Institut für Wasserbau und Wasserwirtschaft

Technische Universität Darmstadt

MITTEILUNGEN

Heft 148 2011

Xiaoyan Zhou

Morphodynamic Response of Yangtze River Estuary
to Sea Level Rise and Human Interferences

Institut für Wasserbau und Wasserwirtschaft

Technische Universität Darmstadt

Morphodynamic Response of Yangtze River Estuary to Sea Level Rise and Human Interferences

dem Fachbereich Bauingenieurwesen und Geodäsie
der Technischen Universität Darmstadt
zur Erlangung des akademischen Grades eines
Doktor-Ingenieurs (Dr.-Ing.)
vorgelegte

Dissertation

von
Xiaoyan Zhou
aus Yichang (China)

Darmstadt im Januar 2011

D 17

Heft 148 **2011**

Diese Mitteilungsreihe hat zwei Wurzeln:

- die “Wasserbau-Mitteilungen” (41 Hefte), begründet 1966 von Prof. Dr.-Ing. Friedrich Bassler, später fortgeführt von Prof. Dr.-Ing. Josef Mock,

- die “Technischen Berichte über Ingenieurhydrologie und Hydraulik” (54 Hefte), herausgegeben seit 1965 von Prof. Dr.-Ing. Dr.-Ing. E. h. Otto Kirschmer, später fortgeführt von Prof. Dr.-Ing. Ralph C. M. Schröder und Prof. Dr.-Ing. Manfred Ostrowski.

Mit dem Dienstantritt von Prof. Dr.-Ing. Ulrich Zanke als Nachfolger von Prof. Mock sind diese beiden Reihen zusammengeführt worden. Die drei Fachgebiete des Instituts für Wasserbau und Wasserwirtschaft

- Ingenieurhydrologie und Wasserbewirtschaftung
- Wasserbau

dokumentieren damit auch nach außen ihre Zusammengehörigkeit. Die neue Numerierung ergibt sich aus der Summe der Hefte beider Vorgängerreihen.

Die “Mitteilungen des Instituts für Wasserbau und Wasserwirtschaft der Technischen Universität Darmstadt” erscheinen in unregelmäßiger Folge im Eigenverlag des Instituts für Wasserbau und Wasserwirtschaft.
(ISSN 1430-3434)
ISBN 3-936146-28-4

FG Ingenieurhydrologie
u. Wasserbewirtschaftung
Petersenstraße 13
64287 Darmstadt
Tel.: 0 61 51/16 21 43
FAX: 0 61 51/16 32 43
E-Mail: ostrowski@ihwb.tu-darmstadt.de

FG Wasserbau
Petersenstraße 13
64287 Darmstadt
Tel.: 0 61 51/16 40 67
FAX: 0 61 51/16 32 23
E-Mail: wabau@wb.tu-darmstadt.de

Aktuelle Informationen über das Institut und seine Lehrangebote finden Sie im World Wide Web unter: http://www.wasserbau.tu-darmstadt.de/wasserbau/index.de.jsp

Referent:	Prof. Dr.-Ing. habil. Prof. h.c. Ulrich C.E. Zanke
Koreferent:	Prof. Dr.-Ing. Chia Chuen Kao
Koreferent:	Prof. Dr.-Ing. Jinhai Zheng
Tag der Einreichung:	25. Juni 2010
Tag der mündlichen Prüfung:	25. Januar 2011

Herausgeber:

Prof. Dr.-Ing. habil. Prof. h.c. U.C.E. Zanke (Wasserbau)
Prof. Dr.-Ing. M. Ostrowski (Ingenieurhydrologie und Wasserwirtschaftung)

VORWORT

Der Yangtze Fluss mündet bei Shanghai in einem aus mehreren Teilästaren bestehenden Mündungstrichter in das Gelbe Meer. Bett und Ufer sind von den vorherrschenden Strömungen leicht beweglich und so befindet sich die Mündung in ständiger Umformung.

Waren für den Hafen Shanghai noch vor wenigen Jahren die natürlichen Tiefen der Mündung um 8,5m ausreichend, so würde der Hafen heute ohne Vertiefung der Zufahrt erheblich an Bedeutung verlieren. Damit sind die derzeitigen Anstrengungen zu verstehen, die Fahrwassertiefen der Mündung in mehreren Abschnitten über 8,5m und 10m auf 12,5 m zu vertiefen. Das zentrale Problem ist bei einer derartigen Maßnahme die Fixierung des Talwegs und die Minimierung der Unterhaltungskosten. Letztere sind zu wesentlichen Teilen Baggerkosten.

Hier setzt die Arbeit von Frau Zhou an. Sie hat zunächst ein topographisches Modell der Mündung des Yangtze aufgebaut und dann verschiedene Szenarien modelliert, um die morphologischen Antworten auf verschiedene natürliche und von Menschen verursachte Einwirkungen auf den Yangtze und seine Mündung zu simulieren.

Um derartige, aussagekräftige Szenarien zu erhalten, mußte sie zunächst die Hydrologie und Morphodynamik der Jangtze-Mündung verstehen und die Wirkmechanismen tangierender Projekte (Wasserumleitungen, Aufforstungen) auf den Fluss und die Mündung analysieren sowie die Gegebenheiten und Ansprüche der Nutzungen der Seeschiffahrt im Mündungsästuar, soweit hier erforderlich, herausarbeiten.

Zugrundegelegt hat Frau Dr.-Ing. Xiaoyan Zhou dann bei den Simulationen verschiedene Szenarien wie extrem hohen und extrem niedrigen Zufluss aus dem Einzugsgebiet des Yangtze. Weiterhin hat sie ein hydrologisches „Ersatzjahr“ entwickelt, mit dem sich die Rechendauer auf ein machbares Maß reduzieren ließ, um die jeweiligen Wirkungen auf den morphologischen Trend herauszuarbeiten.

Ein wesentliches Ergebnis der Arbeit ist, dass die Baggerkosten mit jedem Meter Vertiefung progressiv ansteigen werden. Die Modellsimulationen führten auf die Prognose, dass sich die jährlichen Baggermengen von ca. 7 Mio. m^3 bei 8,5 m Fahrwassertiefe auf ca. 70 Mio. m^3 verzehnfachen, wenn das Fahrwasser auf 12,5 m Tiefe unterhalten werden soll. Soweit bislang erkennbar, bestätigen sich die berechneten Tendenzen in der Natur.

Neben vertieftem Stoff zur Dynamik der Mündung des Yangtze erhält der Leser einen guten Einblick in die komplexen Wirkungszusammenhänge der natürlichen Gegebenheiten und anderer geplanter Großeingriffe.

Darmstadt im Juli 2011

Univ. Prof. Dr.-Ing. habil. U.C.E. Zanke

To my parents Qiyun Zhou, Mingxiang Xiang
and my husband Dong-Jiing, Doong

ACKNOWLEDGEMENTS

I would like to express my gratitude to the German Academic Exchange Service (DAAD) and the China Scholarship Council (CSC) through Sandwich Program, and to the Federal Ministry of Education and Research (BMBF) through IPSWaT Program (IPS 09/10P2) who have financially supported this research.

I would like to express my most sincere appreciations and special gratitude to my supervisor Prof. Dr.-Ing. habil. Prof. h.c. U.C.E. Zanke, who not only always takes good care of me, but most importantly, guided me throughout this work with his profound knowledge and professional experience. I would like to thank my co-supervisor Prof. Yixin Yan for his support and continuous encouragement.

Sincere thanks go to my defense Advisory Committee members for their constructive suggestions, especially to Prof. Dr.-Ing. Chia Chuen Kao and Prof. Jinhai Zheng. I also acknowledge those distinguished guests who came so far to my defense.

Further I would like to show my appreciations to all my colleagues in the Institute of Hydraulic Engineering at the Darmstadt University of Technology for the valuable discussions and the encouragement during my PhD. Much thanks to Dr.-Ing. Andreas Wurpts, Prof. Dr.-Ing. Nicole Saenger, Dr. Zhongchao Yang, Dipl.-Ing. Gregor Dahlem and Dipl.-Ing. Silke Schneider for their help and friendship.

I am deeply grateful for Mrs. Zeitler, Mrs. Wicke and Mrs. Huxhorn, with whom I have good memories.

I could not express my thanks with only a few words to my friends at home and abroad for the great courage and memory of joy that they have brought to me.

I would like to take this opportunity to express my great gratitude to my parents, my brother and other relatives. Special thanks to my husband Dong-Jiing for his constant love, support and patience.

Last but not least, I want to express my thanks and blessings to all those people around the world who have ever helped me in any respect of this study.

ABSTRACT

Estuarine morphodynamics describe the development of estuarine bed over time. The changed morphodynamics have a direct or indirect influence on the wetland resources, water quality and ecological system, biodiversity, channel regulation and coastal protection. The morphology of Yangtze Estuary changed a lot in the past two thousand years, especially in recent 150 years. It is supposed to adjust accordingly with the further changes of water and sediment discharge due to human interferences and the possible sea level rises. To estimate and evaluate the impact on morphodynamics of human interference, like dredging of access channels to ports, and of long-term processes, like sea level rise or a changing discharge regime, is of great importance and much necessity. Therefore, the research goal of this study is to evaluate the morphological response to the variations of hydrodynamic conditions at Yangtze Estuary, based on various unknown scenarios and known project plans. Due to the different spatial and temporal scales involved in the morphological process, both field data analysis and numerical simulations are carried out in order to gain more insight in the historical and future morphological evolution of this area.

Regular and short-term field measurements at Yangtze River as well as the monthly data at Datong station in the past 50 years are analyzed. Results show that the water and sediment discharges of Yangtze River have been changed, and the morphological changes response to the correlation of water and sediment discharges. The major pattern is erosion, and the erosion rate increased 10 times in the past two decades for N-RER reach of Yangtze River. A linear correlation between the deposition volumes with the ratio of water to sediment discharges was found.

The morphodynamic numerical model TIMOR is set up at the Yangtze Estuary. The sensitive parameters are calibrated with measured water level, flow velocities and directions, suspended sediment concentrations. TIMOR is validated with field data from both dry and wet seasons; the model simulation results have very good agreement with the field data.

Simulations are done to check the seasonally and long-term morphological changes. Results show that, deposition happens more frequently during dry season than during wet season. The suspended sediment concentration is greatly influenced by tide propagation and it is in proportion to the current velocity. The spatial and temporal pattern of bathymetry changes predict that, the North Branch would degrade significantly; the South Branch and North Channel has deposition along the river banks; the right bank of South Passage is under deposition.

The major human activity at the Yangtze Estuary, the Deep Waterway Regulation Project, has been examined its influences by simulations. The morphology at Deep Waterway Area is under dynamic equilibrium. Since 2007, the middle waterway started deposition. The idea to heighten the South Training Wall may not be effective to tackle the deposition problem

according to the dredging volume needed as well as the ebb and flood velocities in the channel. To maintain the waterway 15m, huge sediment must be dredged annually.

To predict the morphological response under joint effect of sea level rise and typical water discharges, attempt simulations are made. Under Sea Level Rise scenarios, the morphology of Yangtze Estuary is dominated by deposition. When the sea level rises less than 1 m, the morphological changes are similar. Under the extreme low water discharge and high sea level rise, the Yangtze Estuary is expected to be eroded. Whether extreme large or low water discharges or sea level rise occurs, the South Passage will be deposited.

This study works not only on the hydrodynamic but also the morphological simulation for the entire Yangtze Estuary area considering flows, sediments, currents and winds simultaneously. The human activity influence as the regulation work in the Yangtze has been explored. Exploratory predictions on the joint effect of sea level rise and typical water discharges are made. It is believed that this work can help to improve the understanding of morphological response to the human activities and sea level rise in estuary, thus wished to provide reference for policy-makers, estuary and coastal researchers.

Morphologische Veränderungen im Mündungsbereich des Yangtze hervorgerufen durch den Anstieg des Meeresspiegels und Eingriffe des Menschen

KURZFASSUNG

Morphodynamik beschreibt die zeitliche Entwicklung der Topographie des Meeresbodens. Eine veränderte Morphodynamik hat einen direkten oder indirekten Einfluss auf Feuchtgebiete, die Gewässergüte, ökologische Systeme, die Artenvielfalt sowie die Unterhaltung von Kanälen und den Küstenschutz. Die Morphologie der Yangtze-Mündung hat sich in den letzten 2000 Jahren, vor allem in den letzten 150 Jahren sehr verändert. Dieser Trend wird sich durch weitere Veränderungen in der Abflussmenge und Sedimentfracht hervorgerufen durch menschliche Eingriffe und den möglichen Anstieg des Meeresspiegels fortsetzen. Es ist von großer Bedeutung und von Notwendigkeit abzuschätzen und zu bewerten, welche Auswirkungen durch menschliche Eingriffe, wie Ausbaggern von Kanälen, und langfristige Prozesse, wie dem Anstieg des Meeresspiegels oder einer Änderung des Abflussregimes auf die Morphodynamik entstehen. Das Ziel dieser Arbeit ist die Untersuchung und Bewertung morphologischer Veränderungen im Mündungsbereich des Yangtze anhand verschiedender Szenarien und Projekte. Da unterschiedliche räumliche und zeitliche Skalen an den morphologischen Prozessen beteiligt sind, werden sowohl Analysen der Messdaten als auch numerische Simulationen durchgeführt, um eine verbesserten Einblick in die historische und zukünftige morphologische Entwicklung dieses Gebietes zu gewinnen.

Die Daten von regulären und kurzzeitigen Feldmessungen am Yangtze sowie die monatlichen Messdaten der Datong Station der vergangenen 50 Jahre werden analysiert. Die Ergebnisse zeigen, dass sich die Abflussmenge und Sedimentfracht des Yangtze verändert haben und die morphologischen Veränderungen damit korrelieren. Die größte Veränderung trat bei der Erosion auf. Im Yangtze zwischen Datong und Jiangyin stieg die Erosionsgeschwindigkeit in den vergangenen 20 Jahren um den Faktor 10 an. Eine lineare Korrelation zwischen dem abgelagerten Volumen und dem Verhältnis von Abfluss zu Sedimentfracht wurde gefunden.

Die Yangtze Mündung wird mit dem morphodynamisch-numerischen Modell TIMOR abgebildet. Für die Kalibrierung des Modells werden die Messungen des Wasserstandes, der Strömungsgeschwindigkeiten und –richtungen sowie der Schwebstoffkonzentrationen herangezogen. Das Modell wird mit Messdaten aus der Trocken- und Regenzeit validiert. Die Simulationsergebnisse zeigen eine sehr gute Übereinstimmung mit den Messdaten.

Simulationen, um die saisonalen und langfristigen morphologischen Veränderungen zu überprüfen, werden durchgeführt. Die Ergebnisse zeigen, dass während der Trockenzeit mehr Sediment abgelagert wird, als während der Regenzeit. Die Schwebstoffkonzentration ist stark von Ebbeausbreitung beeinflusst und abhängig von der momentanen Geschwindigkeit. Die räumlichen und zeitlichen Muster der Veränderungen der Meeresbodentopographie sagen vorher, dass der nördliche und südliche Mündungsarm, dass der sich im südlichen Arm

befindliche nördliche Kanal, entlang der Flussufer, und die rechten Ufer der Süd-Passage, Ablagerung aufweisen würden.

Der Einfuss des Baumaßnahmen im Rahmen des „Deep Waterway Regulation“-Projekt, welche in der nördlichen Passage im Bereich der Mündung des Yangtze ausgeführt werden, wird mit Hilfe des in TIMOR implementierten Modellgebietes untersucht. Die Morphologie im Bereich des Projektgebietes ist in einem dynamischen Gleichgewicht. Seit 2007 findet in der Mitte des im Rahmen des Projektes gebaggerten Schifffahrtsrinne Sedimentation statt. Eine mögliche Lösung für das entstandene Problem könnte die Erhöhung der südlichen Wand darstellen. Die Simulation zeigt, dass diese Maßnahme nicht sinnvoll wäre, da sowohl die zu baggernde Menge nicht verringert, als auch die Ebbe- und Flutgeschwindigkeiten nicht positiv beeinflusst würden. Zur Erhaltung einer Tiefe von 15m in der Schifffahrtsrinne müssen jährlich über 70 Mio. m^3 Sediment gebaggert werden.

Die Modellierung verschiedener Anstiege des Meeresspiegels unter Ansatz eines mittleren Abflusses für den Yangtze zeigt, dass die Morphologie der Yangtze-Mündung durch Ablagerungen dominiert wird. Wenn der Meeresspiegel um weniger als 1 m ansteigt, sind die auftretenden morphologischen Veränderungen ähnlich zu einander. Bei einem starken Anstieg des Meeresspiegels und einem sehr niedrigen Abfluss im Yangtze, ist eine starke Erosion in der Yangtze-Mündung zu erwarten. Unabhängig davon, ob extreme hohe oder niedrige Abflüsse oder ein Anstieg des Meeresspiegels auftreten, wird es in der südlichen Passage des Yangtze zu Sedimentation kommen.

Die vorliegende Dissertation beschäftigt sich nicht nur mit der hydrodynamischen, sondern auch mit der morphodynamischen Simulation des gesamten Yangtze-Mündungsbereiches unter gleichzeitiger Berücksichtigung von Abfluss, Sediment, Strömung und Wind. Der Einfluss durch menschliche Aktivität wird ebenfalls betrachtet. Die gemeinsame Wirkung des Anstiegs des Meeresspiegels und verschiedener Abflüsse des Yangtze wird vorhergesagt. Diese Arbeit trägt dazu bei, die morphologischen Veränderungen, welche auf Grund von Eingriffen durch den Menschen und den Anstieg des Meeresspiegels in Flussmündungen entstehen können, besser zu verstehen.

TABLE OF CONTENTS:

LIST OF TABLES:

LIST OF FIGURES:

LIST OF SYMBOLS

A_i	The area of cross section i
$\triangle L$	Distance between sections A_i and A_{i+1}
W	The storage capacity between sections A_i and A_{i+1}
d_{50}	The median particle diameter
f(i,j)	The fraction of the exchange increment
p(j)	The fraction of bed load
F(j)	The fraction of active layer
v	Velocity of flow [m/s]
λ	Friction at the bed
ω_s	Settling velocity [m/s]
ν_{crit}	Threshold velocity [m/s]
E_H	Kinetic energy in the flow direction
E_V	The kinetic energy acting for lifting particles
SF	The shape factor describing the shape of the grain
D*	The sedimentological grain diameter
ρ_s	The density of the sediment
ρ_f	The density of the fluid
g	Gravity constant
ν_{*lift}	The threshold velocity for lifting into suspension
ν_0	The kinematic velocity at 0 degree Celsius
ν	Kinematic viscosity of the fluid
S_{sus}	Suspended load concentration
S_{bed}	Bed load concentration
S_{total}	Total load concentration
γ	A dimensionless friction coefficient
M	The erosion coefficient [kg $m^{-2}s^{-1}$]
q	Transported bed-load volume including voids per unit time and unit width
Us,max	Maximum sediment velocity at the top of the bed
s	Kinematic viscosity of the fluid
h	Water depth
n	Proportions of voids in the sediment at rest
I_B	Bed slope
I_E	Energy slope
R	Risk of grain movement
$\tau_{c,0}$	Shields critical shear stress between the water and the bed
τ_0	Shear stress of the water body at the bottom =ρghI
$\tau^*_{c,0}$	$= \tau_{c,0} / ((\rho_s - \rho) g d) = u^{*\,2}_{c,0} / \rho' g d$ dimensionless critical shear stress

τ^*	= $\tau_0/((\rho_s-\rho)gd) = u_0^{*2}/\rho' gd$ = dimensionless shear stress
τ_b	Bottom shear stress (Nm^{-2})
τ_{ce}	Critical shear stress for erosion (Nm^{-2})
Φ	Angle of internal friction of sediment in the state of motion
$y_{D,eff}$	Distance of the center of thrust from the wall under developed transport
u*	Shear stress
$u^*_{c,0}$	Critical shear velocity at the top of the bed after Shields
u_τ	Shear velocity
ks	Equivalent sand roughness, for natural sediments after v. Rijn(1984) ks≈2d
B	Integration constant for the velocity distribution law
u_m	Average flow velocity at the center of trust of the grains at the surface

LIST OF ABBREVIATIONS

IPCC	Intergovernmental Panel on Climate Change
ALD	Aswan Low Dam
AHD	Aswan High Dam
TGD	Three Gorges Dam
YE	Yangtze Estuary
NB	The North Branch of Yangtze Estuary
SB	The South Branch of Yangtze Estuary
NC	The North Channel of Yangtze Estuary
SC	The South Channel of Yangtze Estuary
NP	The North Passage of Yangtze Estuary
SP	The South Passage of Yangtze Estuary
WSCP	The Water and Soil Conservation Project
SNWDP	The South-to-North Water Diversion Project
WDP	The Water Diversion Projects
DWRP	The Yangtze Estuary Deep Waterway Regulation Project
BOH	Bureau of Hydrology
CWRC	The Changjiang (Yangtze River) Water Resources Commission
SSC	Suspended Sediment Concentration
PS	The Profile Station
FBR	Flow Bifurcation Ratio
SBR	Sediment Bifurcation Ration
N-RER	The Near River Estuary Reach
RER	The River Estuary Reach
OE	The Offshore Estuary
SBM	The Sediment Budget Method
TCM	Topographic Change Method
DEM	Digital Elevation Model
GIS	Geographic Information System
LWL	Low Water Level
MWL	Mean Water Level
RBWL	River-Beach Water Level
FWL	Flood Water Level
1-D	One-Dimensional
2-D	Two-Dimensional
3-D	Three-Dimensional
DHI	Danish Hydraulic Institute
ASMITA	Aggregated Scale Morphological Interaction between a Tidal inlet and the Adjacent coast
USACE	U.S. Army Corps of Engineers
SWE	Shallow Water Equations

MPM	Meyer-Peter and Müller Equation
SMS	Surface-water Modeling System
85NHD	The Chinese 1985 National Height Datum
FC	Friction coefficient
EF	Entrainment factor
EVC	Eddy viscosity coefficient
GSD	Grain size distribution
MF	Morphological factor
ME	Mean Error
STDEV	Standard Deviation of the bias
SE	Smallest Error
RMSE	Root Mean Square Error
MWLE	Mean Water Level Error
MAE	Mean Absolute Error
MSE	Mean Square Error
MFVE	Mean Flow Velocity Error
SD	Standard Deviation
MEV	Maximum Ebb Velocity
MFV	Maximum Flood Velocity
UNFCCC	The United Nations Framework Convention on Climate Change
SLR	Sea Level Rise
MSL	Mean Sea Level
RSLR	Relative Sea Level Rise
PSMSL	Permanent Service for Mean Sea Level
RLR	Revised Local Reference

CHAPTER 1

INTRODUCTION

1.1 Research background

An Estuary is an area where interactions are very strong between land and sea, between natural processes and human activities. An Estuary is a semi-enclosed coastal body of water with one or more rivers or streams flowing into it, and with a free connection to the open sea. An Estuary is also defined as the transition between two distinct water bodies: a river and a sea (Dyer, 1986). The main driving forces affecting the property of an estuary are tide, river runoff, river sediment discharge and littoral sediment transport, waves, and density difference etc. The interactions among these factors, estuary topography and suspended load and bed load characteristics dominate the estuary morphology process and the evolution of the channel and shoal in the estuary. To achieve a complete flowing logic due to the complex interactions between the fluid, the bed, and the particles in the fluid and on the bed is challenging. In most cases, waves, through there are almost ubiquitous, are treated separately from currents. Similarly cohesive and non-cohesive sediments are considered separately, even though there are large areas of the sea bed where the sediments are cohesive until they move, and are non-cohesive until they are deposited (FitzGerald and Knight, 2005). Understanding these interactions has been of interests to coastal oceanography and engineering; e.g. coastal protection, land reclamation, dredging of deepwater navigational channels, estuary regulation works and water quality management.

1.1.1 Natural factors affecting estuary morphodynamics

The erosion and deposition changes in estuaries are very complicate. They are greatly influenced by the flow pattern, namely the total runoff and tide, and also by the sediment sources and sediment concentration. Natural factors which affect estuary morphodynamics can be summarized by four points.

Hydrodynamic factors

Estuary has both river and sea function processes at the same time, and these functions differ with different time and space (Dyer, 1998). River runoff is one-way flow, changes its volume in dry and wet season, while tide is alternating flow, and changes its direction during day and night. River runoff and tide interact with each other. During flood tide, tidal water is in the opposite direction to runoff, their velocities both decreased due to their counteractions. However while during ebb tide, tidal water is in the same direction to runoff, increasing their velocities especially during the wet season. Within this process, sediment sometimes is carried to the estuary and deposit there, sometimes, the estuary is under erosion because of the sediment is carried into the river channel or outer estuary.

The hydrodynamic conditions are influenced by the mixture of saltwater and fresh water. Due to larger gravity of saltwater from seaside, it intrudes into the lower layer of river flow

and forms the salt wedge. The front of salt wedge is always with high sediment deposition (Savenije, 2005). The position of salt wedge shifts back and forth with the changes of runoff and tide. The freshwater can extend far away towards seaside, for example the freshwater in Amazon River (S. American) can run hundreds kilometer away from the estuary, and freshwater in Yangtze River (China) spreads 300 km to Jizhou Island in South Korea in wet season. Wave and current conditions affect the morphology of a river estuary. Erosion or deposition at the river estuary area highly depended on the wave direction.

Bed sediment and sediment supply

Global rivers play the dominant role worldwide in transferring materials from the land to the ocean, including the sediment. Most of these sediments, however, are trapped in estuaries or deposited on adjacent continental shelves. The sediment delivered to the oceans from global rivers has been estimated to be ~20 billion tons per year (Bt/yr) (Milliman and Syvitski, 1992), of which Asian rivers nearly occupy more than 70% (Syvitski et al., 2005; Liu et al., 2007). These large amounts of sediment play an important role in the global geological cycle, the global geochemical cycle, the coastal ecosystems and the evolution of deltas. The sediment in the estuary which comes from river is called terrigenous sediment. Sediment which comes from sea side is the marine sediment, it is carried by tidal current (Dyer, 1998). Due to the different sediment sources and volume, the evolution in estuary region is also different.

The terrigenous sediment is the main source to form the estuary morphology. The amount and size of sediment supply differs due to the characteristics of river basin (Perez, 2000). Some estuaries have large sediment supply from rivers, such as the James river estuary in American has 70% sediment supply from river runoff (Nichols, 1991), but some have relatively small, like the Australian Bega River estuary has only 16% from river runoff (Fryirs, 2001). High energy events can lead re-suspension and re-transportation of sediment in estuary (Baumann, 1984), for example, during the storm surge, sediment can be carried from open sea to estuary.

Geological conditions

Estuaries formed when the sea level rose and flooded valley during the Holocene Epoch, therefore, the original geological background also affects the morphodynamic in estuaries (Dyer, 1998). Estuaries with rock foundation are relatively stable, whole with sand or mud foundation suffer from big turbulence. The estuaries can be classified by tidal influence, river influence, topography, oceanographic, salinity structures, and estuary numbers (Savenije, 2005). In terms of tidal range, the estuaries can be classified as (Davies, 1964): Micro-tidal estuaries (tidal range < 2m), Meso-tidal estuaries (2m < tidal range <4m), Macro-tidal estuaries (4m < tidal range <6m), and Hyper-tidal estuaries (tidal range > 6m). Considering the influence of tide convergence and the friction, the estuaries are defined as (Nichols and Biggs, 1985), Hyper-synchronous estuaries (Convergence > Friction), Synchronous (Convergence = Friction), and Hypo-synchronous (Convergence < Friction). According to topography, estuaries are suggested to be classified as three groups (Pritchard, 1952): Coastal plain estuaries (by Drowned river valleys), Fjords (formed by glacial erosion), Bar-built estuaries (formed by the drowned river valleys), others (formed by volcanic eruptions,

faulting, landslides, or other processes). Based on the characteristics of salinity distribution and stratification structures, estuaries are classified as (Pritchard, 1955, Dyer, 1998), Highly stratified estuaries, Partially mixed estuaries, and Well mixed estuaries.

Sea level changes

During sea advance and sea retreating period, estuary and delta came into being (Boyd, 1992). After the last Ice Stage (about 10000 years ago), the global sea level rose and formed the current world estuaries, much sediment has been deposited in estuary regions, so the estuary in Holocene Epoch were formed during sea advance in the late Ice Stage, and moved towards land with sea level rising (Stanley and Warne, 1994). In estuary, if the sea level rises faster than the supply of sediment, the cut valley will extend to the land further (Dalrymple, 1992) ; if slower, the estuary will be deposited by sediment, till the dynamic and geographic reach balance again (Zaitlin, 1994).

The latest report of the Intergovernmental Panel on Climate Change (IPCC), reflecting the views of scientists from over 130 countries, confirmed that global sea level has already been rising at an average rate of 1.7 mm per year during the 20th century (IPCC, 2007). With continued growth in global greenhouse gas emissions and associated warming, sea level could rise by another one to three meters this century. Most of this anticipated increase is attributable to glacier melt and thermal expansion of oceans. The additional possibility of warmer temperatures unexpectedly breaking up the Greenland and West Antarctic ice sheets, still widely debated among climate scientists, could lead to a devastating five-meter increase.

Future sea level rise will accelerate the evolution of global river estuaries. The mechanism is that the rising sea level will increase the intensity of tidal current, wave and storm surge and decrease the ability to reduce the force of waves on the tidal flat and coastal wetland due to the loss of the coastal area. Therefore, the estuary erosion area will increase, the sedimentation rate of accretion estuary will decrease or even turn accretion into erosion, and the width of tidal flat will reduce. Sea level rise will also increase the salt water intrusion into the river estuary to change the hydrodynamic balance. Altogether, the future sea level rise will bring very large impact to the river estuary area.

1.1.2 Human interferences affecting estuary morphodynamics

Human activities have the most profound influence on the natural coastal environment. Many coasts have been changed by human beings either directly by constructions and dredging, or indirectly by changed environment which affect the sediment, river runoff and climate. Human activities have been strongly affecting the world's river sediment supply to the estuary and ocean since 19th or 20th centuries (Stanley and Warne, 1993; Fanos, 1995; Smith and Winkley, 1996; Guillen and Palanques, 1997; Trenhaile, 1997; Walling, 1999; Milliman, 2001; Yang et al., 2003, 2004). This has been a global concern issue.

Construction of dams or reservoirs

The main sediment at the estuaries area is coming from river runoff. The dam construction

interrupts the continuity of a river system in transporting sediments to downstream and coastal regions (Kondolf, 1997). During the latter half of the 20th century, about 45000 large dams over 15m high and an estimated 800000 small dams had been built worldwide, representing nearly an order of magnitude increase compared to the year 1950 (WCD, 2000). These dams hold up 9.65×10^{13} m^3 runoff, and 15% of annual rainfall (Gornitz, 2000). Subsequently, the global sediment flux from the rivers to the sea has decreased significantly (Milliman, 1997; Syvitski et al., 2005). Recent research showed that 172 of 292 rivers with dams in the world have been affected by the dam construction (Nilsson, 2005).

The influences of dams on the down streams are currently mainly concerned with estuary erosion. It is estimated that more than 30% of the global sediment flux is trapped in dam or reservoirs (Vörösmarty et al., 2003). For example, more than 80% of water and sediment discharge from the Indus River (Asia) has been diverted by large reservoirs and flow diversion (Giosan et al., 2006). Dam and reservoir constructions during the 1950s and 1960s on such major tributaries as the Missouri and Mississippi Rivers (American) have reduced suspended sediment loads reaching the Gulf of Mexico by estimates ranging from 50% to over 70%, thereby resulting in loss of wetlands and delta (Kesel, 1989; 2003). In Spain, after the construction of the Ribarroja-Mequinenza dam in the early 1960s, about 96% of the Ebro River (Europe) sediment has been trapped in the reservoir, also leading to erosion of the river delta (Sanchez-Arcilla et al., 1998). The other example is at the Nile River in Africa. The river bed degradation and bank erosion occurred and serious shore erosion was observed at the river mouth area after the building of Aswan Low Dam (ALD) in 1902 and Aswan High Dam (AHD) in 1964. One of the reasons is the sediment supply has been cut off upstream (Frihy, 1992). In the case of the AHD, the aggregate storage capacity of Lake Nasser, which is twice as large as the annual runoff of the Nile River at the dam site, is sufficient to change both the flow regime and sediment supply. Thus, the annual peak discharge has been reduced to less than a third of its original value in the Nile River.

China has been particularly active in dam construction, building more than half of the world's large dams commissioned since 1950 (Fuggle and Smith, 2000). Over the past 25 years, for example, the Yellow River sediment discharge has decreased by 90% because of dam construction and increased water consumption (Wang et al., 2007). In recent times, concerns about similar impacts of the Three Gorges Dam (TGD) on the middle Yangtze River in China have been raised by many researchers. The aggregate storage capacity of the TGD, however, is 10% of the average annual runoff at the dam site, which may not large enough for a substantial alteration of the flow regime in the downstream river channel. However the primary change of hydrological condition introduced by the implement of TGD in 2003 was a significant reduction of sediment load in the downstream alluvial channel.

Water diversion projects

Stream diversion, both natural and man-made, disrupts the water and sediment supply to downstream areas. With diversion for agriculture or urban use, the results are similar to those produced by dams. Many countries have planned to transfer inter-basin water from rich water resources area to drought region. Famous projects in the world like the Arctic Ocean water diversion scheme of former Soviet Union, North America Water Transfer Project,

New Delta Canal Project in Nile, Amazon Water Transfer Project, Australian Eastern Coast Water Transfer Project, Congo River Water Transfer Project, and Chinese South-to-North Water Diversion Project, etc (Chen, 2000). These water diversion projects reduce the water discharge for the original rivers. It would detrimental to the river's transportation especially in dry season. It also alters the timing of freshwater influx to deltaic environments (Ward and Stanford 1979). Lack of freshwater inflow to deltaic areas affects the salinity, temperature, sediment influx, and nutrient regimes of estuarine habitats (Livingston 1991). Saltwater intrusion situation in the estuary area will possible to be exacerbated. In addition, it may interrupt the sediment transport by the river to accelerate the estuary and coastal erosion and change the estuary morphology.

Degradation of natural capital

The Earth's human population is estimated to be 6.8×10^9 in 2009, more than twice of the population in 1950s. Projection shows the population of around 9 billion by the year 2050. Current population expansion and accompanying increase in usage of resources is a big threat to the earth's environment. Usable land may become less useful through deforestation, desertification, salinization, erosion, and urban sprawl. Some countries, such as the United Arab Emirates and particularly the Emirate of Dubai have constructed large artificial islands, or have created large dam and dike systems, like the Netherlands, which reclaim land from the sea to increase their total land area. In some countries, the inhabitants move to mountain area due to the limited space in the plain. Degradation of natural capital was happened. Human activities, particularly agriculture and deforestation, however, have increased erosion rates, as they tend to remove the protective vegetation and reduce the stability of the soil. In the absence of trees, the harsh environmental factors of wind and water run-off become strong forces eroding the soil. Eroded soil is easily carried away by streams and rivers and is ultimately deposited in estuaries and offshore. In many developing countries, deforestation is a severe problem. Deforestation increases the erosion, and the eroded soil is carried to sea which leads the coastal line move towards sea (Pennant-Rea, 1994). All these human activities in the high mountain or in the river basin are often responsible for accelerated erosion of sediments that can be transported to a river during rainy periods or floods, contributing to sedimentation in estuaries and coastal areas.

Fortunately, the interest and activity in environmental restoration has given rise nowadays. It involves many different approaches and technologies depending on the requirements of the situation such as the planting of trees and other vegetation. For the estuary area, restoration of riparian vegetation in the upper estuary, salt-marsh vegetation in the lower estuary and dune vegetation on the coast line, are environmentally safe and sustainable actions that contribute to retaining sediments in their area of origin, preventing both erosion and loading of massive amounts of sediment into a system.

Sand mining in river and coast

As a dynamic environment, the human impact on sediment balance, especially the sand mining, can have contributed to morphological change. Sand mining in river or coast directly reduces the sediment supply to the littoral system. In most areas of the United States, beach sand can no longer be exploited for commercial purposes because sand is in short supply,

and the health of dunes and biological communities depends vitally on the availability of sand (USACE, 2008). Jia et al. (2007) studied on the impacts of the large amount of sand mining on riverbed morphology and tidal dynamics in lower reaches and delta of the Dongjiang River in Southern China. They found that under the strong sand dredging, the tidal dynamic in the lower reaches and delta of the river occurred. The tidal level dropped, tidal range widened, flood tidal duration became longer, as well as the amplitudes of major tidal components became bigger and tidal dynamics intensified. In addition, the limits of the tidal level, tidal current and salt water moved upstream. The tidal dynamics at the estuary is intensified.

Others

In additional to the above factors, beach nourishment and coastal structures also influence the estuary morphodynamics. Coastal structures such as jetties, groins, seawalls, bulkheads, and revetments are probably the most dramatic cause of man-induced coastal erosion (SPM, 1984). Any coastal structure will have some effect on local sediment dynamics, and in some cases, the drift of sediments may extend downwards for many kilometers. Beach nourishment is the way to add sand back into the littoral system. All of these activities break the sediment balance of the system; may induce the changes of coastal morphology including the estuary region.

1.2 The study site - Yangtze Estuary (YE)

The Yangtze River (Fig.1-1) originates from the Qinghai-Tibetan Plateau at an elevation of 6600m, flowing eastward for more than 6300 km, functions as the golden waterway connecting the west, middle and east China. The basin has an area of 1.8×10^6 km^2, 18% of the total land area of China. It is the longest river in China and Asia in term of water discharge, third in the world in length, ninth in catchment area (Chen and Gupta, 2001), fourth in sediment flux and fifth in water flux (Eisma, 1998). Most of the basin is in subtropical monsoon climate zone, average annual rainfall reach 1100mm, average annual water discharges into sea amount to 10^{12} m^3 ,which is 36% of the total Chinese river runoff volume.

Yangtze River has more than 1000 branch rivers, of which 6 branch rivers are longer than 1000km. There are 45000 reservoirs constructed in the Yangtze River Basin, with the total storage capacity of 140×10^9 m^3. More than 180 cities are located along the river, which including the big cities like Chongqing, Wuhan, Nanjing and Shanghai as shown in Figure 1-1.

Yangtze Estuary is a typical medium tidal estuary with four outlets divided by islands and shoals, of which the dynamical and geomorphologic processes display a unique kinematical rule among the world's estuaries, due to the distinct interactions between runoff and tidal currents. The complicated hydrodynamics in Yangtze Estuary such as the tide, wave and river runoff together with salt-fresh water mixing process exert significant impact on the suspending, mixture and delivery of sediment, thus making estuary sediment issues difficult.

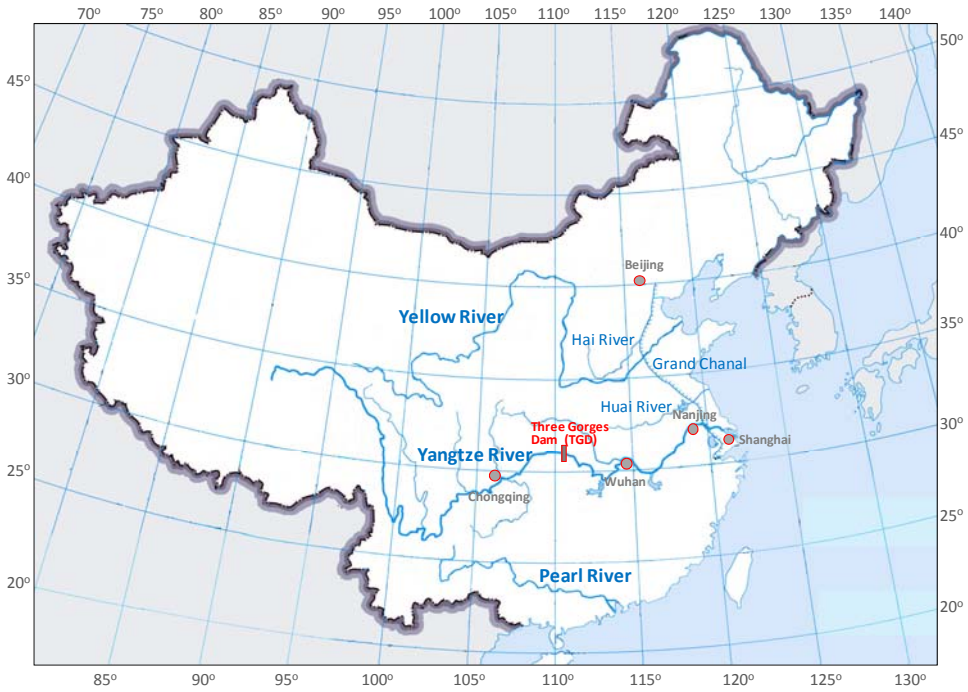

Figure 1-1 Location of Yangtze River in China

The morphology of Yangtze Estuary changed a lot in the past two thousand years. In recent 150 years, it has again experienced some major changes due to flood and human activities. These morphological changes are shown in Figure 1-2. About two thousand years ago, Jiangyin located very close to the river mouth. Nowadays, the distance from river mouth to Jiangyin is 240 km. Great deposition in the river estuary occurred. In 18th century, the Yangtze Estuary had only two branches of the river flow, i.e. the North Branch (NB) and South Branch (SB). During two historic floods in 1860 and 1870, the sill at the entrance of South Branch to North Channel was washed out and the North Channel (NC) and South Channel (SC) came into being. The floods in the period of 1947–1954 settled a frame of North Passage (NP) and South Passage (SP). The current morphology of Yangtze Estuary is shown in Figure 1-3. The North Branch was continuously recessing in the past 100 years due to the upstream reach rapidly fluvial process and the human activities. The abundant river runoff demands the necessary discharge capability of the branches of estuary, thus the North Channel and North Passage were formed during the big wet season. The powerful ebb tide current scoured the shallow area between the main channel (ebb channel) and the flood channel and formed the new branches. In the recent 50 years the regulation works have been executed in river mouth, which effectively interfered with the above natural evolution process. Yangtze Estuary is now becoming a man-controlled river mouth. The width between north and south branch has decreased from 118km to 90km in the past 100 years, while the under water ebb delta extends towards sea. The -5m bathymetry line moves 5-10 km to the seaward. The present three-stage bifurcation of the river mouth has been stabilized, which is favorable for maintaining split ratio of flow and sediment for main bifurcated channels, so that a new stage of bifurcation possibly formed under the flood can be eliminated.

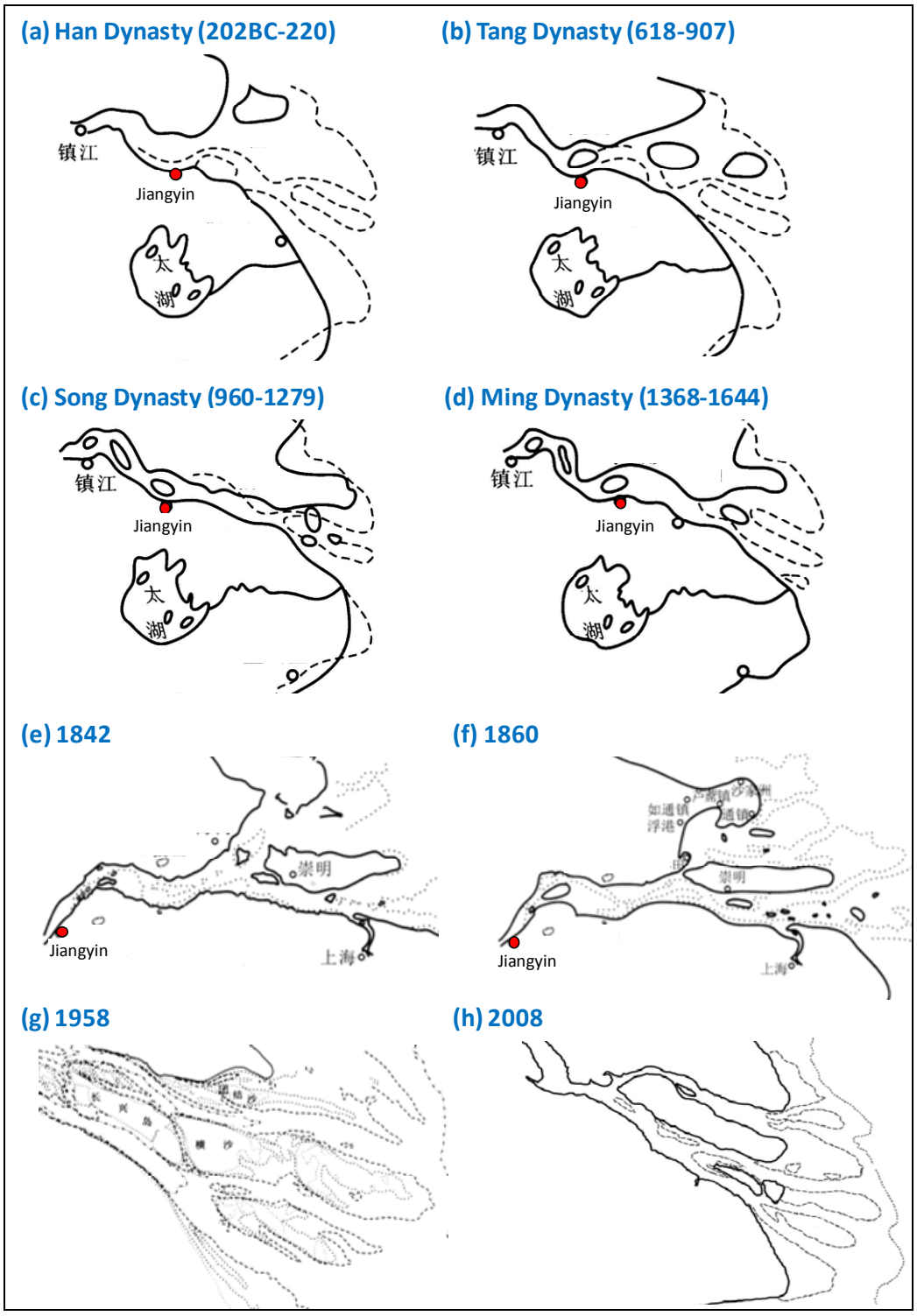

Figure 1-2 Evolution of Yangtze Estuary.
Figures(a) to (d) are modified from Yun (2004); Figures(e) to (g) are modified from Gao (2008)

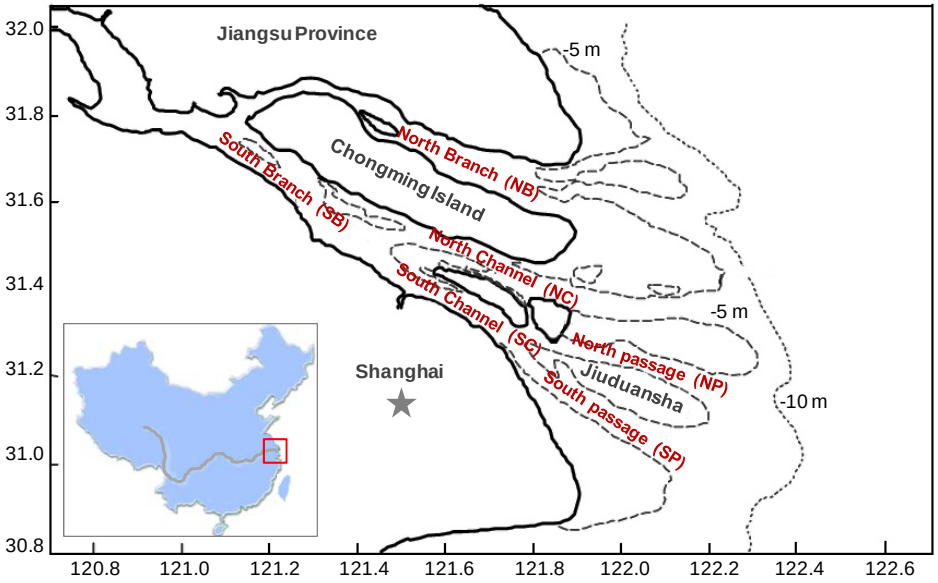

Figure 1-3 Current morphology of Yangtze River Estuary

The morphodynamics of Yangtze River Estuary will be adjusted accordingly with the further changes of water and sediment discharge due to human interferences and the influence of possible sea level rise. The changed morphodynamics will have a direct influence on the wetland resources, water quality and ecological system, biodiversity, channel regulation and coastal protection. The morphodynamic changes in the Yangtze Estuary will directly or indirectly affect the human lives in Yangtze Delta as well as the whole country economically, ecologically and socially. More than 80 million people are living in Yangtze River Delta, therefore, it is of great importance to examine the changed environment and evaluate their interactions.

1.3 Existing situations and problems

Human activities exerted increasing impacts on natural process over time and along the flow directions in the Yangtze River. Construction of water reservoirs or dams greatly reduced the downstream discharge of the sediment load, which will further impact the geomorphological evolution of the river channel of the middle and lower Yangtze River basin, and will also exert tremendous influences on the development of the Yangtze Delta.

The Yangtze River has traditionally carried a vast load of sediment from its upper reaches of the watershed to the East China Sea. Before human activities dominated the Yangtze River, it carried sediment loads of ~480 million tons per year (Mt/yr) to the sea (Wang et al., 1997; Yang et al., 2005). The **Three Gorges Dam (TGD**) was constructed from 1994. Water and sediment began being impounded behind the TGD in 2003, and two years after impoundment, river sediment discharge downstream had decreased to 33% of its 1950-1986 loads (Xu et al. 2006). About 172 Mt/yr of sediment was trapped by the TGD from 2003 to 2008 (Hu et al., 2009). The impact of the TGD on downstream sediment transport was

immediate and sharp. Xu and Milliman (2009) studied the seasonal variations of sediment discharge from the Yangtze River before and after impoundment of the TGD. They presented that the river channel loses a total sediment of 110 Mt/y when considering both the river channel erosion (~70 Mt/yr) and sand extraction (~40 Mt/yr), instead of the TGD trapping (118 Mt/yr). It appeals that the pressure on the Yangtze lower reaches and adjacent coastal areas will get much higher in the near future due to these complicate factors. Many researchers work on the prediction of sediment flux of Yangtze River in the future. Yang et al. (2006a, 2007a, b) suggest that the Yangtze River sediment flux will decrease to about 100-150 Mt/yr in the next six decades. Similarly, Chen et al. (2008) indicated that the Yangtze River sediment flux over the post-TGD period will possibly vary from 112 Mt/yr to 132 Mt/yr or less in ordinary years.

However, the decrease in Yangtze sediment load did not begin with TGD impoundment. The sediment flux at Yangtze River had been decreased since the 1950s (Yang et al., 2006b). The collective changes of reforestation and the construction of many small- and intermediate-sized dams on Yangtze River tributaries have been more important in decreasing the river's sediment load than the TGD (Xu et al., 2006). This illustrates the predominant impact of human activities on the sediment yield, transport and storage in this large river system (Chen et al., 2005; Zhang et al., 2009). Of human activities, dam construction is the dominant factor (88%) contributing to the reduction in Yangtze sediment flux to the sea (Dai et al., 2008). The consequences of TGD trapping were downstream erosion, delta degradation and wetlands loss (Chen et al., 2008). It also posed a great threat to the downstream and coastal ecosystems (Shen and Xie, 2004).

In additional to the dam construction, there are still several ongoing large projects making sediment or water discharge changes therefore influences the estuary morphology. The **Water and Soil Conservation Project (WSCP)** implemented at upper and middle Yangtze River Basin has been started from 1988. WSCP intends to conserve the soil and water loss in Yangtze and its branch rivers by means of planting, returning land for farming to forestry, protecting natural forest and so on. This project benefit the local ecology but also reduces the sediment downloads. The project will keep continuously for next few decades. The **South-to-North Water Diversion Project (SNWDP)** that began in 2002 intends to transfer water from upper, middle and lower Yangtze to meet the demand of northwest and north China. It will be put into full operation in the 2030s. From then on it will divert about 5% (or 450×10^8 m^3) of the Yangtze annual water discharge, leading to 3%-5% of river sediment loss (Yang et al., 2002). The **Water Diversion Projects (WDP)** in lower reach of Yangtze River aims to meet the demand of drinking and industry water in Yangtze River Delta by pumping and diverting water from the River. The Phase III aims to diverse 2.2×10^6 m^3 water per day. The Yangtze Estuary **Deep Waterway Regulation Project (DWRP)** that began in 1998 has built up the south and north dikes with groins in order to reach the design navigation channel depth. This project was planned to take more than 10 years. All of the above large projects, including reclamation at the estuary coasts (1958~) and sand mining at middle and lower reach (1970~) of Yangtze River make very huge influences for the balance of Yangtze Estuary, covering hydrodynamic and ecosystems. Brief of these activities and their influences are summarized in Table 1-1. Considering the factors of the full operation of SNWDP and extension of WSCP as well as the decreasing trend of the erosion capability at downstream

of TGD, Hu et al. (2009) presented that the sediment discharge from Yangtze River to the sea will probably decrease to less than 90 Mt/yr in the coming decades (18% of that in the 1950s).

Both global climate changes and human activities will highly influence the morphology at Yangtze Estuary, but of which the human activities exert a more direct impact. The sediment has been blocked at many reservoirs and reforestation in the upper Yangtze River as well as it has been extracted of huge amount along the river. The water discharge of Yangtze River has been diverged from large diversion projects or regional pumping plans. In additional, big artificial construction is developing directly at the river mouth. All these activities change the water and sediment discharges into the sea. Morphological change at Yangtze Estuary is inevitable.

Table 1-1 List of large projects that have influences for Yangtze Estuary

Name	Period	Place	Description	Influences
Water and Soil Conservation Project (WSCP)	1988~	Upper and middle Yangtze River Basin	WSCP intends to conserve the soil and water loss in Yangtze and its tributaries by planting, returning land for farming to forestry, protecting natural forest, utilizing farm land more reasonably and comprehensive management. By 2008, the total area reforested was estimated at over 90×10^3 km^2. It is planned to protect and recover an additional area of 75×10^3 km^2 in the next decade. (Hu et al., 2009)	WSCP makes a significant reduction in sediment load. WSCP trapped 30 Mt/yr sediment. (Xu et al., 2006) Around 15% of the total sediment reduction (320 Mt/yr in 1993-2002) was attributed to the effects of WSCP (Dai et al., 2008)
South-to-North Water Diversion Project (SNWDP)	2002~	From upper to lower reaches of Yangtze River, incl. East Route (lower Yangtze), Middle Route (Middle Yangtze) and West Route (Upper Yangtze)	SNWDP intends to transfer water from upper, middle and lower Yangtze River to meet the demand of northwest and north China. This project contains three sub-projects to build the east, middle and west routes. The east and middle routes projects both started at Dec. 2002, which plans to transfer 180×10^8 m^3 and 141×10^8 m^3 respectively to the north. The west route will start in 2015. It is planned to divert 170×10^8 m^3 to Yellow River in Northern China.	Water discharge flows into sea decrease, the self-purification capacity weaken and the sediment transport capability also reduce It will be put into full operation in the 2030s. From then on it will divert about 5% (or 450×10^8 m^3) (Chen et al., 2002; Zhu and Zhang, 2008) of the Yangtze annual water discharge, leading to 3%-5% of river sediment loss (Yang et al., 2002)
Three Gorges Dam (TGD) and proposed cascade reservoir upstream TGD	1992-2009	In the Middle Yangtze River near Yichang, 1700km to the river mouth	Main functions of TGD are the generation of power, prevention of flood and enhancement of navigation ability. It is the key project for improvement and development of Yangtze River. TGP began the construction in 1992. The water impoundment has been started since 2003. The dam is 185m high, and has a reservoir 600km long with a total storage capacity approaching 40×10^9 m^3. The project is expected to have a total installed hydroelectric capacity exceeding 22000 MWe.	Water discharge flows into the sea didn't have obvious changes. (this study and Zhou et al., 2008) Sediment loads decreased significantly after TGD. It trapped about 172 Mt/yr of sediment from 2003 to 2008. (Hu et al., 2009). The sediment discharge of Yangtze River will decrease to less than 90 Mt/yr (18% of that in the 1950s) in the coming decades when taking the TGD and proposed cascade reservoir into account. (Hu et al., 2009)

Table 1-1(cont.) List of large projects that have influences for Yangtze Estuary

Name	Period	Place	Description	Influences
Water Diversion Projects in Yangtze River (WDP)	1990-2007	In lower Yangtze River reach (from Datong to the estuary, 640km long)	This is a series project which aims to meet the demand of drinking and industry water in Yangtze River Delta by pumping and diverting water from Yangtze River. 64 water diversion projects have been implemented from Datong to the estuary till 2000. The Phase III aims to diverse 2.18×10^6 m³ Water per day.	Water discharge decreases, especially in dry season. Sediment transportation capability also reduces.
Deep Waterway Regulation Project (DWRP) at the Yangtze Estuary	1998~	At the North Passage (NP) of Yangtze Estuary	DWRP was planned to build very long dikes and groins to deepen the navigation channel in North Passage at Yangtze Estuary. It contains three construction phases. Phase I started in 1998 and finished in 2000. Channel depth is dredged to 8.5m. Phase II started in 2002 and finished in 2006. Channel depth is dredged to 10.0m. The phase III is now under construction. The planned channel depth is 12.5m.	The hydrodynamic conditions changes at the estuary area.
Reclamation	1958~	In the North and South branch of Yangtze River; In the Chongming Island and other shoals; and In the lakes at middle and lower Yangtze River Basin	From 1958 to 1998, much reclamation has been done in the north and south branches, most of them are under 0 m bathymetry level. From 1960s, much reclamation has been done on Chongming Island, which increases its area from 608km^2 to 1086km^2. New technology enhances the reclamation ability to area under -5 m bathymetry level.	Increase the land area for use; The volume in north branch has reduced 56% which increases the saltwater intrusion; sediment erosion; Lakes decrease
Sand mining	1970~	Middle and lower reach of Yangtze River	Since 1990s there are 33 sand mining locations. The annual sand mining amount approaching 53 million tons. In 2004, China has been lifted a ban to constrict the sand mining in Yangtze River.	Pose a threat to flood prevention, shipping safety and dike safety. Sediment load decreases.

1.4 Goal

The hydrodynamic conditions of Yangtze River and its estuary area have been serious influenced by many human activities in the past few decades. This situation may persist and more serious in the coming next few decades. In addition, global climate change is developing. River delta is one the high impact areas by the natural forces. The research goal of this study is therefore designed to understand the morphological response to these variations at Yangtze Estuary, based on various unknown scenarios and known project plans.

For the studies of morphological evolution under unknown scenarios, the projections of water discharge in Yangtze River and sea level rise at the river estuary will be assumed as the future conditions. For the known influences, morphological evolution at Yangtze Estuary before and after the Deep Waterway Regulation Project (DWRP) will be studied. The third phase of this project is still under construction, results on the possible area of erosion or deposition at the project area can provide valid information for the management works. Differences between the simulated morphology at different years can be used to estimate the dredging volume in order to maintain a constant depth of the navigation channel.

Yangtze delta, the great important area to the Chinese economy, is nowadays a good example of the modern morphological evolution of estuaries by the high impacts from human activities and natural environmental changes. This study on morphological changes at Yangtze Estuary is of great importance to ecosystem, economics, and environmental management and, therefore, can receive considerable attention.

1.5 Research approaches

Research on the estuarine processes can be based on the field observations or laboratory scale modeling. The evolution of morphology induced by the human activities or natural impacts will not be clear until few decades or even hundred years. The measurements from the fields are difficult to be implemented continuously and widely in temporal and spatial domains in order to realize the large-scale hydrodynamic conditions and sediment transport systems. On the other hand, the laboratory research has been essentially used as design and verification tools for understanding complex estuarine processes, despite its high cost of construction, maintenance, and operation. Nowadays, numerical modeling of morphodynamics has attracted many research studies by its reasonable, efficient and economical reasons, and is adopted in this study.

The river estuary has complex forms and processes. Analyzing and predicting detailed morphological changes in such areas requires the use of an advanced, process-based morphodynamic model. The third generation morphodynamic numerical model (TIMOR 3) is used in this study. It was developed and improved at the Institute of Hydraulics and Water Resources at the Technical University of Darmstadt. It consists of Hydrodynamic Module, Sediment Transport Module, Morphodynamic Module, and Wave Module. Many studies have been applied TIMOR and have reasonable results for river or estuary morphology simulations (Zanke and Mewis, 2002; Witting, 2004; Witting and Zanke, 2004; Wurpts, 2006).

Since the field data is not easy to discover the long-term and spatial variations of the physical process, it plays the critical role for correct simulation by numerical models. Field data collected in this study will be used to calibrate the model parameters and validate the model results (Chapter 3). In additional, field data are used to study the characteristics of water and sediment discharges of Yangtze as well as the other hydrodynamic properties (Chapter 2). Calibrated TIMOR 3 is applied to study the hydrodynamic and morphological changes influenced by human activities. Most focus is on the influences of the regulation works at Yangtze Estuary (Chapter 4). Studies on the morphological response of sea level rise and the joint effect with typical water discharges is carried out in Chapter 5.

Most of the previous studies focus on the hydrodynamic changes at Yangtze Estuary (Zhu et al., 2001; Hu et al., 2009; Zhou et al., 2009; Gao et al., 2010). This study attempts to work not only on the hydrodynamic but also the morphological simulation for the entire Yangtze Estuary area considering flows, sediments, currents and winds simultaneously. It is an exploratory research for further studies.

CHAPTER 2

HYDRODYNAMIC CONDITIONS AT YANGTZE ESTUARY AND ITS HISTORICAL EVOLUTION ON MORPHOLOGY

2.1 The field data

Field measurement is always very important for getting direct understanding of the investigated objectives. There are many ways to examine the motions of flow and sediment in the estuary domain, like monitoring system, modern measurement technologies, physical model, and numerical model. No matter of which method, the field data, even though consuming time, man power and finance, is necessary and crucial.

In the Yangtze Estuary, where suffers from lots of influence factors like tide, wind, waves and the flow and sediment from upstream, it is of vital importance to have the long-term and short-term field data. The observed long-term variations of the hydrological factors and the time-series changes provide essential initial and boundary conditions as well as verification data for physical and numerical models, thus making these models more powerful and reliable. The modeled results help together with the field data to understand the physics of estuary more, which is at the end, benefit people economically and socially.

Regular field measurements in Yangtze River Basin are conducted by several governmental institutes, such as the Bureau of Hydrology (BOH) of the Changjiang Water Resources Commission (CWRC) takes charge of the basin scale monitoring on hydrology, water quality, sediment and river channel topography. Some other local institutes or universities also make many short-term measurements for research- or project- oriented purposes. Measurement carried out by boat in Yangtze River is efficient, while measurement at a fix location obtains long-term field data. There are more than 100 hydrological stations in the whole Yangtze River Basin; however few of them are systematic and long-term measurements.

Datong station, 640 km far from the river mouth, established by BOH, is one of the important hydrological stations in Yangtze River. Location of Datong station is shown in Figure 2-1. Datong is the only one long-term station at the lower reach of Yangtze River. Datong is also the upper boundary of tidal water influences. It has 170×10^4 km^2 catchment area, equal to 94.7% of the total Yangtze River basin. Since there are still tributaries flowing into Yangtze River at the downstream region of Datong, however they occupy only 1.2% of the total water discharge (Li, 2007). In this study, monthly data of water discharge, sediment discharge, surface suspended sediment concentration (SSC) and the median particle diameter (d_{50}) measured at Datong station from 1950 to 2008 are collected.

In addition to Datong station, there are another several hundred water level stations established in the Yangtze River Basin. Data from eight water level stations locate at the estuary area are used in this study. Station locations are shown in Figure 2-1. Each station represents different nature characteristics. For example, Xuliujing Station (WL1) which locates at the bifurcated node of south-north branches is dynamical dominated by runoff. The tidal influence at Xuliujing is weaker than the runoff influence. It locates at 180 km far away from the mouth. The width of Yangtze River at Xuliujing station is 5.7 km. The other station, Hengsha (WL6) is selected by its location at the mixing area of fresh water and salt water. It is at the river mouth, which is highly influenced by wind. Hourly water levels are obtained from these stations. In this study, data in Feb./Mar. and Sep./Oct. in 2002 are collected. They are used for calibration and validation of numerical models in chapter 3 as well as the statistical analysis in this chapter. In Figure 2-1, the Profile Station (PS) means the locations of profile measurements. Some of them use the ship-board ADCP. Most of them use artificial operation of the current or relative meters. Flow velocity and direction profiles are obtained at these sites. In some sites, surface sediment concentration (SSC) and salt concentration are also collected. Table 2-1 summaries the field data used in this study.

Table 2-1 Description of the field stations

Category	Station Name (abbrev.)	Data contents	Data duration/type	Remark
Hydrological Station	Datong	water discharge sediment discharge SSC[1] d_{50}[2]	1950-2008 / monthly data	
Water level station	WL1 (Xuliujing) WL2 (Chongtou) WL3 (Yanglin) WL4 (Baozhen) WL5 (Gaoqiao) WL6 (Hengsha) WL7 (Zhongjun) WL8 (Lianxinggang)	Water level	Dry season: 2/22-3/22, 2002 Wet season: 9/1-9/30, 2002 / hourly data	
Profile Measurement Section or Station	PS1[3] (near Xuliujing)、PS2(near Baimaogang)、PS3、PS4 (cross Baimaosha)、PS5、PS6 (cross Changxingdao)、PS7、PS8[3]、PS9、PS10	Flow velocity and direction profile; SSC[1] salt concentration	Dry season: 2/22-3/22, 2002 Wet season: 9/1-9/30, 2002 / hourly data	PS1(X1~X3)、PS2(Y1~Y3)、PS3(Z3)、PS4(Y4~Y6)、PS5(Z4)、PS6(Y7~Y12) PS7(WL7)、PS8(WL6)、PS9(Z6~Z9)、PS10(Z1~Z2)
others	SS[3] (Sheshan)	SSC[1]	1998/8~2001/7 /monthly data	

[1] SSC: surface suspended sediment concentration

[2] d_{50}: median particle diameter

[3] The stations have monthly SSC data from 1998/8 to 2001/7

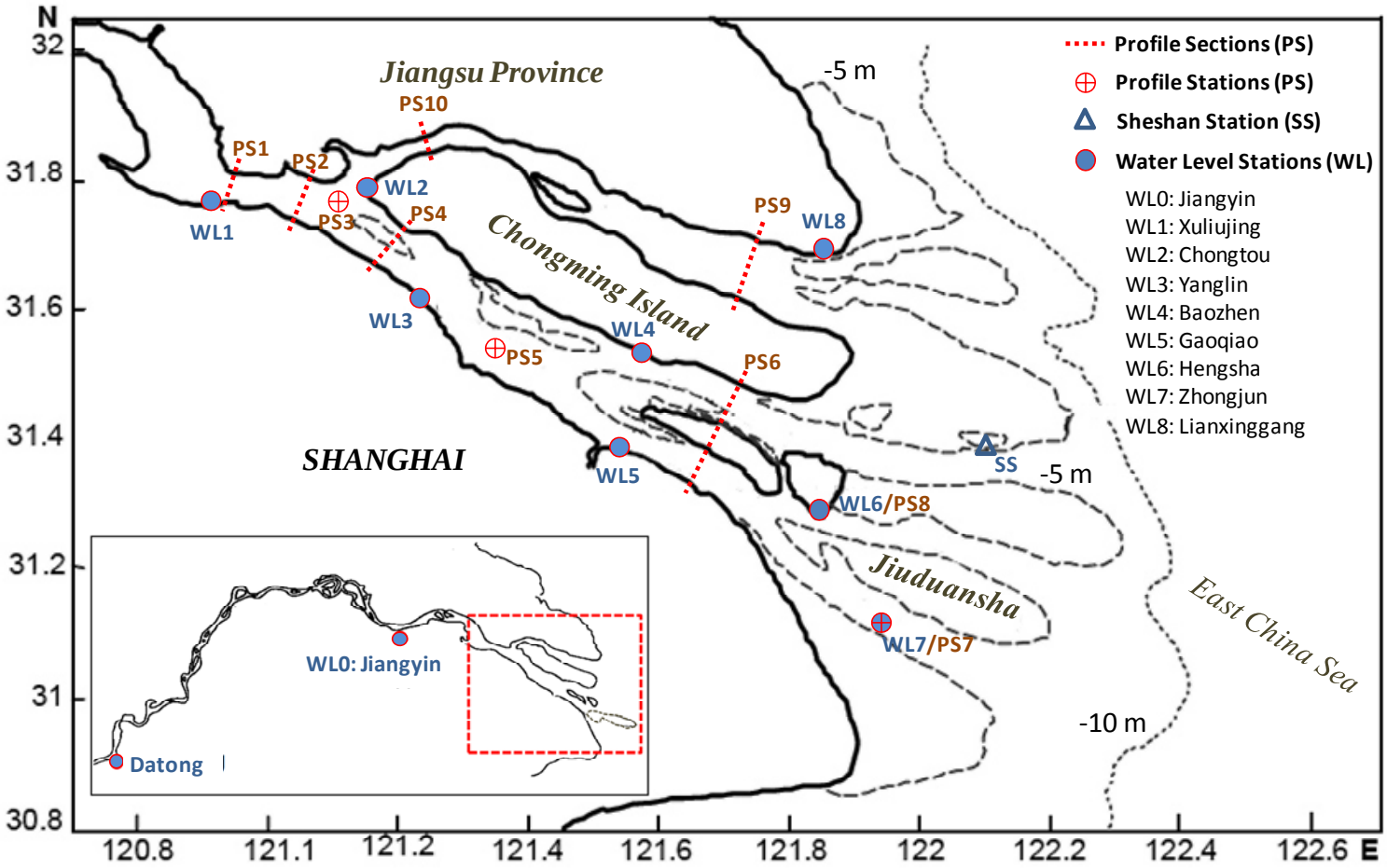

Figure 2-1 Location of the field stations

2.2 Hydrodynamic and sediment conditions

Yangtze Estuary is famous for its large runoff and high suspended sediment concentration. Yangtze delta is the area having medium tidal range. The spatial-temporal change of runoff and tidal current is the main factor for the morphological changes of Yangtze Estuary. It is necessary to understand the hydrodynamic and sediment conditions at Yangtze Estuary before studying its morphological evolution.

Runoff

Table 2-2 shows the monthly discharge and runoff at Datong station from 1950 to 2006. The average monthly discharge is 28419m^3/s. It is 40128m^3/s for the wet season (May to October) and 16710m^3/s for the dry season (November to April). For the runoff, the average monthly runoff is $750\times10^8 m^3$. The total runoff of Yangtze River flowing into East China Sea in one year is $8994\times10^8 m^3$. In the past few decades, the max monthly discharge was recorded as 92600m^3/s that occurred in August 1954. The min monthly discharge was recorded as 4620m^3/s that occurred in January 1979. The runoff distribution of Yangtze River is unsteady in a year. The wet season occupies 70.9% of runoff; the dry season occupies 29.1%. The max monthly runoff always happens in July as well as the min runoff happens in February.

Table 2-2 Statistics of monthly water discharge and runoff
(Data from Datong Station, 1950-2006)

		Average water discharge (m^3/s)	Average runoff ($\times10^8$ m^3)	Average water discharge (m^3/s)	Total runoff ($\times10^8$ m^3)
Dry season	Nov	22913	594	16710	2615 (29.1%)
	Dec	14218	381		
	Jan	11103 (min)	297		
	Feb	11899	288 (min)		
	Mar	16189	434		
	Apr	23940	621		
Wet season	May	33728	903	40128	6379 (70.9%)
	Jun	40237	1043		
	Jul	50033 (max)	1340 (max)		
	Aug	43748	1172		
	Sep	40058	1038		
	Oct	32964	883		
	Monthly	28419	750		
	Annual	341030	8994 (100%)		

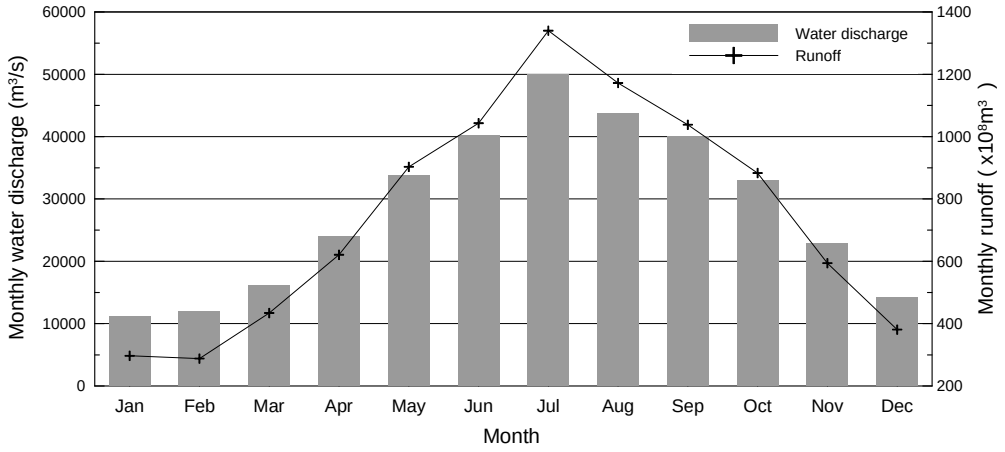

Figure 2-2 Monthly discharge and runoff of Yangtze River
(Statistics from the data of Datong Station from 1950-2006)

Tide and tidal current

The Yangtze River Estuary is the estuary of medium intensity tide. Due to the effects of estuarine shape, river discharge, bottom and bank friction etc., the tidal condition is complex at Yangtze River Estuary. The tidal range of the South Branch is reduced upstream from the mouth because of the gradual change of its width and depth. Since the channel of the North Branch is trumpet-shaped, the tidal range is larger than that of the South Branch. The statistics at Zhongjun Station (WL7 in Figure 2-1) shows that the average tidal range is 2.66m, maximum is 4.62m and minimum is 0.17m (Zheng, 2002). This area is influenced by two tidal systems. One is the rotating tidal system drove from Yellow Sea; the other one is the progressive tidal system drove from East China Sea. It is mainly the progressive tide inside the river channel. The tidal limit is about 640km from the river mouth; the tidal current limit is about 240 km from the river mouth.

The tidal ranges at various locations of Yangtze Estuary are shown in Table 2-3 (Li, 2008; Yu and Tian, 2003). The mean tidal ranges changes from 2.66m at Zhongjun (WL7) to 1.64 m at Jiangyin (WL0). At Nanjing where locates around 400km to river mouth, the mean tidal range is still 0.52 m. Datong is the boundary of tidal influence for Yangtze River in the dry season.

In South Channel and North Channel, the tidal current is a kind of to-and-fro flow. The velocity of ebb current is larger than that of flood current. During spring tide, the average velocity of tidal current during ebb tide period is around 1.0~1.2 m/s. The maximum velocity can reach 1.5~2.2 m/s (Gao, 2008). In South Passage and North Passage, the tidal current transfers from to-and-fro to rotary flow with clockwise. The tidal currents are clockwise flow outside the estuary.

Table 2-3 Tidal ranges at Yangtze Estuary

Location	Datong	Nanjing	Jiangyin (WL0)	Xuliujing (WL1)	Gaoqiao (WL5)	Zhongjun (WL7)
Distance to river mouth	640 km	400 km	240 km	180 km	80 km	0 km
Max tidal range (m)	0	0.69	3.39	4.49	4.66	4.62
Mean tidal range (m)	0	0.52	1.64	2.03	2.36	2.66

Wind

The wind systems that influence Yangtze Estuary are from the winter storm and summer typhoon. The prevailing wind direction is coming from SE-ESE. Strong wind is coming from direction NW~NNW that happens frequently in January and December (Dou, 2003). Mu et al. (2006) analyzed the in-situ wind data measured at the offshore station Yinshuichuan (121°34′ E, 31°19′ N) and used a high resolution model to simulate the wind field for the whole Yangtze Estuary area in order to assess wind energy. They found the average wind speed at Yangtze Estuary is around 4~6 m/s. In addition, several storms hit Yangtze Estuary annually (both tropical cyclones and cold fronts), with about 13% of storms having wind speeds greater than 25 m/s. However mean wind speed more than 30m/s has ever happened during the typhoon Paibian in 2000 (Yang et al., 2003). This is the result based on the statistics of Yinshuichuan station.

Waves

Wind-induced waves dominate the sea state at Yangtze Estuary area, which occupies 77%. Swell takes about 23%. Due to the effect of topography at the estuary, the wave height is decreasing and the wave period is shortening when it's propagating into the channels. The average significant wave heights (periods) at offshore station Yinshuichuan (121°34′ E, 31°19′ N) and inner estuary Gaoqiao station (WL 5 in Figure 2-1) are 0.9 m (3.7 s) and 0.35 m (2.4 s), respectively. The maximum wave height and wave period were 6.2 m (8.0 s) and 3.2 m (4.5 s) at the two stations (Liu, 2008). Hu et al. (2003) applied SWAN model to simulate waves induced by two typhoons for the waters around Yangtze Estuary. The simulated results show the max significant wave height is approaching 10 m for the offshore area however the field measurement at deep sea buoy is 8 m. Yan et al (2006) compared WAVEWATCH and SWAN models in terms of forecasting wave conditions in East China Sea. Dou (2003) presented the maximum wave period is 12 s in Sheshan (SS in Figure 2-1) and 4.5 s in Gaoqiao respectively.

At Yangtze Estuary area, the dominant wave direction is generally consistent with the wind direction. Waves are mainly coming from NW in winter and SSE in summer (Liu, 2008). For typhoon waves, the directions highly depend on the typhoon tracks.

Salinity

Salinity is the saltiness or dissolved salt content of a body of water. It has been traditional to express salinity not as percent, but as parts per thousand (‰). The salinities of world's oceans are from 30 ‰ to 35 ‰. Due to huge runoff flowing into the sea, the estuary waters of Yangtze River has lower salinity than the open sea. The salinity is around 30 ‰ offshore Yangtze Estuary. The isoline of salinity 30 ‰ reaches 125°E (300 km offshore the river mouth) in wet season and 122°30'E (50 km offshore the river mouth) in dry season (Liu, 2008). The salinity distribution at Yangtze Estuary is not uniform in temporal and spatial domains. Generally, the salinity is higher in the open sea than in the river estuary, as well as higher salinity at deep layer than at shallow layer of the water column.

Gao (2008) presented the salinity measured in North Passage where the DWRP project is developing varies from less than 5 ‰ to 15 ‰. From the field data collected in Liu (2008), the salinity is highest in Feb. (the dry season). It is around 20.9 ‰ at the river mouth (Station Yinshuichuan, near WL7). The salinity is lowest 8.85 ‰ at the same location in Jul. The average salinity has good negative correlation to the monthly water discharge.

As mentioned, the distribution of the salinity is very complex due to the joint effects of runoff (dry and wet season), tide (spring, mean and neap tide) and the topography. In general, the North Branch has most serious salt water intrusion problem (Liu, 2008) because of its low river runoff. During the spring tide in dry season, the salt water intruding into NB may flow into SB. Due to the salinity gradient, a gravitational circulation with a net flow to the sea at the surface and a net flow in landward direction at the bottom is formed. It may result the net landward sediment transport due to the fact producing high sediment concentration in deep layer of the water. At the force balance location of the landward sea water and downstream fresh water, the turbidity is always very high. In this area there is high sediment concentration with high siltation due to the effect of clay flocculation.

Sediment

Yangtze River has abundant sediment, which comes from both river and sea. Based on the statistic of data at Datong Station, the average of annual sediment discharge is 408. 09 Mt/yr, in which 90% of them are suspended load. The average sediment concentration is 0.361kg/m^3. The sediment transport has similar characteristics to the river runoff. Sediment discharge in wet season accounts for 87.4% of the total quantity. Outside the estuary at the west of 10m isobathic line, the sediment concentration is about 0.4 kg/m^3 however at the east is 0.1 kg/m^3 where is controlled by the tidal flow.

It has almost zero sediment load at the stream of North Branch because of its negative net runoff. The sediment load between North Channel and South Channel is about 1:1; the same as North Passage and South passage. Sediment concentration is influenced by tide propagation and in proportion with the current velocity. The maximum sediment concentration occurs when the maximum velocity occurs during ebb and flood tide. The minimum value occurs when the tidal current velocity is low. For a vertical water column, the

maximum sediment concentration occurs near the bottom, decreasing from the bottom to the water surface.

The d_{50} of suspended load in Yangtze Estuary varies from 0.0065 to 0.0301 mm. The median d_{50} is about 0.0086. The particle size of suspended load in South Passage is the largest, in North Passage the second and in North Channel the third. Contrarily, the particle size of bed load in North Channel is the largest, and in South Passage the smallest. Due to the salt water intrusion, suspended load is easy to be flocculated. According to the field survey Gao (2008), the d_{50} of bed load is 0.0325 mm in South Branch. 0.0079-0.0685 mm in North Channel; 0.0232-0.0677 in South Channel; 0.0063-0.0159 mm in North Passage and 0.0076-0.0148 mm in South Passage as shown in Table 2-5. This means that the South Passage has more favorable conditions for sediment flocculation and deposition than the other channels. The values in Table 2-5 have large variation. It depends to the measurement locations. During a typhoon or winter storm, the sediment in the shoal area is stirred up and transported by current to the channel area.

Wash load is the portion of sediment that is carried by the river flow, such that it always remains near the free surface. In Yangtze Estuary when fresh water flows to contact with salt water, wash load is easy to be flocculated. The settling velocity increases. When it reaches the river bed, it becomes part of the bed load.

Table 2-4 Statistics of monthly sediment concentration and discharge
(Data from Datong Station, 1950-2006)

		Average sediment concentration (kg/m^3)	Average sediment discharge ($\times 10^4$ m^3)	Average sediment concentration (kg/m^3)	Total sediment discharge ($\times 10^9$ m^3)
Dry season	Nov	0.293	1742.0	0.177	5153 (12.6%)
	Dec	0.174	664.8		
	Jan	0.103	305.9		
	Feb	0.102	293.4		
	Mar	0.153	663.7		
	Apr	0.239	1483.5		
Wet season	May	0.339	3050.5	0.545	35656 (87.4%)
	Jun	0.402	4176.9		
	Jul	0.705	9458.0		
	Aug	0.672	7840.7		
	Sep	0.656	6785.7		
	Oct	0.493	4344.0		
	Monthly	0.361	3400		
	Annual	341030	40809 (100%)		

Table 2-5 Bed Load size distribution in Yangtze Estuary

d_{50} (mm)	North Branch	North Channel	North Passage
	0.093*	0.0079-0.0685	0.0063-0.0159
d_{50} (mm)	South Branch	South Channel	South passage
	0.0325	0.0232-0.0677	0.0076-0.0148

*data from Liu (2008); the other data are from Gao (2008)

2.3 Field data statistics

2.3.1 Long-term trend

Variations of water and sediment

Since 1950s, the total water discharge of Yangtze River that flowing into the East China Sea has no obvious changes although the establishment of TGD. Zhou (2008) applied statistical test to proof the conclusion. Figure 2-3 shows the time series of annual water discharge and runoff. The data are from Datong Station. We find the discharge has mild decrease since 2002. However, it starts to increase again in 2007. This is just due to climate scenario of the time such as 2006 is an extreme dry year. Tong et al. (2008) used wavelet analysis to study the water discharge records in the past 50 years. He found the water discharge of Yangtze River has the repeat circles every 2, 3, 5, 7, 15 and 23 years.

The variation of sediment of a river can be evaluated by two aspects, i.e. its concentration and discharge, and the grain size. Figure 2-4 shows the variations of sediment concentration and sediment discharge from 1951 to 2008. It shows that the variations can be divided to three phases. The first phase is from 1950 to 1985. The sediment concentration and discharge are nearly constant in this phase. From 1986 to 2002, it is the second phase. The sediment concentration and discharges began to decrease in the second phase. TGD was operated in 2003. After 2003 is the third phase. The decreasing rates of sediment concentration and discharge increase. The effect of the dam construction to intercept the sediment transportation from upstream to downstream is obvious from the time series. Zhou (2008) verified this conclusion. The average sediment discharge drops from 471 Mt/yr (1950~1985) to 346 Mt/yr (1986~2002) and finally to 226 Mt/yr (2003~2008). We find the variation of water discharges is less than that of sediment discharges in the past 50 years at Yangtze River.

Figure 2-5 shows the time series of the grain size of suspended load and bed load at Datong Station (reanalyzed from Chen et al., 2007). The grain size of bed-load size is increasing. However, there is no significant change for the grain size of suspended load in the past 30 years.

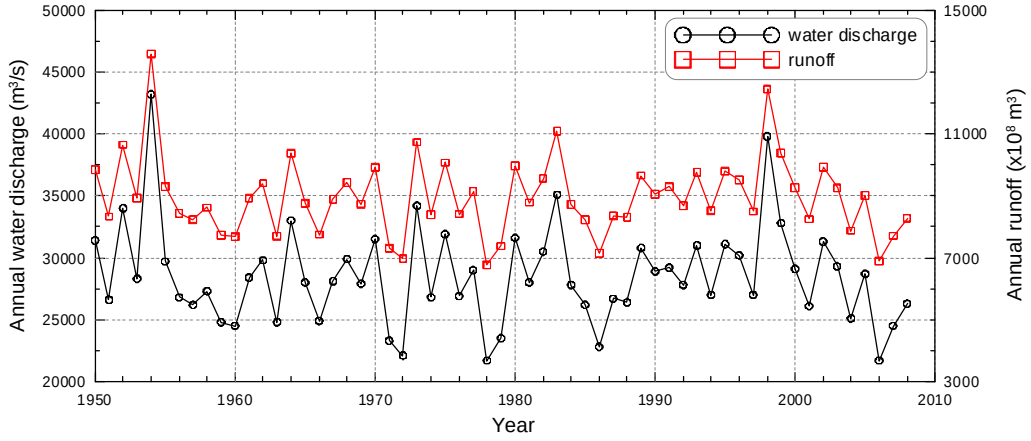

Figure 2-3 Annual water discharge and runoff (Data from Datong Station)

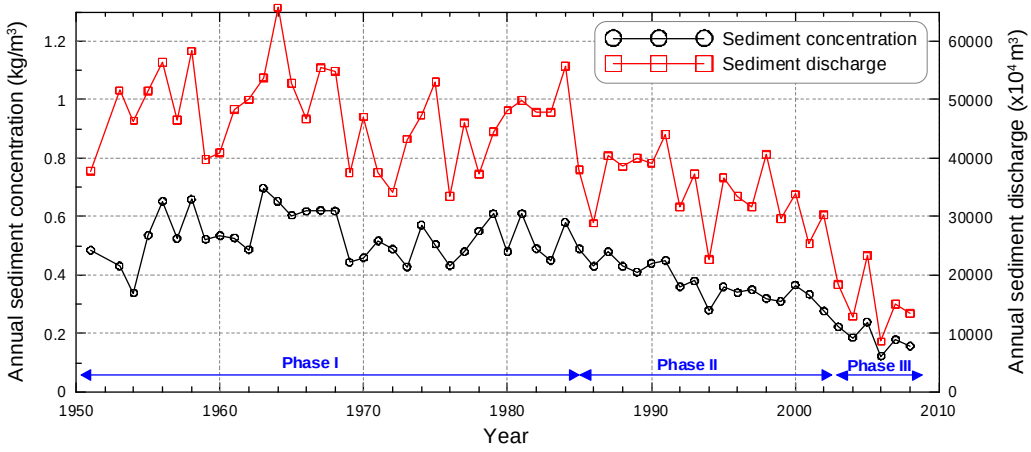

Figure 2-4 Annual sediment concentration and sediment discharge (Data from Datong Station)

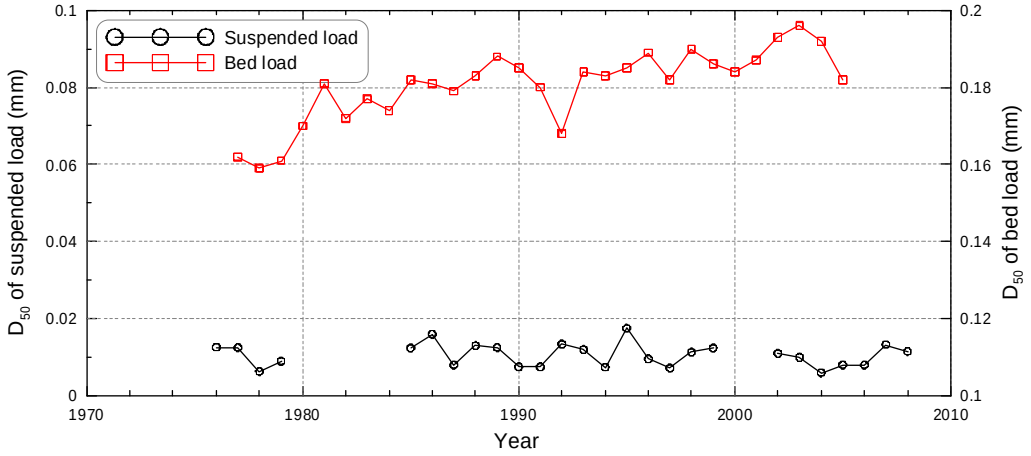

Figure 2-5 Variation of suspended load size and bed load size (Data from Datong Station)

Monthly variation

Figure 2-6 shows the changes of the monthly water discharges before and after the TGD operated in 2003. The distribution of the monthly discharge has been changed after the dam operated. The water discharge increases in dry season especially from December to March as well as it decreases in wet season especially in July. This result identifies the anticipated benefit of TGD which improves the flood protection on the middle and lower reaches of the Yangtze River. Historically, people living along the Yangtze River have suffered tremendous losses from flooding. In 1931, 145,000 people drowned, and over 300,000 hectares of agricultural land flooded. In 1954, 30,000 more died in Yangtze floods or the subsequent diseases. In 1998, a flood in the same area caused billions of dollars of damage. More than 2000 km^2 of farm land was flooded, and over 1500 people were killed (CTGPC, 2002). From the result, TGD reduces the flood runoff but infuse the water to the river in dry season. This also maintains the consistency of the river runoff in a year.

After the implementation of WSCP since 1989 and TGD since 2003, the sediment discharges of Yangtze River are obvious decreasing. They blocked the sediments at upstream. In addition, the implementation of SNWD which started since 2002 has influenced the water discharges, especially from the east route sub-project. It has reduced the transport capability for suspended load. However by the operation of the TGD dam, the water discharge may hold the same amount which has been preliminary verified in the measurement data (Figure 2-3). Due to the reduction of sediment, this may lead to erosion in the river or at the estuary area.

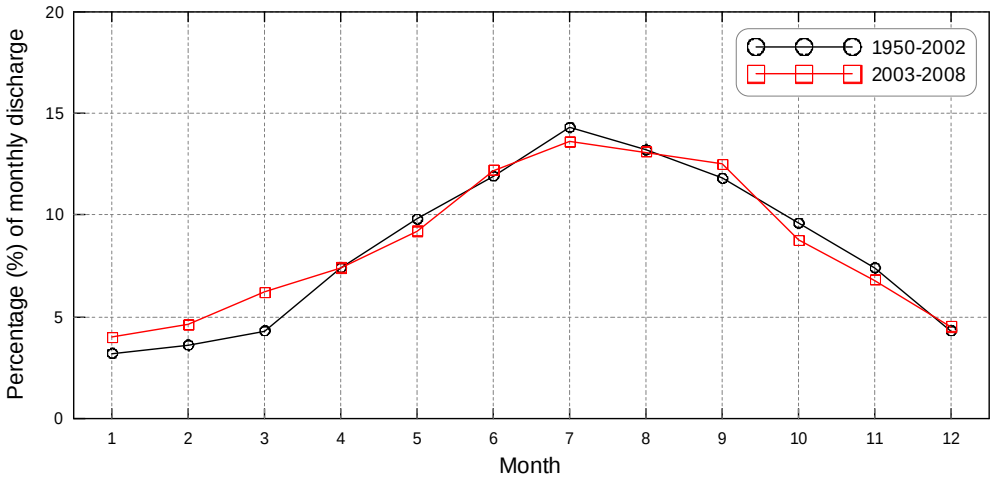

Figure 2-6 Changes of the monthly discharge after TGD operated with respect to that before

2.3.2 Variations in the estuary area

Tidal motion

From Hu et al. (2000)'s results, there exist regular semi-diurnal tides out of the river mouth,

and irregular semi-diurnal tides inside the river channel. Two tidal waves systems exist in the region. One is the travelling tidal wave system of the East China Sea including semi-diurnal tides, M_2, S_2, K_2 and N_2. The other is a rotary tidal wave system of the Yellow Sea including diurnal tides, K_1 and O_1. The energy of the travelling tidal wave system (semi-diurnal tides) mainly comes from the northeast of the outer sea, and the energy of the rotary tidal wave system (diurnal tides) enter this sea area from the direction of NE. The semi-diurnal tides of M_2 and S_2 are the largest ones within the constituents. The diurnal tide of K_1 is a little larger than that of K_2 or N_2 and O_1 is a little smaller (Hu et al., 2000). The duration of the M_2 semidiurnal tide is a 12.4-hour period. Near the Yangtze mouth M_2 travels as a progressive wave due to its convergent character, whose amplitude decreases and phase grows upstream. Tide wave propagation along the channel makes the wave to be laterally compressed by river shores; however, friction exceeds convergence and causes tide height to decrease along the channel.

Figure 2-7 and Figure 2-8 show the propagation of the tidal waters during dry and wet seasons, respectively. The data are from station WL1, WL3, WL5 and WL7 as shown in Figure 2-1. Their locations are from river mouth (WL7) to river channel (WL1). From the results, we find the tidal shape is distorted. This is also mentioned by Gao (2008). We also find the duration of ebb-tide is longer than it during flood tide period either in dry season or wet season. In addition, the duration of flood tide gradually shortens and that of ebb tide gradually increase when the tidal water propagates from river mouth into the river channel. The tidal range decreases during the propagation. There is a time lag between different locations. The time lag of the max water level between the river mouth (WL7) with inner channel (WL1) is around 3 hours. The distance between the two stations is around 180 km, representing the tidal wave (a kind of long-wave) propagation speed during flooding tide period is around 60 km/hr (16.7 m/s). We find the speed is constant in flood and dry seasons. However the decrease of tidal range in dry season (0.6 m) is less than it in wet season (1.0 m).

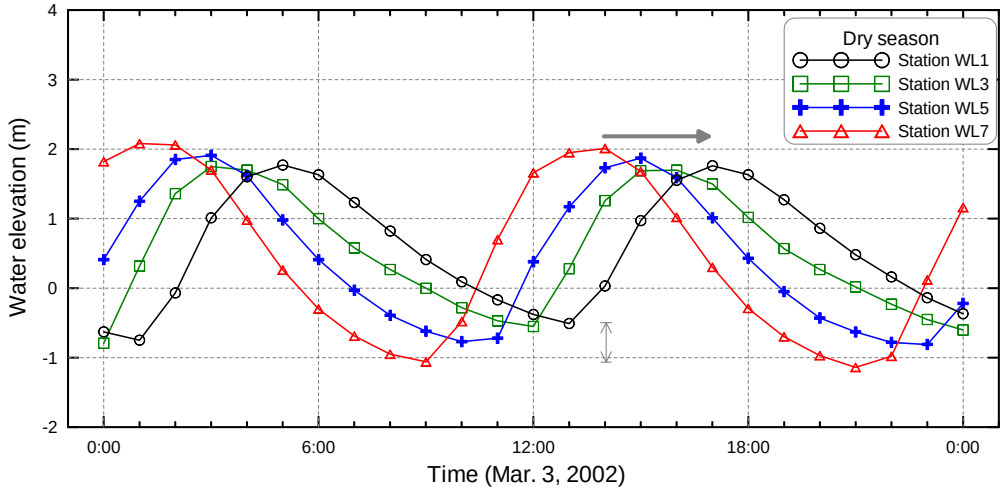

Figure 2-7 Tidal wave propagation upstream in dry season demonstrated by the tidal current at different stations

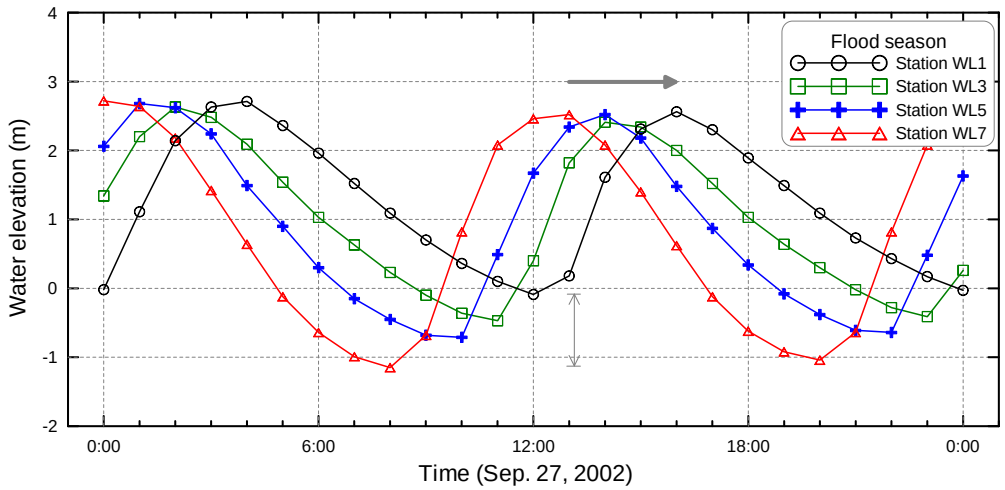

Figure 2-8 Tidal water propagation upstream in wet season demonstrated by the tidal current at different stations

Flow velocity and direction

There are two flows at the Yangtze Estuary area. One is the river flow; the other one is the flow of tidal current. The river flow velocity is influenced by many factors such as the channel morphology, sediment transport, water depth and so on. Chen et al. (2007) measured the flow velocity along the Yangtze River. He found the average flow velocity of the lower Yangtze ranged from 1.4 m/s to 1.8 m/s. Unfortunately, they didn't make the measurements for the estuary area. Interaction of the river runoff and tidal motion dominate the flow condition at Yangtze Estuary. The influence of the tidal current can reach Jiangyin (WL0), 240 km to the river mouth. Yangtze Estuary is a partial mixed estuary, the mixture of salt-water and fresh-water changes water density producing the baroclinic effect of density. The baroclinic effect of density accelerates the flow velocity of flood tide, but reduces the flow velocity of ebb tide. It makes the distribution of flow velocity in the estuary more complicate. Due to the difference of the salinity at upper and lower layers of the water column, the vertical circulation also exists at Yangtze Estuary. Except the salt-water intrusion and topography transformation, Ippen (1968) said that the Coriolis forces and the centrifugal forces inducing transverse fluid motion due to rotation of the earth and due to the curvature of the estuary channel. Yu (2006) studied the velocity distributions of Yangtze Estuary which induced by the Coriolis forces based on both surveyed data and numerical model calculation. Horizontal and transversal circulations were found at the river estuary reach. Hu et al. (2000) used a 2D numerical model to simulate the current field for Yangtze Estuary. They applied advanced numerical schemes to improve the correctness of the current simulation. The to-and-fro current and rotary current were found in the estuary area. The rotary current exists in the outer sea and its direction is most clockwise by the effect of the Coriolis force. Near the river mouth, the rotary current is gradually transformed to the to-and-fro current by the restrictions of water depth, islands, coasts and channels.

Figure 2-9 and Figure 2-10 show the max average flow velocities within the flood and dry

seasons, respectively. Figures for flooding tide and ebb tide are plotted separately. Measurements for wet season were done on Feb. 22 to Mar. 8, 2002. It was on Sep. 22 to 30, 2002 for dry season measurements. To-and-fro currents are obvious found in the figures. From the limited data, we find the max average flow velocity is occurred near the bifurcate point of NB and SB (PS3 in Figure 2-1). The max average velocity is 2.49 m/s (Figure 2-9 left) occurred at flooding tide period within wet season. This is because of the salt water flowing from NB into SB. Figure 2-11 shows the current velocity profile at four locations, PS3, PS6, PS7 and PS9 (see Figure 2-1), from upstream to downstream and in the NB mouth. Variation of the current velocities at different water depths is up to 30% (PS3). At PS6, where in the narrow bifurcated channel, the flow velocity is accelerated and the difference at upper and lower layer of the water is large. At the river mouth, the differences of the flow velocities at the surface and bottom are 25% (PS7 at SP) and 20% (PS9 at NB). From Table 2-6, it is found that the average flow velocities measured at these four locations are from 1.17 m/s to 1.28 m/s (flood tide) and 1.51 m/s to 1.9 m/s (ebb tide) within dry season. Generally, the flow velocity in ebb tide period is higher than that in the flooding tide period. Besides, it has higher velocity within wet season than it within dry season, except the bifurcate point, PS3.

Table 2-6 The average flow velocity measured at some locations at Yangtze Estuary during spring tide period within dry season (The measurements were done on Mar. 1 and 2, 2002).

Unit: m/s

Station	PS3 (SB)	PS6 (SC)	PS7 (SP)	PS9 (NB)
Flood tide period	1.28 @2002.03.02 00:00	1.30 @2002.03.01 21:00	1.56 @2002.03.01 20:00	1.17 @2002.03.02 05:00
Ebb tide period	1.51 @2002.03.01 15:00	1.90 @2002.03.01 13:00	1.71 @2002.03.01 12:00	1.60 @2002.03.01 23:00

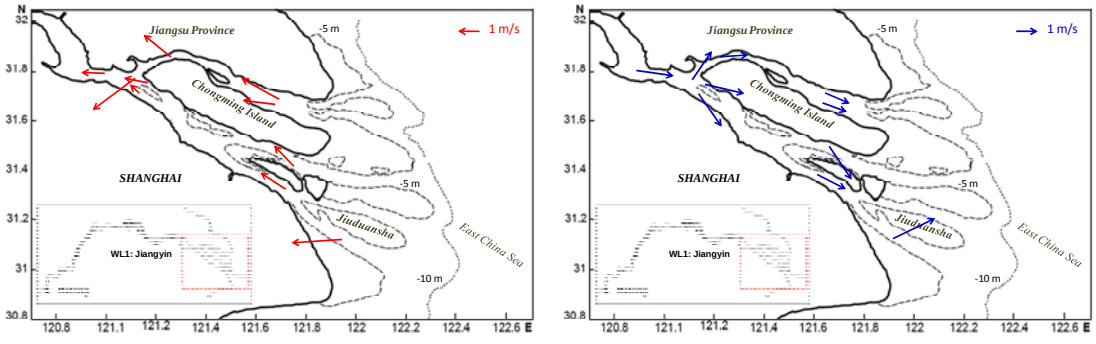

Figure 2-9 Maxima of the observed average flow velocities. (left) flooding tide period; (right) ebb tide period. Measurements were made in Sep. 2002 (wet season).

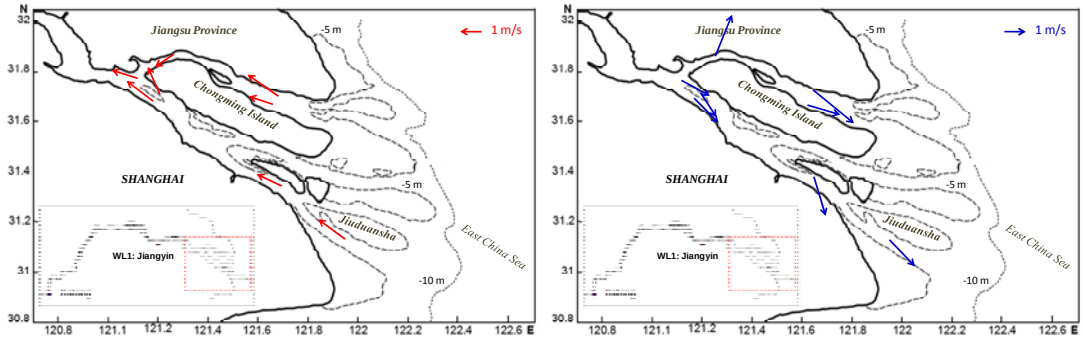

Figure 2-10 Maxima of the observed average flow velocities. (left) flooding tide period; (right) ebb tide period. Measurements were made in Mar. 2002. (dry season)

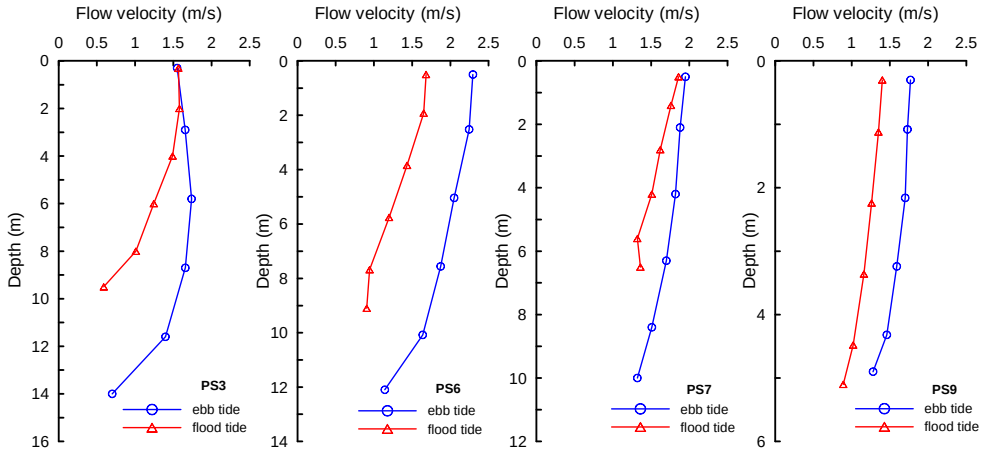

Figure 2-11 Flow velocity profiles at the time when max average flow velocity (in Fig. 2-10) occurs during the measurements (dry season); Measurement station see in Fig.2-1

Suspended Sediment Concentration (SSC)

Suspended sediment concentration (SSC) in river channel and estuary area is one of the most important hydrologic data in solving engineering problems ranging from hydraulic design, river restoration, to water quality improvement and coastal zone management. Understanding of characteristics of the suspended sediments at Yangtze Estuary is therefore essential in this study. The geomorphologic studies concerned with the development and changes of shoals or the maintenance of navigation channels require detailed information on sediment dynamics and in particular its spatial and temporal distribution. In Yangtze estuary, SSC varies significantly both in time and in space in response to freshwater discharge, tidal variability, and channel geometry. Many studies focus on the measurements of SSC, such as based on the acoustic instruments. (Holdaway et al., 1999; Gartner, 2004; Hoitink and Hoekstra, 2005; Bai et al., 2009). Studies on the SSC distribution or related problems are also very large amount especially from the Chinese scholars (Qing et al., 2003; Yang et al., 2002, 2003; Dou, 2003; Chen et al., 2003; Lu and Zheng, 2004; Han et al., 2006, Hu et al., 2009, Chen and Wang, 2008)

This study re-analyzes the data in Table 2.16 in Zhou (2008). The result is shown in Figure 2-12. They are the monthly SSC data measured at Xuliujing (PS1), Hengsha (PS8) and Sheshan Station (SS) from Aug 1998 to July 2001. The 36 months length SSC data are significant. Locations of three stations represent the inner channel (Xuliujing, PS1), sand bar area at river mouth (Hengsha, PS8) and outer river mouth (Sheshan station, SS), respectively. At PS1, river runoff is the main driving force for sediment movement. All of runoff, tidal flow and wave and their interactions are the factors to influence the SSC variation. From figure 2-12, we find the mean SSC is highest at the outer river mouth SS (0.4195 kg/m^3). At inner channel PS1, it is 0.1370 kg/m^3. Three times difference exists. This result shows high impact to the SSC is from the wave- or tidal- induced turbidity at outer river mouth. From further analysis, the suspended sediment in inner estuary shows higher concentration during wet season than during dry season while the result is reversed at the outer estuary. For the comparison of the SSC during different tide periods, all three locations have the same trends, i.e. SSC is higher during flood tide period than it during ebb tide period. Table 2-7 shows the quantitative results. The sediments from the Yangtze River are resuspended due to marine dynamic actions including tidal current and wind wave. The SSC show a neap-spring tidal cycle and seasonal fluctuations, temporally. The tidal current control the neap-spring tidal cycle, and the wind wave control the seasonal fluctuation (Cheng et al. 2004). They are which the two predominant factors controlling the SSC distribution at the Yangtze Estuary.

Figure 2-13 shows the SSC profiles at the time when max average flow velocity (in Fig.2-10) occurs. They are the results from the measurements in dry season. We find the SSC has small variations at river mouth stations, such as PS7 at SP and PS9 at NB. At the inner estuary stations, there are higher SSC near the river bed.

Table 2-7 Quantitative results of the SSC measurements (Unit: kg/m^3)

Station	Xuliujing (PS1)	Hengsha (PS8)	Sheshan Station (SS)
Wet season	0.1583	0.3382	0.3285
Dry season	0.1157	0.3752	0.5106
Flood tide period (all data period)	0.1465	0.3659	0.4593
Ebb tide period (all data period)	0.1343	0.3487	0.3840

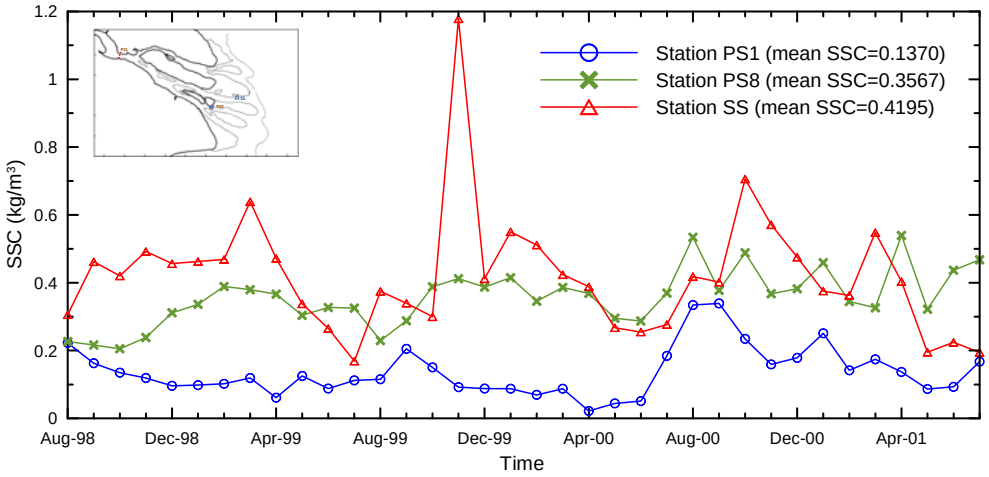

Figure 2-12 Distribution of the observed SSC from 1998 to 2001 (Unit: kg/m^3)

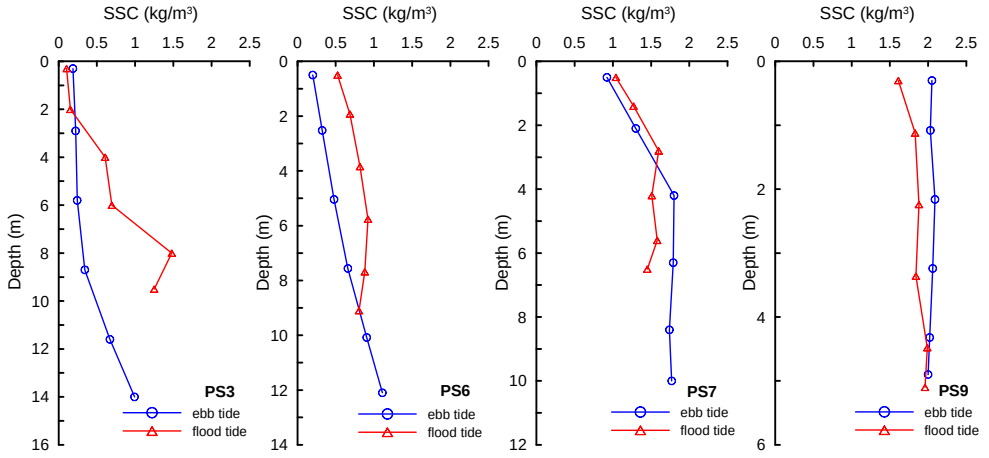

Figure 2-13 SSC profiles at the time when max average flow velocity (in Fig.2-10) occurs during the measurements (Dry season); Measurement station see in Fig.2-1

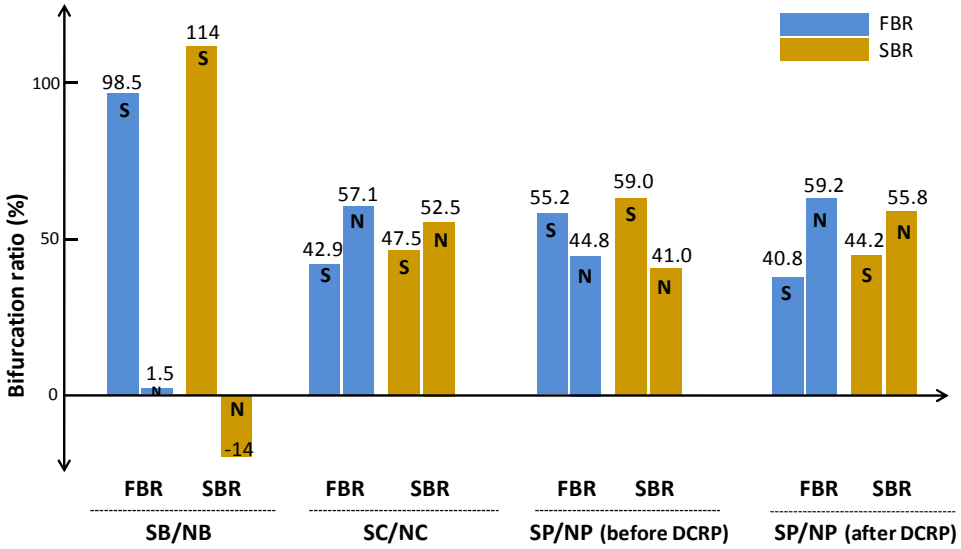

Figure 2-14 FBR and SBR at SB/NB, SC/NC and SP/NP

Flow bifurcation ratio (FBR) and sediment bifurcation ratio (SBR)

Flow bifurcation ratio (FBR) is the ratio of the net runoff flowing into different bifurcated channels. Similar definition is used for sediment bifurcation ratio (SBR). Due to the complexity of the morphology at the Yangtze Estuary, the ratios are significant for the morphological evolution. This study re-analyzes the FBR/SBR data from Zhou (2008). The data are obtained from non-continuous in-situ measurements from 1964 to 2002. Figure 2-14 shows the results of the ratios at SB/NB, SC/NC and SP/NP. For SP and NP cases, results of ratios before and after the DWRP are also compared. From Figure 2-14, an obvious fact is found. Both of the FBR and SBR of NB are very low, even the SBR is negative. It means most of the runoff from upstream flow into SB. The values in Figure 2-14 are the average results from several years' measurement including wet season and dry season. During dry season, serious intrusions of salt water and sediment from NB to SB occur. The ratios of FBR and SBR are not different too much for SC/NC. Generally, NC has higher capability for runoff and sediment transportations. At the river mouth, large percentage of the runoff and sediment move into SP. However, both of FBR and SBR increase about 15% at NP after the DCRP started in 1998. This is the result based on the investigation from 1998 to 2000.

Time series at Xuliujing (WL1) and Zhongjun (WL7)

Xuliujing (WL1) and Zhongjun (WL7) are the two important locations at the Yangtze Estuary area. WL1 is at the bifurcate location of Yangtze Estuary reach. WL7 is at the river mouth. It is interesting and helpful to understand the properties of hydrodynamic conditions at the two locations. Time series of water level (incl. river runoff and tidal flow), flow velocity and direction (incl. river flow and tidal flow), SSC and salinity at WL1 are shown in Figure 2-15 and Figure 2-16, for the flood and dry season measurements, respectively. Plots for WL7 are shown in Figure 2-17 and Figure 2-18. In the figures, the positive flow velocity means that stream flows into the sea. The definition of direction is flowing to with angle accumulation clockwise from north.

From the time series, a very interesting phenomenon is found according to the correlation of water level and flow velocity. The fact is that the net flow velocity is higher during ebb tide than it in flood tide period. In addition, the flow direction is going to upstream during the flooding tide and vice versa, whether at WL1 or WL7. We find that there is a time lag between the intrusions of tidal water and tidal current. This means when the water level gauge reflects the arrival of tidal water (or maybe the effect of backwater); the flow changes its direction some hours later. This happens both in flood and ebb tide periods, flood and dry reasons and at river mouth and inner estuary. During wet season, the time lag is the same for flood and ebb tide periods. They are 5 hrs at WL1 but 4 hrs at WL7 (Figure 2-15 and Figure 2-17). During dry season, the time lag is shorter in flood tide than in ebb tide. It is 3 hrs (flood tide) and 8 hrs (ebb tide) at WL1. It is 5 hrs (flood tide) and 7 hrs (ebb tide) at WL7. From the data statistics in section 2.2, the monthly runoff in dry season is only 42% of the runoff in wet season. This leads to have stronger upstream driving force of tidal water in dry season than in wet season.

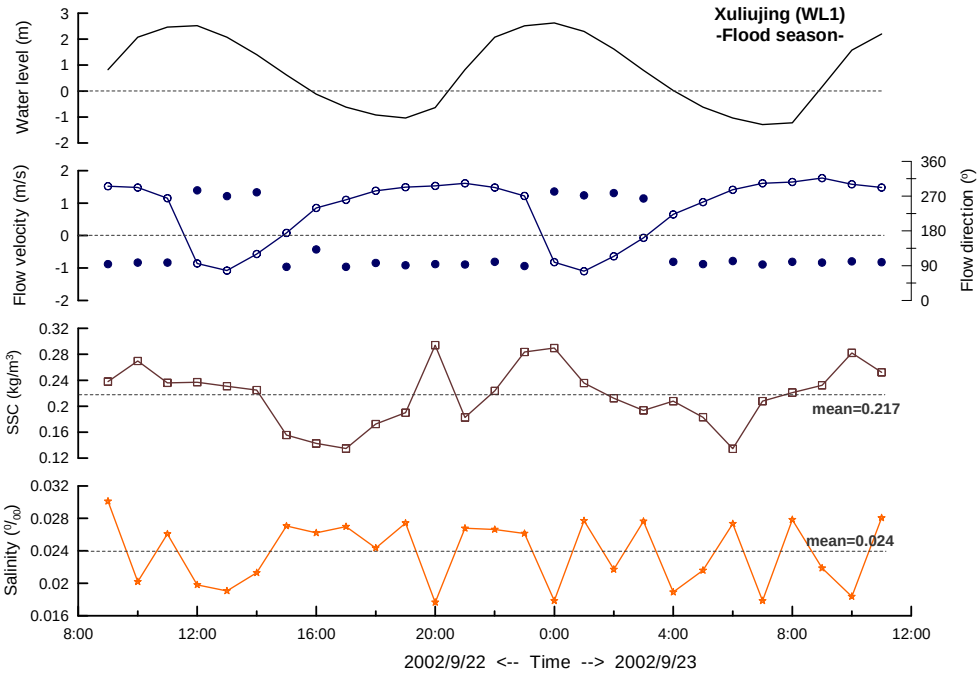

Figure 2-15 Time series of the observed hydrodynamic conditions at Xuliujing (WL1) (wet season data); the full point represents the flow direction

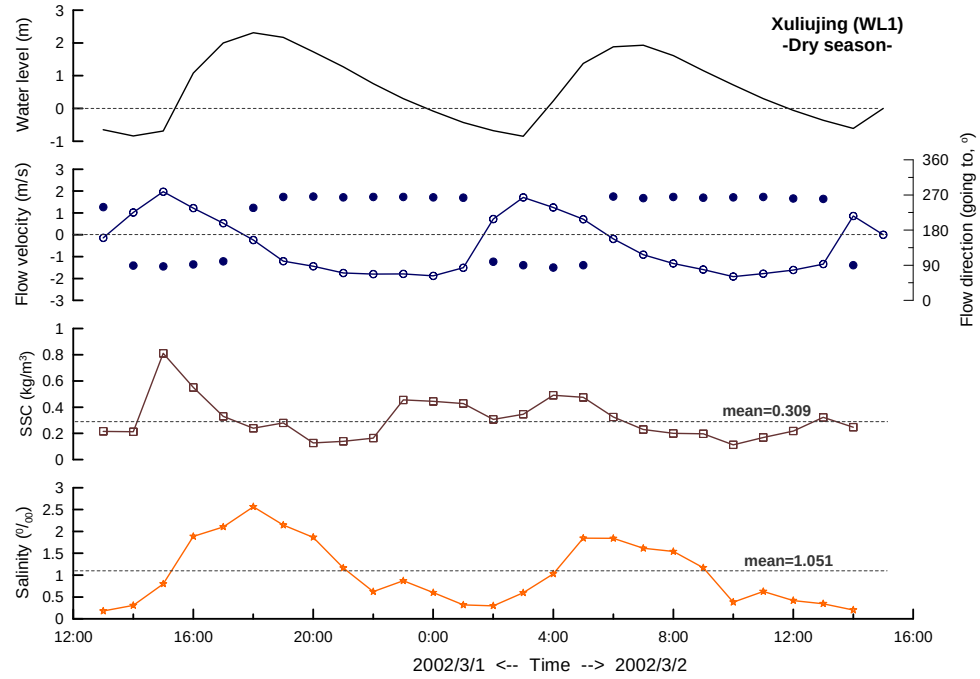

Figure 2-16 Time series of the observed hydrodynamic conditions at Xuliujing (WL1) (dry season data); the full point represents the flow direction

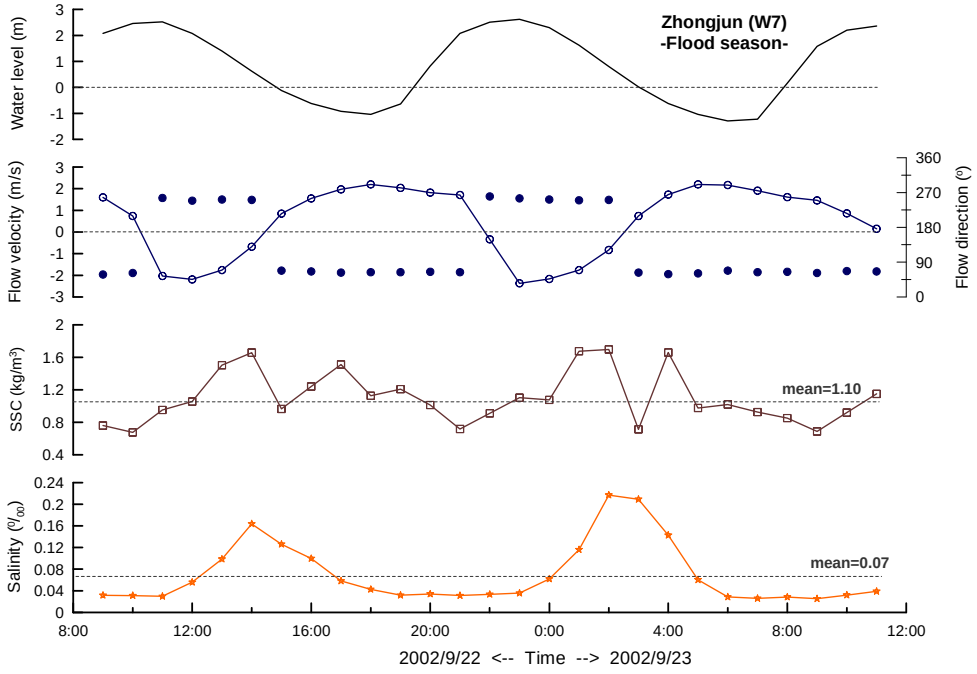

Figure 2-17 Time series of the observed hydrodynamic conditions at Zhongjun (WL7) (wet season data); the full point represents the flow direction

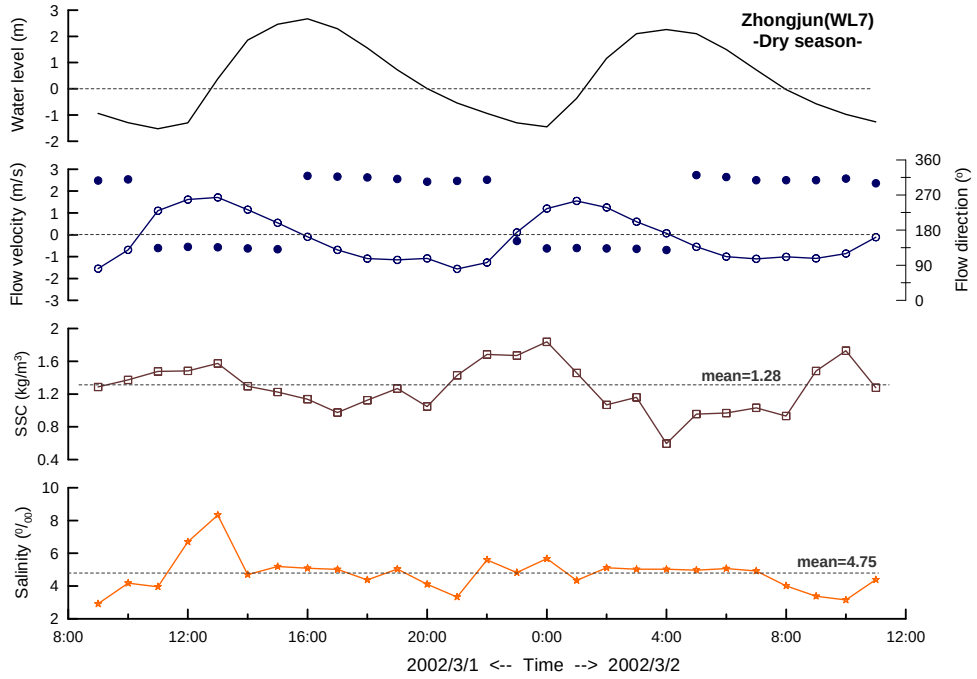

Figure 2-18 Time series of the observed hydrodynamic conditions at Zhongjun (WL7) (dry season data); the full point represents the flow direction

2.4 Morphological evolution analysis by field data

Reaches of the Yangtze Estuary

The lower reach of Yangtze River can be divided into three sections as shown in Figure 2-19. The Near River Estuary Reach (N-RER) is from Datong to Jiangjin which its length is 400 km long. Datong is the location of boundary of tidal level influence in dry season. Jiangyin is the location of boundary of tidal current influence in wet season. The boundaries of tidal level and tidal current influences have different definitions that represent the areas which water level is affected by tide and flow velocity is affected by tidal current, respectively. Generally, the boundaries of tidal level influence and tidal current influence are not the same for wet season or dry season such as for the Yangtze River. The River Estuary Reach (RER) is from Jiangyin to the river mouth. It is 240 km long. The Offshore Estuary (OE) is the area that eastern of river mouth.

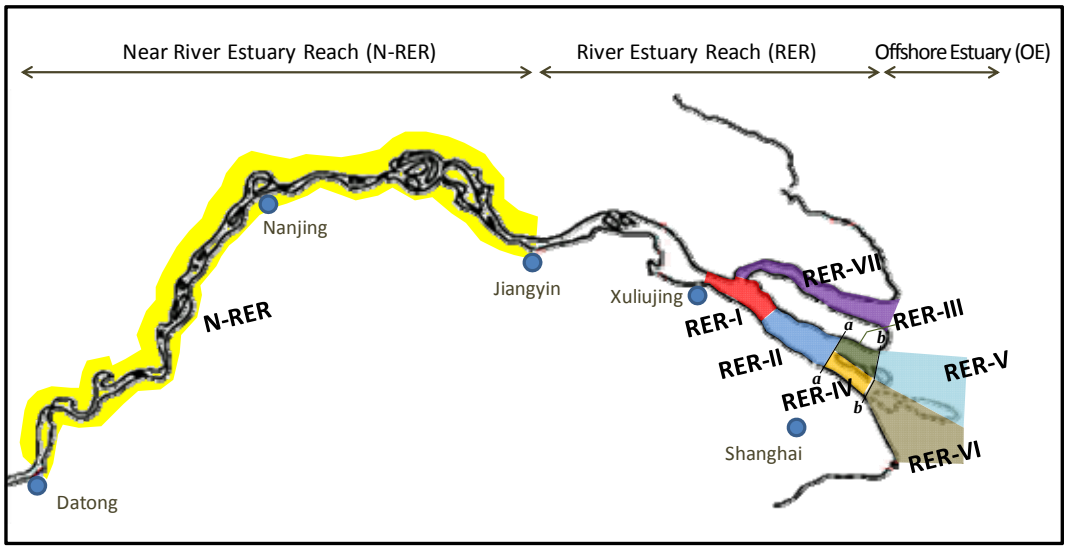

Figure 2-19 River reaches at Yangtze Estuary

At the Yangtze RER, the 240 km river has the special property that called “third-class bifurcation and four river mouths”. It is further divided into three river sections according to the dynamics of the runoff and tidal current for the RER. First, from Jiangyin to Wusongkou (section a-a in Fig.2-19) which is 147km long, where the morphological changes are dominated by runoff. From Wusongkou to Hengsha Island (section b-b in Fig.2-19) which is 32km long, where the morphological changes are jointly dominated by runoff and tidal current. The last section is at the downstream of Hengsha Island, where the morphological changes are mainly dominated by tidal current. In Figure 2-19, the partition of reaches by different color is used for morphological analysis in the next section.

Congming Island divided the Yangtze Estuary into North Branch (NB) and South Branch (SB). The main stream of Yangtze River goes through the SB. It is therefore unstable and has complex mechanism of topography evolution at SB. SB has therefore significant effect on the evolution of Yangtze Estuary compared with that at NB. In SB, Changxing Island and Hengsha Island have divided the SB into North Channel (NC) and South Channel (SC). Jiuduansha has divided the SC into North Passage (NP) and South Passage (SP). The morphological evolution at Yangtze Estuary is jointly affected by the interaction of runoff and tidal current. In addition, mixing of salt water and fresh water has also significant impact. Many factors including the river water discharge (in wet season or dry season), tidal conditions (during flood tide, ebb tide or high tide, low tide) and their interaction make the morphological evolution at this area very complex and nonlinear. It is difficult for modeling and forecasting quantitatively.

Topographic change method

The purpose of this section is to study the morphological evolution at Yangtze Estuary. The methods for calculating the erosion or deposition of the river reaches are the Sediment Budget Method (SBM) or Topographic Change Method (TCM). If there are long-term and continuous field data of water and sediment discharges, SBM can be applied. It is theoretically based on the balance of sediment transportation in the river reach. Alternately, the amount of erosion or deposition can also be estimated from the difference of topographic maps in different era. This is so called the TCM. Geographic Information System (GIS) and digital elevation model (DEM) are common technologies in modern geomorphology and topography analysis because of their powerful spatial analysis and spatial database management capability (Milne and Sear, 1997; Li and Chen, 2004; Antonelli *et al.*, 2004). Wang et al. (2009) used GIS technique and the DEM of channel topography at Jiangsu reach of Yangtze River to evaluate the dynamic changes of sedimentation and erosion from 1959 to 2003. Their results indicated that the main course of the Yangtze River in Jiangsu Province had experienced an obvious switch from sedimentation to erosion status around 1985. They thought one of the possible reasons of that it converted from sedimentation to erosion status is the sea level rise.

Topographic maps are digitalized to be used by TCM. In order to estimate quantitatively the erosion or deposition, the topographic cross-section scheme is applied. Several cross-sections in the river are made. According to the gradient of adjacent cross-sections, the storage capacities of the cross-sections are found. Based on the changes of these storage capacities, the amount of erosion or deposition is then calculated. The storage capacity of a cross-section is calculated by the formula shown below (Dong, 2009; Su and Tan, 2009).

$$W = A_i + A_{i+1} + \sqrt{A_i A_{i+1}} \Big/ 3\Delta L \tag{2-1}$$

where A_i is the area of cross section i. ΔL is the distance between sections A_i and A_{i+1}. W is the storage capacity between sections A_i and A_{i+1}. Some considerations need to be care when applying the topographic cross-section scheme.

Firstly, the cross-sections are better set to perpendicular to the flow direction. For the area of large variation on topography, the number of the cross-sections should be increased. Second, it is generally along the axis of geometric center of the cross sections to calculate the distance between two sections. Finally, water levels have to be decided for the calculation of deposition. These water levels always reflect the discharges under flood and dry seasons. They can be obtained from the rating curves at the control sections.

2.4.1 Near-River Estuary Reach (N-RER)

The Near-River Estuary Reach (N-RER) is firstly considered to assess its morphological change. The location of the N-RER is shown in Figure 2-19. It is the river reach from Datong to Jiangyin that the length is around 400 km. Topographic data surveyed in the year of 1981, 1998, 2001 and 2006 are collected. The elevation base is corrected to the "85 National Datum". Four water levels including low water level (LWL), mean water level (MWL), river-beach water level (RBWL), and the flood water level (FWL) are used to calculate the deposition. The water levels are according to the water discharges 10000, 30000, 45000 and 60000 m^3/s at Datong station. They are the representative discharges of central deep-channel flow, daily flow, river-beach high flow, and the flood flow, respectively. The result is shown in Table 2-8.

From Table 2-8, we find the N-RER reach of Yangtze River was scouring. The most serious erosion area is at the river central deep-channel. Base on the calculation of setting water level to LWL, it was $6.5\times10^8\ m^3$ sand scoured in the past 25 years (1981-2006). The period of most serious scouring was from 1991 to 1998. This may be due to the flood event of Yangtze River in 1998 (Yin and Li, 2001). The average rate of the scour for the whole N-RER is $0.16\times10^8\ m^3$ per year. However, the scouring rate was increasing for this reach, varies from $0.03\times10^8\ m^3/yr$ to $0.3\times10^8\ m^3/yr$. It increased for ten times in the past two decades. Many factors may cause the case. From Figure 2-3 and Figure 2-4, we know the water discharge didn't have obvious changes but the sediment discharge decreased, especially since 1985 (the Phase II in Fig. 2-4). Human activities such as protection of upstream forecast, river sand mining, and the construction of dam or reservoir are all the possible causes.

We try to formula the estimation of the scouring volume. It is assumed the volume is correlated with the ratio of water discharge to sediment discharge. Figure 2-20(a) shows the result. There is a linear correlation of the scouring volume to the ratio. The coefficient of correlation is 0.98. Unfortunately, the sample is too short to have high confidence. In Figure 2-20(b), we don't find the correlation between these two parameters. However, there is another linear correlation between the scouring volumes with sediment discharge, as shown in Figure 2-20(c). This shows that the variation of sediment discharge dominated the scouring at the reach N-RER. Water discharge is not the critical parameter since it didn't vary too much from 1981 to 2006, compared to sediment changes.

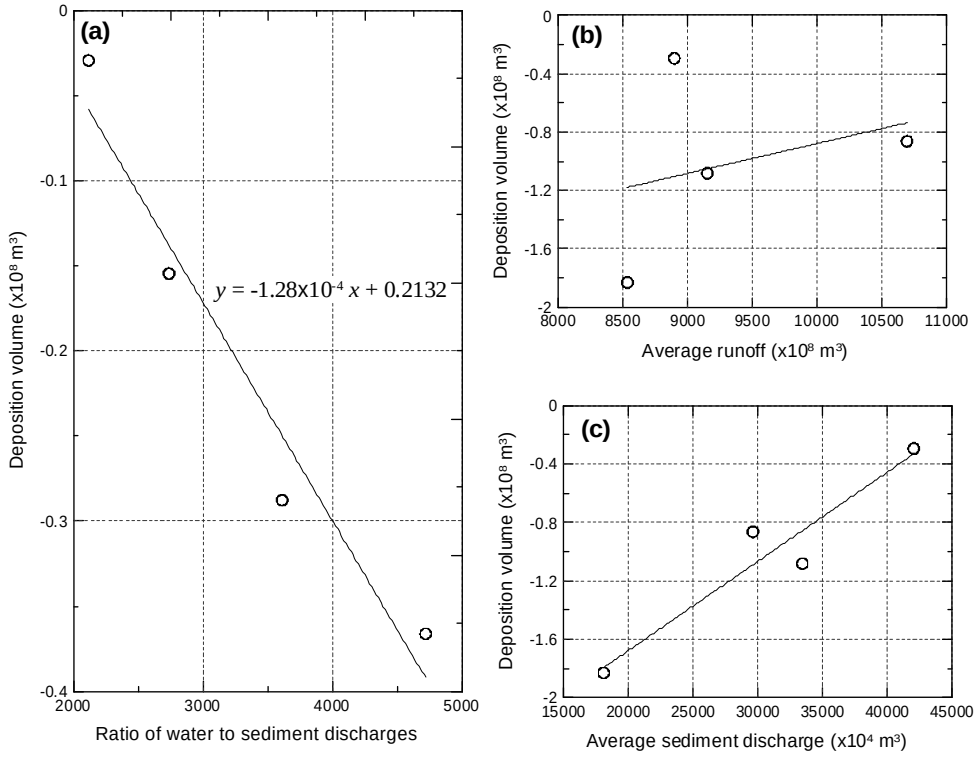

Figure 2-20 Correlations of the deposition volume at N-RER to the (a) ratio of water to sediment discharges; (b) average runoff; and (c) average sediment discharge.

Table 2-8 Deposition calculation results for the Yangtze N-RER reach

Period	Deposition volume (Unit: $\times 10^8$ m^3)					Average ($\times 10^8$ m^3/yr)
	FWL-RBWL	RBWL-MWL	MWL-LWL	under LWL	Summation	
1981-1991	0.25	-0.02	-0.24	-0.29	-0.30	-0.03
1991-1998	-0.03	0.81	1.60	-3.46	-1.08	-0.15
1998-2001	0.05	0.23	0.46	-1.59	-0.85	-0.28
2001-2006	-0.29	-0.10	-0.26	-1.18	-1.83	-0.37
Summation	-0.02	0.92	1.56	-6.52	-4.06	-0.16

2.4.2 River Estuary Reach (RER)

In this section, we discuss the morphological changes at the River Estuary Reach (RER). It is the reach at downstream of Xiuliujing. According to the morphology, it is divided into 6

sections at SB which are labeled from RER-I to RER-VI. Their ranges are shown in Figure 2-19. RER-I is the reach of upper SB covering the island of Baimaosha. RER-II is the reach of the main channel of SB. RER-III is the left-hand reach of the Changxing Island, i.e. the NC. RER-IV is the right-hand reach of the island, i.e. the SC. At the left-hand region (NP) of the Hengsha Island is the RER-V as well as RER-VI is at the right-hand side (SP). In addition, RER-VII is defined as the reach of NB.

Topographic cross-section scheme is applied to calculate the morphological changes from the topographic data of different times. Table 2-9 shows the annual deposition for each sub-reach within RER that are re-analyzed from the output by Zhou (2008). The datum for the deposition calculations is 0 m which means the results represent the morphological changes for the deep-channel area. We find in the Table 2-9 shows that most of the reaches at the RER are scouring since 1973, except RER-VI (SP) and RER-VII (NC). Compared to the result for N-RER, the RER reach has more serious scouring condition. The lower segment is influenced by both river flow and tide current. When the river flow and tide current go in the same direction, it can significantly intensify the channel erosion. Within RER, the scouring rate decreases from upstream (-0.094×10^8 m^3/yr at RER-I) to downstream (-0.022×10^8 m^3/yr at RER-IV). Channels (NB and SB) at the both sides of Changxing Island are scoured. The scouring at NB (i.e. the rate at RER-III: -0.031×10^8 m^3/yr) is serious than SB (i.e. the rate at RER-IV: -0.022×10^8 m^3/yr). Offshore the river mouth, it was scoured at the north river passage (NP) but deposited at south passage (SP). The annual deposition rate for the SP is 0.143×10^8 m^3/yr. North Passage (NP) is the location of Deepwater Channel Regulation Project (DCRP). The result is based on the data until 1997 that the construction didn't start. For the reach of North Branch (NB) (i.e. RER-VII), it has been also scoured since 1992. According to the hydrodynamic conditions described in section 2-3, it is assumed that the deposition at NB is due to its intrusion of sea water to reduce the flow velocity. In Table 2-9, the deposition volume increased after the implementation of TGD in 2003 is also found.

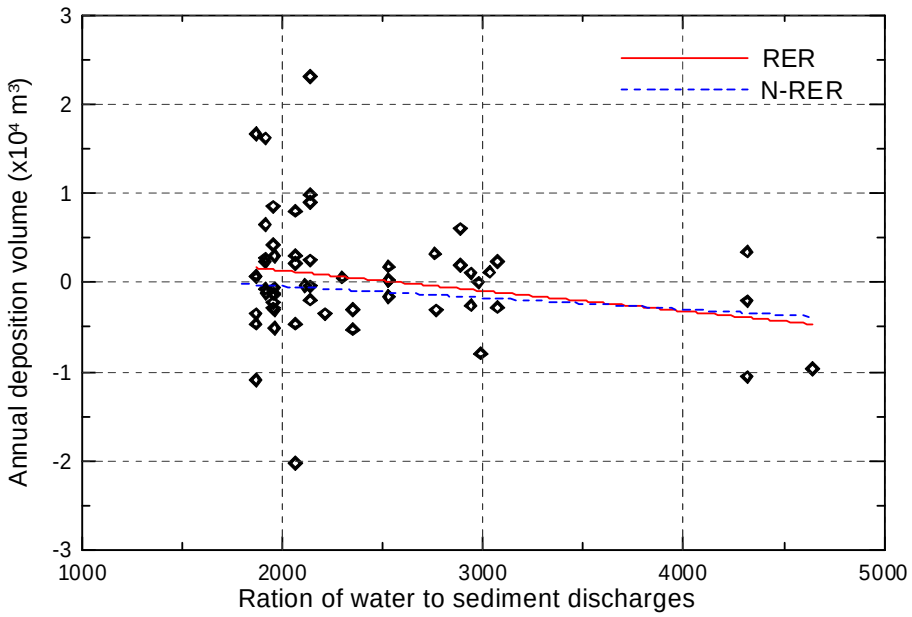

Figure 2-21 Correlation of deposition volume at RER to ratio of water to sediment discharges

Table 2-9 Annual deposition for the Yangtze RER reach (RER-I~RER-VII)

Unit: $\times 10^8\ m^3/yr$

RER-I		RER-II		RER-III	
period	Deposition Volume	period	Deposition volume	period	Deposition volume
1973-1976	0.897	1973-1976	0.253	1973-1976	-0.040
1976-1978	-0.460	1976-1978	0.215	1976-1978	0.305
1978-1980	0.080	1978-1980	-0.460	1978-1980	0.060
1980-1984	-0.118	1980-1982	0.270	1980-1982	0.225
1984-1990	-0.035	1982-1984	-0.510	1982-1984	0.295
1990-1992	-0.305	1984-1986	0.855	1984-1986	-0.225
1992-1994	-0.260	1986-1988	-0.350	1986-1997	-0.161
1994-1997	-0.793	1988-1990	0.055	1997-1999	-0.280
		1990-1992	-0.525	1999-2002	0.193
		1992-1994	0.105	2002-2004	-0.210
		1994-1996	0.115		
		1996-1998	-0.002		
		1998-2000	0.325		
		2000-2002	-0.310		
		2002-2004	0.345		
		2004-2006	-0.970		
$\sum$	-2.260	$\sum$	-0.924	$\sum$	-0.970
average	-0.094	average	-0.029	average	-0.031

Table 2-9(cont.) Annual deposition for the Yangtze RER reach (RER-I~RER-VII)

RER-VI		RER-V		RER-VI		RER-VII	
period	Deposition volume	period	Deposition volume	period	Deposition volume	period	Deposition volume
1973-1976	-0.197	1973-1976	0.990	1973-1976	2.310	1992-1998	0.123
1976-1978	0.805	1976-1978	-2.025	1976-1978	-5.785	1998-2001	-0.048
1978-1980	-1.090	1978-1980	-0.350	1978-1980	1.665	2001-2003	0.044
1980-1982	-0.070	1980-1982	0.650	1980-1982	1.620	2003-2006	0.136
1982-1984	-0.310	1982-1984	-0.065	1982-1984	-0.135		
1984-1986	0.420	1984-1986	-0.290	1984-1986	-0.120		
1986-1997	0.022	1986-1997	0.029	1986-1997	0.182		
1997-1999	0.235						
1999-2002	0.603						
2002-2004	-1.055						
$\sum$	-0.67	$\sum$	-0.87	$\sum$	3.42	$\sum$	0.255
average	-0.022	average	-0.036	average	0.143	average	0.018

2.5 Summary

Estuaries, coastal water bodies and its adjacent environment are subjected to continuous stress by natural and man induced perturbations. Hydrodynamic information in the region of interest is very essential. Yangtze Estuary is the lower, tide-affected part of the Yangtze River. The morphology of Yangtze Estuary is directly affected by the hydrodynamic parameters including river runoff, sediment and tide, as well as their interactions. Water movement and sediment transport of such a tidal estuary differs from an un-tidal river. The characteristics of asymmetrical and un-invariableness are much more extrusive, and the movement directions of both water and sediment are bi-directional. Besides, wave and mixed of salt-water and fresh-water are also the factors determining dynamic evaluative process of riverbed. Conditions such as wet/dry seasons, flood/ebb tide, spring/neap tides make the hydrodynamic characteristics very complexity at this area. This chapter collects and analyzes the in-situ measurement data, as well as the data from tables in the referred papers or reports, in order to understand the hydrodynamic and sediment conditions at Yangtze Estuary. At the last section of this chapter, topographical maps of different times are used to learn the historical evolution of morphological changes at lower reach of Yangtze River and the estuary area. Summary conclusions are given below.

For understanding of hydrodynamic conditions:

Water discharge and runoff

- The average monthly water discharge is 28419m^3/s. It is 40128m^3/s for only the wet season (May to Oct) and 16710m^3/s for the dry season (Nov to Apr). The temporal distribution is very non-uniform. Max and min discharges in the records are 92600m^3/s and 4620 m^3/s, respectively. The total runoff of Yangtze River in a year is 8994×10^8 m^3 which 70.9% is occupied in wet season.

- At Yangtze Estuary reach, the main stream splits into three smaller rivers and flow into the sea from four mouths. The Flow Bifurcation Ratio (FBR) is average 98.5% and 1.5% for South Branch and North Branch, 42.9% and 57.1% for South Channel/North Channel and 55.2% and 44.8% for South Passage/North Passage. The flow of North Branch often intrudes to South Branch, especially during flood tide period in dry season. After Deep Waterway Regulation Project, the FBR for North Passage (where the construction site is) increases 15%.

- No significant change was found on the annual water discharge in the past 50 years, even after the implementation of Three Gorge Dam. However, the distribution of monthly discharge changes (after the Three Gorge Dam). Monthly water discharge decreases in wet season but increases in dry season.

Sediment

- The annual total sediment discharge is 40809×10^4 tons/yr, in which 90% of them are

suspended load. The average sediment concentration is 0.361 kg/m^3. They have also high variations (87.4% sediment is transported in wet season, 12.6% in dry season).

- Base on the analysis of field data at Datong station, the average d_{50} is 0.0106 mm for suspended load and 0.1805 mm for bed load. There is no obvious change for suspended load but the trend of the bed load size is increasing.

- The SSC (Suspended Sediment Concentration) increases from inner estuary (station WL1: Xuliujing 0.1370 kg/m^3) to the river mouth (station SS: Sheshan 0.4195 kg/m^3). It exists highly variations for different flow and tide conditions.

- The Sediment Bifurcation Ratio (SBR) is higher than 100% at South Branch, means the sediment moves from North Branch to South Branch. After Deep Waterway Regulation Project, SBR for North Passage (where the construction site is) increases also about 15%. This is the result based on the investigation from 1998 to 2000.

- Decreasing trends were found on the sediment discharge and concentration in the past few decades, especially after 1986. After the Three Gorge Dam started to operate in 2003, the decreasing rate increases. The average sediment discharge drops from 471×10^6 tons/yr (1950~1985) to 346×10^6 tons/yr (1986~2002) and finally to 226×10^6 tons/yr (2003~2008), only 48% reserved.

Tidal motion

- Outside the Yangtze Estuary, it belongs to semi-diurnal tide. M_2 and S_2 are the largest ones within the constituents. At the inner estuary, it is irregular semi-diurnal due to complicate river topography and water depth.

- The average tidal range is 2.66 m (varies from 0.17 m to 4.62 m) at Yangtze Estuary. This range decreases from river mouth to inner estuary. The max length of tidal level influence is 640 km (at Datong) from river mouth. The max length of tidal current influence is 240 km (at Jiangyin) from river mouth.

- There exists a time lag between the intrusions of tidal water and tidal current. Water level is always responded faster at a station than the arrival of tidal current. The estimated tidal wave propagation speed is 60 km/hr (16.7 m/s) in the river channel; however, the tidal current velocity is from 1.17 m/s to 1.28 m/s (flood tide) and 1.51 m/s to 1.9 m/s (ebb tide) in dry season. This lagging phenomenon happens both in flood and ebb tide periods, flood and dry reasons and at river mouth and inner estuary. The lag time is the same for flood and ebb tide periods in wet season. But in dry season, the lag time is shorter in flood tide than it in ebb tide.

Wind, Wave and Salinity

- Monsoon and typhoon are the main impacts for the wind and wave conditions at

Yangtze Estuary. The average wind speed is 4~6 m/s. Wind speed that larger than 30 m/s during a typhoon has ever happened.

- Long-term statistics shows that the average significant wave heights (periods) at the river mouth and inner channel are 0.9 m (3.7s) and 0.35 m (2.4s), respectively. Maxima values are 6.2 m (8.0s) and 3.2 m (4.5s). Numerical simulation shows 10 m significant wave height for the estuary area.

- Salinity distribution is also highly non-homogeneous and unsteady at Yangtze Estuary area due to the complex hydrodynamic conditions. Generally, the 30 ‰ salinity isoline can reach 300 km offshore from the mouth. At the Deep Waterway Regulation Project construction site, the salinity varies from 5 ‰ to 15 ‰. At the inner estuary, NB has higher salinity because of serious salt-water intrusion.

For analysis of morphological changes:

The lower Yangtze reach is divided into Near-River Estuary Reach (N-RER, from Datong to Jiangyin) and RER (from Xuliujing to river mouth) for morphological evolution analysis. Historical topographic maps are used and the Topographic Change Method (TCM) is applied. The results show the whole N-RER and most parts of RER were scouring. Only the RER-VI (at South Passage) and RER-VII (at North Channel) were accumulating.

For N-RER reach, the main scoured region is at the river central deep-channel. The average rate of scouring is 0.16×10^8 m^3/yr. It has been increased 10 times for the past two decades. On the other hand, the scouring rate decreases from upstream (0.094×10^8 m^3/yr at RER-I) to downstream (0.022×10^8 m^3/yr at RER-IV) in the RER reaches. Before the Deep Waterway Regulation Project started, the result shows it (RER-V, North Passage) was scoured. However the annual deposition rate for the South Passage is 0.143×10^8 m^3/yr.

This study found a linear correlation between the deposition volumes with the ratio of water to sediment discharges. These two regressions from N-RER and RER data are close. It was also found the deposition volume is dominated mainly by sediment discharge, instead of water discharge. Add the samples to reduce the uncertainty for the regression equation in the future can increase the confidence of application.

CHAPTER 3

ANALYSIS OF MORPHOLOGICAL EVOLUTION AT YANGTZE ESTUARY BY NUMERICAL MODEL

3.1 Morphodynamic Models Worldwide

Morphodynamics is the evolution of the shape of a system such as river estuary, including the water movement, sediment dynamics and salinity distribution as a function of the driving forces (sea level, tide, river flow, human interference). Development of morphodynamics modeling has been worldwide raised for representing the response of sediment dynamics to natural driving forces and human intervention. Prediction of morphological changes with numerical models is a powerful technique (van Rijn, 2001). It is nowadays a topic of increasing interest in the fields of coastal and estuarine management, environment protection, and water resource exploitation. Operated over timescales of months to decades, the morphodynamics model can provide information on how the morphology of an estuary should evolve in response to natural or man-made forcing (Lesser et al., 2004; Sutherland et al., 2004a, 2004b). However, the research and development of these models are still in progress and not finished. Morphodynamics modeling often perform poorly in detail due to several reasons. First of all, the longer term morphological changes are driven by shorter term processes such as flow, tidal and sediment motions. Many aspects of the complex interrelation between flow, waves, sediment flux, bottom change, morphological time scales and vice versa are not definitely investigated sophisticated for long term applications. Especially for practical applications, the secure prediction of morphological changes is often required. Second, sediment characterization is very complex due to the presence of both cohesive and noncohesive materials, originating from the river, the sea, and/or from wind transport. The study of sand–mud mixtures is still one of the pioneering areas in sediment transport modeling (Toorman, 2001). Furthermore, the behavior of cohesive sediments is influenced by a large amount of parameters and processes, which are often difficult to describe and that introduce large uncertainties in the morphodynamics model prediction. Over the recent decades, there have been continuing efforts to enhance the understanding of morphodynamics models. State-of-the-art models are becoming increasingly sophisticated in their attempts to model the flow condition and sediment transport accurately (Benkhaldoun et al. 2009).

Cronin et al. (2007) summarized the models used for estuaries to be classified into empirical models, process-based models and abstracted models. The equations in empirical models are based on observations in nature or are purely experimental. Dynamic or process-based models, on the other hand, are based on the mathematical description of water and sediment motions. Generally, the dynamic models have a better theoretical basis than empirical models. At the other end of the dynamic model scale are abstracted models. The processes driving the dynamics of the coastal system are described by a minimum number of variables and relationships (Huntley et al., 2004). According to the consideration of the physical processes and the assumption for governing equations, the morphodynamics models have been developed from one-dimensional (1-D) to two-dimensional (2-D) and then

to a three-dimensional (3-D) model. The 1-D assumption simplifies the equations, but neglects the effects of alongshore variations on near shore dynamics. 2-D modeling is required for increased accuracy of morphology predictions in the nearshore. 3D models may provide detailed descriptions of the physical processes but increased computational time may not be appropriate for use by environmental managers, where speed and ease of application is important (Gleizon et al., 2003). Table 3-1 summarized the recent published morphodynamics models.

One of the first morphodynamic models which have been successfully used for the planning phase of big harbor projects ad on question of the environment is the model TIMOR. TIMOR is a quasi 3D hydro- and morphodynamic model. It was developed by Prof. U. Zanke since 1992 in the Technical University of Darmstadt, Germany. It consists of Hydrodynamic Module, Sediment Transport Module, Morphodynamic Module, and Wave Module. TIMOR has been applied to several studies and have reasonable results (Zanke and Mewis, 2002; Witting, 2004; Witting and Zanke, 2004; Witting et al., 2004; Mewis and Zanke, 2006; Wurpts, 2006; Zhou et al., 2008). TIMOR 3 will be used in this study. More detail description will be given in next section. TIMOR has not been commercialized.

There are several famous morphodynamics models worldwide such as the Delft3D, Mike21, SISYPHE and so on. Some of them can be commercial obtained. Morphodynamics model is always drove by the hydrodynamics model, for example the currents in a river environment, waves in a coastal environment, or a combination of both in an estuarial environment. Therefore, most of the morphological simulation is carried by two-stage simulation, i.e. hydrodynamic model to simulate the flow condition and the morphodynamics model to simulate the sediment condition. Delft3D, developed by WL | Delft Hydraulics is a process-based model (WL | DELFT HYDRAULICS, 2005). It performs computations for coastal, river and estuarine areas and simulates flows, sediment transport, waves, water quality, morphological developments and ecology. Delft3d-FLOW is the centre of the model system simulating flow, by solving unsteady shallow water equations. Many reports used Delft3D for studying the morphodynamics at estuaries (Vriend, 2003; Nghiem et al., 2006; Cañizares and Irish, 2008; ….more) but most of them focus only on the hydrodynamic simulation. Another morphodynamics model is the SISYPHE (Villaret, 2005; Hervouet, 2007). SISYPHE is part of the TELEMAC system and was developed by the Laboratoire national d'hydraulique et environnement of Electricité de France (LNHE-EDF, Chatou, France). SISYPHE morphodynamical model has been developed to obtain realistic estimates of bed movements and sediment transport patterns driven by currents and/or waves. The bottom evolution equation is solved, using either a finite element or a finite volume method, yielding the bottom evolution and the solid transport rate at each node of the model. Coupling of the depth-averaged hydrodynamic model TELEMAC-2D (Hervouet and Bates, 2000) and the SISYPHE morphodynamics model were run on the same computational mesh to estimate the hydrodynamics and suspended sediment transport in the IJzer estuary in Belgium (Giardino et al., 2009) and in the central part of the Gironde macro-tidal estuary in France (Villaret et al., 2010). MIKE 21, developed by DHI (Danish Hydraulic Institute) in Denmark is a package for the simulation of flows, waves, sediments and ecology in rivers, lakes, estuaries, bays, coastal areas and seas in two dimensions. MIKE 21 HD simulates water level and flow variations. The water levels and flows are resolved using a rectangular nested grid or tin or finite volume grid covering the area of interest, using the river channel and floodplain topography, bed resistance coefficients, and hydrographic boundary conditions.

Besides the commercial models, many individual researchers work hard on the improvement of the morphodynamics models. Benkhaldoun et al. (2009) studied the application of a finite volume method to morphodynamics models on unstructured triangular meshes. Their model is based on coupling the shallow water equations for the hydrodynamics with a sediment transport equation for the morphodynamics. The quasi-steady approach formulated by the finite volume method and the approach of coupling hydrodynamics and sediment transport system within the same time step are applied and compared. Their results point out that the coupled approach performs better than the quasi-steady approach only when the bed–load rapidly interacts with the hydrodynamics. Vriend (2003) used examples from research project and studies on the morphological evolution of sandy estuaries and coastal lagoons in The Netherlands to demonstrate the added value of simultaneously applying different morphodynamics methods. Zhou et al. (2009) presented a two-dimensional morphological model for unsteady flow and both suspended-load and bed-load transport of multiple grain size to simulate transport of graded sediments downstream from the Three Gorges Reservoir. The model system includes a hydrodynamic module and a sediment module. Data assimilation technique that is common used in atmospheric and oceanographic models has been used in the coastal area morphodynamics modeling (Scott and Mason, 2007). Zhu et al (2001) applied the junction control method in the numerical model of unsteady flow and suspended-sediment transport in river networks. Liu (2006) analyzed the hydrodynamic problems associated with man-made constructions. Ding (2004) developed a model to estimate the typhoon-induced sedimentation in the Yangtze Estuary. Numerical models have high performance but also high uncertainty. Some researchers such as Eidsvik (2004) thought the abstracted model is another choice especially for environmental managers, where speed and ease of application is important. The ASMITA (Aggregated Scale Morphological Interaction between a Tidal inlet and the Adjacent coast) model developed by Stive et al. (1998) is one of the abstracted model.

Nowadays, most of the morphodynamics models are commercialized. However many individual researchers or research groups still work hard on the development of the models. Normally this can be improved faster than commercial ones and is helpful for student education by means of using the model. For example, CH3D is a Curvilinear-grid Hydrodynamics 3D model developed by Dr. Y. Peter Sheng during 1983-1986 (Sheng, 1987). It can be used to simulate the flow and sediment transport in various water bodies under the forcing of winds, tides, freshwater inflows, and density gradients with the influence of the Coriolis acceleration, complex bathymetry, and shoreline geometry. An integrated modeling system entitled CH3D-IMS, includes circulation (CH3D), wave, sediment transport (CH3D-SED3D), water quality (CH3D-WQ3D), light attenuation (CH3D-LA), and seagrass models (CH3D-SAV) has been developed and applied to several estuarine systems in US. CH3D-SED3D includes a fine sediment transport model as well as a coarse sediment transport model. The fine sediment transport model is based on the theory described in the 3-D sediment transport model developed for USEPA (Sheng et al., 1991). The coarse sediment transport model uses some theory described in van Rijn (1991). The processes included in the CH3D-SED3D are advection, turbulent mixing, settling/flocculation, deposition, and resuspension, and wave-current interaction inside bottom boundary layer. The bottom sediment layer is also updated.

Table 3-1 Summary of worldwide morphological models

Name	Description	Institution	Version/ year	Dimension	Numerical skill	Application areas	Reference
MIKE 11	Simulation of flow and water level, water quality, sediment transport and morphology in rivers and other inland water bodies.	DHI, Denmark	2009	1-D	implicit finite difference scheme	rivers and channels	DHI homepage http://www.dhigroup.com/
HEC-RAS	Computations for steady flow water surface profile, unsteady flow simulation, movable boundary sediment transport computation, and water quality analysis.	U.S. Army Corps of Engineers (USACE), USA	V4.1 2010	1-D	Preissmann implicit scheme	rivers, reservoirs and open channels	USACE homepage http://www.hec.usace.army.mil/
ISIS	Prediction of sediment transport rates, bed elevations and amounts of erosion/deposition throughout a channel system.	Wallingford Software Ltd, UK	V3.3 2003	1-D, 2-D	Preissmann implicit scheme	Rivers, channels and irrigation canals	ISIS homepage http://www.wallingfordsoftware.com/
UnTRIM+ SediMorph	UnTRIM is the hydrodynamic model to simulate flow conditions. SediMorph is a morphodynamics model to compute the sedimentological processes.	Federal Waterways Engineering and Research Institute (BAW), Germany	V1.1 2005	1-D, 2-D	Finite volume method	Free surface flow such as rivers, lakes, estuaries, bays, coastal areas and seas.	BAW Homepage http://www.baw.de
SOBEK	Application for flood forecasting, drainage systems, irrigation systems, sewer overflow, river morphology, salt intrusion and water quality.	WL|Delft Hydraulics, Netherlands	V2.12 2009	1-D, 2-D		in a river, an estuary, a canal or in a sewer network	WL|Delft Hydraulics homepage http://delftsoftware.wldelft.nl/
MIKE 21	Simulation of flows, waves, sediments and ecology in rivers, lakes, estuaries, bays, coastal areas and seas in two dimensions.	DHI, Denmark	2009	2-D	Explicit scheme	rivers, lakes, estuaries, and coastal areas. For non-cohesive Sediment transport	DHI homepage http://www.dhigroup.com/
DELFT 3D	Simulation of hydrodynamics, sediment transport and morphology and water quality for fluvial, estuarine and coastal environments.	WL|Delft Hydraulics, The Netherlands	V3.3 2009	2-D, 3-D		For fluvial, estuarine and coastal environments	WL|Delft Hydraulics homepage http://delftsoftware.wldelft.nl/

Table 3-1(cont.) Summary of worldwide morphological models

Name	Description	Institution	Version/ year	Dimension	Numerical skill	Application areas	Reference
CCHE2D / CCHE3D	simulation of steady and unsteady river flows, non-uniform sediment transport, morphologic processes, coastal processes, pollutant transport and water quality.	National Center for Computational Hydroscience and Engineering, the University of Mississippi, USA	V3.26.7 2010	2-D, 3-D	control volume approach and efficient element method.	simulate non-uniform sediment (both non-cohesive and cohesive)	CCHE homepage http://www.ncche.olemiss.edu/software/cche2d
SED2D	computation of depth-averaged transport of cohesive or a representative grain size of noncohesive sediments and their deposition, erosion, and formation of bed deposits.	U.S. Army Corps of Engineers (USACE), USA	2006	2-D	Finite Element Method	non-cohesive and cohesive sediment	USACE homepage http://chl.erdc.usace.army.mil/sed2d
ECOMSED	a three-dimensional hydrodynamic and sediment transport model. The hydrodynamic component of ECOMSED is based on Princeton Ocean Model.	HydroQual, Inc, USA	2010	3-D	a mode-splitting technique with finite difference method	River, lake, reservoir, estuary, ocean	HydroQual homepage http://www.hydroqual.com/ehst_ecomsed.html
CH3D-SED3D	simulate the flow and sediment transport in various water bodies under the forcing of winds, tides, freshwater inflows, and density gradients with the influence of the Coriolis acceleration, complex bathymetry, and shoreline geometry.	originally by Dr. Y. Peter Sheng since 1983	-	3-D	finite volume approach	in lakes, estuaries, harbors, and coastal waters	CH3D homepage http://ch3d.coastal.ufl.edu/
MIKE III	simulations of flows, cohesive sediments, water quality and ecology	DHI, Denmark	2009	3-D	Alternating Direction Implicit (ADI)	in rivers, lakes, estuaries, bays, coastal areas and seas.	DHI homepage http://www.dhigroup.com/
TIMOR 3	a quasi 3D hydro- and morphodynamic model, fully coupled with wave model	Technical University of Darmstadt, Germany	2009	2-D, 3-D	Finite Element Method	Simulate tides, currents, waves, wind, salinity, cohesive and non-cohesive sediments	Zanke 1993, 1994, 1995,2002

3.2 Tide Morphodynamic Model (TIMOR3)

TIMOR, a quasi 3-D hydro- and morphodynamic model, has been developed at the Institute of Hydraulics and Water Resources at the Technical University of Darmstadt. TIMOR is a dynamic modeling system that simulates the flow and sediment transport in lakes, estuaries, harbors, and coastal waters and can be used to simulate the flow and sediment transport in various water bodies under the forcing of winds, tides, freshwater inflows, and density gradients with the influence of the Coriolis acceleration, complex bathymetry, and shoreline geometry. In this thesis, TIMOR is applied to simulate the morphological changes under tide, current, wind and waves in the Yangtze Estuary.

The history of TIMOR traced back to 1992, when the first German 2-D morphodynamic simulation system TIMOR2 came into being (Zanke, 1993; 1994). It was applied to simulate unsteady two dimensional flow in the horizontal plane coupled with morphological computations. It could handle salt and uniform sediment transport, but the sediment bed was assumed to be infinite. In 1995, TIMOR3 was developed (Zanke, 1995). The sediment bed was divided into a finite number of layers. Up to 12 sediment sizes per layer could be accommodated. In each layer under each node, a distributed sediment could exist. Thus the bed could be described fractionized and fully 3D. The dredging as well as the dumping sediments could be simulated. In 1998, modules were incorporated to simulate silt transport and deposition including biodynamic effects. Since 1999 the TIMOR3 was coupled with wave model SWAN (Roland et al., 2009). Meanwhile, SWAN was replaced by WWM II. The TIMOR3 is still improving, to have more correct results and better performance.

TIMOR3 is based on FEM (finite element method) using triangular elements. It can handle multi-fractional 3-D bed evolution and suspended sediment transport based on the vertical integrated SWE (shallow water equations), which is solved with an eddy viscosity turbulence approach (Mewis, 2002). The model is able to handle different grain sizes (graded sediment transport). It accounts for bed load and suspended load using an arbitrary number of discrete grain sizes in order to numerically resolve the resulting grain size distribution. The seafloor is divided into slices of arbitrary magnitude with the upper slice being the active mixing layer, a layer in which the sediment composition is changeable (Witting and Zanke, 2004). Transportation of non-cohesive material is calculated with the formula presented by van Rijn (1993) where additionally increased mixing due to the turbulence of breaking waves and the effect of gravitation on the bed load transport on slopes is taken into account.

In most sediment transport problems, the mathematical modelling of morphodynamics relies on a system of four equations: three equations (shallow water equations) describing flow continuity and momentum conservation with shallow water assumptions, and one equation (Exner equation) expressing the sediment continuity (Benkhaldoun et al., 2009). TIMOR solves the bed evolution equation in order to account for the bed evolution equation (3-1) and the advection diffusion equation in order to estimate the suspended sediment transport rates. The vertical concentration distribution is considered by the analytical approach of Rouse (1937). Also the changes of near bed flow directions due to secondary

flows are taken into account by analytical solutions. The stirring up and the outfall of sediments from the water column is solved as a feedback process using van Rijn (1993)'s entrainment approach. Figure 3-1 shows the model conceptual scheme of TIMOR3.

$$\frac{\partial z}{\partial t} = \frac{\partial q_{tx}}{\partial x} + \frac{\partial q_{ty}}{\partial y} + E - S \tag{3-1}$$

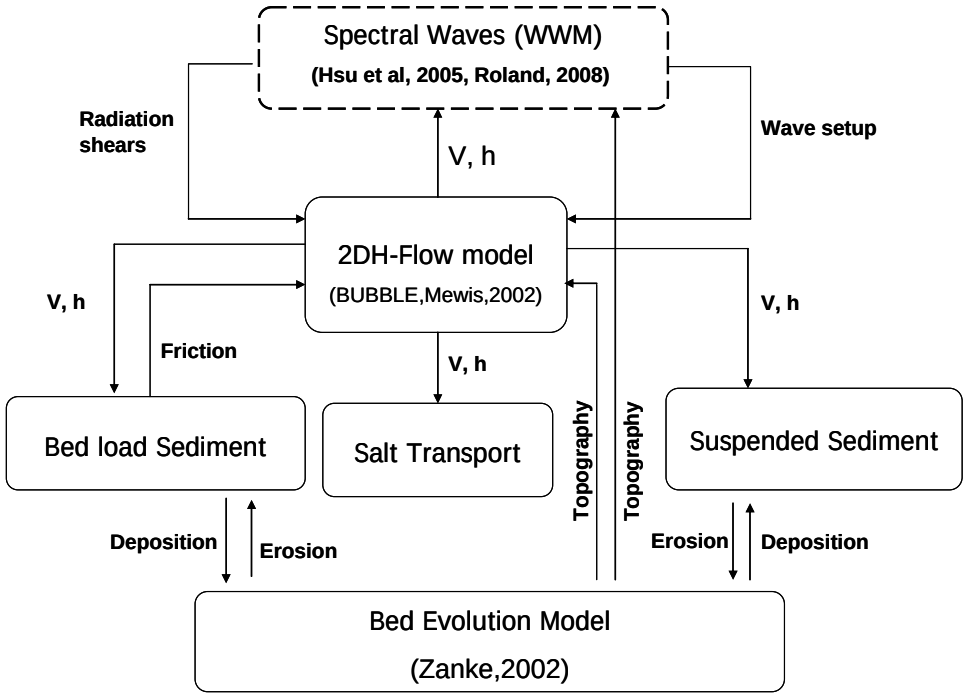

Figure 3-1 Conceptual scheme of TIMOR3 model

Active layer

Under most circumstances, sediment exchange between the flow and the river bed remains limited to a thin layer near the water-sediment interface. It is possible to define a rather thin active or exchange layer with thickness which is typically taken to correspond to some multiple of characteristic surface grain size or dune height. The active layer concept was proposed by Hirano (1971) and later advanced and utilized by others (Parker, 1990; Cui et al., 1996; Toro-Escobar et al., 1996) for modeling the morphodynamics of gravel-bed rivers, including downstream fining and armoring. TIMOR also uses the active layer approach. This is a more intuitive and transparent method. It can form a coarse or fine active layer, and, with an appropriate exchange increment, it may be preferable in some cases for modeling mobile armor systems. This approach divides the substrate into active (mixing or surface) layers that are available for transport, and inactive layers that have no influence on the computations for a given time step. Since the active layer and inactive layers are composed of different gradations, there is a gradational discontinuity between them. As the bed aggrades and degrades material is passed across this interface in order to reset the active layer to the specified thickness. In the erosive case, computing the gradational composition of this exchange increment is trivial. Material from upper one of the inactive layers is

brought up into the active layer. The depositional case could be a simple matter of assuming that the material added to the active layer is fully mixed. Resetting the active layer thickness would involve transferring some of this mixed active layer material to the inactive layer. Alternately, in the fully unmixed scenario, bed load material would be deposited on the top of the active layer, and unmixed material from the bottom of the active layer would be moved to the upper of inactive layer, the active layer would then be fully mixed before the next computational time step.

Toro-Escobar et al (1996) advanced the idea that the depositional exchange increment was a combination of the active layer gradation and the bed-load gradation. They generated an approximate weighting function from their tests (without claiming generality) : f(i,j)= 0.7p(j)+0.3F(j) where: f(i,j), p(j) and F(j) represent the fraction of the exchange increment, bed load and active layer respectively, associated with grain class (i). This is the default assumption in TIMOR. During deposition, when using the active layer method, the exchange increment is composed of 30% of the composition of the active layer from the beginning of the time step and 70% of the gradation of the deposited material. For example, if 10 tons of material were deposited for a given time step (assuming the active layer would be transferred to the inactive layer, 7 tons of the deposited material would be added to the inactive layer. The 3 remaining tons of the deposited material would then be mixed into the active layer. Figure 3-2 shows the conceptual structure of TIMOR3.

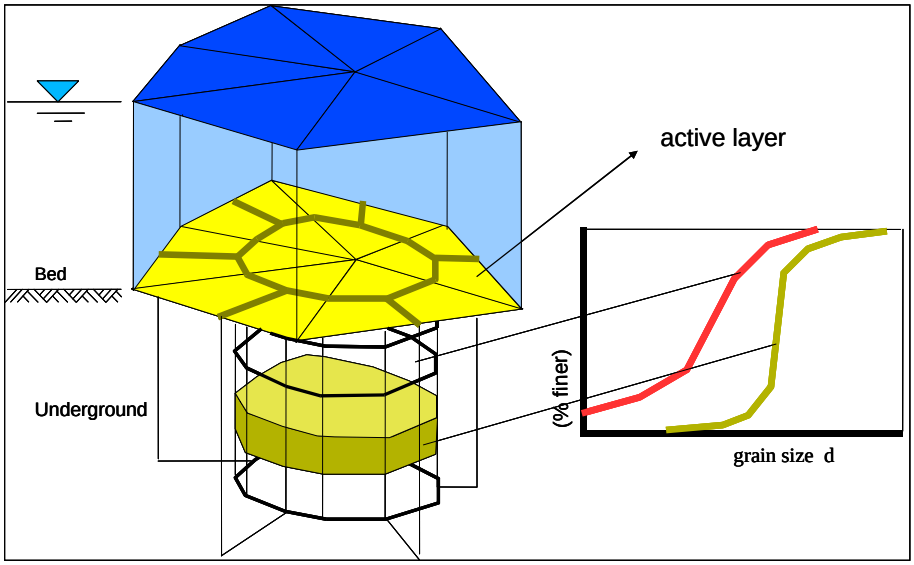

Figure 3-2 Conceptual structure of TIMOR model (Zanke, 2002)

Morphological factor

Analyzing and predicting detailed morphological changes in those areas with complex plan forms and processes, such as tidal inlets, river mouths, estuaries and bays requires the use of advanced, process-based morphodynamic models. One of the key issues in carrying out longer-term simulations with morphodynamic models is the strategy applied to bridge the gap between short-term hydrodynamic and transport processes, varying over hours to days,

and morphological changes, often taking place over much longer time periods. Different strategies have been developed and the “morphological factor” approach has been used in TIMOR3.

The morphological factor approach exaggerated the amplitude of short-term changes due to tide and varying wind and wave conditions still puts a limit on the morphological factor that can be applied. Now it is extended by running multiple simulations in parallel, where the evolving bathymetry is modified by a weighted superposition of all simulations and all processes share the resulting bathymetry. This method allows for smooth, long-term simulations, which take into account short-term variations in an efficient, parallel-processing way.

This is a complete different approach to run flow, sediment transport and bottom updating all at the same small time steps. In case an advection-diffusion scheme is solved for the sediment transport this has to be done with comparable time steps as the flow solver. The updating of the bottom takes very little computation time. However, this “brute force” method does not take into consideration the difference in time scales between the flow and morphology. This method was tested and implemented into TIMOR in 1992, but not published. Later, Lesser et al (2004) described the same method. In 2008, Zanke published an extensive study on this method. This factor n simply increases the depth change rates by a constant factor, so that after simulation over one tidal cycle we have in fact modeled the morphological changes over n cycles. The bottom evolution is then computed in much smaller time steps, even when relatively large values of n are used.

An advantage of this method is that short-term processes are coupled at flow time-step level, which makes it easy to include various interactions between flow, sediment and morphology, and which also removed the need to store large amounts of data between processes. The treatment of areas that may be drying or wetting also becomes more straightforward, and especially in these areas it is a great advantage to take many small morphodynamic time steps. To compute long-term morphological changes, a morphological factor can be used in order to save time, man power and computational facilities. Roelvink (2006) has also proposed this technique, which supposes the bottom change due to the difference in sediment transport is quite slow as compared with the hydrodynamic change of flow, so the change of the bottom topography can be “accelerated” using a morphological factor with less impact to the flow and tidal hydrodynamics. By using this technique the computational time for a long period simulation is reduced significantly.

Sediment transportation formulas

The sediment transport $S = S(\nu, \lambda, d_{xx}, \omega_s, \ldots)$ is a function of

Velocity of flow	ν [m/s]
Friction at the bed	Manning, Chezy…parameter λ
Grain size parameter	d_{xx} [mm]

Settling velocity ϖ_s [m/s]

Threshold velocity v_{crit} [m/s] and further parameters

And other parameters

For practical use the sediment transport rates are to be determined by experiments. There are dozens of transport functions, some take bed load and suspended load individually, and some are for the total load (bed load plus suspended load). Following are a brief summary of those formulae by name of the author.

In the literature, there are numerous formulae. Principally, all of them can be implemented in each MD-code. In TIMOR, a selection of the most well known is implemented such as AW (Acker and White, 1973), EH (Engelund and Hansen, 1967), MPM (Meyer-Peter-Müller, 1948), Rijn (Van Rijn, 1984), and also Zanke (Zanke, 1999; 2001), which was ranked high in ASCE proceedings.

There are several sediment transport formulae available in TIMOR3. They are Vollmers/Pernecker formula, Engleund/Hansen formula, Meyer-Peter/Müller formula, Ackers/White formula and Zanke's formula. A brief and qualitative note on the use, applicability, and sensitivity of some formulas is given below.

Bed load transport formula defined by Zanke(2001) is as follows

$$q_B = u_{s,\max} s \frac{1}{2} \frac{\left[1+\frac{2}{3}\frac{s}{h}\left(n+\frac{\rho_s}{\rho}(1-n)\frac{I_B}{I_E}\right)-R\frac{\tau_{c,0}}{\tau_0}\right]}{\left[1+\frac{1}{2}\frac{s}{h}\left(n+\frac{\rho_s}{\rho}(1-n)\frac{I_B}{I_E}\right)-R\frac{\tau_{c,0}}{\tau_0}\right]} \tag{3-2}$$

While

$$\frac{s}{d} = \frac{\tau^*_{c,0}}{(1-n)\left(\tan\Phi - \frac{\rho_s}{\rho_s-\rho} I_B\right) - n\tau^*\frac{d}{h}} R\left(\frac{\tau^*}{\tau^*_{c,0}} - R\right) \tag{3-3}$$

The average maximum velocity $U_{s,max}$ of grain covering the bottom is

$$u_{s,\max} = u_m \chi = \frac{\left[\left[\left(y_{D,eff}\right)\frac{u^*}{v}\right]^{-2} + P_{yt}\left[2.5\ln\left(\frac{y_{D,eff}}{k_s}\right)+B\right]^{-2}\right]^{-1/2}}{2.5\left[\ln\left(\frac{h}{k_s}\right)-1\right]+B}\left(1-0.7\frac{u^*_{c,0}}{u^*}\right)u_m \tag{3-4}$$

For the general case of s/h $<\approx$ 0.1, the Formula (3-2)can be simplified to:

$$q_B \approx \frac{1}{2} u_{S,\max} s \tag{3-2a}$$

For a given sediment ρ_s, n and Φ are constant, $I_B << \tan\Phi$, and in many cases n τ^* d/h may be neglected. Then s is a direct function of the grain diameter d and $\tau^* / \tau^*_{c,0}$:

$$\frac{s}{d} \approx 2.8R\left(\tau^* - R\tau^*_{c,0}\right) \tag{3-3a}$$

For $\tau^* / \tau^*_{c,0} > 2$, Formula (3-3) becomes

$$\frac{s}{d} \approx 2.8\left(\tau^* - \tau^*_{c,0}\right) \tag{3-3b}$$

For the above formulas, q_B= transported bed-load volume including voids per unit time and unit width, $U_{s,max}$= maximum sediment velocity at the top of the bed, s= kinematic viscosity of the fluid, *v*= kinematic viscosity of the fluid, h= water depth, n= proportions of voids in the sediment at rest (≈0.3for natural sediments), ρ_s= density of the sediment, ρ= density of the fluid, I_B= bed slope, I_E =energy slope, R= risk of grain movement, $\tau_{c,0}$= shields critical shear stress between the water and the bed, as exerted by the water body, τ_0= shear stress of the water body at the bottom = $\rho g h I$, $\tau^*_{c,0} = \tau_{c,0} / ((\rho_s - \rho) g d) = u^{*\,2}_{c,0} / \rho' g d$ = dimensionless critical shear stress after Shields for the grains at the top of the bed, τ*= $\tau^* = \tau_0 / ((\rho_s - \rho) g d) = u_0^{*2} / \rho' g d$ = dimensionless shear stress related to the grains, Φ= angle of internal friction of sediment in the state of motion, ≈27° for natural sediment, ≈34° for every angular and splintered material, $y_{D,eff}$ = distance of the center of thrust from the wall under developed transport, u*= shear stress, $u^*_{c,0}$ = critical shear velocity at the top of the bed after Shields, k_s= equivalent sand roughness, for natural sediments after Rijn(1984) $k_s \approx 2d$, B= integration constant for the velocity distribution law, u_m= average flow velocity at the center of trust of the grains at the surface.

Entrainment and deposition process in TIMOR

The entrainment rate is computed separately for non-cohesive and cohesive sediments in TIMOR. The entrainment rate for non-cohesive sediment can be computed using the formula developed by Rijn (1984):

$$E = 0.00033 D_*^{0.3} T^{1.5} \rho' g d \tag{3-5}$$

$$T = \frac{\tau - \tau_{cr}}{\tau_{cr}} \quad , \quad D_* = d_{50}\left[\frac{(s-1)g}{\nu}\right]^{1/3} \tag{3-6}$$

The entrainment rate for cohesive sediment is computed by the formula developed by Talmon (1995):

$$E = M\left(\frac{\tau_b}{\tau_{ce}} - 1\right) \tag{3-7}$$

The deposition rate is computed by assuming that the sediment is distributed vertically according to Rouse and the distribution is largely determined by the fall velocity (Zanke, 2002)

$$\omega = 14.7 \times \frac{\nu}{d}\left(\sqrt{1 + 5.7 \times 10^{-3} D^{*3}} - 1\right) \quad \text{(for natural sediments)} \tag{3-8}$$

$$\omega = 1.1 \times \sqrt{\rho' g d} \ \text{(for coarse sediment)} \tag{3-9}$$

$$D^* = \left(\frac{\rho' g}{\nu^2}\right)^{1/3} . d_m = \left(\frac{\mathrm{Re}_d^{*2}}{\tau^*}\right)^{1/3} \tag{3-10}$$

The suspended sediment is distributed both in vertical and horizontal directions because of turbulence. This phenomenon causes sediment dispersion. Sediment dispersion in the horizontal plane is parameterized though a dispersion coefficient, Dx,y, which is computed as

$D_{x,y}$= konst h u_τ (3-11)

Where M = erosion coefficient (kg m^{-2} s^{-1}), τ_b = bottom shear stress (Nm^{-2}), τ_{ce} = critical shear stress for erosion (Nm^{-2}), h= flow depth, u_τ = shear velocity.

3.3 Model Setup

In order to evaluate the influences of human interferences and sea level rise on the morphological evolution of the Yangtze Estuary in the long-term and on the large scale, a

process-based morphodynamic model on the basis of both cohesive and non-cohesive sediment transport module TIMOR3 is used. Model input is very important for enhancing simulation accuracy. For numerical models the input data always includes initial conditions, bathymetry and water body boundaries, physical coefficients, water surface elevations or flow rate at open boundary, and time sequences of hydrological conditions. This section introduces the setup of TIMOR3.

3.3.1 Model Area

TIMOR3 is used to simulate the hydrodynamic and morphodynamic conditions at Yangtze River Estuary. The model area is wide considering the strong current and tide dynamics at the Yangtze estuary area. The upstream boundary is set to be at Jiangyin (WL1 in Fig.2-1), where is a water level station 220 km away from the Yangtze Estuary with latitude E 121^{o}. Hangzhou Bay where locates at the southern Yangtze Estuary is included in the study domain. The north boundary is to Lvsi Port with latitude N 32.5^{o}; south boundary is with N 29.25 ^{o}; east boundary is to the outer sea with the longitude E 124.5^{o}, at the isobath of -50m. The model area is around 8×10^{4} km^{2}. It is shown in Figure 3-3.

3.3.2 Grid Generation

Grid generation is a general task for all kind of applications from mechanics to fluids. It is a backbone for any computational approach. Grid generators for Finite Difference Method are commonly based on geometric rectangular cells of variable size. Each cell represents an averaged water-depth. Adaption to geometrically complicated boundaries is cumbersome. Coastal Engineering applications mostly deal with complex coastline situations so that triangular grids are favorable. They are pretty flexible for adaption to geometrically complicated situations and mostly used within Finite Element Method based numerical models.

In this simulation, the Surface-water Modeling System (SMS) is used to generate triangular grid. SMS includes 2D finite element, 2D finite difference, and 3D finite element modeling tools. Much attention has been paid to the project area, where the bathymetry changes greatly due to the on-going hydraulic structures, in order to reflect the tidal field much accurately. Besides the encrypted grid is generated in the whole channel area, the dikes and groins and its surrounding areas have been taken into consideration for the depth gradient. Totally there are 128294 triangle elements and 65946 nodes with the triangle length from 90m to 6700m in the model of the Yangtze Estuary.

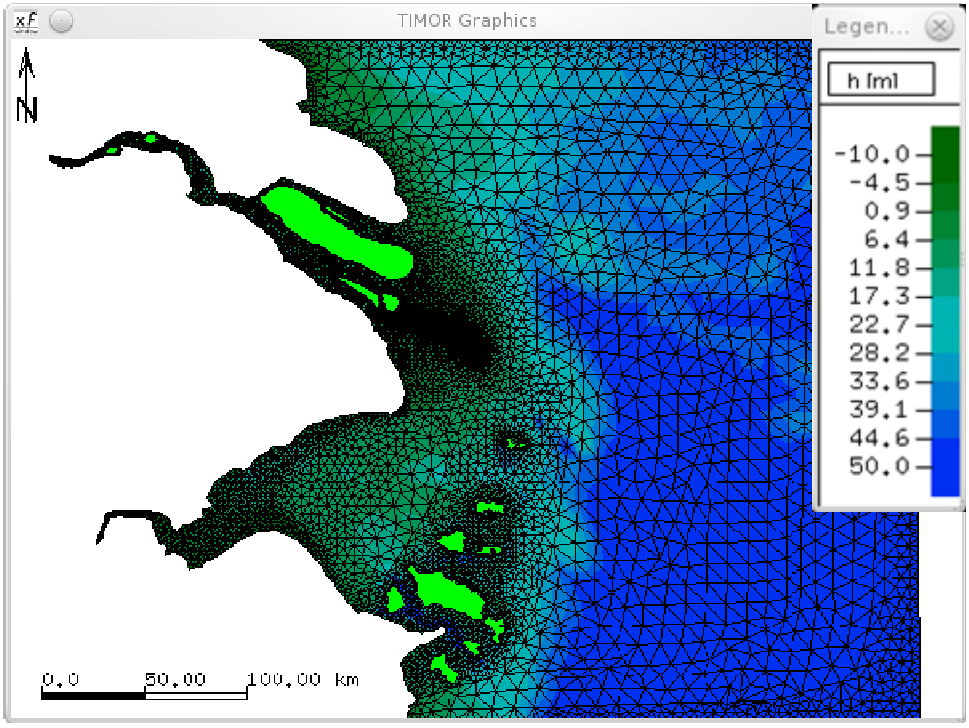

Figure 3-3 The model area and the mesh in the domain

3.3.3 Model input data

Bathymetry data

The bathymetry data used in this study were collected by Bureau of Hydrology (BOH) of the Changjiang Water Resources Commission (CWRC) in 2002, and part in 2005. The elevation was transferred to the 1985 National Height Datum (85NHD) in China. The density of the measured data is not uniform within the study domain. From Jiangyin to the estuary near -20m isobath depth, distance of the data points is densely with 50m to 2000m. The open sea is far from interested area, so the measured data are relative few there. The further the open boundary is from the area of interest, the less impact it will have on the desired solutions due to later arrival and increased damping in transit of errors propagated. Distance of data points in other regions is from 4000m to 30000m.

Hydrological data

Corresponding to the bathymetry data, the tidal records from Feb. 24 2002 to Mar. 31 2002 and Sep. 1 2002 to Sep.30 2002 are used in this study. They include data of tidal level, flow velocity and suspended sediment concentration (SSC). These data are used for model calibration and validation purposes respectively. Data in Feb represent the hydrological characteristics in dry season as well as Sep. data for wet season. In addition, the records cover the periods of spring, mean and neap tides. The layout of the measurements is shown in Figure 2-1.

3.3.4 Boundary Conditions

Upper boundary (flow and tide)

Either water level or water discharge can be used for the upper boundary condition. Both have been tried to work as upper boundary to see the difference and then find the best one to do further simulation. Measured water discharge was finally chosen as input data for the upper boundary at Jiangyin. With respect to the period of measured data for validation and calibration, the periods of water discharge as the upper boundary were from Feb.24 2002 to Mar.31 2002 and from Sep.1 2002 to Sep.30 2002. Both the bed load transport and the suspended load transport are considered in the model. Due to the lack of sediment load transport information at Jiangyin Station, there is no suspended sediment concentration adopted as constant input at the upper stream boundary, but in the application of the model, some techniques has been made to lighten the problem.

Seaside boundary (tide)

The water level at seaside boundary is derived from East China Sea Model (Lin et al., 2000). The harmonic constants of 8 principal tidal constituents (Q1, O1, P1, K1, N2, M2, S2 and K2) are used to predict the tide (water level) within the East China Sea tidal model. The data are from Feb.24 2002 to Mar.31 2002 and from Sep.1 2002 to Sep.30 2002.

Project boundary (hydraulic structures)

The bathymetry data survived in 2005 provides more detail information, mainly at the DWRP project area at the estuary. This is necessary for correct simulation of morphodynamics conditions for the construction area.

3.3.5 Model Parameters

Besides the boundary conditions, the proper initial conditions are also one of the main concerns of validation process. Frequently models are started from rest and it is assumed that due to the propagation properties together with dissipative features of the model the initial disturbances disappear over the boundaries and with time. So some of them are only needed to set an initial value according to the available experience, and they will become stable during the simulation. Some of them need to be calibrated with measured data in order to make the model more applicable.

The results of simulation depend greatly on the parameters, because some of the formula are empirical, the parameters in them should be calibrated according to the current situation of the modeled area before model application. Table 3-2 gives the parameters needed to be computed in TIMOR. For the hydrodynamic simulation, the most important factors are Friction Coefficient and the Eddy Viscosity Coefficient. For the morphodynamic simulation, dozens of parameters have to be set. The calibration will be concentrated on

grain size distribution and entrainment factor in this study. Field data will be used to calibrate those important parameters to find the best values. Detailed results will be introduced in the following sections.

It should be mentioned that the morphological time step is a multiple of the flow simulation to save the computation time, because the rates of erosion and sedimentation are small and the changes in bed per time step of flow simulation are insignificant for changes of velocities on the flow time step base.

Table 3-2 Main parameters in TIMOR

Parameter (symbol/abv.)	Parameter description	Values
FC*	Friction coefficient	0.0012
EF*	Entrainment factor	1.2 (dry season) 1.5 (wet season)
EVC*	Eddy viscosity coefficient	10
GSD*	Grain size distribution	in Table 3-5
Density (t/m^3)	Sediment grain density	2.65
Porosity	Sediment grain porosity	0.3
Density (t/m^3)	Flow medium density	1
Initial value	Suspended load concentration	0
Erosion factor	Bank stability criteria	
Angle of repose	Bank stability criteria	> 28°
Zanke (1999,2001)	Sediment transport formula	
Max. velocity	For computing Courant Number	
Max. wave height	For computing Courant Number	
Min. water depth[1] (m)	For dry and wetting criteria	0.2
Min. water depth[2] (m)	For computing bed level change	
MF	Morphological factor	choose
v_{crit} (m/s)	Depth averaged critical velocity	Depends on grain size
w_s (m/s)	Fall velocity	Depends on grain size
Water temperature		17°
Secondary currents		Enable/disable
Transverse sediment transport		Enable/disable
Dredging		Enable/disable
Suspended load transport		Enable/disable
Resuspension		Enable/disable
Dumping of sediments		Enable/disable
Transport of salt		Enable/disable
Time step[1] (s)	For hydrodynamic simulation	4.5
Time step[2] (s)	For suspended load simulation	135
Time step[3] (s)	For bed load simulation	135
Time step[4] (s)	For landslide check	30
Latitude	For calculating Coriolis value	N 31.5°

3.4 Calibration

Numerical models contain parameters which are either representing material or system properties. Mostly the values or data of these parameters are not known and have to be determined by trial and error processes. Material parameters may be determined by experiments; in real systems however, the distribution of material is not well known and the variability of properties is huge. Typical material parameter is the hydraulic conductivity in ground water flow. System parameters are such which are dependent on the state of the system, like turbulence or friction etc. They are represented by parameterized relations. The parameters contained have to be specified a priory and then adapted by iterative model simulation runs in order to obtain reasonably agreeing results in comparison to measurements.

Friction Coefficient (FC) Calibration

To compute flow resistance, different formulae have been developed, what follows is a brief introduction to each formula. The relationship among each is shown in Table 3-3.

Friction is represented by the parameter r in a non-linear formulation. Friction is dependent on the tension stresses at the bed which varies with material; it is also dependent on the velocity profiles and thus turbulence and mixing. So r represents a system parameter which has to estimated and adapted to the actual flow conditions.

Newton-Taylor: $$gI = r_f \frac{uq}{H^2}$$ [dimensionless] (3-12)

Darcy-Weisbach: $$gI = \frac{\lambda}{8}\frac{u^2}{H}$$ [dimensionless] (3-13)

Manning-Strickler: $$gI = \frac{1}{\kappa_{ST}^2}\frac{gu^2}{r^{4/3}} = \frac{1}{\kappa_{ST}^2}\frac{gu^2}{H^{4/3}}$$ [unit: $\frac{m^{1/3}}{s}$] (3-14)

Chezy: $$gI = \frac{gu^2}{C^2 H}$$ [unit: $\sqrt{m}/s$] (3-15)

In TIMOR, there are two ways of treating roughness data, either assume the same value of roughness over the whole area of investigation, the uniform roughness approach, or the vary roughness over the domain if the modeler has a good idea of the variation of the roughness characteristics. Flow resistance due to friction is modeled in TIMOR by using the Newton-Taylor Formula. The Newton-Taylor Formula parameterizes energy loss due to friction through a dimensionless friction coefficient r . Moreover, the loss due to the friction depends on flow velocity and flow depth. According to the past experience for setting FC

(here means r) of Yangtze River simulations, different values of FC (0.0010, 0.0012, 0.0015 and 0.0020) have been tried in the model. Results of the comparisons of the simulated and measured water levels at various sites are shown in Table 3-4. Assessment indexes including the ME (mean error of the simulation), STDEV (standard deviation of the bias between model results and measurements), SE (smallest error), and the RMSE (root mean square error) are applied. From the results, it is found that when friction coefficient is 0.0012 there is the best simulation on the water level.

Table 3-3 Relationship among different friction coefficient formulae (Mewis, 2007)

	Newton-Taylor	Darcy-Weisbach	Manning-Strickler	Chezy
Newton-Taylor	1	$r=\frac{\lambda}{8}$	$r=\frac{g}{\kappa_{ST}^2 H^{1/3}}$	$r=\frac{g}{C^2}$
Darcy-Weisbach	$\lambda=8r$	1	$\lambda=\frac{8g}{\kappa_{ST}^2 H^{1/3}}$	$\lambda=\frac{8g}{C^2}$
Manning-Strickler	$\kappa_{ST}^2=\frac{g}{rH^{1/3}}$	$\kappa_{ST}^2=\frac{8g}{\lambda H^{1/3}}$	1	$\kappa_{ST}^2=\frac{C^2}{H^{1/3}}$
Chezy	$C^2=\frac{g}{r}$	$C^2=\frac{8g}{\lambda}$	$C^2=\kappa_{ST}^2 H^{1/3}$	1

Table 3-4 Results of the friction coefficient calibration

Cases	Stations	ME	STDEV	SE	RMSE
FC=0.0010	WL7 (Zhongjun)	1.349	0.184	0.008	3.903
	WL8 (Lianxinggang)	0.684	0.143	0.006	14.266
	WL5 (Gaoqiao)	1.482	0.205	0.009	4.634
FC=0.0012	WL7 (Zhongjun)	1.336	0.198	0.008	3.987
	WL8 (Lianxinggang)	0.637	0.133	0.006	13.014
	WL5 (Gaoqiao)	1.431	0.229	0.010	4.187
FC=0.0015	WL7 (Zhongjun)	1.342	0.228	0.009	4.146
	WL8 (Lianxinggang)	0.763	0.138	0.006	13.456
	WL5 (Gaoqiao)	1.409	0.263	0.011	4.687
FC=0.0020	WL7 (Zhongjun)	1.492	0.282	0.012	4.439
	WL8 (Lianxinggang)	0.965	0.172	0.007	14.014
	WL5 (Gaoqiao)	1.447	0.311	0.013	4.264

Entrainment Factor (EF) Calibration

One of the important parameters is the entrainment factor which can effect how much sediment will enter into water body from bed. This should be calibrated in the model. The measured SSC (suspended sediment concentration) is used to tune this parameter. Figure 3-4 shows the results of calibration of EF parameter for dry season case. It is found that the EF parameter has great affect on the SSC. From the figure we find the best fit EF parameter is 1.2 (for dry season) whether during spring tide, mean tide and neap tide periods. Another result shows the best fit EF is 1.5 for wet season case.

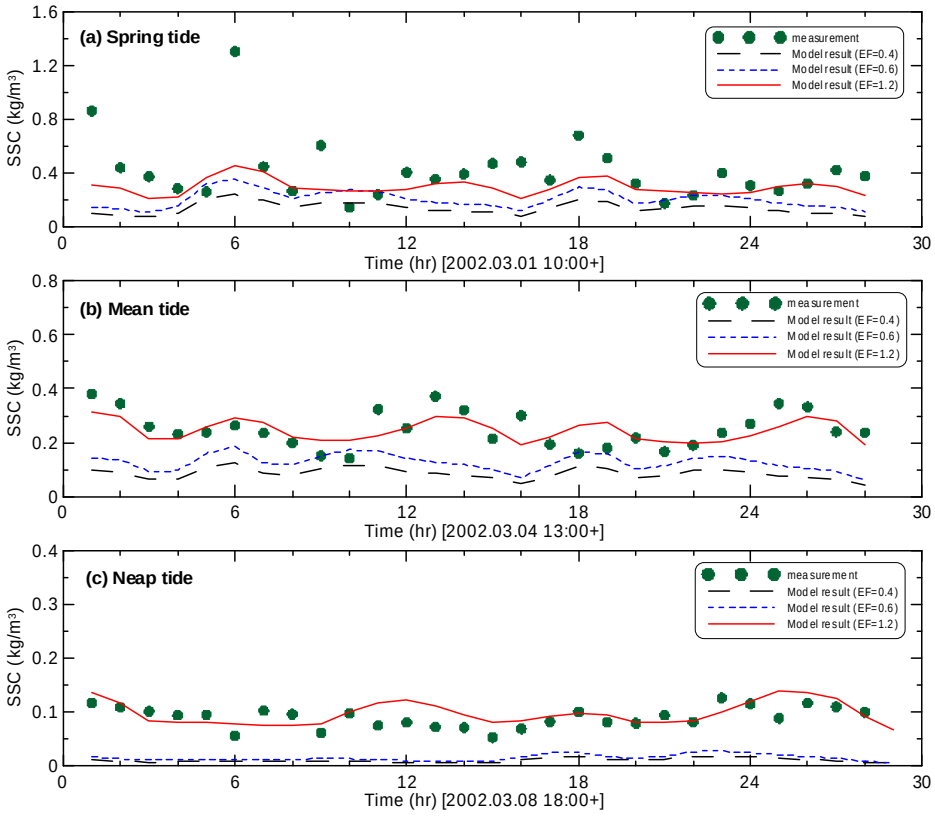

Figure 3-4 Calibration of the model entrainment factor (EF). Results at Station PS2.

Grain Size Distribution Calibration

The other important input data in sediment simulation is the sediment gradation curve, given as series of ordered pairs of points of sediment size and their percentage. TIMOR can handle up to 24 sediment sizes or even more, if needed. Purpose of this calibration is to find an appropriate group of gradation curve as initial value. In this study, two distribution cases have been tried, one is the grain size distribution for coarse sediment, and the other is for fine sediment, as shown in Table 3-5. Each group has a range of medium size using 10 logarithmically distributed fractions. The initial given gradation curve will be reorganized during the calculation by hydraulic sorting.

The results are shown in Figure 3-5. The SSC measurements are from Station PS4 in South Branch (see Figure 2-1). From the figures it is found the case of coarse sediment GSD has better fitting to the field measurements, especially for the spring and mean tide periods. During neap tide period, both cases have similar results. Therefore, the coarse sediment grain size distribution is used in TIMOR for this study.

Table 3-5 Two distribution cases of GSD calibrated in this study

Case 1: coarse sediment										
d_{50}(mm)	0.03	0.08	0.125	0.15	0.24	0.25	0.4	0.7	1.0	1.5
%	5	40	10	20	0	15	4	2	2	2
Case 2: fine sediment										
d_{50}(mm)	0.006	0.008	0.01	0.01	0.01	0.01	0.03	0.04	0.04	0.1
%	10	15	15	10	10	15	5	10	5	5

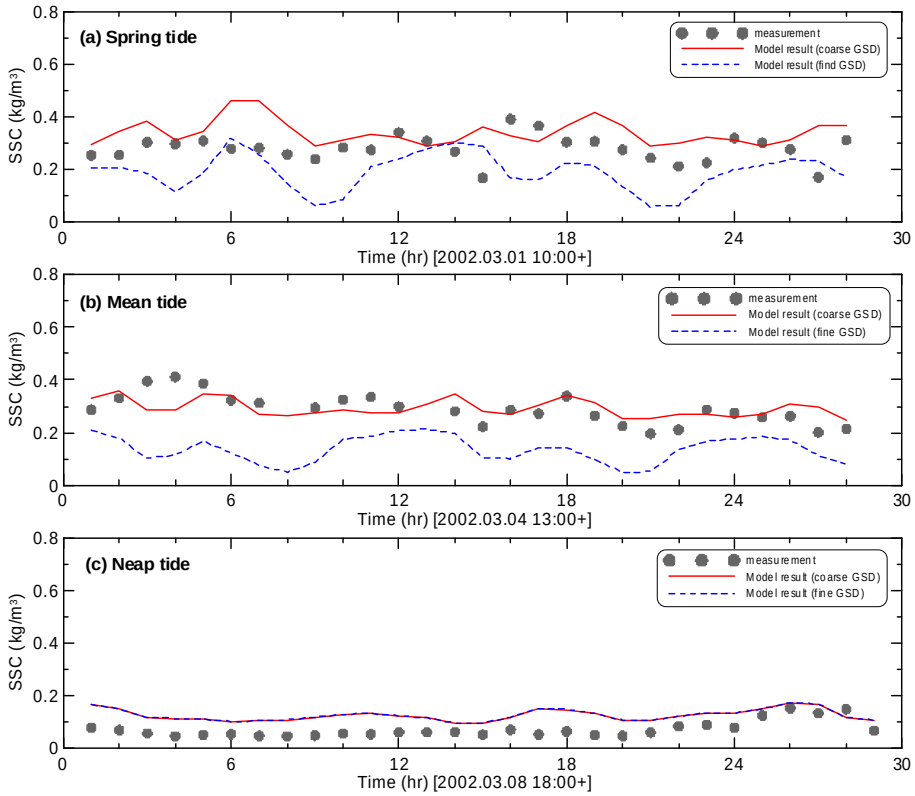

Figure 3-5 Calibration of the model grain size distribution (GSD). Results at Station PS4.

Eddy Viscosity Coefficient (EVC) Calibration

Eddy viscosity presents in first approximation turbulence of flow. Energy contained in turbulent cells decays towards smaller cells by absorbing energy. This process is modeled the decay and specific kinetic energy. Eddy viscosity is anisotropic, and on a rule viscosity is 10 times stronger in flow direction than orthogonal to the flow. However, because of computational expense mostly simplifications are made by taking eddy viscosity constant in all directions. In TIMOR, frequent approach has been taken, which the eddy viscosity remains constant. Four values (0, 1, 10 and 100) are used to tune the model. It is found the best

simulation is when setting eddy viscosity to 10.

3.5 Validation

After the calibration of the model important parameters, this section shows the results of model validation. This work includes the validation on water level, flow velocity, flow direction, and SSC that simulated by TIMOR. Again, field measurements are used to validate the model result. Field data both of dry season from Feb. 24, 2002 to Mar. 31, 2002, and wet season from Sep.1 to Sep 30, 2002 are used. However, the validation data are from different site compared to the calibration process in order to avoid dependent results.

Water level validation

There are 8 water level stations selected for validation of water level simulation. They are WL1 (Xuliujing), WL2 (Chongtou), WL3 (Yanglin), WL4 (Baozhen), WL5 (Gaoqiao), WL6 (Hengsha), WL7 (Zhongjun) and WL8 (Lianxinggang). These stations distribute homogeneous in the model domain. The station locations are shown in Figure 2-1. Validation results are shown in Figure 3-7, which the horizontal axis means the accumulative time from 00:00 on Mar. 11, 2002, the vertical axis is the water level. The solid points are the field data, while solid lines are the simulation results of TIMOR. Since the model stable time needs around 25 hours and the consideration of clear check of the validation results, 10 days simulation results are plotted. This covers the periods of spring tide, mean tide and neap tide.

From Figure 3-6, it is found the model simulation results have very good agreement with the field data in all stations. The water level simulation at WL1 and WL2 have very good agreement with the field data may due to its location is close to the upper boundary. The stations WL7 and WL8 which locate at the river mouth have also good agreement that can be also assumed also to its location at the seaside boundary. However it is found that some stations in the South Branch like WL3, WL4, WL5, and WL6, have a little higher simulation results for the high water level, which may be induced by the value of friction factor. Table 3-6 shows the quantitative results. All the assessment indexes show very small biases between the simulation and measurements. The average of mean square error (MSE) is 0.10m, validating TIMOR has very high performance on the water level simulation.

Table 3-6 Result of water level validation

	MWLE (m)	MAE (m)	MSE (m)	R
WL1: Xuliujing	0.005	0.081	0.074	0.92
WL2: Chongtou	0.006	0.090	0.101	0.92
WL3: Yanglin	0.020	0.150	0.091	0.93
WL4: Baozhen	0.023	0.186	0.127	0.93
WL5: Gaoqiao	0.023	0.176	0.127	0.92
WL6: Hengsha	0.015	0.123	0.111	0.93
WL7: Zhongjun	0.019	0.144	0.116	0.92
WL8: Lianxinggang	0.008	0.061	0.054	0.92

Remark: **MWLE** (Mean Water Level Error); **MAE** (Mean Absolute Error); **MSE** (Mean Square Error); **R** (Correlation Coefficient)

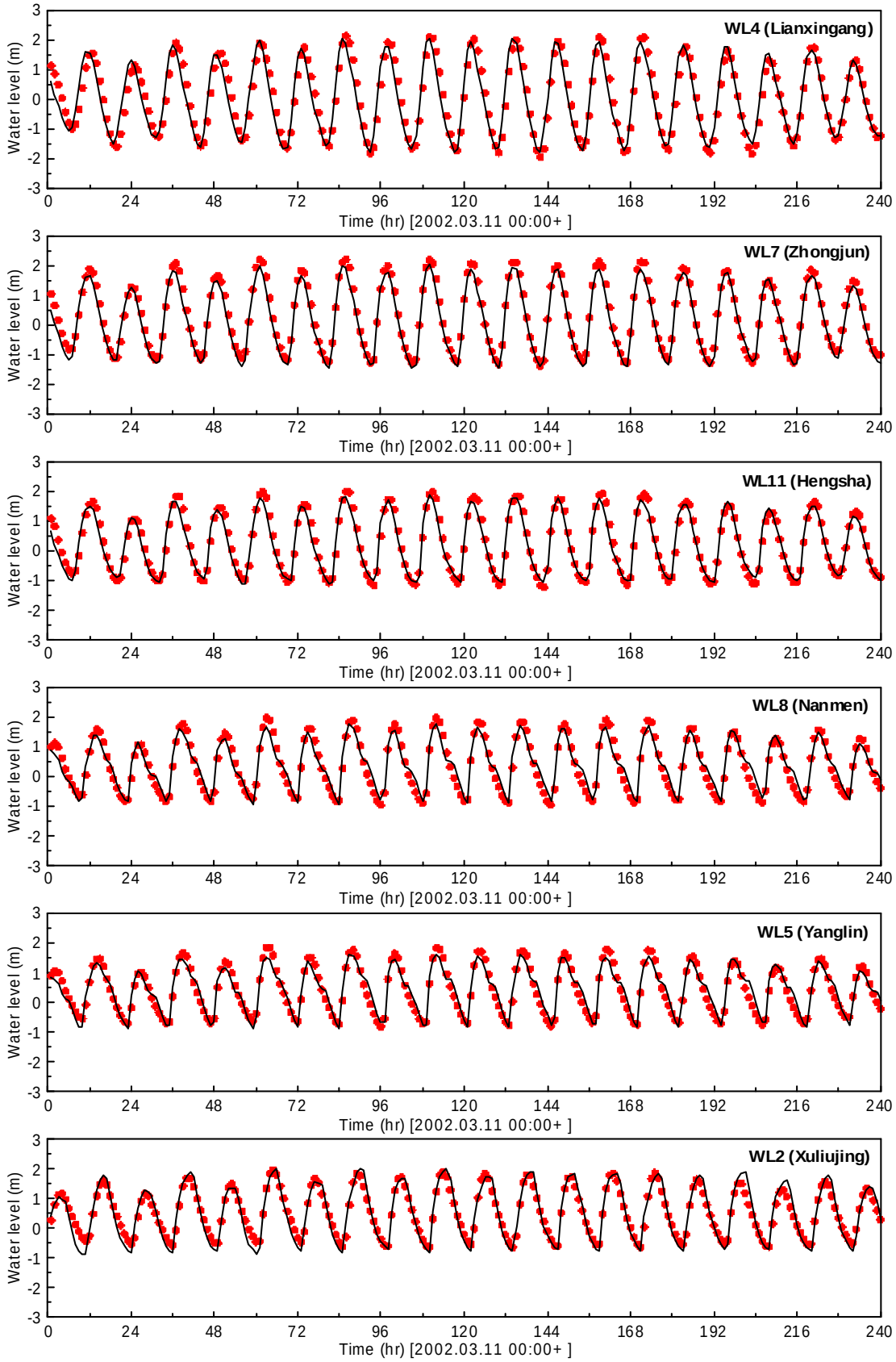

Figure 3-6 Validation of water level simulation

Flow velocity/direction validation

The profile stations (abbreviated by PS) in Figure 2-1 measure the flow conditions including the flow velocity and direction. Again several stations distributed homogeneous in the model domain are used for the flow validation. These stations are PS1 (at upper stream), PS3 (at the bifurcation point of South Branch/North Branch), PS5 (at South Branch), PS8 (at the South Branch mouth), PS9 (at the North Branch mouth) and PS10 (at North Branch). Detail locations are shown in Figure 2-1.

The validation results are shown in Figure 3-7~Figure 3-12. Validation of the flow condition during spring, mean and neap tide periods are included in each figure. Validations of flow velocity and flow direction are both covered. The flow direction is defined as the direction of flowing to with the angle accumulated clockwise from north. Generally, variation of flow condition is not easy. One reason is due to the existing uncertainties in the measurement. Another reason is that the flow velocity obtained from the hydrodynamic model is the depth-averaged vertical velocity that is not the same as measurements.

From the results we found the simulated flow directions are generally close to the measurements, except the station PS10. PS10 is located at the upper reach of North Branch. At this area, serious saltwater intrusion was observed. Discharge at PS10 has large variation. These are all possible reasons to explain the poor hydrodynamic simulation near PS10. However the flow simulation for the lower reach of North Branch (station PS9) has very good result on the flow direction simulation as well as the flow velocity simulation. Regarding to the flow velocity simulation at other stations, the results are very satisfied. Better simulation is found for the cases during mean tide period, such as at PS5, PS8 and PS9. Simulations for both spring tide and neap tide periods show good mostly agreements with field measurements. Table 3-7 gives the quantitative results. The values show the mean flow velocity error (MFVE) over the simulation period is 0.093 m/s (for spring tide period), 0.077 m/s (for mean tide period), and 0.063 m/s (for neap tide period). This is the statistics exclude the station PS10. PS5 where locates at the main stream of South Branch has the best simulation results. The mean absolute error (MAE) on flow direction simulation is 5.5^{o}, 7.1^{o}, and 9^{o} for spring, mean and neap tides respectively. Simulation of the flow direction at neap tide period raises higher error that may be due to less water in the river channel. However the error is less than 10^{o} which is satisfied in this study.

Table 3-7 Results of the flow velocity and direction validation

Location	Period	Flow velocity validation			Flow direction validation	
		MFVE	MAE	MSE	MAE	Sd.
PS1	Spring tide	0.017	0.258	0.138	6.1	4.6
	Mean tide	0.121	0.434	0.292	5.6	4.4
	Neap tide	0.102	0.276	0.103	9.3	7.7
PS3	Spring tide	0.165	0.354	0.184	4.8	3.3
	Mean tide	0.074	0.334	0.150	8.5	6.2
	Neap tide	0.012	0.253	0.105	4.3	3.8
PS5	Spring tide	0.122	0.204	0.072	8.8	4.6
	Mean tide	0.049	0.186	0.057	11.9	5.5
	Neap tide	0.019	0.182	0.056	5.1	5.4
PS8	Spring tide	0.058	0.289	0.143	4.9	3.4
	Mean tide	0.021	0.144	0.034	5.9	3.0
	Neap tide	0.117	0.218	0.066	8.1	5.4
PS9	Spring tide	0.103	0.303	0.176	3.0	1.7
	Mean tide	0.121	0.233	0.099	3.7	2.2
	Neap tide	0.065	0.227	0.076	18.2	11.3
PS10	Spring tide	0.451	0.521	0.476	58.1	42.9
	Mean tide	0.313	0.353	0.169	32.2	33.3
	Neap tide	0.521	0.523	0.342	43.3	40.1

Note: **MFVE** (Mean Flow Velocity Error); **MAE** (Mean Absolute Error); **MSE** (Mean Square Error); **Sd.** is the standard deviation.

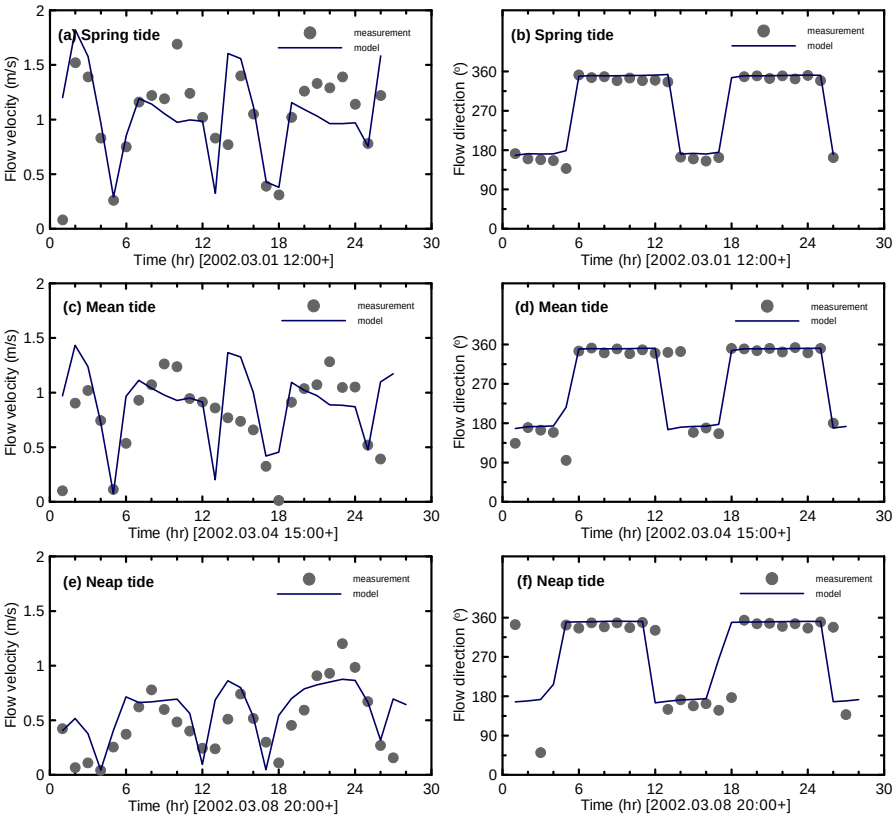

Figure 3-7 Validation of flow simulation at PS1 (Location: South Branch upper stream)

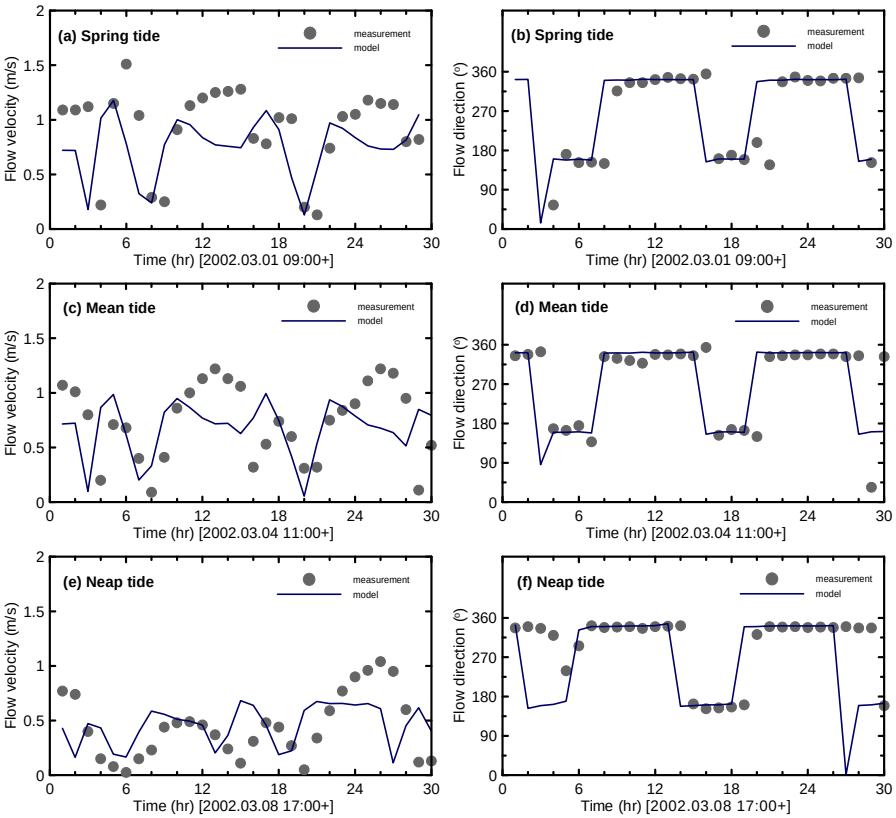

Figure 3-8 Validation of flow simulation at PS3 (Location: bifurcation point of South Branch/North Branch)

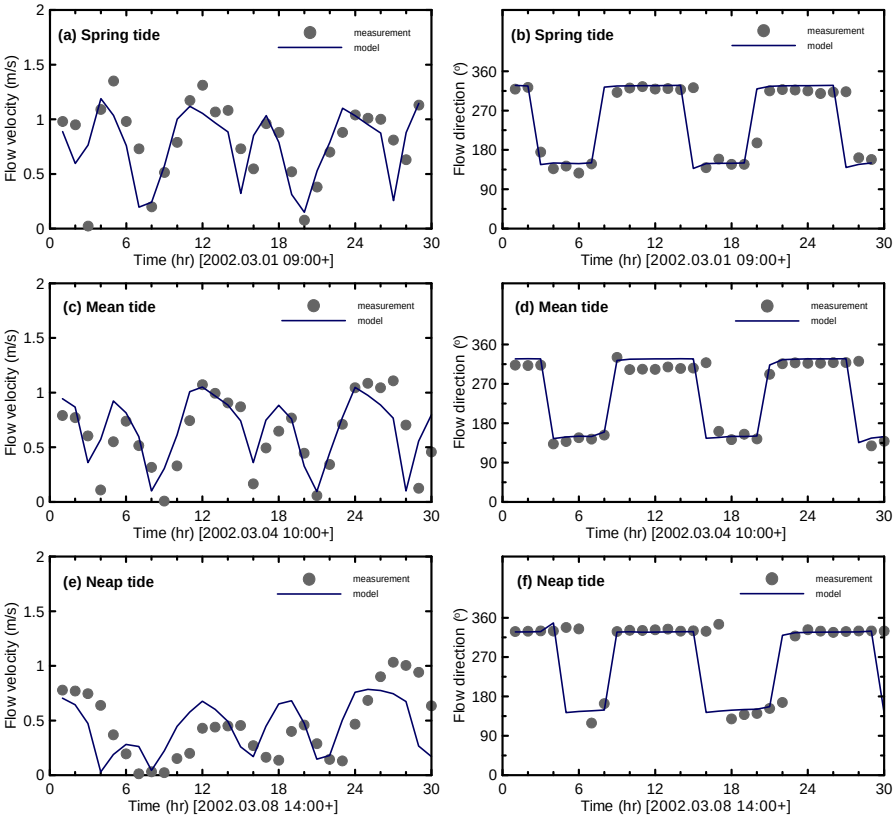

Figure 3-9 Validation of flow simulation at PS5 (Location: South Branch main stream)

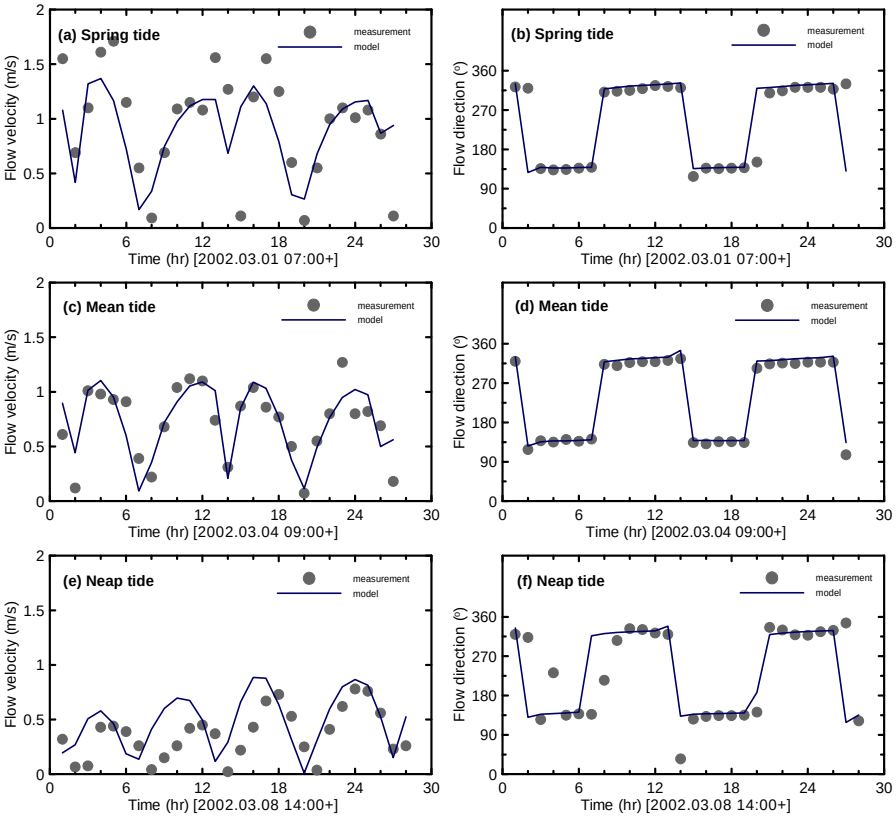

Figure 3-10 Validation of flow simulation at PS8 (Location: South Branch river mouth)

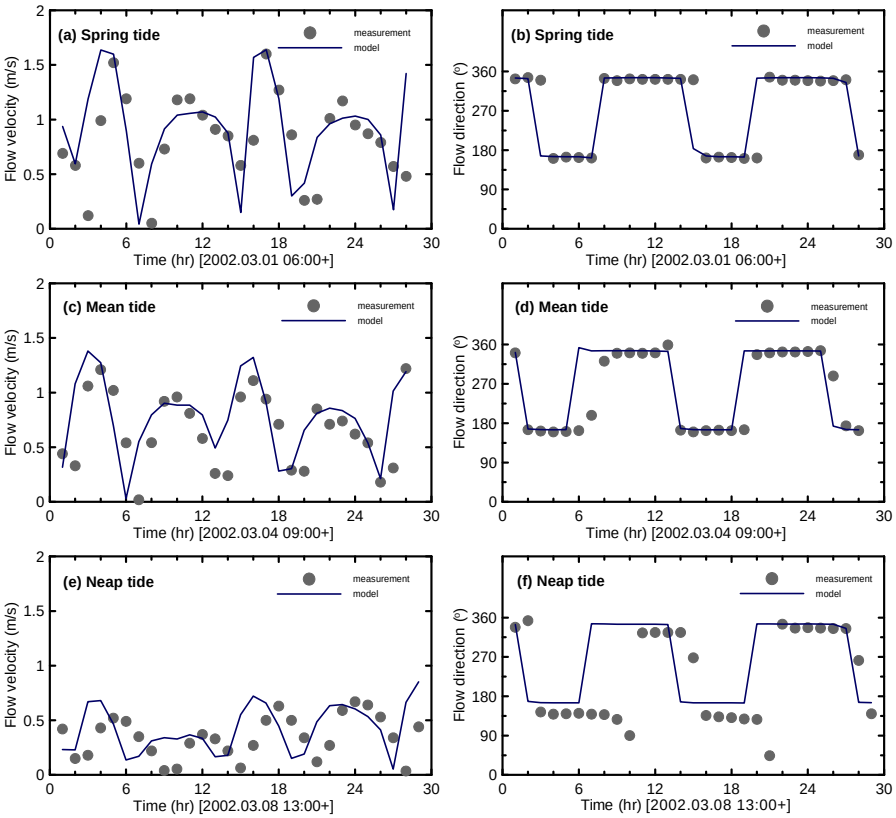

Figure 3-11 Validation of flow simulation at PS9 (Location: North Branch river mouth)

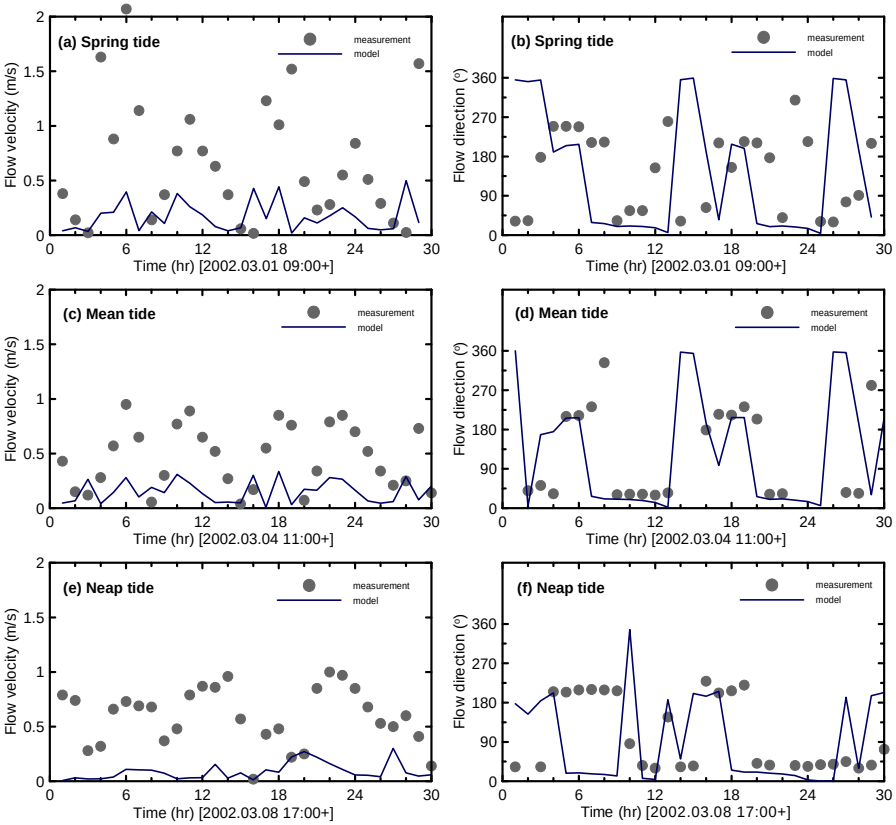

Figure 3-12 Validation of flow simulation at PS10 (Location: North Branch upper stream)

SSC validation

From the experiences and also from many previous studies, the SSC is the most difficult hydrodynamic parameter to be simulated because of the SSC is affected by many factors like the waves, the salt water, and the flocculation. Field data from Stations PS3 (bifurcation point of South Branch/North Branch), PS4 (upper reach of South Branch), PS5 (main stream of South Branch), and PS9 (North Branch river mouth) are used for SSC validation. The results are shown in Figure 3-13~Figure 3-16. The results show reasonable trend on the SSC simulation. The quantity of SSC simulation in this study is in the same scale of field measurement. Station PS5 at the main stream of South Branch shows the best SSC simulation result, for spring, mean and neap tide periods. At PS9, where locates at North Branch river mouth, has relative higher bias to the measurements. Compare to the other stations, PS5 locates at relative simple environment. Taken as a whole, the results of SSC validation are in the reasonable scale and satisfied in this study.

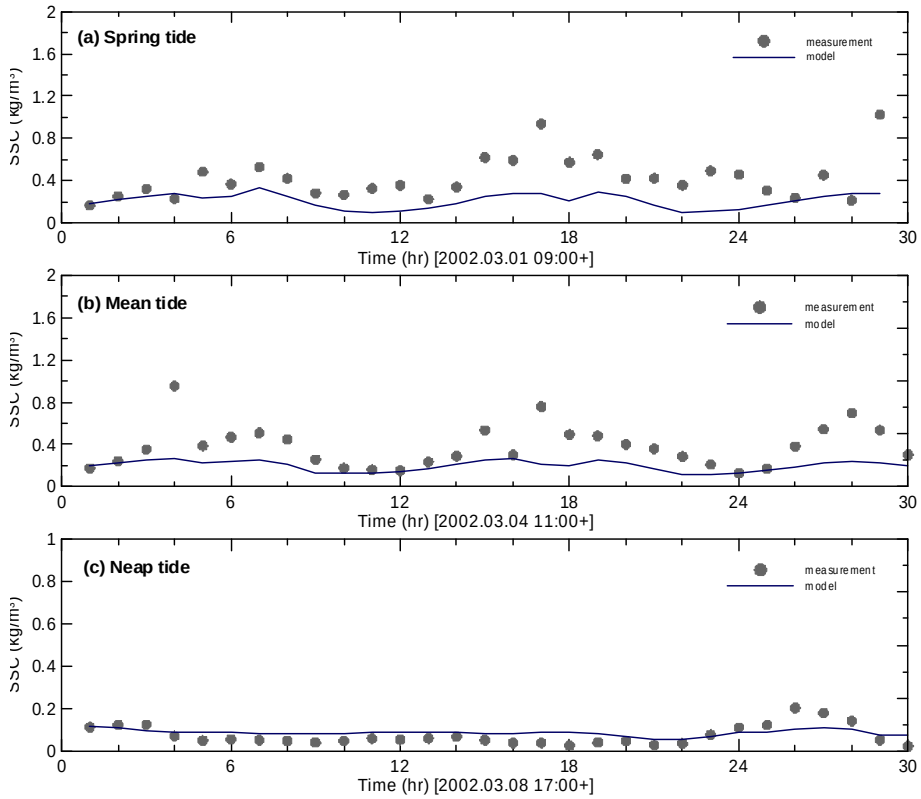

Figure 3-13 Validation of SSC simulation at PS3 (Location: bifurcation of South Branch/North Branch)

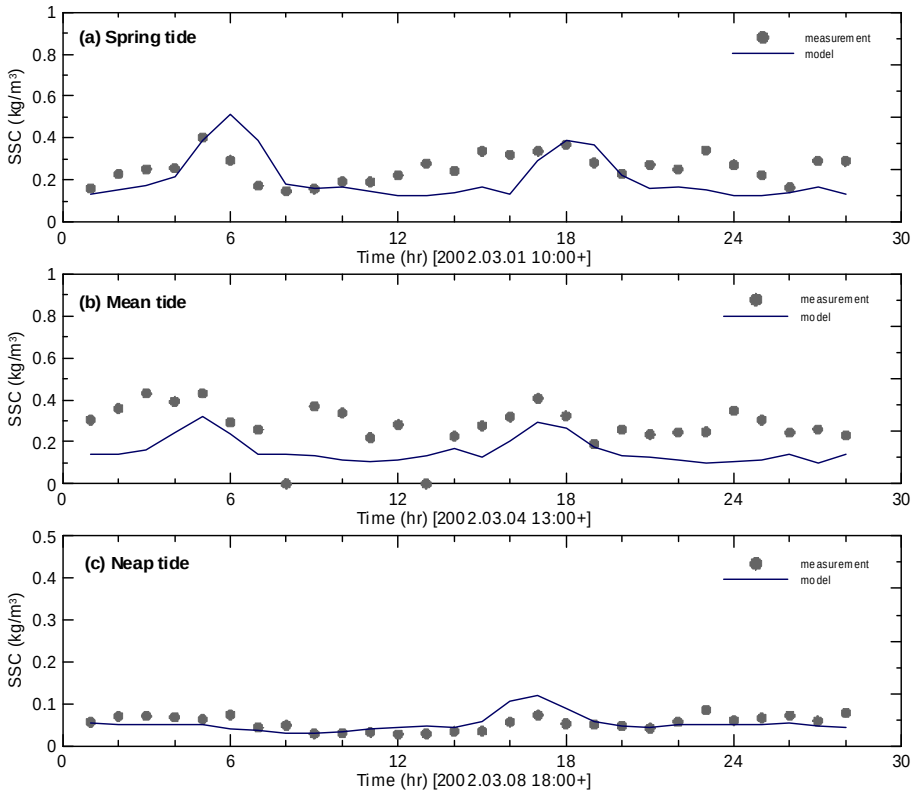

Figure 3-14 Validation of SSC simulation at PS4 (Location: upper stream of South Branch)

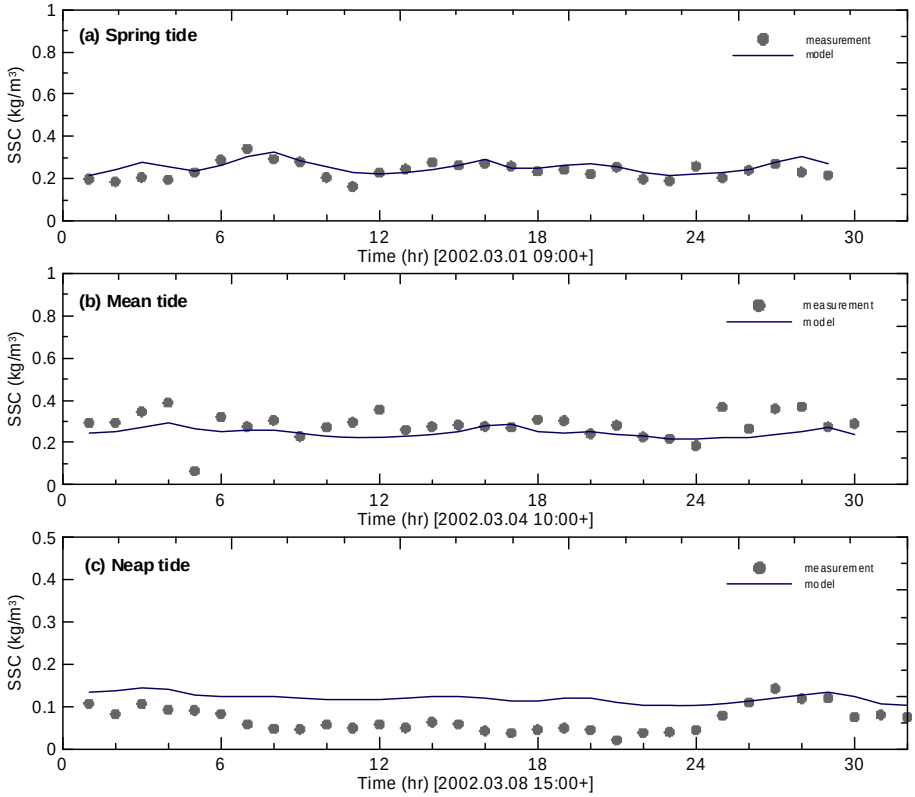

Figure 3-15 Validation of SSC simulation at PS5 (Location: main stream of South Branch)

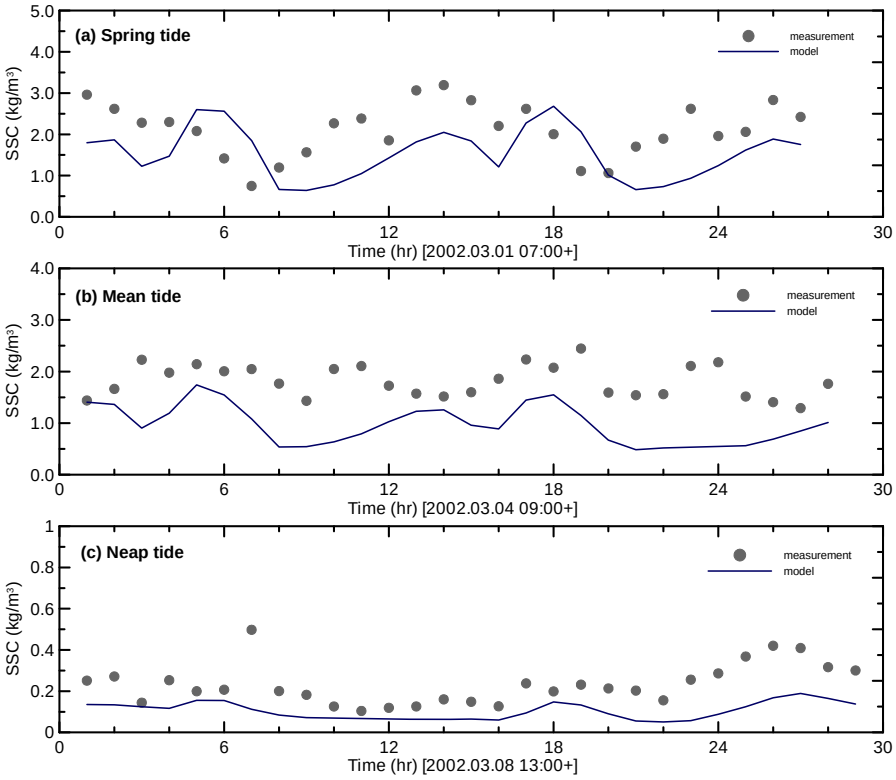

Figure 3-16 Validation of SSC simulation at PS9 (Location: North Branch river mouth)

3.6 Morphological simulation by TIMOR 3

The numerical simulation, comparing to the field measurement and physical model, can present the spatial distribution of physical quantity. In this study, the process-based morphological model TIMOR 3 after fully validation and calibration is used to examine the hydrodynamic characteristics and bathymetry changes of Yangtze River Estuary in huge domain.

3.6.1 Calculated flow patterns

Residual sediment transport is influenced by tidal asymmetry, residual currents and diffusion. Understanding the hydrodynamic processes is therefore an essential precondition for an evaluation of the sediment transport problem. In fact, the accuracy of cohesive sediment transport prediction is strongly contingent upon the degree of accuracy with which the flow field is described (Mehta et al., 1989). The hydrodynamic and sediment conditions in Yangtze Estuary, as illustrated in chapter 2, is a very complex system, due to the effects of estuarine shape, river discharge, bottom and bank friction, etc. The simulated results of hydrodynamics at initial stage are analyzed as follows for better understanding the sediment processes. Due to the great seasonal variation of runoff in Yangtze River, two groups of calculations are carried out, based on the upper boundary at WL0 (Jiangyin, see Figure 2-1) with water discharge from dry season (Feb.22 0:00-Mar.22 4:00, 2002) and from wet season (Sep.01 0:00-Sep.30 4:00, 2002). The seaward boundaries with tidal level were located in -50m isobath of East China Sea, far away from the upper boundary, to minimize the effect of boundary conditions on water and sediment transport within the area of interest.

Figure 3-17 to Figure 3-20 show the strength and directions of the flow velocity during spring tide and neap tide in dry season. Figure 3-21 to Figure 3-24 show the flow velocity during spring tide and neap tide in wet season. In those figures, the length of these triangles represents the strength of the velocity. Since the tidal current meets the river runoff while entering into the Yangtze Estuary as it propagates upstream along the channels, the tidal shape transforms, thus it is unable for the whole domain to reach maximum ebb velocity or flood velocity simultaneously. Here we set the water level observation station WL7 (Zhongjun) as a reference point. The strengths and directions of the current velocities are plotted when the WL7 reaches Maximum Ebb Velocity (MEV) or Maximum Flood Velocity(MFV) during spring tide, neap tide in dry season and wet season respectively.

From the figures we can see that, the tide comes into the estuary from a direction between south and east, and leaves the estuary from a direction between north and west. The tidal current in the South Channel and North Channel is to-and fro flow, while in the South Passage and North Passage or in the lower stream of Hengsha Island it transforms into rotary flow with clockwise.

The flow velocities during spring tide in the Yangtze Estuary are notably greater than the velocities during neap tide. The velocities in wet season are greater than those in dry season.

In dry season during spring tide and neap tide, the average velocities of tidal current are around 0.5m/s and 0.3m/s respectively. In wet season during spring tide and neap tide, the average velocity of tidal current are about 1m/s and 0.4m/s respectively.

The time series of the water level and velocity at WL7 show that there is a 1-3 hours phase lag between the water level and velocity. The maximum ebb velocity during spring tide in dry season happens at 150.75hour but the minimum water level happens 1.5hours later, at 152.25hour. The maximum flood velocity during spring tide in dry season happens at 154.5hour but the maximum water level happens 2.25hours later, at 156.75hour. The ebb tide duration is generally longer than the flood tide duration. This agrees with previous studies based on field measurements (Milliman, 1983; He, 2003; Gao, 2008), which revealed that, the maximum velocities of ebb currents are usually observed on the flow surface just before the minimum water level is reached during the ebb tide. Minimum (or maximum backflow) current velocities are observed just before the maximum water level is recorded during the tide.

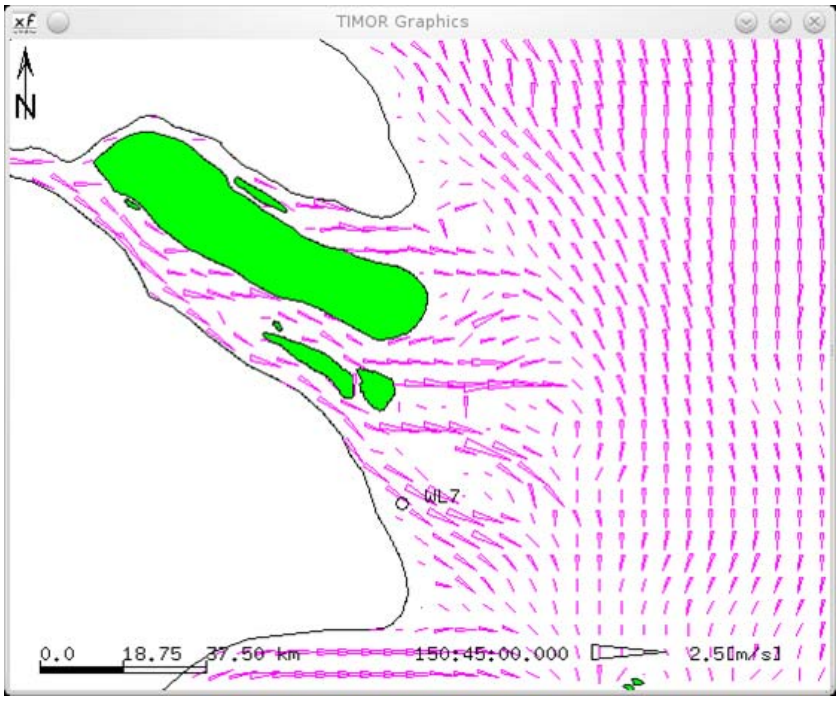

Figure 3-17 Calculated flow velocity during spring tide in dry season
At 05:45 Feb.28, 2002 (150.75h), when WL7 reaches Maximum Ebb Velocity (0.951m/s)

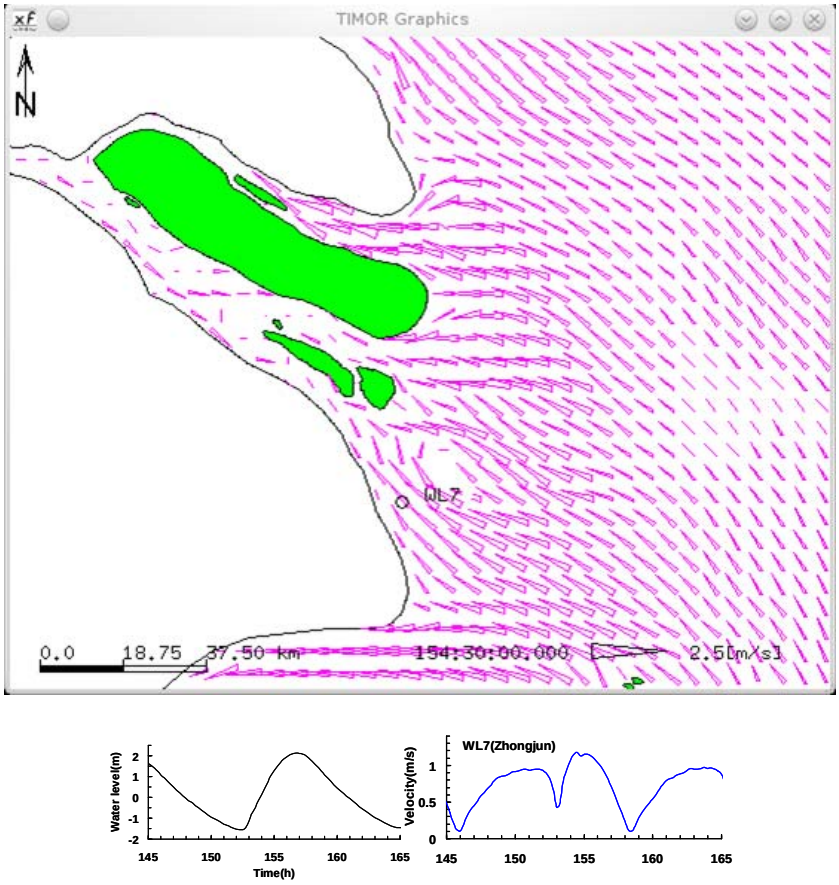

Figure 3-18 Calculated flow velocity during spring tide in dry season
At 09:30 Feb.28, 2002 (154.5h), when WL7 reaches Maximum Flood Velocity (1.176m/s)

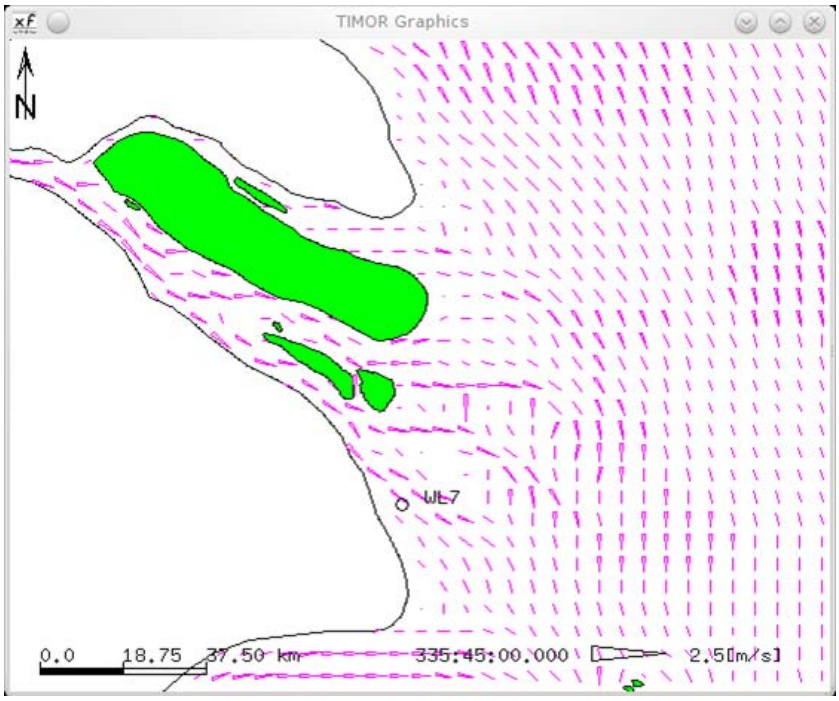

Figure 3-19 Calculated flow velocity during neap tide in dry season

At 22:45 Mar.07, 2002 (335.75h), when WL7 reaches Maximum Ebb Velocity (0.586m/s)

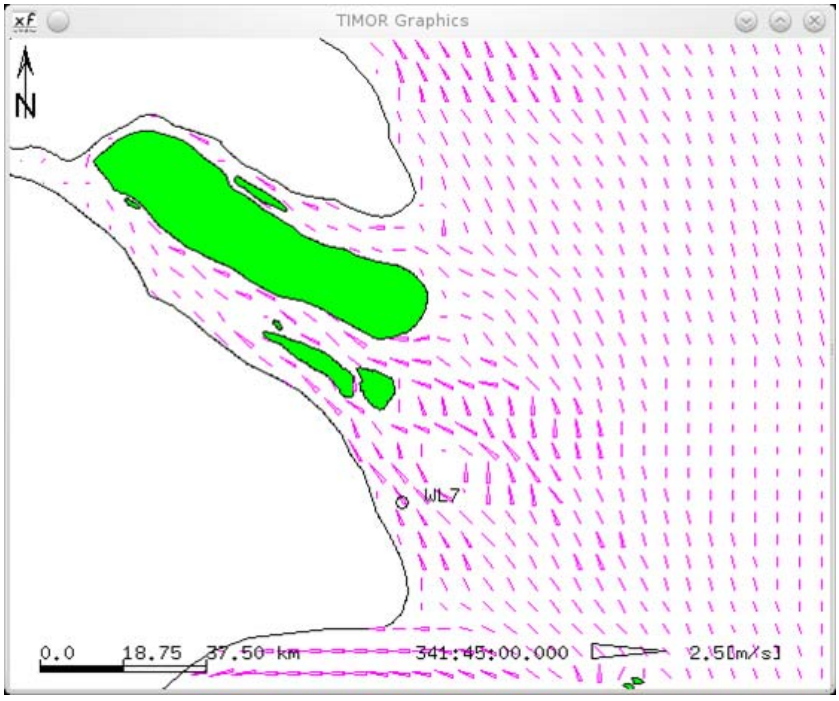

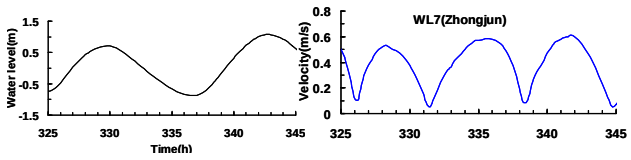

Figure 3-20 Calculated flow velocity during neap tide in dry season

At 04:45 Mar.08, 2002 (341.75h), when WL7 reaches Maximum Flood Velocity (0.611m/s)

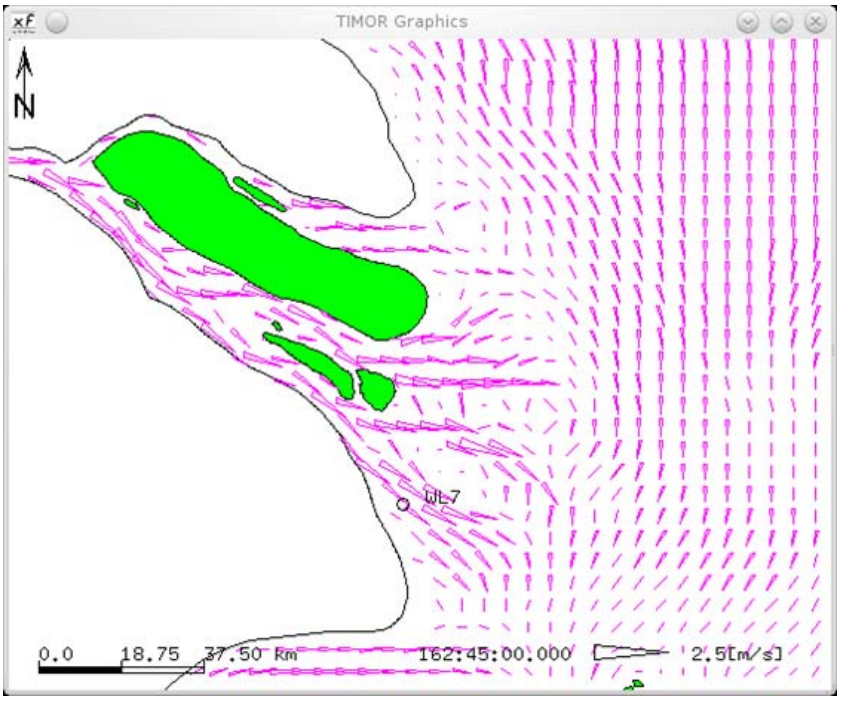

Figure 3-21 Calculated flow velocity during spring tide in wet season

At 17:45 Sep.07, 2002 (162.75h), when WL7 reaches Maximum Ebb Velocity (1.284m/s)

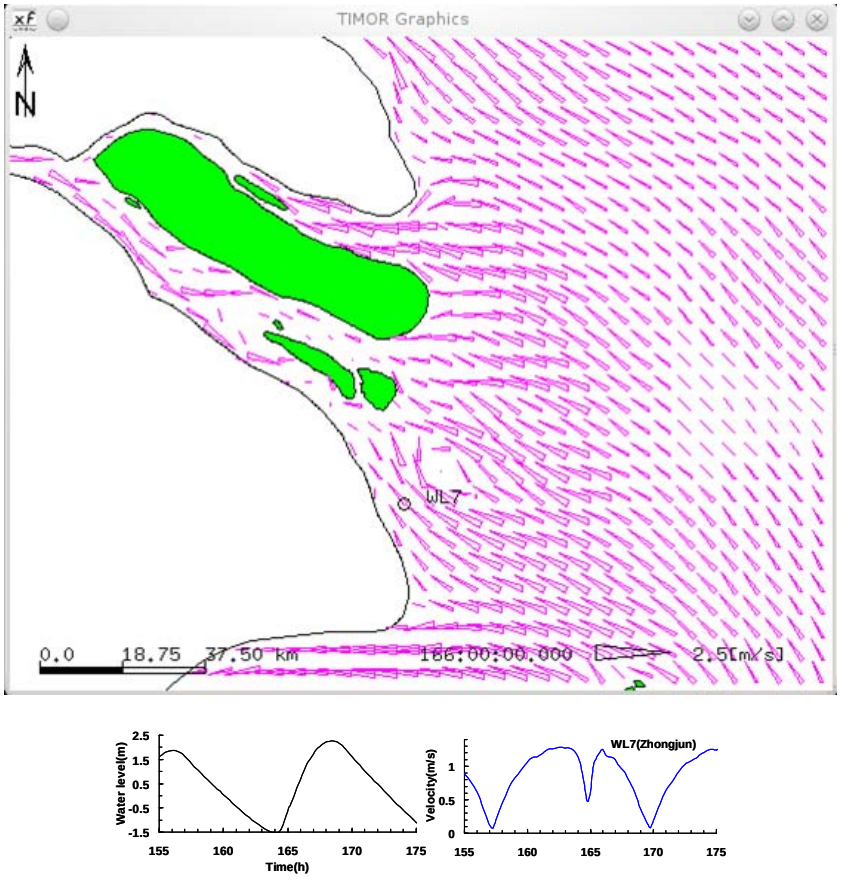

Figure 3-22 Calculated flow velocity distribution during spring tide in wet season

At 21:00 Sep.07, 2002 (166h), when WL7 reaches Maximum Flood Velocity (1.253m/s)

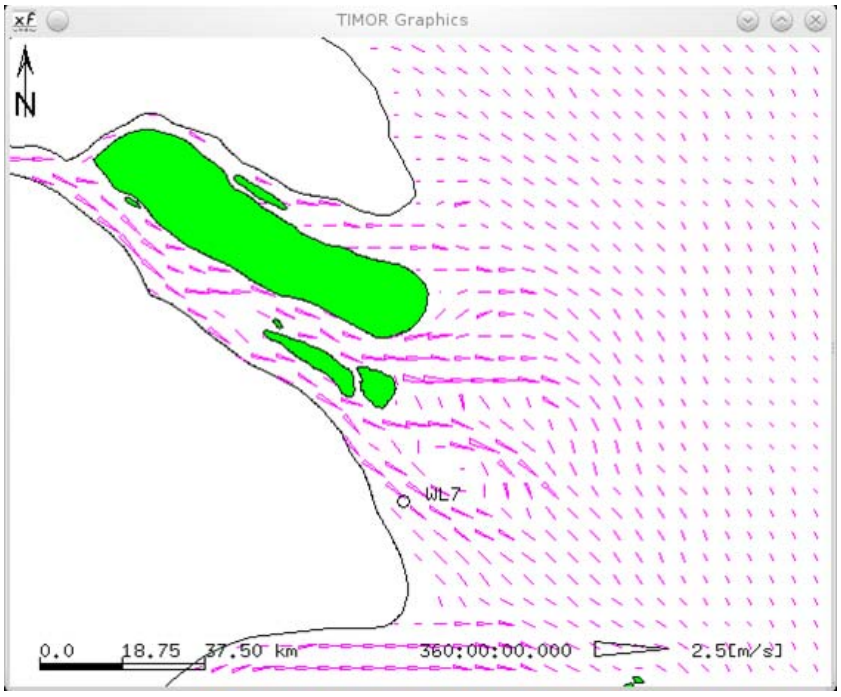

Figure 3-23 Calculated flow velocity during neap tide in wet season

At 23:00 Sep.15, 2002 (360h), when WL7 reaches Maximum Ebb Velocity (0.543m/s)

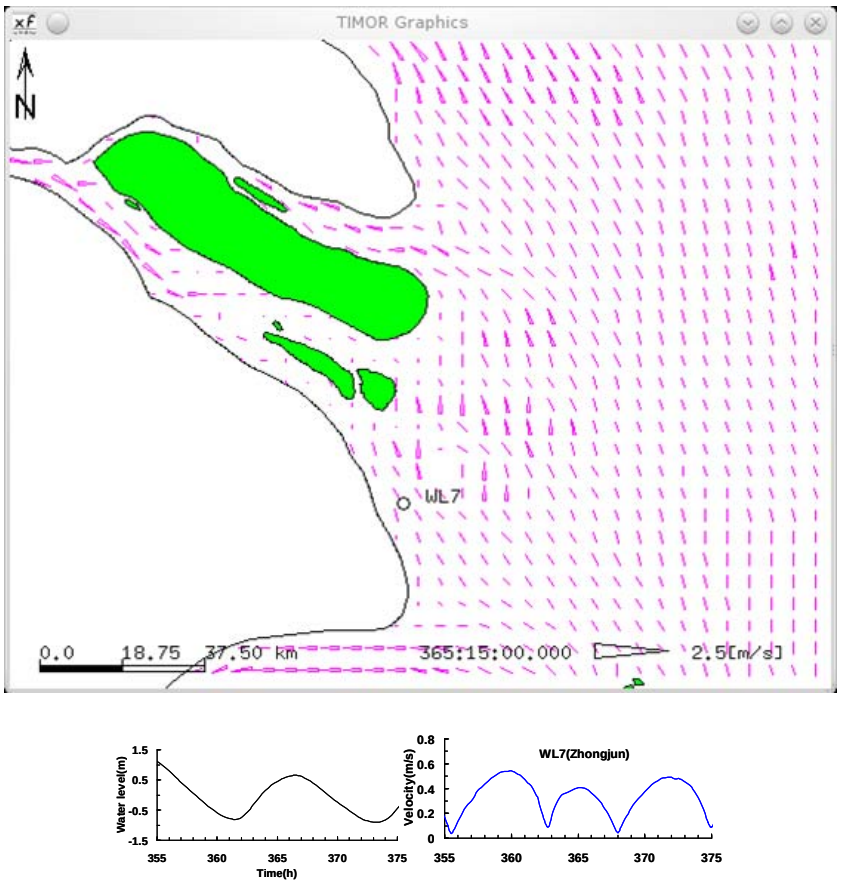

Figure 3-24 Calculated flow velocity during neap tide in wet season

At 04:15 Sep.16, 2002 (365.25h), when WL7 reaches Maximum Flood Velocity (0.406m/s)

3.6.2 Sediment simulation

Suspended Sediment Concentration (SSC)

Calculated suspended sediment concentration as well as the flow velocity of Yangtze Estuary during spring tide and neap tide in wet season is shown in Figure 3-25. The range of SSC is almost between 0 and 2.5kg/ m^3, with high SSC in the lower section of North Branch and North Channel, in the South Passage, and the Jiuduansha shoal (position see in Fig. 2-1).

During spring tide, the flood tide brings sediment into all channels of Yangtze Estuary. The velocity in North Branch reaches about 1m/s but the SSC in the lower section reaches 2.5 kg/m^3. The shoal between North Branch and North Channel has SSC ranging from 1.5 kg/m^3 to 2.5 kg/m^3. The whole North Passage has SSC more than 1.5 kg/m^3, especially in the lower section of it, which reveals that the strength of flood tide decreased. The whole Jiuduansha has high SSC, with some areas more than 2.5 kg/m^3, which could be explained by that, not only the flood tide transport sediment in this area but also the wind and waves lift the fine cohesive sediment into water column. It is of interest to notice that the SSC in the upper section of South Branch is comparatively high. The velocity direction reveals the fact that, when WL7 reaches the maximum flood velocity, the upper section is still under ebb tide. So the high SSC is carried by the ebb tide. This matches well with previous studies in chapter 2, that the range of tidal current influence is about 240km from the river mouth, while the upper boundary WL0(position see in Fig.2-1), which has a mean tidal range of 1.64m (see in Tab. 2-3), is just 240km away from the river mouth.

During spring tide, the ebb tide brings the sediment back to the seaside along the main channels. The whole area is under ebb tide. The South Passage, the North Passage, the North Channel as well as partial of the North Branch are under high SSC over 2 kg/m^3. The high SSC area shows the route as well as the strength of the ebb tide. It is obvious that much ebb tide flows into the North Channel, which, from the other side of view, will weaken the dominant position of ebb tide in the South Channel. But the ebb tide in the North Passage is stronger than that in the South Passage from the prospect of SSC. Generally speaking, the SSC during flood tide is higher than during ebb tide.

The SSC during neap tide is lower than that during spring tide. During neap tide, there is no big difference of SSC under flood tide or under ebb tide. The average SSC in main high SSC areas during spring tide are about 0.5 kg/m^3 bigger than during neap tide. The average SSC in other areas during spring tide are about 0.2 kg/m^3 bigger than that during neap tide. The North Branch has lower SSC both in flood tide and ebb tide, which show the weak current power in this area. Comparing the velocity in figure 3-25 (a) and (c), it can be found that during spring tide, the ebb tide in the upper stream meet the flood tide at WL5 (Gaoqiao, 80km from the river mouth), but they meet each other at WL3 (Yanglin, 130km from the river mouth) during neap tide. Comparing to spring tide, the flood tide has stronger power than the ebb tide during neap tide.

The calculated SSC during wet season in Yangtze Estuary is generally from 0.2kg/m^3 to 1.0kg/m^3, except for the shoals and some specific high SSC areas. This results match well with the statistics of monthly sediment concentration from 1950-2006 (see Tab.2-4), which shows that the average sediment concentration in wet season is between 0.339kg/m^3 and 0.705kg/m^3. The SSC is greatly influenced by tide propagation and it is in proportion with the current velocity. The depth-averaged flow velocity and SSC distribution show that, the SSC in Yangtze Estuary is higher during flood tide than during ebb tide, as well as higher during spring tide than during neap tide.

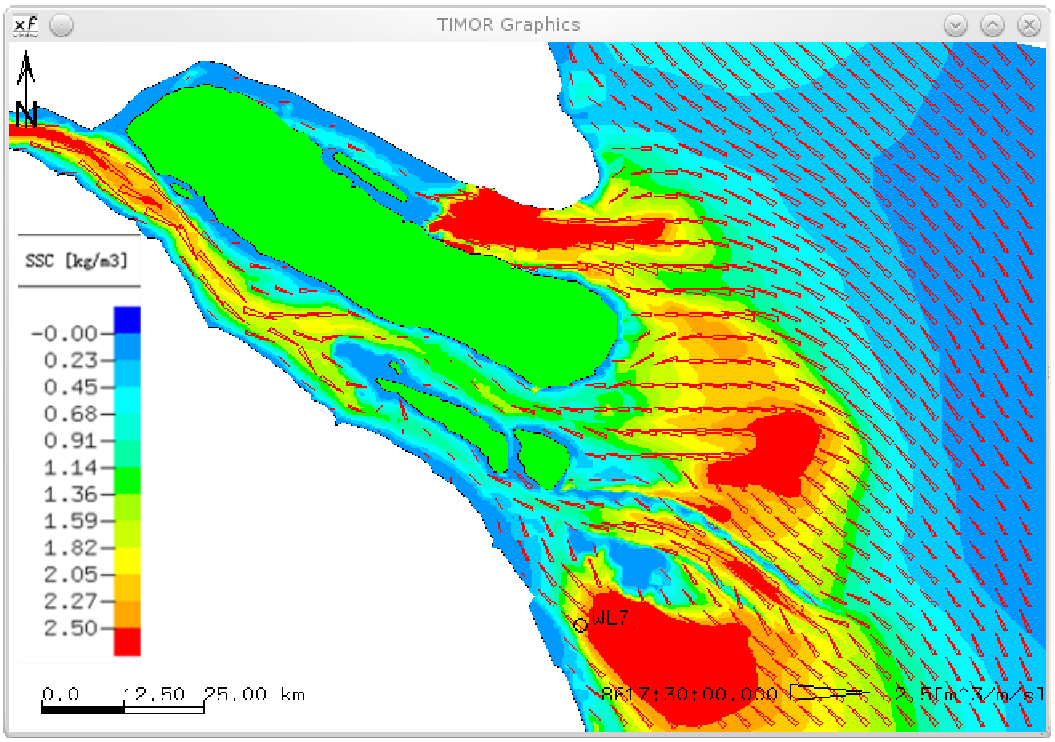

Figure 3-25(a) Depth-averaged flow velocities (m/s) and SSC (kg/m^3)
during spring tide, when WL7 reaches Maximum Flood Velocity (1.17m/s)
(triangles show flow velocity; color shows SSC)

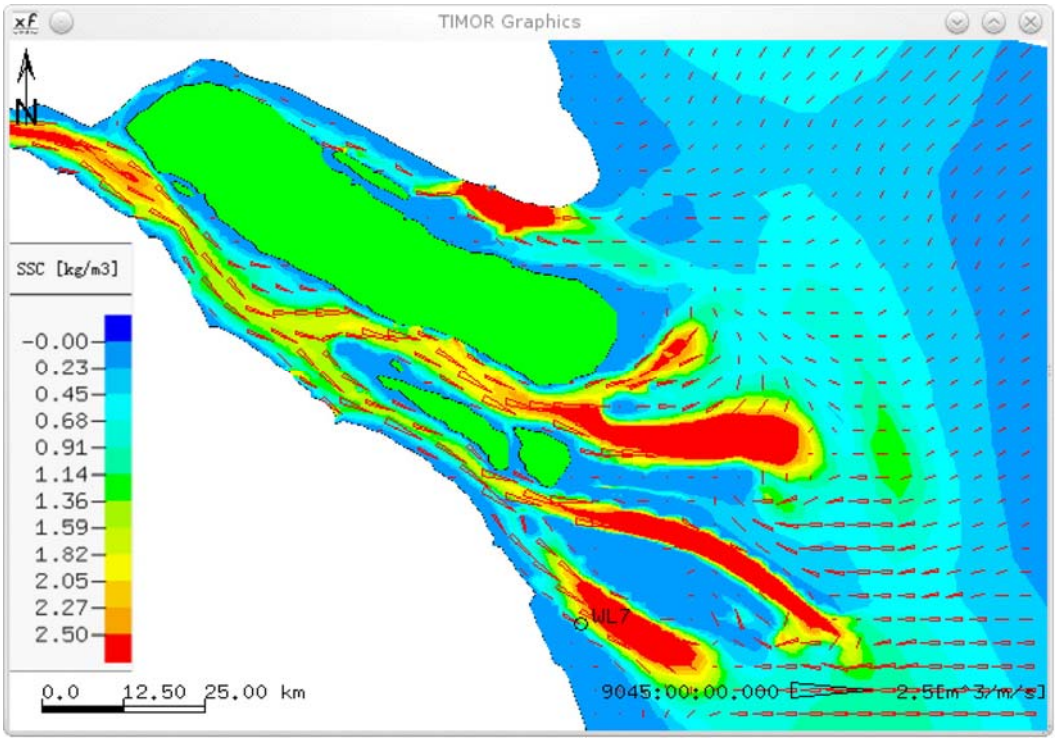

Figure 3-25(b) Depth-averaged flow velocities (m/s) and SSC (kg/m^3)
during spring tide, when WL7 reaches Maximum Ebb Velocity (1.07m/s)
(triangles show flow velocity; color shows SSC)

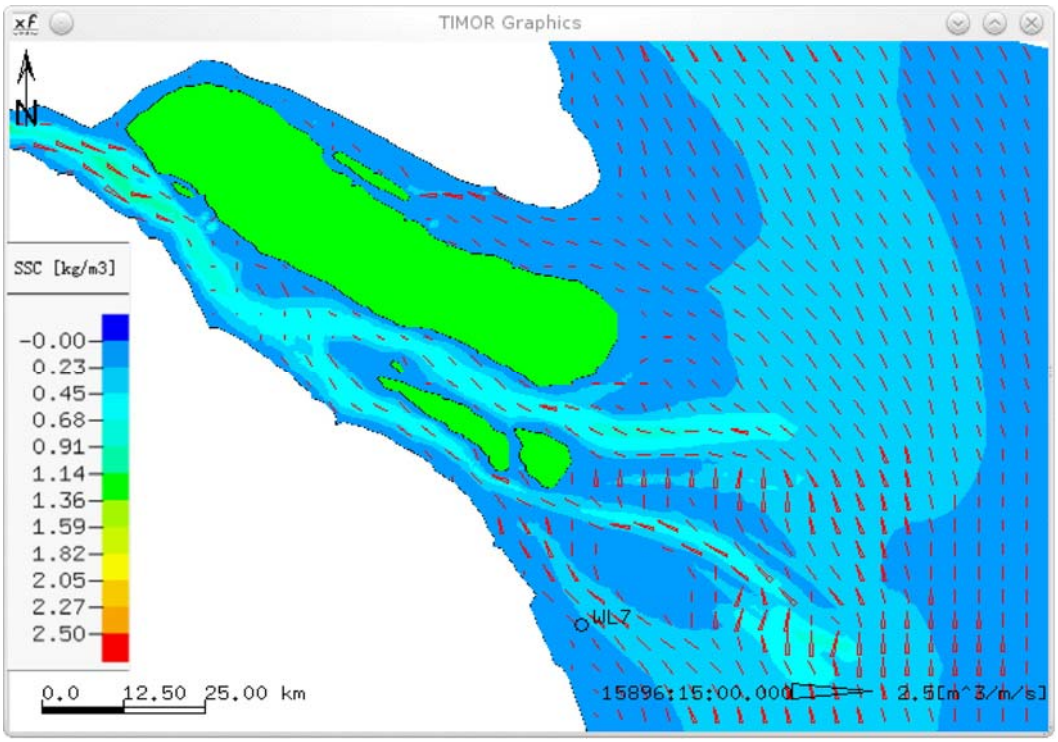

Figure 3-25(c) Depth-averaged flow velocities (m/s) and SSC (kg/m^3)
during neap tide, when WL7 reaches Maximum Flood Velocity (0.71m/s)
(triangles show flow velocity; color shows SSC)

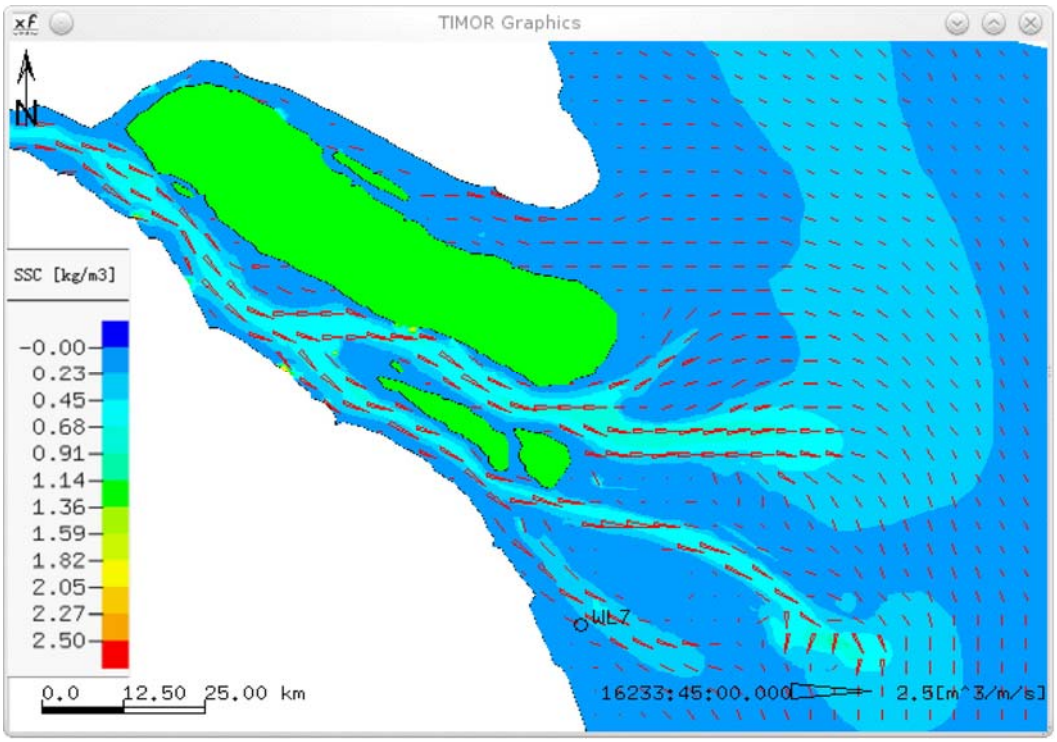

Figure 3-25(d) Depth-averaged flow velocities (m/s) and SSC (kg/m^3)
during neap tide, when WL7 reaches Maximum Ebb Velocity (0.74m/s)
(triangles show flow velocity; color shows SSC)

Grain size distribution d_{50} of bed load

Figure 3-26 show the calculated results of medium grain size (d_{50}) distribution of bed load, which developed in the model by hydraulic sorting itself, starting from well mixed initial conditions (Fig3-26a). Figure 3-26 (b), (c), (d) are calculated results at 3 years, 6 years and 9 years respectively. The initial gain size distribution as input data is taken as the case 1 in Table 3-5. The size and percentage of each size is assumed according to the statistics of averaged grain size. The well mixed initial conditions of grain size distribution shows no big difference among these channels. However, the South Branch has bigger grain size of bed load than other channels, which matches well with the field data analysis in chapter 2.

The distribution pattern in figure 3-26 (b), (c) and (d) are similar. The grain size noticeably decreases from the channel to the mouth area. The sediment along the main current route is coarser than those areas near the river bank, which is especially obvious in the South Branch. The North Channel, North Passage and South Passage have grain size about 0.13mm, but as time goes on, the grain size of South Passage is getting smaller. The North Branch has grain size about 0.08mm with no significant changes as time increases. It is of interest to find that at the end of North Passage, an area with grain size more than 0.2mm is growing up. The current velocity in Figure 3-25 could explain one of the reasons, in that the ebb tide is strong in this area, which takes away the sediment into sea and remains the coarse ones.

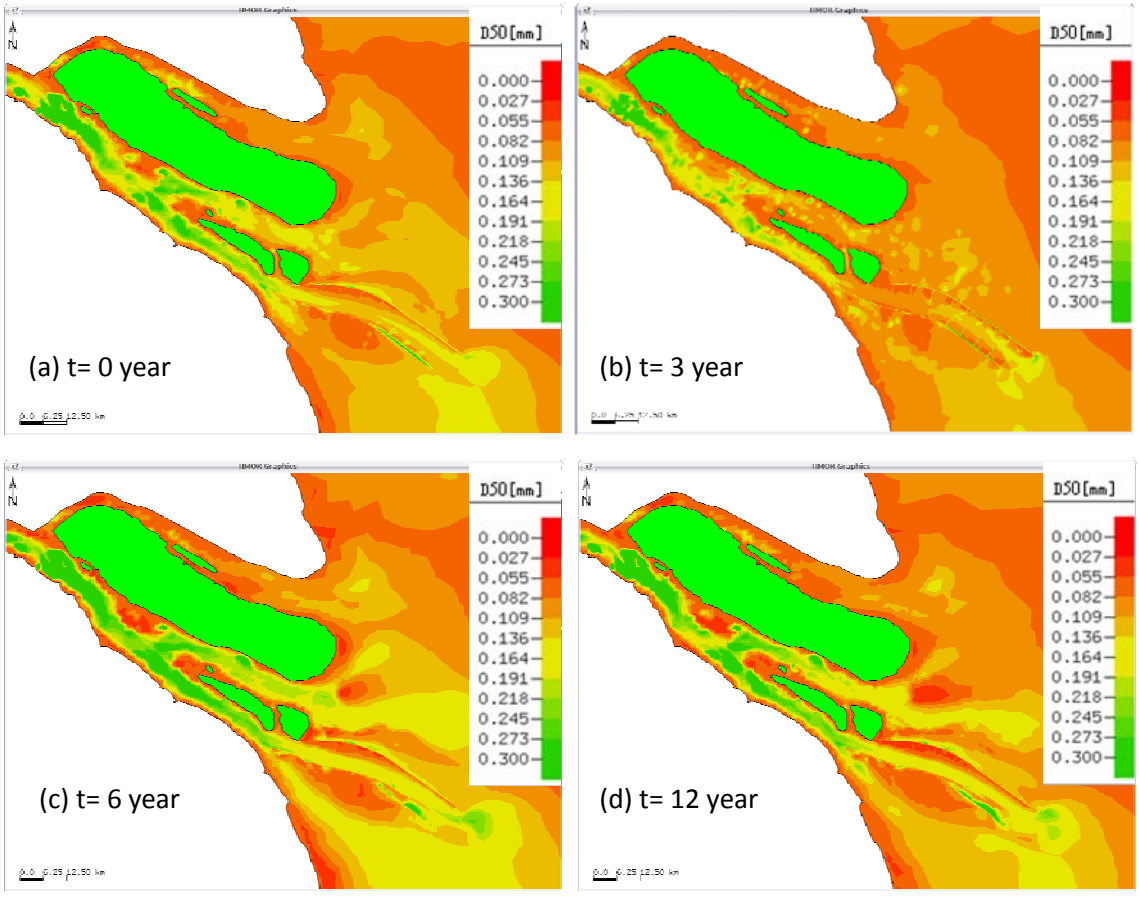

Figure 3-26 Calculated medium grain size distribution of bed load (d_{50})
at initial condition and after 3, 6 and 9 years

3.6.3 Morphological evolution

Simulated seasonally bathymetry results

The uneven seasonally water runoff distribution in the Yangtze Estuary makes it meaningful to treat the influence of dry season and wet season respectively. The hydrodynamics under different seasons and the simulated SSC and grain size distribution have been analyzed above. Figure 3-27(a-h) give the initial bathymetry at 0 year and the simulated bathymetry results in 3 years, 6 years and 9 years in dry season and wet season. The red means shallow water; blue means deep water.

The original input data of bathymetry keeps the same during dry and wet season. The local bathymetry in the North Passage in the input data has updated to 2005, when the implementation of Phase II of DWRP (Deep Waterway Regulation Project) has been finished. It is obvious to find the 10m deep waterway in the North Passage.

The bathymetry after 3 years show that, the North Branch is under deposition. The North Channel gains much current power and has relatively favorable water depth. The difference between result in wet season and in dry season is that, a little bit more deposition happens in the South Branch during dry season.

The results of 6 years have the same pattern as of 3 years, but the North Passage in wet season suffers much from erosion. A very small channel from south and east direction in parallel with the deep waterway is forming. The end of North Passage has strong current power in wet season, while a tiny partial of the Jiuduansha shoal has been separated.

(d) and (h) show the modeled bathymetry results after 9 years in dry and wet season. The North Branch has very tiny water depth and is almost blocked. The main current channels are South Branch, North Channel, and North Passage. Especially the North Channel has obvious current power advantages. The South Passage is also under heavier deposition comparing to the North Passage. The form of the small channel near the North Passage is now much clear after 9 years. But the water depth in dry season seems to be larger than that in wet season, which may be explained by that during dry season less runoff from riverside comes and the North Passage suffers more impact from the seaside tidal current.

The figures show that the general pattern of the bathymetry in 9 years remains no big changes. The North Branch has very shallow water depth. The South Branch, North Channel, and South Passage are main current routes, while the North Channel has extremely good water conditions. Partial of Jiuduansha shoal is separated in wet season. There is a small channel coming into being parallel to the deep waterway in North Passage.

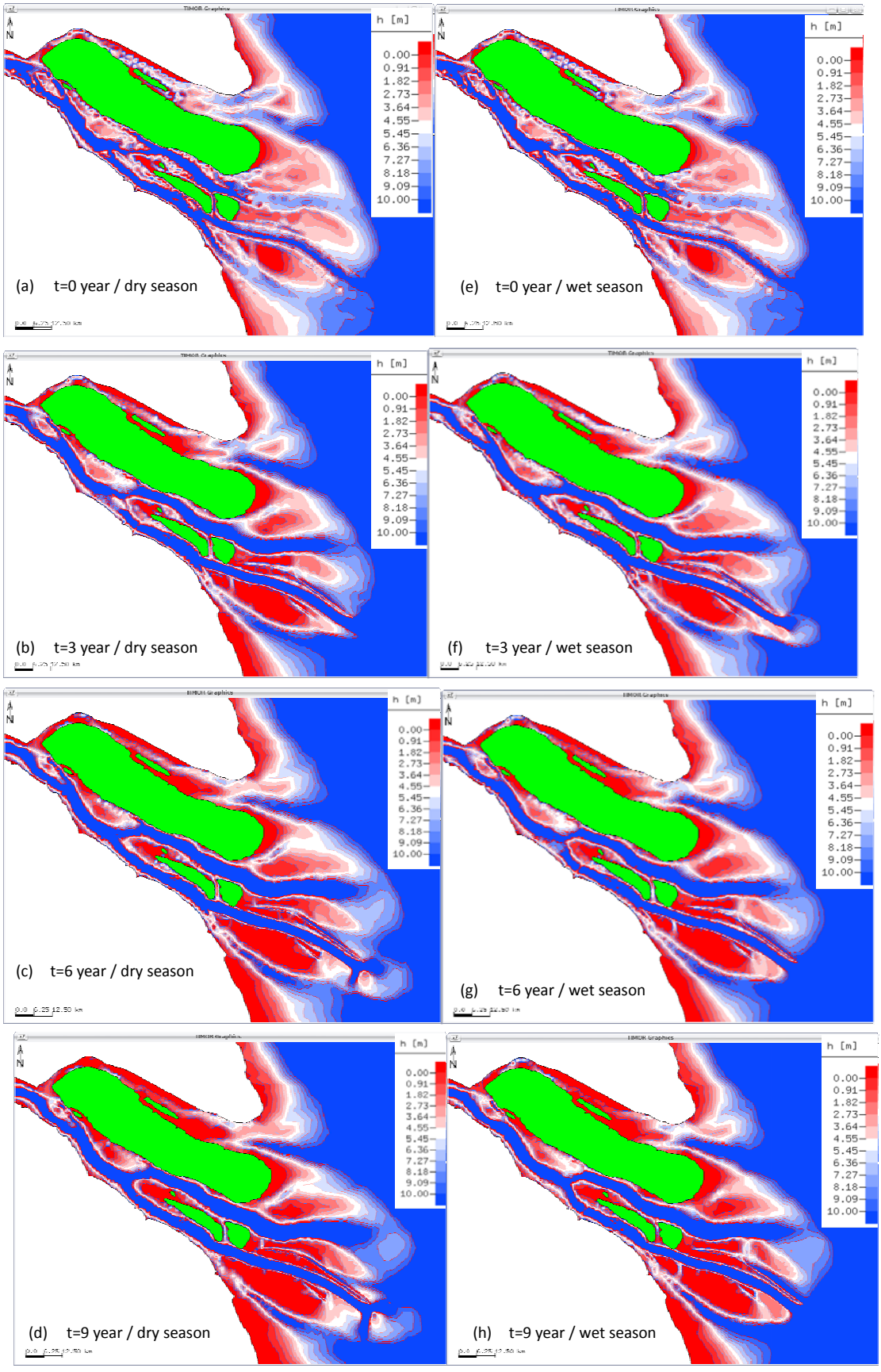

Figure 3-27 Simulated bathymetry for different years under dry season (left) and wet season (right) (red means shallow water; blue means deep water)

Velocity and water depth profile

It is of great interest to explore the changes of velocity and water depth in North Branch (North Branch) and South Branch (South Branch). The flow bifurcation ratio and sediment bifurcation ration in different channels of the Yangtze Estuary has been analyzed in Chapter 2 based on long-term field data. Here we plot simulated results of PS10 in North Branch and PS4 in South Branch to analyze their velocity and water depth in 1 year, 3 years, 6 years and 9 years.

Modeled velocity profile of PS10 and PS4 are shown in Figure 3-28 and Figure 3-30. Modeled water depth profiles are shown in Figure 3-29 and Figure 3-31. The water depth above 0m means dried, while the number below 0m represents the depth.

The velocity pattern at PS10 and PS4 are similar to each other. The velocity remains no big change in the first three years with an average velocity of 0.4 m/s and maximum approximately 0.6 m/s. But after then a huge jump happens in the next 3 years. The average velocity is getting at 0.9 m/s and the maximum reaches 1.2 m/s. After this jump, the velocity of profile PS10 remains little change. However, the velocity of PS4 is always increasing. The maximum velocities of both profiles happen always at the middle of each profile.

The water depth patterns of both profiles are in the form of "w". In the middle of profile, PS10 has a water depth of 4.5m but PS4 has 5.5m. The water depth at the right side of each profile is the deepest, with the maximum water depth 21m of PS10 and 18m of PS4. One of the reasons that could be explained is due to the effect of Coriolis force, which has studied by Gao (2008) that the ebb current usually lies at the south part of the channels and the flood current is located on the North. The water depths of both profiles in the next 9 years remain the same pattern, but they are approaching much gentle and the height difference is decreasing.

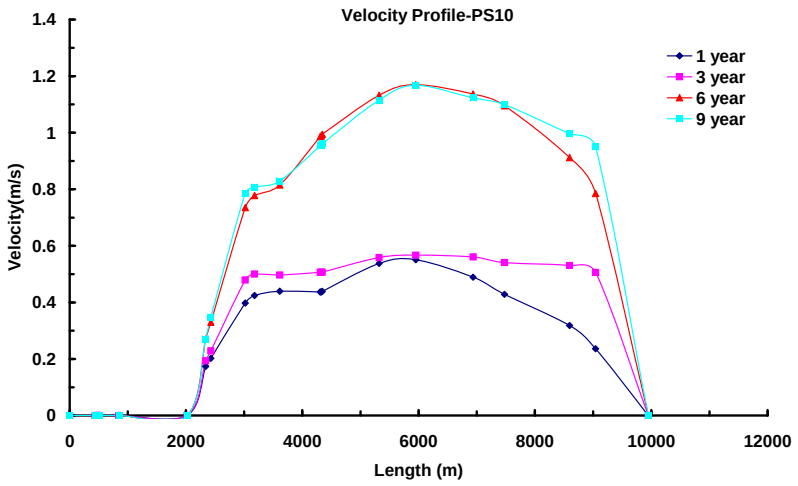

Figure 3-28 Simulation of flow velocity profile at PS10
(this shows only part of the cross-section)

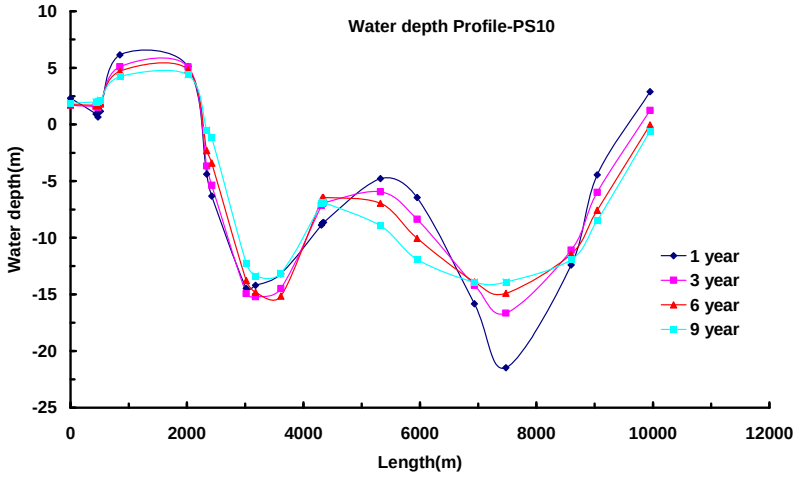

Figure 3-29 Simulation of cross-section bathymetry profile at PS10 (this shows only part of the cross-section)

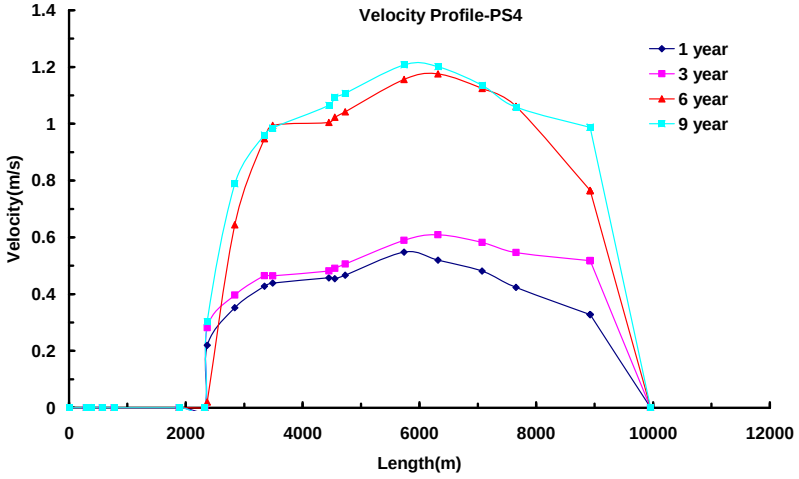

Figure 3-30 Simulation of flow velocity profile at PS4

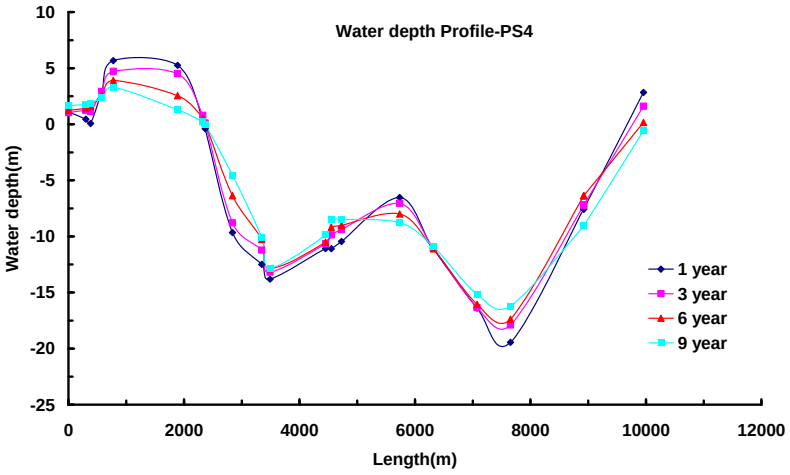

Figure 3-31 Simulation of cross-section bathymetry profile at PS4 (this shows only part of the cross-section)

Input data of "a whole year"

The simulated results of bathymetry changes under dry season and wet season show the influence of seasonal variation of water discharges. This is very special for the Yangtze, since the runoff distribution of Yangtze River is uneven timely during the year. The wet season (from May to October) has 71.1% of runoff amount, while the dry season (from November to April) has 28.9%. It is of great interest to have a whole hydrological data considering both wet season and dry season characteristics as input boundary. But due to the reality, even with high-performance computers, it consumes time and energy. For long-term morphodynamic modeling which neither goes into the details of small-scale processes, nor extends to scales far beyond those of interest, one of the key elements is input reduction (De Vriend, 1991, 1993). The methods (Latteux, 1995) have been proved to be efficient regarding the reduction of computer time requirements for long-term morphological simulation: reduction of the inputs, applying techniques for flow adjustment to bed changes and for increase of morphological time step to save a lot of CPU time without too significant error. The input filtering techniques is applied in the Yangtze to get an input data of "a whole year" as boundary conditions.

For the upper boundary, it would be perfect if having the water discharge of a typical hydrological year during the past centuries as input data, but due to the scarcity of this data, the monthly averaged water discharges in 2002 will be taken and filtered as "a whole year' input data. Figure 3-32 (a-d) show the process of making an input data of "a whole year" with input filtering techniques. (a-b) are taken as the input data for simulations in dry season and wet season respectively. (c) is the averaged water discharge in each month in a whole year. (d) is the filtered data of the whole year water discharge by extracting out the knee points.

For the seaside boundary, due to the fact that the Yangtze River has semi-diurnal tide outside its mouth, irregular semi-diurnal inside, repeating one full tide with spring, mean and neap tides to represent the whole year variety of the tidal changes is possible and acceptable.

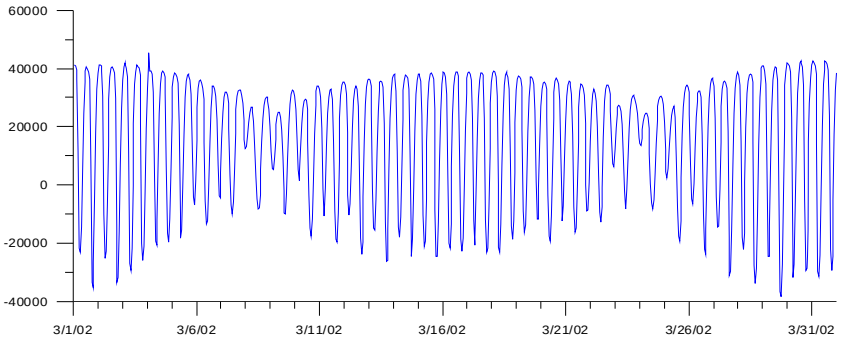

Figure 3-32 (a) Water discharge in Mar.1-31.2002 at WL0 (Jiangyin)

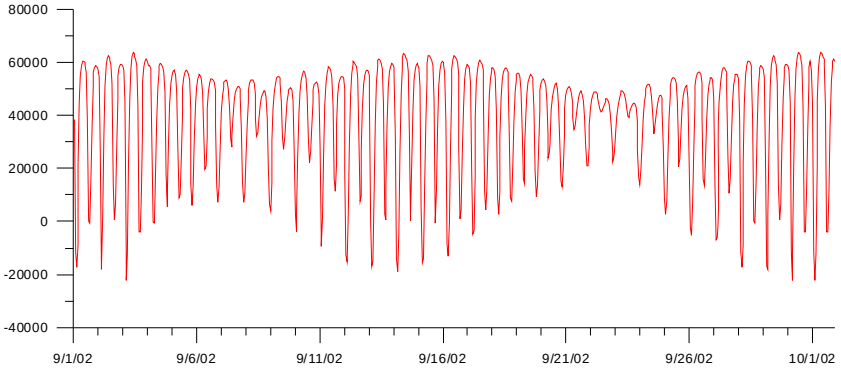

Figure 3-32 (b) Water discharges in Sep.1-30.2002 at WL0 (Jiangyin)

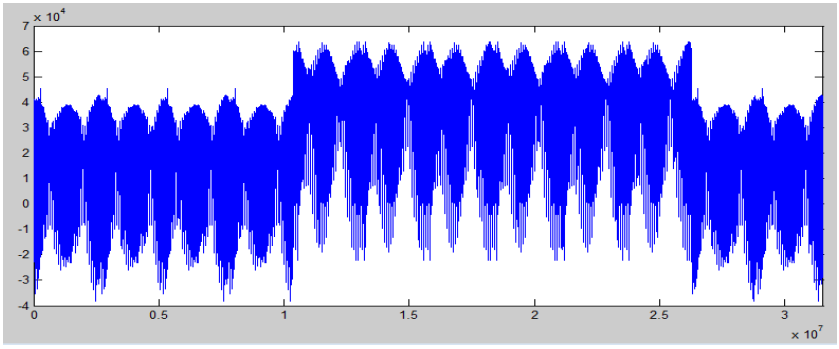

Figure 3-32 (c) Averaged monthly water discharges in a whole year

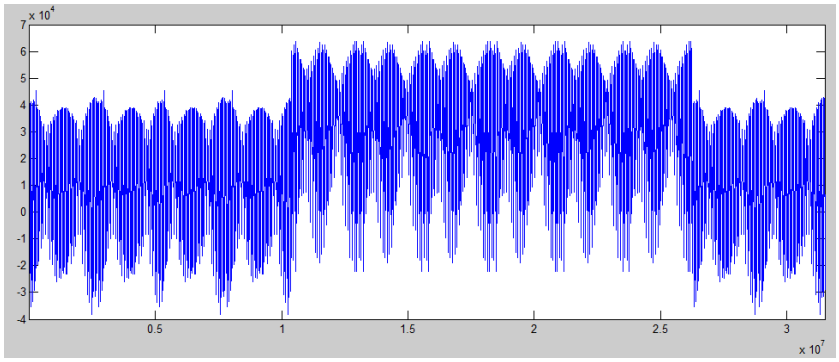

Figure 3-32 (d) Filtered data of a whole year water discharge

Long-term model results

Based on the input data of “a whole year”, long-term morphological simulations are made to see the spatial and temporal pattern of bathymetry changes in the Yangtze Estuary. Figure 3-34 (a-d) are the difference of bathymetry changes between the modeled year (t=6, 12, 24, 36 years) and the original bathymetry (t= 0 year). The negative value represents deposition and is colored in red; the positive value means erosion and is colored blue. The area colored in white means balance between deposition and erosion.

The patterns of morphological evolution remain little changes in the long-term scales. Most area of the Yangtze Estuary is under balance between deposition and erosion in long-term. But the whole North Branch is still under obvious deposition, which corresponds to those modeled results in Figure 3-28. The South Branch has deposition along the river banks, while the middle area is under balance. The North Channel is the same like South Branch, deposition along river banks. The right bank of South Passage is under deposition. But the whole North Passage is generally under balance, except the deep waterway, which is maintained for a certain water depth by dredging.

This modeled results exhibit the general pattern of morphological evolution in the long-term, however, much more influencing factors such as the storm surges, waves, typhoons and floods have to be considered for more accurate predictions. This is big challenge for long-term and large-scale morphological simulations.

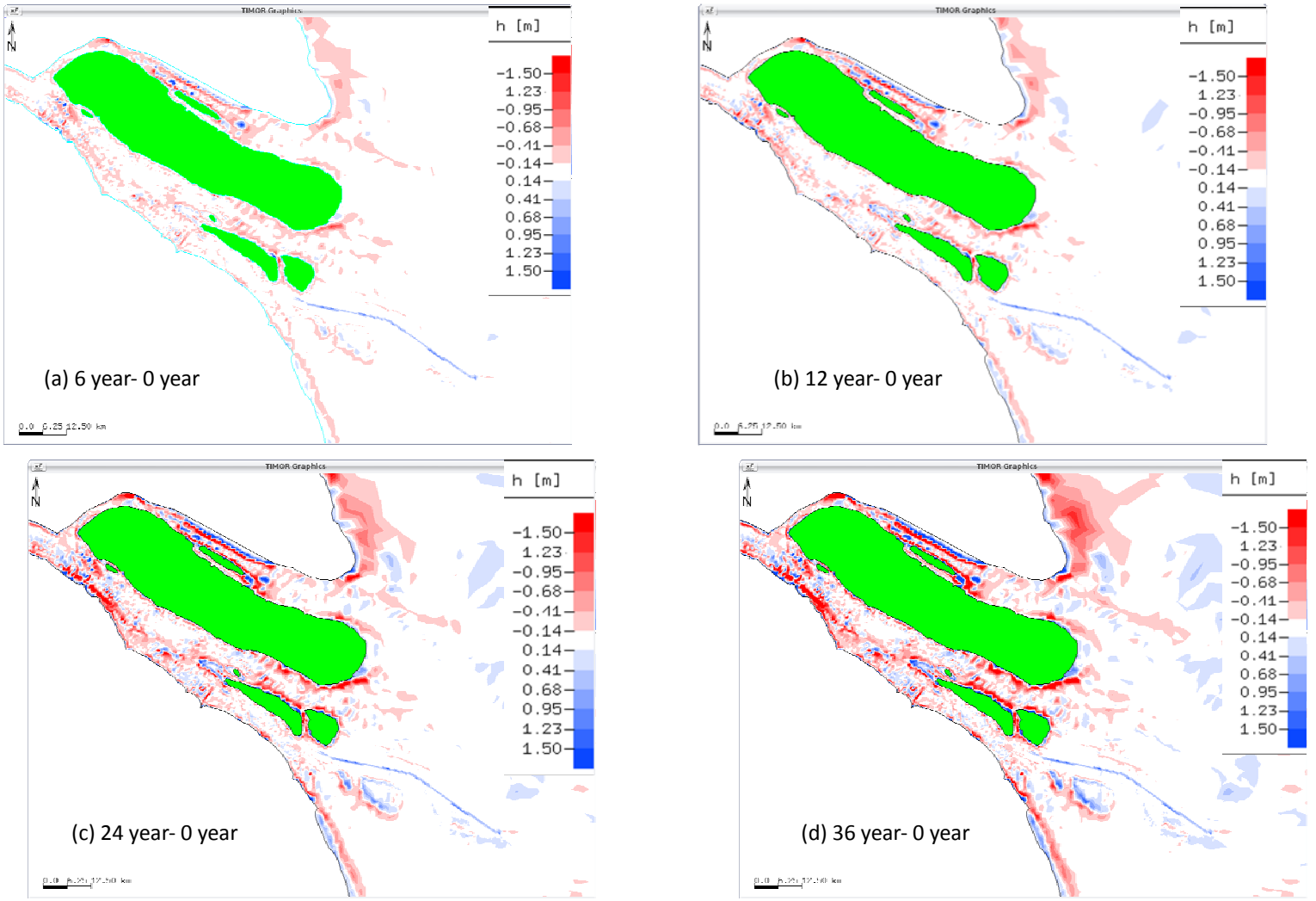

Figure 3-33 Simulated bathymetry difference with “a whole year” input data (Red: deposition; Blue: erosion)

3.7 Summary

Morphodynamic models have been developed for representing the response of hydrodynamic and sediment dynamics to natural driving forces and human interventions. Over the past decades, continuing efforts are made to enhance the understanding of morphodynamics models. Besides the commercial models, many individual researchers work hard on the improvement of the morphodynamic models. The recent published morphodynamic models have been summarized in this chapter. The quasi 3D hydro- and morphodynamic model TIMOR, developed by Prof. U. Zanke since 1995 in the Technical University of Darmstadt, has been introduced and applied in this study.

In TIMOR, advanced technical approaches are adopted, like the active layer concept, which is aimed to tackle the problem with the sediment exchange between the flow and the river bed. In addition, the morphological factor concept to bridge the gap between short-term hydrodynamic and transport processes is presented in TIMOR. The latter concept reduces significantly the computational time for long period simulation.

The hydrodynamic and morphodynamic conditions at Yangtze River Estuary are simulated by TIMOR. The model is then set up with bathymetry and hydrological input data, upper and seaside boundary conditions, generated mesh and a series of model parameters. The sensitive parameters such as the friction coefficient (FC), the entrainment factor (EF), the grain size distribution (GSD), and the eddy viscosity coefficient (EVC) are calibrated with field data. It is shown that the best fitting parameters are FC=0.0012, EF=1.5, EVC=10, and the best GSD for Yangtze Estuary is from the case of coarse sediment. After calibrating the important parameters of the model, validations on simulations of water level, flow velocity, flow direction, and SSC are carried out with field measurements. These validations are for different stations distributed homogeneously at the Yangtze Estuary, for different seasons (wet season and dry season), for different tidal conditions (spring, mean and neap tides), in order to obtain the overall performance of the simulation by TIMOR. The model results have good agreements with the field measurements as showed by. The average of mean square error (MSE) of water level simulation is 0.10m, the mean flow velocity error (MFVE) is 0.093 m/s (spring tide period), 0.077 m/s (mean tide period), and 0.063 m/s (neap tide period), and the mean flow direction error is less than 10^{o}. Since the SSC simulation doesn't have the same error level with previous parameters, they do have the same trend with field measurements and the results are quite reasonable. The TIMOR is validated as a reasonable model for the hydrodynamic and morphodynamic simulation for Yangtze Estuary area.

The simulated hydrodynamics show that, the tide comes into the estuary from a direction between south and east, and leaves the estuary from a direction between north and west. The tidal current in the South Channel and North Channel is to-and fro flow, while in the South Passage and North Passage or in the lower stream of Hengsha Island it transforms into rotary flow with clockwise. The values of flood and ebb currents during spring tide in the Yangtze Estuary are notably greater than the respective values during neap tide. The values in wet season are greater than those in dry season. There is a 1-3 hour phase lag between the water level and velocity both in dry and wet season. The ebb tide duration is generally

longer than the flood tide duration. This agrees with previous studies based on field measurements (Milliman, 1983; He, 2003; Gao, 2008).

Model results show that the SSC is greatly influenced by tide propagation and in proportion with the current velocity. The modeled results of depth-averaged velocity and SSC distribution with ebb and flood current during spring and neap tide reveal that, the SSC in Yangtze Estuary is higher in flood current than that in ebb current, as well as higher during spring tide than during neap tide. The grain size distribution pattern of bed load show that, the sediment along the main current route is coarser than those areas near the river bank. The North Channel, North Passage and South Passage have grain size about 0.13mm, but as time goes on, the grain size of South Passage is getting smaller. At the end of North Passage, the grain size is growing more than 0.2mm. This could be explainable due to the strong ebb tide, which takes the sediment away into the sea and remains the coarse ones.

Due to the uneven seasonally water runoff distribution in the Yangtze Estuary, simulations are done to check the seasonally bathymetry results in 1 year, 3 years, 6 years and 9 years. The velocity and water depth profile in South Branch and North Branch is also plotted and analyzed. For long-term morphodynamic modeling, the input filtering techniques is applied in the Yangtze to get an input data of “a whole year” as boundary conditions. Based on this input data, the long-term morphological simulations are made; and the spatial and temporal pattern of bathymetry changes in the Yangtze Estuary is analyzed. In long-term scale, the general pattern of morphological evolution is under balance. The whole North Branch is under obvious deposition. The South Branch and North Channel has deposition along the river banks. The right bank of South Passage is under deposition. But the whole North Passage is generally under balance, except the deep waterway, which is maintained for a certain water depth by dredging.

CHAPTER 4

MORPHODYNAMIC RESPONSES TO HUMAN INTERFERENCES AT YANGTZE RIVER ESTUARY

4.1 Effect of human interferences on morphodynamics

4.1.1 Effect of dams and reservoirs

Almost half of the world's large dams (defined as dams higher than 15 meters) built since 1950 are in China (Fuggle and Smith, 2000). On the Yangtze alone, there are an estimated 50,000 dams with a total storage volume 713×10^8 m^3, including the largest in the world, the Three Gorges Dam project (Gleick, 2009). The Three Gorges Dam (TGD) and associated infrastructure is the largest integrated water project built in the history of the world. The construction began formally in Dec. 1994. The water was impounded since 2003, and the physical dam was mostly completed in 2006. The TGD is designed as 175m high, and has created a reservoir 600 km long, 1084 km^2 area. The average depth of the dam is 70m, max is 170m behind the dam. The total storage capacity of TGD is 393×10^8 m^3, is less than 10% of the average annual runoff at the dam site (4510×10^8 m^3) and is only 5% of the average annual runoff of Yangtze River. At its completion, sometime after 2010, the project is expected to have a total installed hydroelectric capacity exceeding 22000 MWe. In addition to the originally proposed power supply function, the other benefits of the project include flood protection on the historically dangerous Yangtze River and improvements to river navigation for thousands of kilometers.

According to the statistics in Chapter 2, the annual water discharge didn't have significant change before and after the dam construction, however the seasonal adjustment exists. But, TGD has a significant impact on sediment loads in the Yangtze. The Yangtze River has traditionally carried a vast load of sediment from its upper reaches of the watershed to the East China Sea. This sediment load has varied with annual climatic factors, and more significantly, with the level of deforestation, and subsequent reforestation in the upper watershed. The completion of TGD, however, has led to a rapid and significant decrease in downstream sediment load. Sediment volumes have been declining from the late 1990s due to reforestation efforts and the construction of many small- and intermediate-sized dams on Yangtze River tributaries. In 2003, the implementation of TGD caused a further severe decrease. Yangtze carried sediment loads of ~480 Mt/yr to the sea (Wang et al., 1997; Yang et al., 2005). Two years after impoundment, sediment load at Datong, near the Yangtze's delta dropped to only 33% of the 1950–1986 levels (Xu et al., 2006). Yang et al. (2007) found that 151 Mt/yr of sediment has been retained by TGD since it began operation (2003–2005). In response to this, significant erosion has occurred in the downstream riverbed. This erosion did not offset the sediment lost in the reservoir, and the sediment flux into the estuary decreased by 85 Mt/yr (31%) (Yang et al., 2007). Hu et al. (2009) showed that the sediment discharge from Yangtze River to the sea will probably decrease to less than 90 Mt/yr in the

coming decades (18% of that in the 1950s) when considering the effects of TGD and other large projects such as SNWDP and WSCP.

In response to the decrease of large amount sediment trapped by TGD, it has lead to conversion from propagation to recession in the delta front and has great impacts for delta ecosystem and human development (Yang et al., 2001). Changes in surface textures of river bed sediments corresponding to variation in the rate of sediment supply have been reported in the previous flume and field studies (Lisle et al., 1993). It is very common that, when deprived of sediment, poorly sorted bed surfaces typically coarsen through size-selective winnowing of fine grains (Leopold et al., 1964). Bed forms usually respond to changes in surface sediment distributions, as in the Nile estuary (Fanos, 1995) and the Elbe estuary (Trenhaile, 1997). Subaqueous dunes are well developed in the Yangtze Estuary (Cheng et al., 2004). The factors that have significant influence on the morphological changes of dunes are flow regime, channel pattern and bed materials. As the result of lack of sediment supply trapped by TGD, the shoals in the bifurcation of the North and South Channel become less stable and had been severely eroded (Li et al., 2005). The erosion of the shoals has led to a large quantity of coarser sediments being transported into the South Channel (Jin et al., 2006), resulting in a significant coarsening of the bed material in the South Channel. Hence, the sediment discharge decline in the Yangtze Estuary caused by TGD is believed to be the root cause for the dune field extension seaward about 11.7 km during dry seasons in the South Channel over the period from 2002 to 2006 (Li et al., 2008).

4.1.2 Effect of water diversion project

The South-North Water Diversion Project (SNWDP) (Chen et al., 2002; Mei, 2006; Zhang, 2009) in China is a multi decade project in order to divert water from the Yangtze River to the Yellow River and Hai River in North China (see Figure 4-1). This is because the heavily industrialized Northern China has a much lower rainfall and its rivers are running dry. When finished, the work will link China's four main rivers - the Yangtze, Yellow River, Huaihe and Haihe - and requires the construction of three diversion routes, stretching south-to-north across the eastern, central and western parts in China. The western route is in the western headwaters of the rivers where Yangtze River and Yellow River are closest to one another; the central route is from the upper reaches of the Han River (a tributary of Yangtze River) to Beijing and Tianjin; and the eastern route using the course of the Grand Canal. This massive scheme has already taken 50 years from conception to commencement and is expected to take almost as long to construct. Planned for completion in 2050, it will eventually divert 38-48×10^9 m^3 of water annually to the population centres of the drier north (Chen et al., 2002; Zhu and Zhang, 2008).

Construction on the Eastern Route officially began in December 2002, and water is supposed to reach Tianjin by 2012. This route will transfer about 26×10^9 m^3 of water to Northern China. Construction of the central route began in December 2003. Initially designed to transfer 9.5×10^9 m^3 of water, by 2030 some 22×10^9 m^3 will be flowing along this system. The central route project was scheduled for completion by 2010 but has been postponed to 2014. Construction of the western route, which involves working on the Qinghai-Tibet Plateau between 3000-5000m above sea level, is scheduled to begin in 2010 and will involve overcoming some major engineering and climatic challenges. Once completed in 2050, the

project will bring 4×10^9 m^3 of water from tributaries of the Yangtze to northwest China.

Although only a small share of Yangtze water would be diverted, the strong possibility that each transfer would generate a range of negative impacts on local and regional environments has long been recognized (Biswas, 1983). SNWDP would result in the decrease of water and sediments discharging into the estuary, the change of the morphological process and dynamic aggradation, and therefore affect the estuarine environment. In the eastern route, it might aggravate saltwater encroachment in the estuary as well as add to sediment deposits in the lower Yangtze. Zhao (2006) showed that due to decrease of sand and water discharges influenced by both of SNWDP and TGD, the underwater bars were eroded and the channel volume was growing in South Branch (SB), South Channel (SC) and the upstream side of North Channel (NC) as well as the siltation speed decreased. The Yangtze Estuary may change from deposition to erosion.

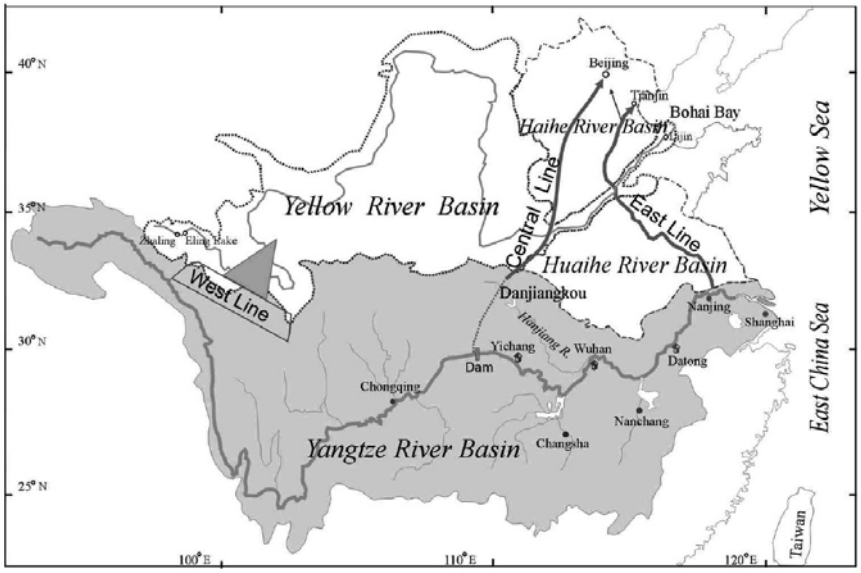

Figure 4-1 Sketch map of the SNWDP (Chen et al., 2002)

4.1.3 Effect of Water and Soil Conservation Project (WSCP)

China is one of the countries suffering from most serious soil and water loss in the world. Due to the natural, geographic, social and economic conditions, as well as human activities, soil and water loss has caused ecological and environmental degradation. They include overlogging, overfarming and overgrazing, neglect of protection during construction and development (Liu, 2004). The Water and Soil Conservation Project (WSCP) at upper and middle Yangtze basin, begun in 1988, intended to conserve the soil and water loss in Yangtze and its tributaries by planting, returning land for farming to forestry, protecting natural forest, utilizing farm land more reasonably and comprehensive management. By 2008, the total area reforested was estimated at over 90×10^3 km^2. It is planned to protect and recover an additional area of 75×10^3 km^2 in the next decade (BYRS, 2000; Hu et al., 2009). WSCP makes a significant reduction in sediment load. It trapped 30 Mt/yr sediment in the Jialing River, a tributary of Yangtze (Xu et al., 2006). Around 15% of the total sediment reduction (320 Mt/yr in 1993-2002) was attributed to the effects of WSCP (Dai et al., 2008). Xu and Milliman (2009) thought one of the reasons of that the lower reach of Yangtze River (from Yichang to Datong)

changed from deposition to erosion in 2002 is due to the reforestation on the Yangtze tributaries.

4.1.4 Effect of reclamation

Reclamation is a very common disturbance to the alluvial lands of estuaries. Along with the economic development in Yangtze Delta, the area of cultivated land is decreasing. Reclamation is one of the effective ways to countervail the decrease of tilth and alleviate conflict in land use. For example, Shanghai coast has been long beneficial from the Yangtze siltation such as the new Pudong airport of Shanghai was built on the reclaimed coast. Chen et al. (2000) indicated that the reclamation land is about 84,042 ha in the Shanghai inland from 1953 to 2000. The reclamation land distributes at Nahui East Beach, north beach of Chongming Island, Chongming East Beach and north beach of Qiantang Estuary. After beach reclamation, the hydrodynamic conditions in front of the bank become weakened, and then the sand deposits and the beach develops. In addition to the sediment carried by the Yangtze, the dredging quantity of Deep Waterway Regulation Project (introduce in section 4.2.2) constructed in the North Passage is estimated 200×10^6 m^3 (even more). Taking into consideration of the environment impact and the soil utilization, the dredged silt was deposited to Hengsha East Beach, which benefits both the need in land usage and the dredged silt disposal. Qi and Zhang (2003) applied a numerical model to simulate the environmental impact of reclamation work at Hengsha East Beach. They found the mentioned reclamation work has no negative effect on the flood control in the Yangtze Estuary and the velocities of ebb and flow in the North Channel will decrease. However the reclamation makes influences on the bifurcation rations for both SC/NC and SP/NP. The hydrodynamic conditions are changed.

4.2 Regulation works in estuaries

4.2.1 Worldwide projects (examples)

Estuaries form a transition zone between river environments and ocean environments and are subject to both marine influences, such as tides, waves, and the influx of saline water; and riverine influences, such as flows of fresh water and sediment. A mouth bar is typically created in the middle of the channel at the estuary that is created by the positive feedback between mid-channel deposition and flow divergence (Edmonds, 2007). Presence of mouth bar interrupts effluent flood flow into the sea. The navigation capability decreases also due to mouth bar. Since the 19th century, the worldwide cargo transport as well as the ship size has been increasing, with the development of world industrialization and the innovation of ship building. The navigation channel depths are demanded to fit the developments. Therefore many regulation works have been carried out at the estuary or in the nearby harbors such as to expend the harbor capacity, renew the facilities, or dredge the harbor and the channel accessing to the harbor. The carried out regulation works have put into influences for the estuary morphodynamics.

The regulation works carried out in different estuaries in the world have a long history. In the 19th century, dredging is the main approach to increase the channel depth. But with the

increasing draft of ships, local dredging could not cure the problem of deeper water depth. In addition, hydrodynamic conditions are changed by the dredging. In some cases, the dredged channel was again under deposition in very short time. Sometimes the deposition speed was always faster than the dredging. Long-term monitoring is therefore necessary after the regulation works. Furthermore, not only the dredged channel depth was obviously restricted, but also the channel after dredging was fragile to storms or floods. In the 20th century, regulation works at estuaries changed to take combination of dredging and regulation. Besides, hydraulic experiments have been used to study the performance of regulation works since 1930. Furthermore, the numerical modeling was developing. Implementation of estuary regulations became more confident and predictable. This section is going to review several large scale estuary regulation works worldwide. Their locations are shown in Figure 4-2. Summaries are given in Table 4-1.

Mississippi Estuary

Mississippi Estuary is a braided estuary with weak tide and material supplied by river runoff. The sediment discharge was about 500 Mt before 1950.The spring tidal range is only 0.45m during the dry season (Fan, 2006). Before regulation, the lowest depth on the mouth bar was about 2.7m. In 1836, dredging works was carried out in the southwest passage to achieve 5.0m water depth (Wright, 1971). But the channel was frequently silted up during storms. In 1875, the new regulation works was implemented in the south passage, regulating structures and dredging works were combined together to achieve the 9.0 m water depth in 1879. From 1904, regulating structures with dredging works were carried out in southwest passage intending to achieve 10.5 m water depth. But the project got only a 6.0 m channel depth after being finished, so a lot of research was done and the regulating structures were adjusted, the channel direction was modulated too. In 1921 the water depth achieved 10.5m, and after that the channel depth was continuously regulated and reached to 13.7m in 1993.

Seine Estuary

The Seine Estuary is one of the largest estuaries on the northwestern European continental shelf. It is characterized by strong tide with a tidal range of 8.5m at the mouth and tidal penetration of 170 km inside the continent (Lafite, 2001). Before regulation, shoals and mouth bar developed in the river mouth with low and unstable channel depth. Since 1848, two long training jetties, each with 60 km long, 300~500m wide, were built between la Risle river and la Mailleraye river to attempt to deepen the navigation channel (Parthiot, 1981). Due to the widths between two jetties were too narrow it was unable to accept enough influx, and part of the upper and lower regulation passage was seriously deposited because of the flood tide discharge decreased. After long-time discussion and testing, part of the old north jetty has been removed in 1959 due to unstable flow condition. In 1960, the new north jetty was built with the combination of dredging and regulating, which increased the channel depth by 2.5m. Shifts with draft of 8.0m and 10.0m can enter the city Rouen during high tide and low tide, which prompted the rapid development of Rouen. Since 1970, a new low jetty with 5.0km long was built to increase the water depth, together with the engineering of dredging the sediment at the 6.0km long middle river reach which was earlier hard to be carried away by the runoff. Since 1977, the north low jetty was extended to 17km long. In 1979, the channel depth increased to 2.0-2.4m. In 1980, vessels with 35,000 DWT could enter the Rouen Harbor. The regulation works for Seine Estuary spend nearly 200 years. The

lower Seine River was changed from a natural system to one that was controlled (Lesourd et al., 2001). The removal of islands, polder management, and the diking of the river bed has created a single but deep channel up to Rouen. The flow condition has been improved with reduced water volume and increased current velocities. And in this highly controlled system, the fine-grained sediments in the fluvial estuary are hard to deposit in areas which sheltered from erosion by river and tidal currents.

Rhine Estuary

The River Rhine is one of the longest and most important rivers in Europe. It runs through four countries - Switzerland, Germany, France and Netherlands, before emptying into the North Sea at Rotterdam. In the mouth of the Rhine annually 10.5 Mt of material are dredged out (Eisma, 1988) which is a far larger amount than the total load of the Rhine across the German/Dutch border (Kempe et al., 1981). In 1863, The Netherlands began to regulate the Rhine River, a new water channel and two dikes were built (Walter, 1974). It was expected to obtain deep water depth by current scour and to carry away the deposited sediment in the estuary by tide, however the expectations didn't come true. After half century's effort, a general river regulation plan has been implemented and got big achievements. Since 1960, the new navigation channel was successful with combination of dredging and regulating after enlargement of new port in Holland Bay. Regular dredging is always needed to maintain the deep water depth besides the north and south jetties.

Columbia Estuary

The Columbia River Estuary is the second largest river in the United States and the largest river flowing into the eastern North Pacific. Fist regulation applied to Columbia Estuary was implemented in 1885 (O'Brien, 1971). The south dike and four groins were constructed to create a deep navigation channel of 9.1m. In 1902, the channel developed into three branches and the water depth went back to 6.7m, the navigation conditions went worse. In 1905, a regulation plan was made to in order to get 12.2 m water depth in the river mouth. The south dike was strengthened as well as the north dike and groins were built together with dredging measurements to guarantee a 2.4 km long, 12.2 m deep channel. And it reached to 14.3m at the end of 1927. In 1931, the water depth in the mouth bar has been reduced to 13.1m due to the deposition in the west and north direction according to the development of shoals in the north dike. These shoals decrease the water depth but protect the north dike. In order to stabilize the channel, dredging has to be done every year. The total dredging volume was approaching 13.3×10^6 m^3 in 1948. In 1954, the mouth bar plan has been readjusted in order to meet the demands of modern shipping. A navigation channel with 810 m wide and 14.6 m deep was dredged. The dredging record in 1956 and 1957 showed that the channel became seriously deposited in winter through with a water depth of 14.6 m by dredging. In 1958, measurement demonstrated that the dredged sediment came back to the channel; therefore the dredging and dumping method has been changed to dump all the dredged sediment to the outer, which improved the situation a lot.

Elbe Estuary

The Elbe Estuary is located at the Germany North Sea Coast (see Figure 1). The tide at the Elbe estuary is semi-diurnal. Tidal ranges reach around 3 m in the mouth. The North Sea coastline of Germany is devoid of cliffs and has wide expanses of sand, marsh, and mud flats.

Sediment sources for the Elbe estuary are both from riverine and marine. The tidal Elbe River has a tendency for sedimentation due to the asymmetrical tide. On a very small scale locations can be found with alternating erosion and sedimentation. This is mainly due to morphological adjustments to human induced changes (dredging, fixing the shipping route, canalisation, land reclamation). Since the beginning of the last century, the Elbe estuary has been deepened several times to allow ships of increasing cargo capacities and draughts to reach the Port of Hamburg. The most recent deepening by about 1 m to 14.4 m depth was carried out during spring 1999. A further deepening to a depth of about 16 m along the whole longitudinal profile is recently planned. The objective of the deepening project is to allow vessels with an actual draught of 13.5m to use the Lower and Outer Elbe estuary without any tidal restrictions. Moreover, vessels with a draught of 14.5m must be able to enter and particularly leave the port with the corresponding tides. To create these improved access conditions the present fairway will have to be deepened by between 1.5m and 2.4m. However, as the present channel bed is above the required depth only in certain sections, the project will involve dredging only specific stretches of the Elbe estuary, and not the entire 130 km. In total, 38.5 million m^3 of material will be dredged out of the channel, 75% of which will be used to build underwater structures, 22% will be relocated in the estuary and 3% will be used to charge and partly recharge polders (Osterwald et al., 2008). The morphology of the Elbe estuaries has been adapted by humans in order to optimize their function as shipping routes. Upstream, at the narrow end that leads into the docks, the channel was given a funnel like shape (Kausch, 1993). The canalization has resulted in a loss of intertidal and shallow sub tidal areas and in an increase of the tidal range (4 m at spring tide) in Hamburg. Other hydrological parameters like the diurnal asymmetry of the tides, the flow velocities during low and high tide (Kappenberg and Grabemann, 2001) are long-term trends and cannot be associated with a specific deepening event. It is also found that the outer southern shore is mostly subjected to sedimentation. The northern coastline shows a constantly changing process of erosion and sedimentation.

Mersey Estuary (UK)

The Mersey Estuary is a strongly tidal estuary located on the West coast of the UK. Compared with the typical open funnel shape of many other estuaries, the Mersey Estuary has a relatively large inner basin which is constricted at its seaward end by rock outcrops. Since 1833, Mersey Estuary was started to be dredged (Thomas et al., 2002). Several major civil engineering works have been undertaken in the estuary and Liverpool Bay area that may have contributed to changes in estuary morphology in the past 100 years (Thomas et al., 2002). Within Liverpool Bay these included: (1) Dredging of the bar at the seaward end of Queens Channel beginning in 1890 to a depth of 6.4m increased to 9m by 1895. By 1908 1 Mt of material was being removed from the bar annually. (2) Dredging of the sea approach channels, 10 Mt was removed annually in 1908, increased to a maximum of 17 Mt between 1910 and 1917. (3) Construction of training walls, commencing with a 3.6km length on the outside of Crosby Channel bend, extended to the west and augmented between 1914 and 1935 by training walls on both the east and west sides of Crosby Channel. Between 1945 and 57 the training walls were extended in a seawards direction. According to Thomas et al. (2002), the establishment of a stable state is attributed to a reduction in the calculated transport of sediment across Liverpool Bay reducing the supply of sediment to the estuary mouth.

Douro Estuary

The Douro River is 930 km long, rising in the Picos de Urbión in northern Spain, and flowing generally westwards to the Atlantic Ocean (Portela, 2008). The Douro estuary has a length of 22 km and average only 400m wide. It is a highly energetic zone due to tides, waves and river discharge. At its mouth, a sand spit protects the inner zone, with its river banks and beaches, against incoming waves. Dredging to maintain the nautical depth is only carried out in the estuary. Due to the morphology of the estuary, the tidal prism is relatively small. The lower river banks have cyclically been flooded, and, in recent years, a weaker, and more protracted, spit has also allowed direct sea-wave attack of the northern bank, with southwesterly storms flooding the adjacent urban area. Although the upper river reaches have been equipped with infrastructures such as ship locks and berths, the unstable configuration of the estuary mouth has hampered the connection with the sea, and so inhibited the full navigation potential of the river. In order to improve navigation condition, some form of structures had to extend from both banks. To protect the north bank and adjacent urban areas against sea-storms, the Cabedelo sand spit had to be strengthened and brought outward, near its original position. To promote the spit's tombolo-like growth, a detached, shore-parallel, breakwater was designed. To ensure the good functioning of this system, and to avoid sand spilling into the navigation channel, a semi-submerged structure connecting the breakwater with the spit was also built. Sediments arriving at the spit would thus be held in a position further seaward than at present by the combined action of the breakwater and its transverse connection to the spit head, reconstituting this way the original robust spit (Ramos, 2006a).

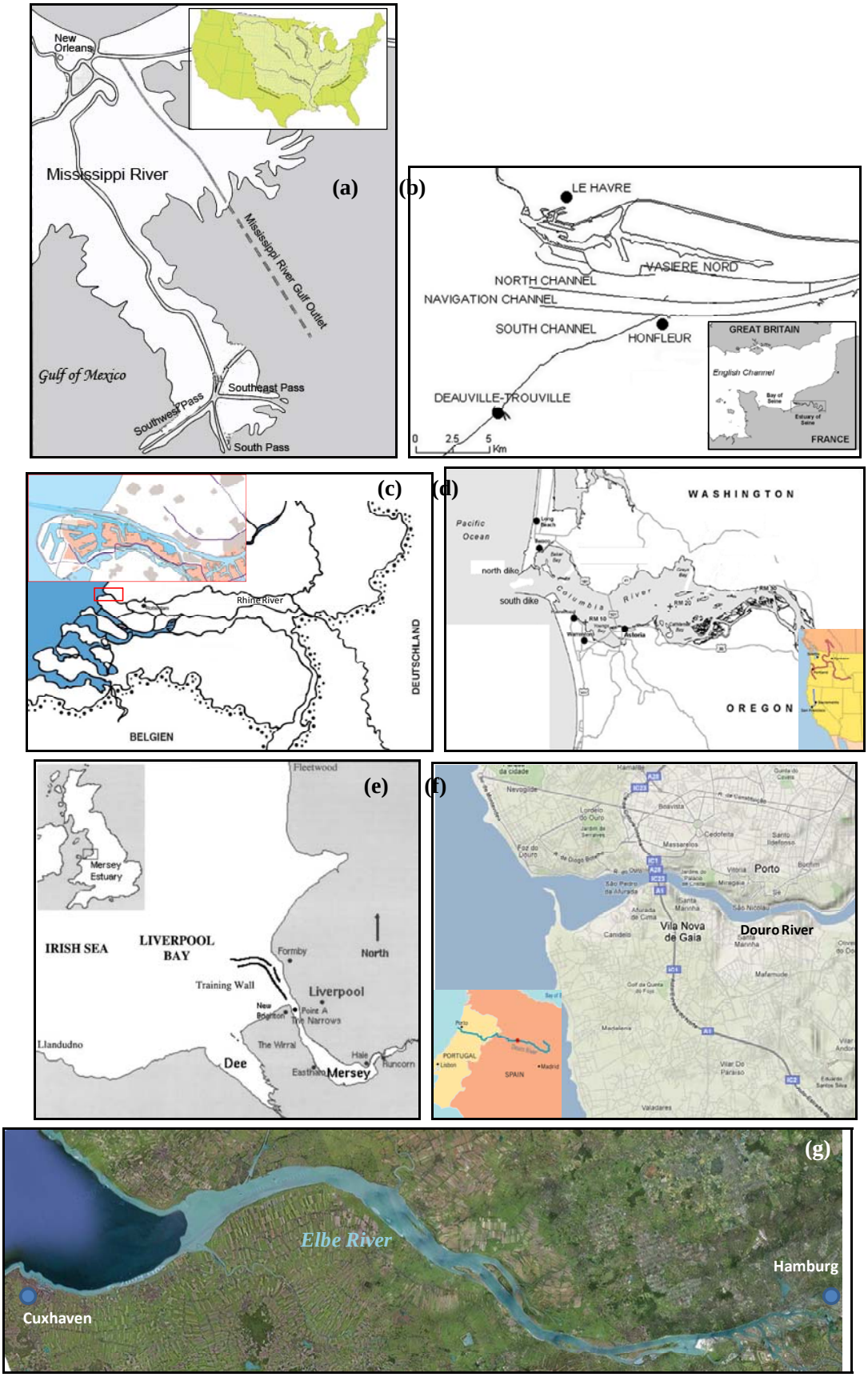

Figure 4-2 Examples of worldwide estuary regulation works. (a) Mississippi Estuary; (b) Seine Estuary; (c) Rhine Estuary; (d) Columbia Estuary; (e) Mersey Estuary; (f) Douro Estuary; (g) Elbe Estuary

Table 4-1 Summary of large estuary regulation works in the world

		USA	USA	UK	Germany	France	The Netherland
		Mississippi Estuary (South Passage)	Columbia	Mersey Estuary	Elbe Estuary	Seine Estuary	Rhine Estuary
Initial time		1904-	1885-1958	1890-	1938-	1848-	1863-
Catchment (x10^4 km^2)		324	67	0.477	14.85	7.86	16
Annual discharge (m^3/s)		16800 (min.1420;max.61000)	7420 (min.1000;max.32000)	52.7	700 (min.130;max.3900)	400 (min.15; max.2000)	2140 (min.630; max.13500)
Tidal range (m)		0.5	2.0	6.37	2.87	3.5~7.2	1.6
Sediment condition		dominated by land sediment. 500 Mt/yr (1950s) 100~200 Mt/yr (1970s)	dominated by land sediment. ~ 8.4 Mt/yr	dominated by sea sediment	dominated by sea sediment	dominated by sea sediment. ~ 3.5 Mt/yr	dominated by sea sediment.
Regulation initial time		1904-	1885-1958	1890-	1938-	1848-	1863-
Regulation contents		Initially double dikes then groins. Dike interval is 1100 m. Width of regulation line is 432m.	Initially South dike, then North dike and North groins. Dike interval is 2.4km.	Initially dredging, then 60km double dikes (1914-2057). Dike interval is 400-500 m.	Initially dredging, then 9.25km single dike. Continuous to extend 3km for avoiding erosion.	A high dike with groin at North river bank; Submerged dike at South bank. Improve to build the double dikes. Dike interval is 500m.	Double dikes. The interval was reduced from 900m to 700m. Dike elevation decrease from nearshore to offshore.
Channel depth (m)	Natural	2.7	6.1	3~3.6		2.4	3.6
	After regulation	12.2~13.7	14.6	13.6	13.5	10.5	13.0
Channel width (m)		180~240	150~670	-	-	200	350~600
Regulation length (km)		35.4	37	-	-	30	45.6
Annual dredging volume (× 10^4 m^3)		1150	376	130~260	very few	500	2300

4.2.2 The Yangtze Deep Waterway Regulation Project (DWRP)

Regulating structures in combination with dredging works are favorable measures for most estuary regulations. After regulating, the maintenance dredging is usually needed to maintain the water depth. Like most regulation works in the worldwide estuaries, the guideline of the Deep Waterway Regulation Project (DWRP) at Yangtze Estuary is to combine remediation and dredging. There are various layouts for the regulation work during planning period. They are “single dike”, “double dikes”, “single dike with groins” and “double dikes with groins” etc (Yang, 1997). Choosing the a correct layout highly depends on the water and sediment conditions, the strength of tidal current and runoff as well as the shape of the estuary. Due to the nature characteristics of Yangtze Estuary and some other considerations, “double dike with groins” was decided for the project as shown in Figure 4-3. It was suggested that this layout has benefit for guiding the current, preventing sediment from sand shores and relieving deposition in the navigation channel.

The Yangtze Estuary is a medium tidal estuary. It has sediment sources from both seaside and upstream river. There is a sand bar at the Yangtze River mouth which called “mouth sandbar”. The shallow water depth condition because of the mouth sandbar has seriously restricted the further economic and social development of Shanghai and other cities along Yangtze River. Large-scale and container ships could not freely go into Shanghai harbor. The “golden waterway” didn’t bring its function into full play. It is of great importance and necessity to enhance the navigation water depth. Scholars domestic and overseas have done much feasibility research. The Chinese government has paid great attention on it. As early as in 1960, the Yangtze Estuary Regulation Group was established by the Ministry of Communications to take responsibility of regulation work (Yan, 1981). Yan (1992; 1996; 2001) did a lot of site investigations, drown domestic and overseas experience on regulation works, and provided many valuable and feasible suggestions on the regulation work in Yangtze Estuary. Chen (1995) and Wang (1994, 2002) summarized the causes of mouth sandbar and analyzed its evolution law. Chen et al (1994; 2005; 2006) carried out physical experiments on the layout program of DWRP based on previous research achievements. Dou (1999) used numerical model to simulate the sediment problems in the regulation channel. Yan (2001) discussed the advantageous regime of regulation area, namely the North Passage from the point of diversion ratio. Le (2006) made an overview of the previous researches on the regulation work and illustrated the overall regulation program. The DWRP has finally been taken into implementation after more than 40 years investigation and verification.

The North Passage (Fig.4-3), which was chosen as the deep navigation channel for regulation works, has 6.0m natural water depth under lowest tide level (Yan et al., 2001). Influenced by incoming water and sediment from riverside, the sandbar in Yangtze Estuary suffers from erosion in dry season and deposition in flood season (Chen, 1995; Yang et al., 2001). The Yangtze Estuary width is 90km, however only the sandbar beach at North Passage occupies 69km. The wind waves are easy to lift the sediment from the shore area as well as the tidal currents can carry them to move inner channel or outer estuary. In 1984, the North Passage was functioned as the main navigation channel by means of dredging. Before DWRP, the upper section of the North Passage needed dredging (range for 16 km in length) to maintain a channel with 7m water depth, while the middle and lower sections of the North Passage

have natural water depth more than 7m. The annual dredging volume amounted to 12×10^6 m^3. It varies in different seasons. In flood season, it takes 65% volume of the total (Zhang et al., 1993).

The whole project was divided into three phases and was planned to take 10 years. The double-way navigation channel with 92.2 km length and 350-400 m width will be carried out. The designed water depths are 8.5m, 10m and 12.5m respectively for different phases. After completion, the third and fourth generation container ships as well as 50,000 tons vessel can enter Shanghai Port under all weather conditions. Furthermore, the fifth generation and sixth generation container ships, 100,000 tons full-load vessels and 200,000 tons empty vessel can entry depending on the tide.

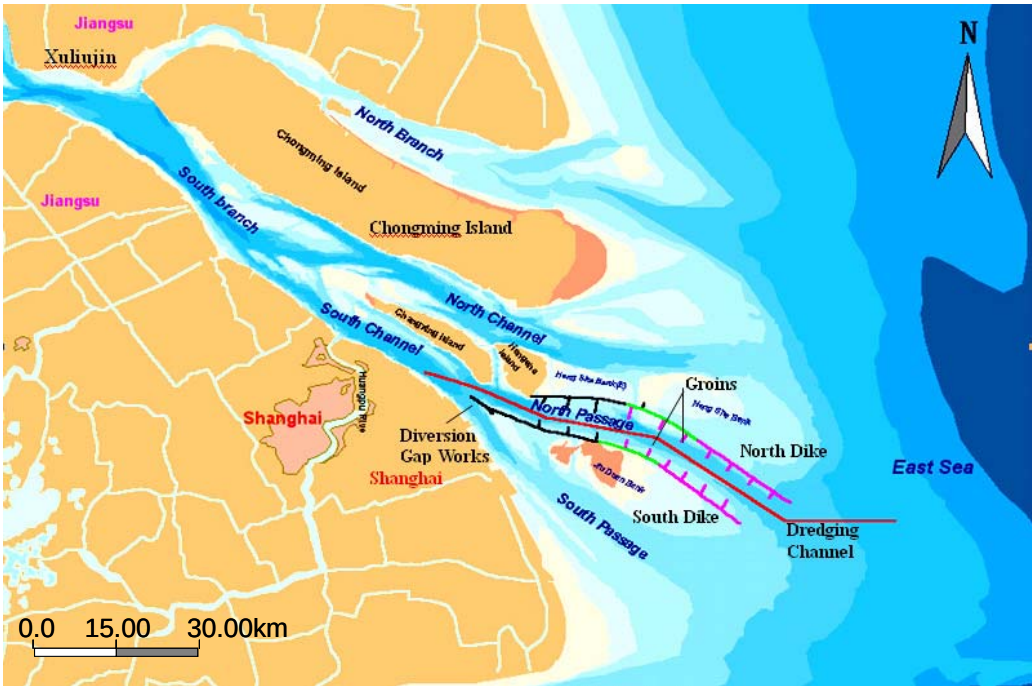

Figure 4-3 Layout of Deep Waterway Regulation Project at Yangtze Estuary
(Dikes and groins in black color are the construction in Phase I; in green color means the improvement construction of Phase I; the pink color means Phase II constructions. Dredging Channel is in red with a length of 92.2km, width of 350~400m, water depths of 8.5m, 10m, and 12.5m as objectives in different phases)

The project, based on as the guideline for the design, is set to construct the diversion gap control works, training dikes and groins alongside the passage. (a) Diversion gap works: The work consists of the 3.2km submerged dike, 1.6km south diversion dike and part of south dike. The location is at the head of the South Jiangya Shoal as shown in Figure 4-3. The objective of this work is to stabilize the South Jiangya Shoal in order to maintain a proper flow and sediment bifurcation ratio for North Passage and South Passage. (b) South and North training walls: The work consist of 49.2 km North training wall and 48.0 km South training wall. They are set to create the river-shape flow in North Passage and provide support for the groins to form the regulation lines. They can also reduce the sediment at side shoals to be stirred up to the channel by waves. In addition, the dikes can interrupt the ebb current diverted from Jiangya north passage and make it turn towards North Passage. (c)

Groins: The work consist of 19 groins is set to form a reasonable regulation line of the channel and make the distribution of the flow field beneficial to the shaping and maintenance of the deep-draft channel without changing the flow distribution rates of North Passage. (d) Dredging: The work is set to dredge the channel to reach the design for navigation depth of 12.5m and the reasonable maintenance of dredging volume on the basis of regulating structures and exerting the functions of water diversion, sand retaining and silt reduction to stabilize the river regime (YEWAB, 2007).

This project constructed the diversion gap works to stabilize the river regime and have better flow and sediment conditions for the main navigation channel; built south and north training wall to prevent the sediment from sand shores and channeling grooves into the channel; and block the ebb current from other channels. 19 Groins were built to regulate and improve the inner channel flow conditions. Based on the regulation works, dredging is necessary to maintain the water depth in the channel (Liu, 2008). The construction works of Phase I and Phase II have been finished. Phase I works finished in July 2000. An improvement work was implemented. The south and north training walls were extended and two more groins at each side were constructed in order to improve the flow and sediment conditions to obtain design water depth. Phase III that mainly focus on channel dredging was supposed to be finished in 2009. However, due to unexpected back-silting in the middle section of the channel (observed in 2006), the government has assigned several institutions to carry out the improvement suggestions through physical experiments, numerical simulations and field investigations. Detail information of the planned project and the progress are shown in Table 4-2.

Social and economic benefits have been obtained after implementation of the Project Phase I and II. The completion of 10m deep channel enhances the waterway capacity step by step (Table 4-3). The navigation conditions for large-scaled ships have been improved. The direct economic efficiency of DWRP is significant. In Phase II, part of dredged material is used for reclamation in order to make full use of the soil resources. The reclamation area was approaching 36 km^2 in Phase I and 31.3 km^2 in Phase II. This will be an important means to deal with the dredged materials in the future. Favorable social assessments have been achieved. It is of great significance to carry on implementation of the third phase of the project.

Table 4-2 The construction scale and progress of DWRP in Yangtze Estuary (data from Liu 2008)

Stage		Phase I		Phase II	Phase III	Summary
		Original	Improvement			
Period (planned)		Jan 1998 -Jul 2000	Nov 2000 -Jun 2001	May 2002 -Mar 2005	Sep.2006 -Sep.2009	
Progress		Finished	Finished	Finished	postpone	
Diversion gap works	SP Dike (km)	1.6				1.60
	Submerged dike (km)	3.2				3.20
South training wall (km)		20	10	18.08		48.08

North training wall (km)	16.50	11.41	21.29		49.20
Groins (number/km)	6 / 5.97	4 / 5.23	14 / 18.9		19 / 30.10
Water depth (m)	8.5		10.0	12.5	12.5
Width of channel (m)	300		350~400	350~400	350~400
Dredging length (km)	51.77		74.47	92.20	92.20
Dredging volume ($\times 10^4$ m^3)	4074 (3182)		7635 (5920)	16960	

Note: The dredging volumes include designed volume and actual volume. Those in brackets are the actual dredging volume according to the statistics. The statistics for Phase I was from July 1999 to Mar 2000; statistics for Phase II was from Jan 2004 to Mar 2005.

Table 4-3 Throughput and international place of Shanghai harbor (Data provided by YEWAB)

Year	1997	2000	2003	2004	2005
Container throughput (10^4 TEU)	253	561	1128	1455	1809
International place		6	3	3	3
Goods throughput(10^8 TEU)	1.64	2.00	3.16	3.79	4.43
International place			3	2	1

4.3 Morphodynamic evolution induced by regulation work at Yangtze River Estuary

To tackle the problems occurred in the regulation works, various methods can be adopted. In most estuaries, physical and numerical models are combined into research, which not only shorted the research period but also saved a lot of money. Furthermore, it can enhance the efficiency of estuary regulation work. But experience obtained from those regulation works in worldwide estuaries could not be easily applied to one Estuary due to the different characteristics and hydrodynamic complexity of each estuary. Since the 1970s, numerical models only for hydrodynamic investigations have been widely used to the mouth bar regulation works. Since the 1990s, morphodynamic simulations have been developed.

TIMOR3 has been fully validated and calibrated with measured water level, flow velocities, flow directions, and suspended sediment concentrations in dry and flood seasons. The bathymetry of 2002 has been put into TIMOR3; local bathymetry in the regulation work area has been updated to those in 2005. The modeling area remains the same (see Figure 3-1) which takes a huge region in order to minimize the boundary error caused by deformation. The boundary condition for the riverside is hourly water discharges from Feb.22 0:00 to Mar.22 23:00, 2002 and from Sep.1 0:00 to Sep.30 23:00, 2002. The boundary condition for the seaside is the hourly tidal level in the same period as the riverside. All the parameters are in consistency with the calibrated parameters in Tab.3-1. The morphological factor due to different purposes has changed.

4.3.1 Morphological changes with and without the regulation works

Simple case

In order to examine the function of training works, a simple test case is made by setting 5 groins on each side of training dikes. Under the same bathymetry and boundary conditions within the same mesh, the comparison has been made between two systems, with and without test training works. Figure 4-4 shows the layout of training works, while Figure 4-5 shows the test result.

The grain size used in this simulation was generated by a pre-run and ranged from 0.03 mm up to 1.5 mm using 10 logarithmically distributed fractions. The morphological factor was set as 35 for both suspended and bed load, and the calculating period is equal to 2 years 9 months in nature. The compared parameter in Figure 4-5 is the difference of water depth under the water reference level between two systems. The negative value colored in red represents deposition, while positive value colored in blue represents erosion. It can be seen from the figure that as expected, the model calculated a trend for erosion in the area of the groin heads and between the “groins”, there is tendency for deposition (Zhou, 2009). The simple case showed the reliability of the numerical model.

Case of Deep Waterway Regulation Project (DWRP)

- Layout of the training works according to DWRP

After the test case, it is necessary and meaningful to simulate the real case of DWRP. The available measured data and statistics will help to calibrate the model. The numerical model TIMOR, however, with its flexibility and convenience, can explore the possible problems and make predictions.

As the DWRP Phase I and II have constructed the south and north dikes, the groins and the diversion gap works, the generalized engineering measures are built in the numerical model in accordance with the prototype (Figure 4-6).

In order to examine the local flow field and sediment transport more accurately, the mesh in these engineering area has been refined. The whole modeling area has 45439 elements, and 23799 nodes. While in the project area, there are 10197 elements and 5200 nodes with minimum triangle length 70m. The south and north training dikes have an elevation of +2m under Wusong Datum (Wusong Datum-1.63m=1985 National Datum). The 19 groins (10 groins in the south training dike, S1-S10; 9 groins in the north training dike, N1-9) have +2m at the root of groins, +0m at the head of groins under Wusong Datum. The submarine dike has an elevation from western side to eastern side -2m to +2m under Wusong Datum. Its eastern side connects with the south training dike. The water depth in the modeling area is under 1985 national datum, so the bathymetry of nodes in the project area has to be carefully considered and assigned through numerical methods according to the actual project data (Figure4-7).

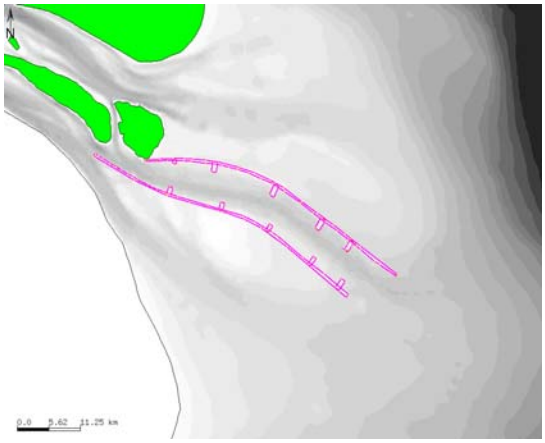

Figure 4-4 Layout of training works

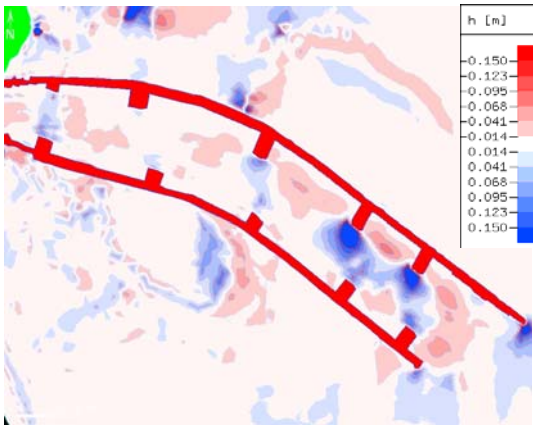

Figure 4-5 Morphological difference within 2.75 years between two systems (with-without training works)

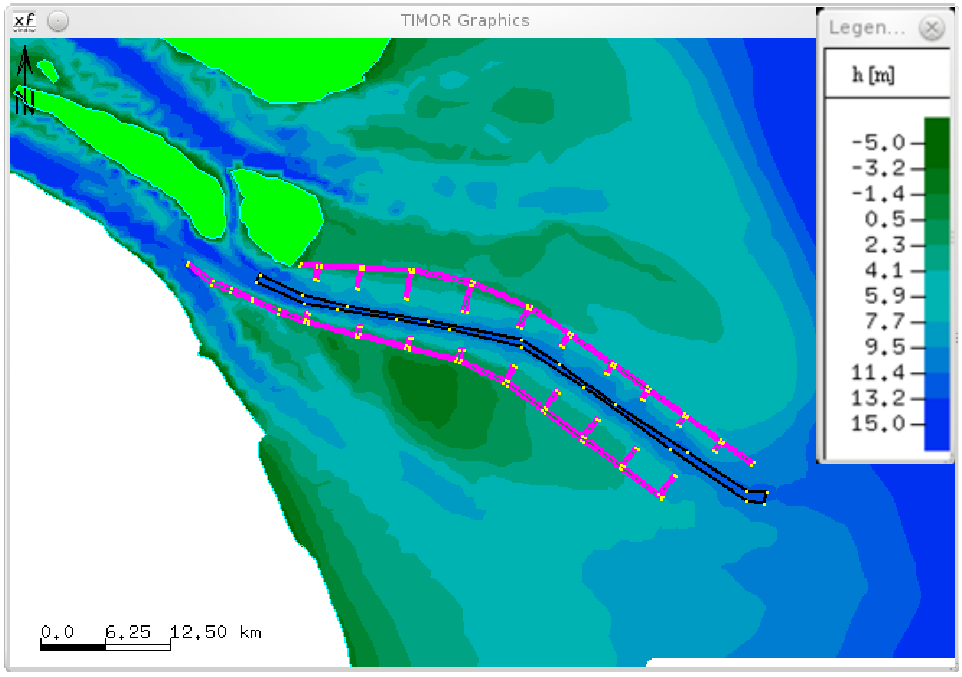

Figure 4-6 Bathymetry with engineering measures

The south and north training walls, the merging dike, and 19 groins are in red, the navigation channel with 92.2km long and 350m wide is in black. (blue= deep water; green= shallow water)

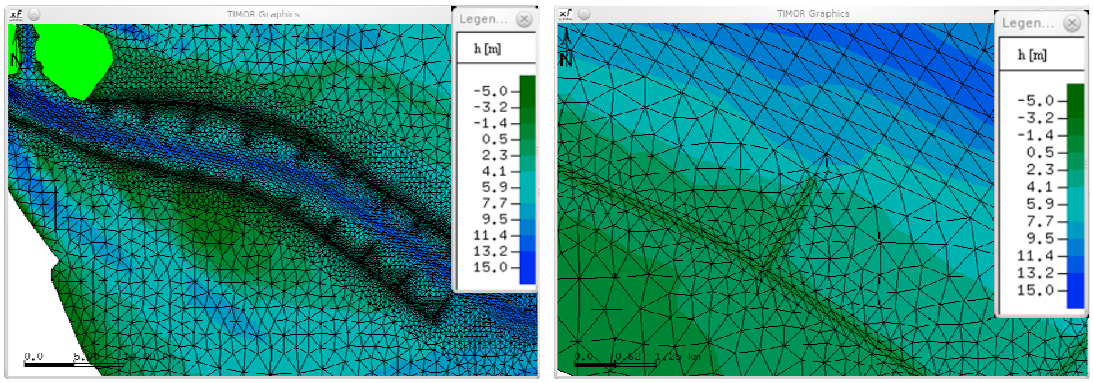

Figure 4-7 High resolution mesh for the project area at Yangtze estuary. (left) the DWRP; (right) a groin of the project. (blue= deep water; green= shallow water)

- Bathymetry changes with and without training works

The simulations here are like in the above simple case. Two systems have been taken, one without training works (which is the original input bathymetry), the other is with training works (Figure 4-6). A morphological factor as 70 is set to get 5 years morphological changes in the simulated area. Figure 4-8 and Figure 4-9 show the bathymetry changes in one year without and with training works respectively. Figure 4-10 and Figure 4-11 show the difference of bathymetry changes in one year between systems with and without training works. The purpose of this simulations are to see how much effect the DWRP will have on the bathymetry changes, whether the training works will fulfill its designed principle as guiding the current, preventing sediment from sand shores and relieving deposition in navigation channel.

The bathymetry changes in two systems with and without training works have same tendency. In the upper section of the channel, a little bit erosion occurred. In the lower section of the channel, deposition took the main position. But the deposition area without training works is larger than that with training works. The difference of bathymetry changes in one year showed that, the channel in the upper and middle section has obvious erosion with training works. The groin head in the south training dike has erosion as well, and meanwhile, there is a deposition area in the lower section of the channel in the direction of SE~NW. The difference of bathymetry changes in two years showed that, the whole channel is under erosion, the mouth bar disappeared. This is a case to test the function of the training works.

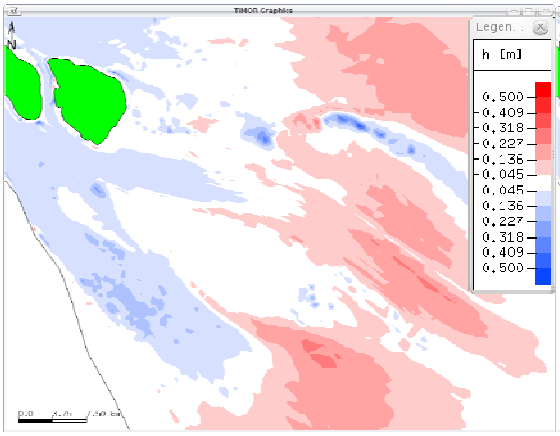

Figure 4-8 bathymetry changes in one year without training works

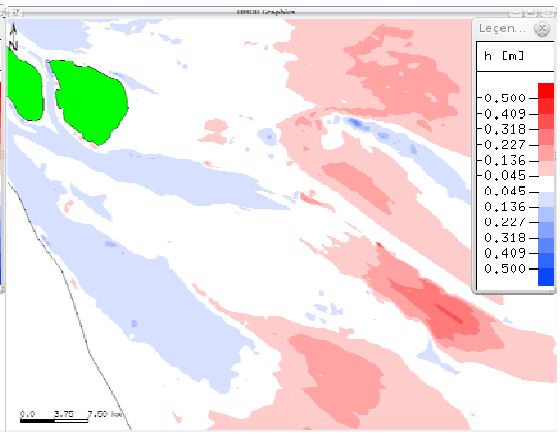

Figure 4-9 bathymetry changes in one year with training works

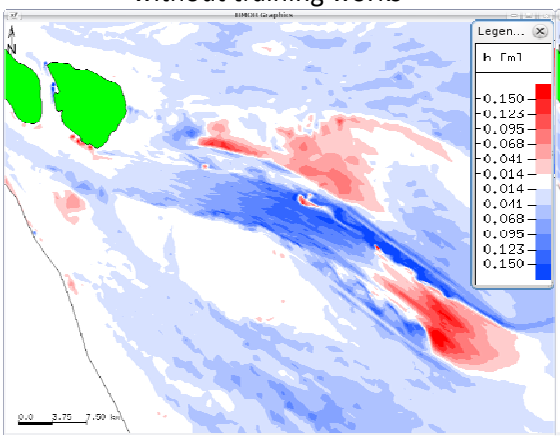

Figure 4-10 Difference of bathymetry changes in one year (with–without training works)

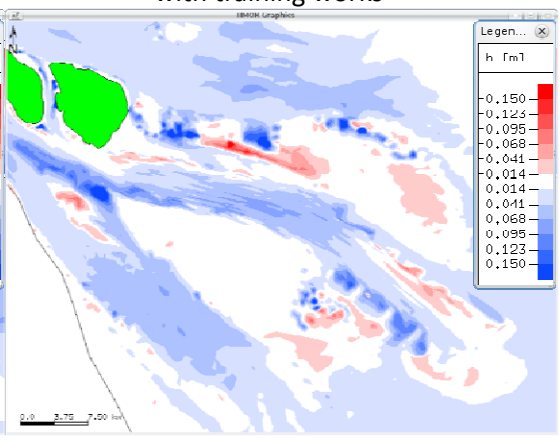

Figure 4-11 Difference of bathymetry change in two years (with–without training works)

- Hydrodynamic changes with and without training works

The relationship between tidal current and SSC (Suspended Sediment Concentration) in Yangtze Estuary can be concluded as that, the SSC is higher during spring tide than other tidal period; and higher during flood tide period than ebb tide period. It is necessary to check the hydrodynamic changes with and without training works.

The maximum velocities during flood and ebb represent the starting ability of sediments. The bed load sediment in the North Passage is quite fine, with the average medium grain size between 0.02mm and 0.04mm. The starting velocity of such kind of sediment is bigger than its stirring velocity, which means, once the sediment is started to move, it become then suspended sediment and not easy to settle down again. Therefore, the maximum flood velocity and maximum ebb velocity have great impact on the riverbed evolution and channel back-silting (Liu, 2008).

Figure 4-12 shows the difference of maximum ebb velocity in one year between two systems with and without training works. Figure 4-13 shows the difference of maximum flood velocity in one year between two systems with and without training works. The maximum ebb velocity is bigger in the upper section with training works than without training works (Figure 4-12), which means the ebb tide is stronger in that area and could bring much more sediment into the sea. The maximum flood velocity in the upper section is also stronger (Figure 4-13), so the total effect of tidal currents makes the upper section of the channel erosion. The maximum ebb velocity in the lower section is weak comparing to the upper section (Figure 4-12), but what important is, the maximum flood velocity in the lower section is stronger than the upper section (Figure 4-13). In this case the flood tide transport the sediment from seaside to the lower section of the channel and the weak ebb tide could not carry them out of the channel, so deposition occurs. This could explain very well the deposition in the lower section of the channel in Figure 4-10.

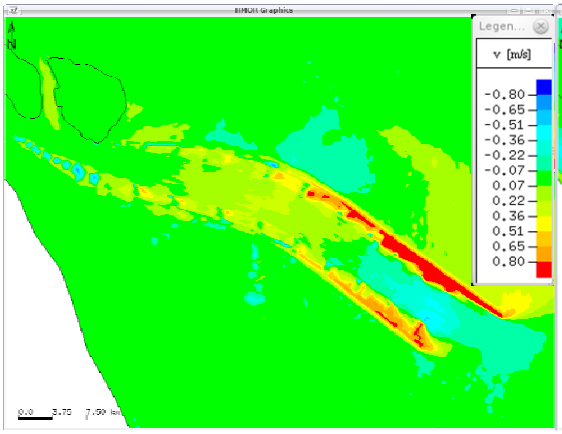

Figure 4-12 Maximum ebb velocity difference in one year (with-without training works) (red= high velocity)

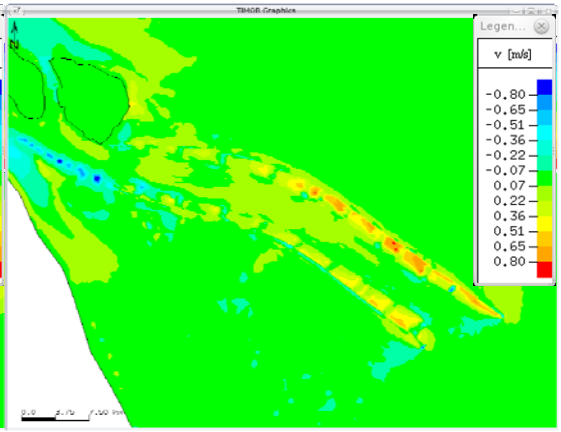

Figure 4-13 Maximum flood velocity in one year (with-without training works) (red= high velocity)

Remarks

A simple case and the case of DWRP have been simulated by the numerical model TIMOR with the purpose of getting intuitive impression of training works. The simple case showed that the simulation result is reasonable to the basic regular pattern of sediment transportation. The training dikes can narrow the flow and enhance the flow velocity. The groins which guide the current in the one hand and trap the sediment on the other hand. The case of DWRP has done a more detailed examination of the morphological changes with and without the regulation works. The bathymetry changes in one year with and without training works have been given. The difference of bathymetry changes in one year and two years have been made between two systems. The deposition and erosion area corresponds well to the changes of maximum ebb and flood velocities.

4.3.2 Long-term morphological changes with regulation works

Two cases discussed above have illustrated the function of training works. In this section, the long-term morphological changes caused by the regulation works are simulated by TIMOR with the purpose of calibrating the calculated results with available measured data to lay a solid foundation for the future predictions.

Observed geomorphology before and after DWRP

Figure 4-14 and Figure 4-15 gave the observed geomorphology in the year of 1997 and 2005, before and after the DWRP respectively. Before DWRP, due to the horizontal gradient of water surface, the North Passage exchanges flow current with the North Channel through East Hengsha Passage and Hengsha groove; and exchanges flow current with the South Passage through North Jiangya passage and Jiuduansha groove. An uneven longitudinal section was formed due to the ebb tide and flood tide. The ebb current divers from the North Passage to the North Jiangya passage and Jiuduansha groove, which weakened its erosion effect for the mouth bar in the upper section of the North Passage. In the middle section of the North Passage, a pool with 10m depth was formed as the ebb current entered into it from the East Hengsha passage. In the lower section of the North Passage, the natural water depth is bigger than 7m.

After the Phase II of DWRP, the response of morphology to the training works is obvious. A smooth and micro-bend navigation channel has been obtained. The mouth bar in the upper section disappeared, and the channel could be maintained with 10m water depth by dredging. This could be explained that, the north training dike of DWRP has blocked the East Hengsha passage; while the south training dike has blocked the North Jiangya passage and Jiuduansha groove, thus the sediment from these grooves have been prevented from entering into the channel. The joint function of groins and training dikes has strengthened the hydrodynamic power and guide the current.

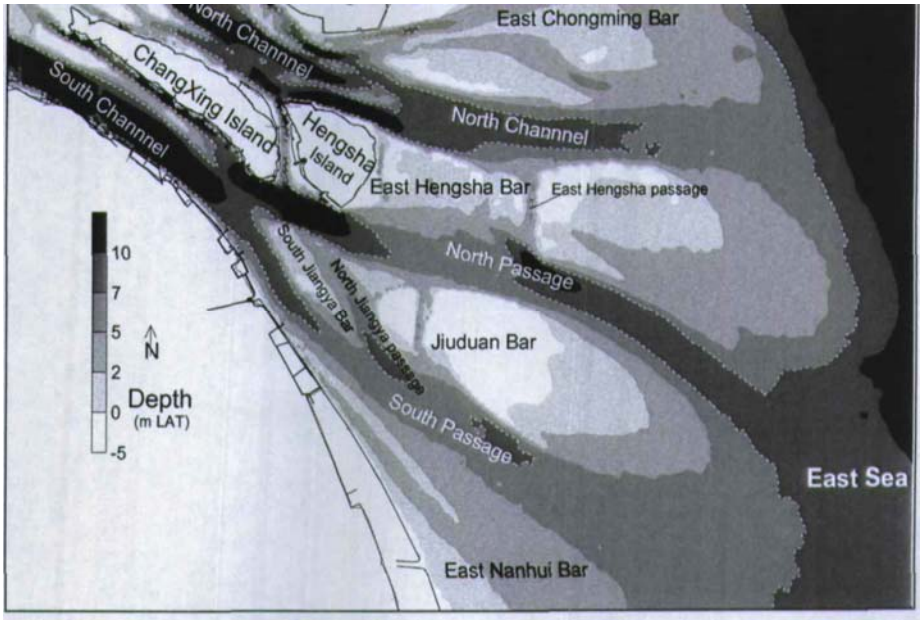

Figure 4-14 Geomorphology before the DWRP in 1997 (Liu, 2008)

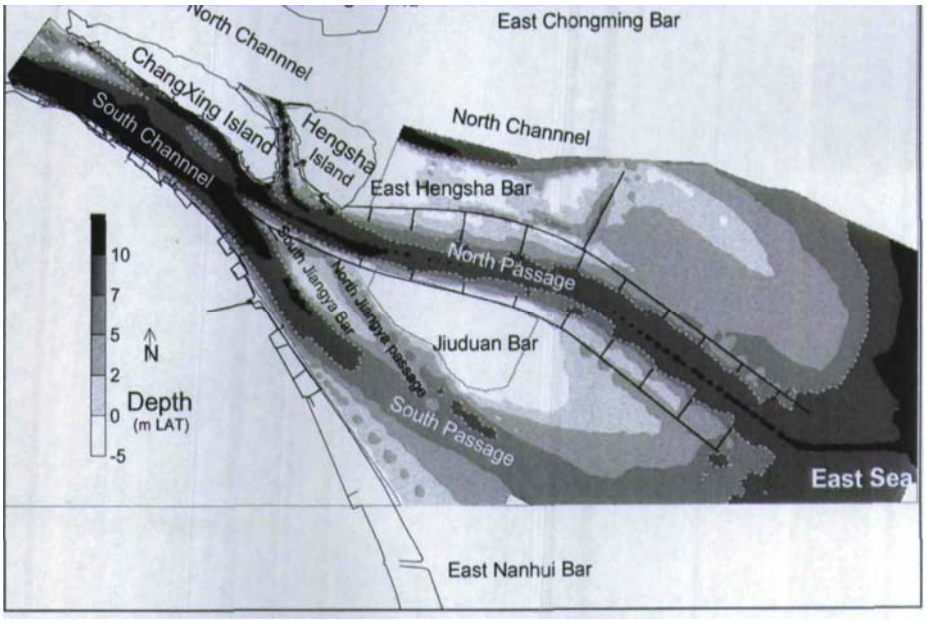

Figure 4-15 Geomorphology after the DWRP in 2005 (Liu, 2008)

Comparison of measured and modeled results between 2002 and 2005

After understanding the general changes of geomorphology before and after DWRP, simulations have been made to examine further the effect of the training works. Under the same hydrodynamic condition and the same topography with unchanged calculating parameters, simulations with training works (Figure4-5) have been carried out.

The period from May 2002 to May 2005 is the period for the improvement construction of Phase I and the construction of Phase II. During this period, total 19 groins have been built, while the south and north training dikes have been stretched to their current length (Tab.4-2). Figure 4-16 is the measured erosion and sedimentation map from May 2002 to May 2005.

Figure 4-17 is the calculated map of erosion and sedimentation by TIMOR3.

The three months from Feb to May in 2005 is just after the establishment of Phase II. All the constructions have been finished and the morphology is under adjustment. Figure 4-18 is the measured from February to May in 2005. Figure 4-19 is the calculated map of erosion and sedimentation by TIMOR3 during the same period.

The measured data in Figure 4-16 showed that, the middle and lower section has obvious erosion, while the upper section and areas among the groins is under deposition. The calculated results in Figure 4-17 showed great agreement with the measured data. The erosion position and erosion strength in the simulated results are in the same trend with the measured ones. The whole area among those groins on both sides of north and south training dikes is under deposition, but the whole channel is under erosion. The upper section has much heavier deposition comparing to the middle and lower section. The morphology readjusted itself to the implementation of DWRP. The hydrodynamic conditions in these parts have been greatly improved by the added groins and extension of training dikes, which fulfills the original purpose of maintaining a navigation channel.

Figure 4-18 is the measured data for three months, just after the establishment of Phase II. Even though the lower section has erosion (less than 1m) comparing to the upper section of the channel, the morphology of the whole North Passage reached a relative dynamic equilibrium. The calculated results in Figure 4-19 showed the same equilibrium, but the erosion in the lower section is not obvious. What has to mention is that, the area among groins in the middle part of the training dikes is not under deposition any more.

The calculated results agree quite well with the measured one which shows the feasibility of the morphological model. Simulated results after 2005 will be plotted for discussion and analysis.

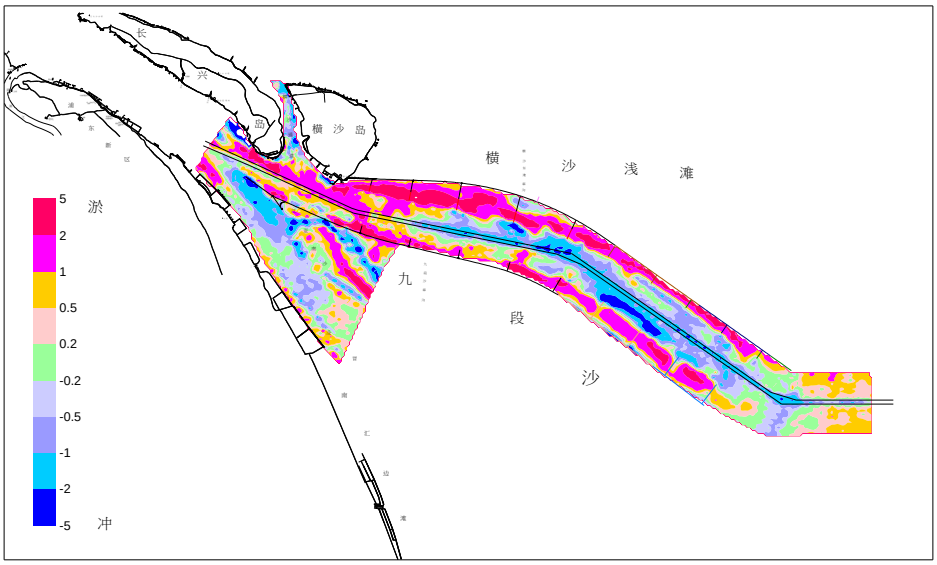

Figure 4-16 Measured erosion and sedimentation map from May 2002 to May 2005 (blue= erosion; red= deposition)

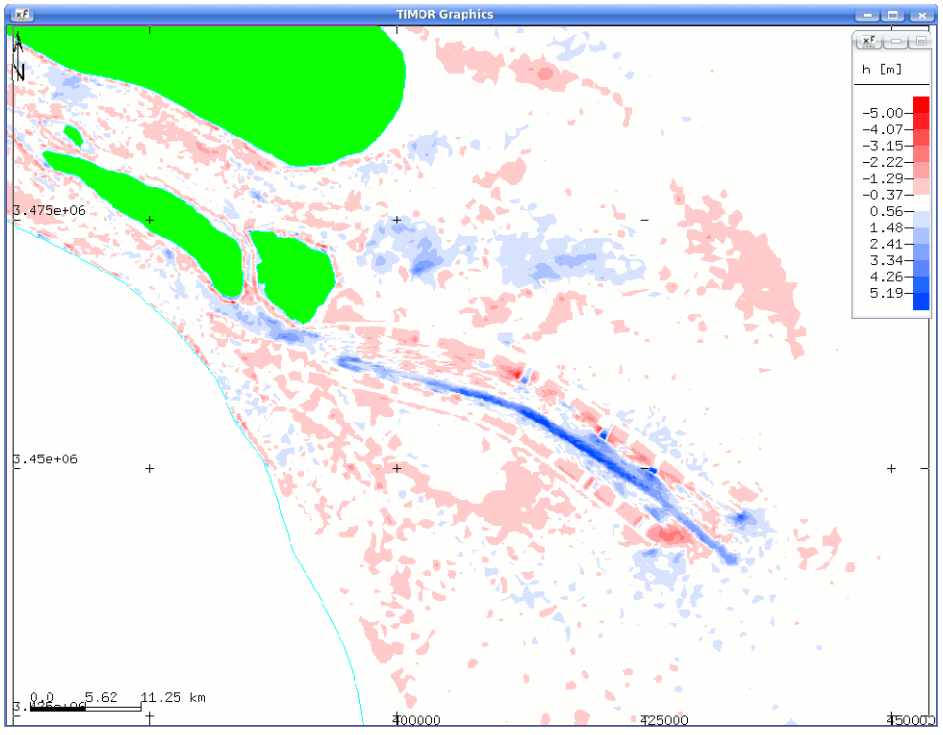

Figure 4-17 Calculated erosion and sedimentation map from May 2002 to May 2005 (blue= erosion; red= deposition)

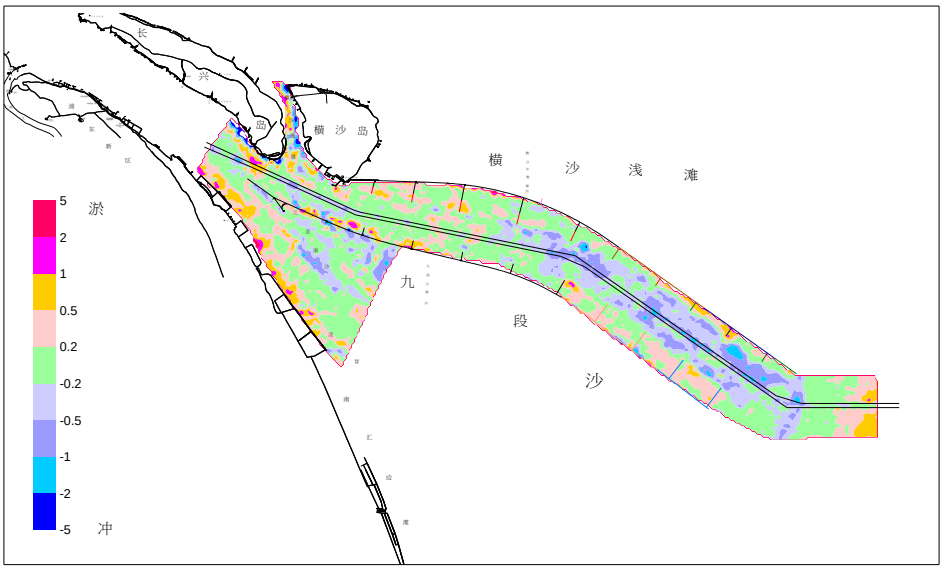

Figure 4-18 Measured erosion and sedimentation map from February 2005 to May 2005 (blue= erosion; red= deposition)

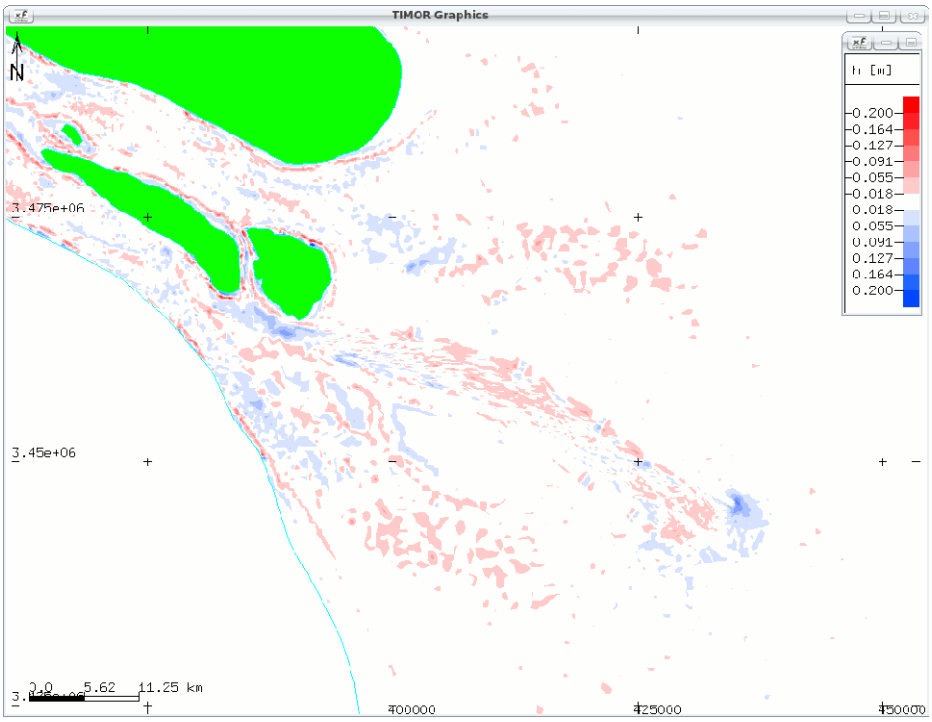

Figure 4-19 Calculated erosion and sedimentation map from February 2005 to May 2005 (blue= erosion; red= deposition)

Simulation of bathymetry changes from 2005 to 2007

After the comparison between the measured data and calculated results, a systematic analysis of bathymetry changes in the year after the Phase II of the project is given. Figure 4-20, 4-21, 4-22, and 4-23 showed the bathymetry changes of the model results from 2002 to 2007.

It is obvious from those figures that not only the area among groins but also the whole channel is under deposition, especially the middle section. Many reasons should be

accounted for. Firstly, due to the deposition in the area among groins after 2002, the total volume of the channel in the North Passage was decreasing, which changed the pattern of the morphology. The total flood current is strengthening, and ebb current is decreasing, which lead more sediment from seaside to be transported to the channel. Secondly, the sediment source for the continuing deposition needs to be analyzed. As the analysis from Figure 2-4 (the annual sediment concentration and sediment discharge), after 2003, the sediment discharge is decreasing, which means, the sediment source besides from the riverside, has much from the seaside as well. In recently years, the sediment came also from the Jiuduansha Shore into the channel. The artificial sand mining in Ruifengsha provided rich sediment source. Besides, part of the dredged material which is thrown into the mud storage pit could deposit in the channel.

In general, after the establishment of Phase II in 2005, the main channel appeared with continuous deposition, which has somehow weakened the effect of training works. There are mainly two phases for the readjustment of morphology with the regulation form as “double dikes + groins”. The first phase is during the construction, which characterizes as obvious erosion in the main channel and deposition in the groin areas. This phase lasts for 1 year. The second phase is after the construction of the training works, the main channel appears with continuous deposition with the continuing deposition of area among groins. This phase of deposition will last for 6~7 years (Liu, 2008).

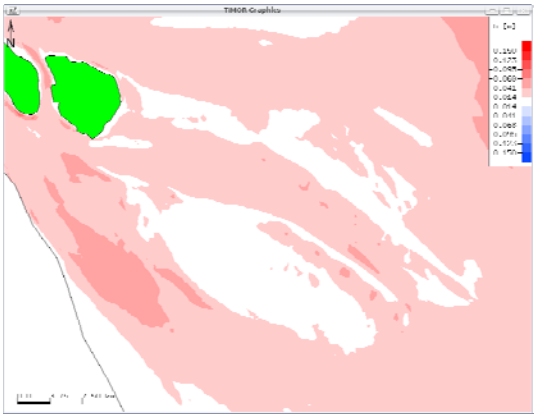

Figure 4-20 Calculated bathymetry changes during 01-12.2005

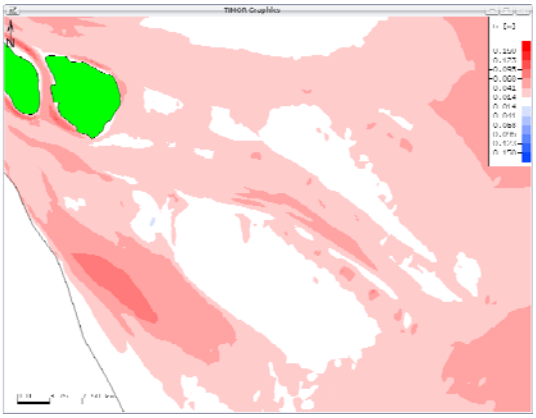

Figure 4-21 Calculated bathymetry changes during 01-12.2006

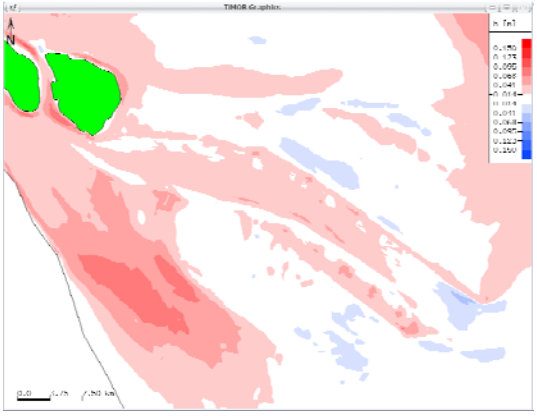

Figure 4-22 Calculated bathymetry changes during 01-12.2007

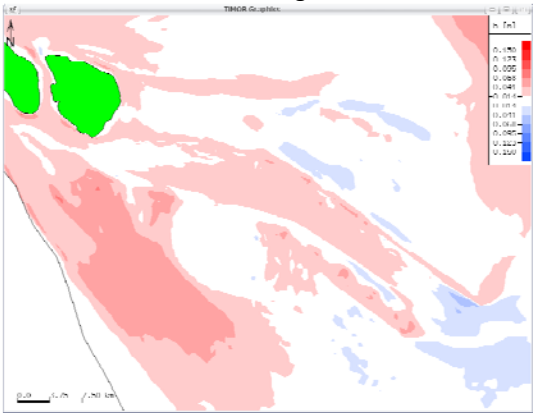

Figure 4-23 Calculated bathymetry changes during 01.2005-12.2007

(for all the figures here, blue=erosion; red=deposition)

Hydrodynamic changes from 2005 to 2007

The hydrodynamic changes have direct relationship to the bathymetry changes. The maximum ebb and flood velocity changes in the year of 2005, 2006, 2007 and the changes between 2005 and 2007 have been plotted in Figure 4-24 (a-d) and Figure 4-25 (a-d) for analysis.

The maximum ebb velocity in 2005 is increasing, especially in the main channel, seen in Figure4-24(a). Meanwhile, the maximum flood velocity is decreasing a little bit, seen in Figure4-25(a). This hydrodynamic changes match with the erosion and deposition map in Figure 4-19, but as mentioned, there are many other reasons for the deposition. The maximum ebb velocity in 2006 is increasing (see Figure4-24(b)), but the maximum flood velocity is increasing much more (see in Figure4-25(b)), which resulted in deposition in the whole channel (Figure4-21). Both the maximum ebb velocity and flood velocity in 2007 (Figure4-24(c), Figure4-25(c)) are decreasing, however, the maximum ebb velocity decreased in a more degree than that of maximum flood velocity, that's why the year of 2007 has deposition in general (Figure4-22). The changes of maximum ebb and flood velocity between 2005 and 2007 are obvious, the maximum ebb velocity is decreasing, while the maximum flood velocity is increasing, which resulted in deposition (Figure4-23).

The changes of maximum ebb and flood velocities correspond to the bathymetry changes, which tell us that the hydrodynamic conditions have obvious effect on the morphology.

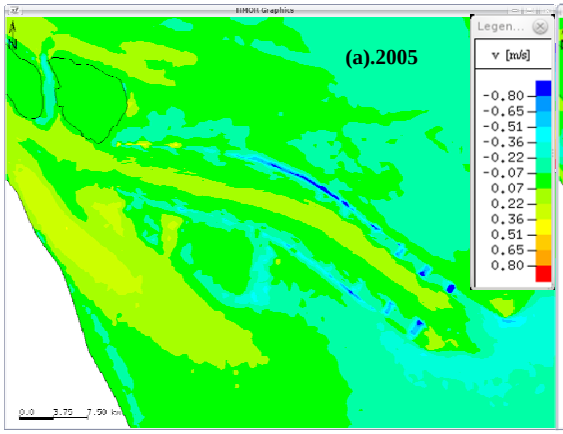

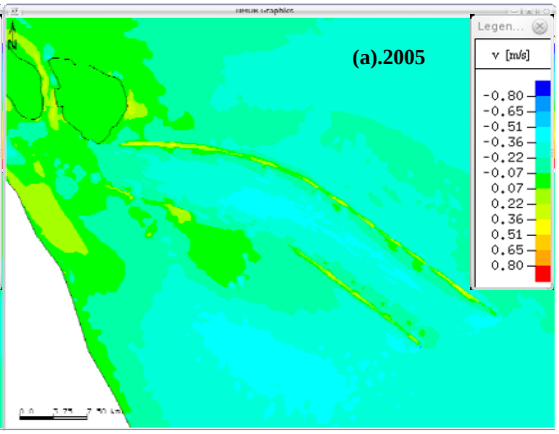

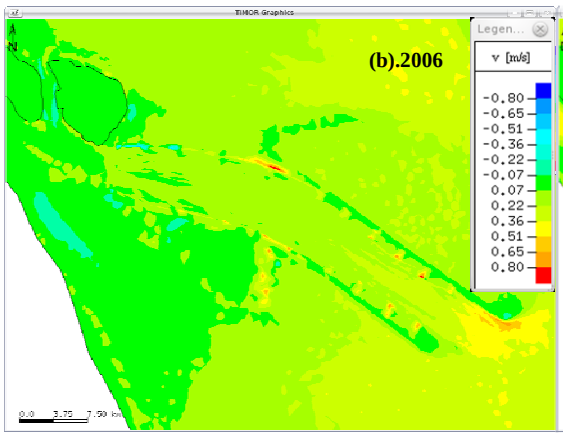

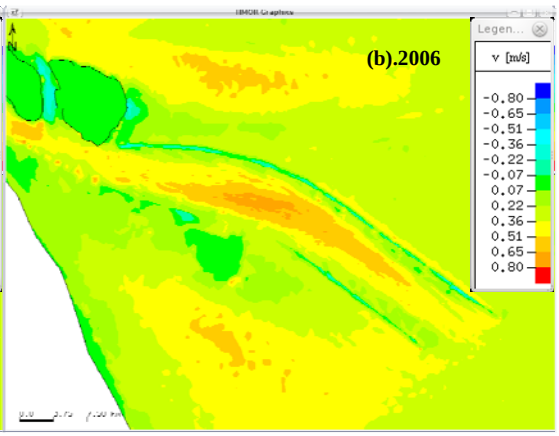

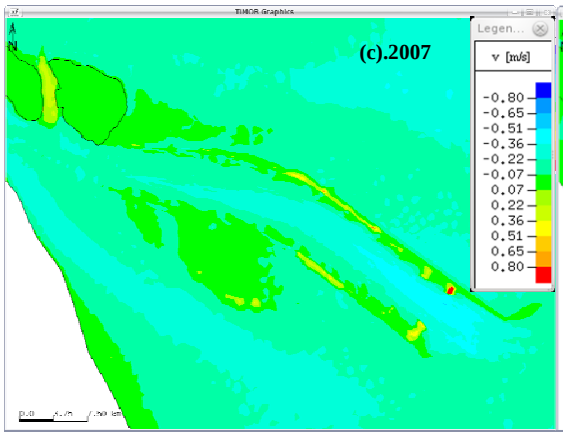

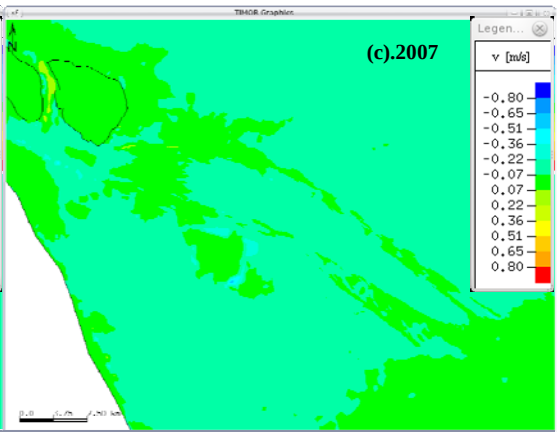

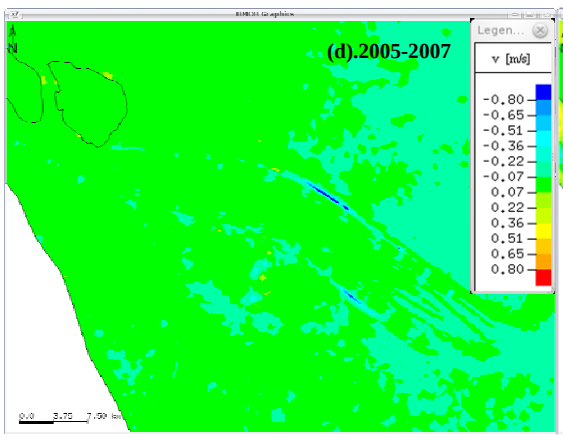

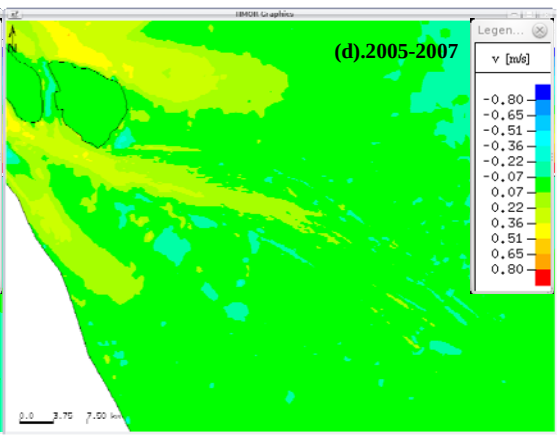

Figure 4-24(a)-(d) Changes of maximum ebb velocity

Figure 4-25(a)-(d) changes of maximum flood velocity

4.3.3 Analysis of dredging volume

The purpose of the regulation works in the mouth bar of estuaries is to get bigger water depth with little maintenance dredging volume and to ensure the long-term navigation possibility of the channel. After dredging, the original equilibrium of sediment transport is broken, and the channel is resulted in sedimentation. The major dynamic factors affecting the sedimentation are river runoff, tidal current, waves, salt wedge density flow, and alongshore currents. The sediment factors include the different sources, from seaside and from riverside. Besides, they also conclude the flocculation characteristics of cohesive sediments, and the maximum turbidity zone. The sedimentation in the channel is the joint effect of different dynamic factors and sediment factors. Furthermore, it also depends on the layout of the regulation works, the position of the channel axis and the elevation difference between channel and shoal.

It mainly depends on dredging to maintain the water depth in the regulated channel, so the dredging volume after each phase of project becomes the key research topic of DWRP. In the feasibility study of this project, different methods have been used to make predictions of the dredged volume. However with the implementation of the project, the topography is continuously changing, together with the variable incoming water and sediment discharges from the upper Yangtze River. New problems occur now and then, so it is of great necessity to monitor the dynamic hydraulic and sediment environment changes and calculate the dredging volume respectively.

The numerical model TIMOR has been thoroughly validated and calibrated with measured water levels, current velocities and directions, suspended sediment concentrations, as well as the bathymetry changes. The calibration results meet the demand of precision and criterion of engineering. Therefore further calculations have been made with the model. The calculated dredging volume is compared to the available statistics of dredging volume. Predictions are made based on dredging volume calibrations.

Simulation method and process

Two groups of simulations for calculating the dredging volume have been carried out with TIMOR. One group is calculating the dredging volume without training works for maintaining water depth 7m, 8.5m and 10m. Another group is calculating the dredging volume with training works for maintaining water depth 8.5m, 10m, 12.5m and 15m, which are the target water depth for three phases of the DWRP and the long-term goal. The only one difference between the two systems is with or without building of training works. In order to consider the variable water discharges in a year in the Yangtze Estuary, the model calculated one month with spring tide, mean tide and neap tide both during flood season and dry season (calculation time). With the morphological factor 35, the simulated results represent 3 year (simulation time).

A polygon along the channel (Figure4-5) is made in the model and set to have the different maintenance water depth. The dredging process set in the model is that, when the water depth in the channel is less than the target of maintenance water depth, the deposited material in the channel will be dredged. The topography will be updated after the dredging.

Simulation results

There are many results from the simulations, and here we draw out the meaningful ones for comparison and analysis. Figure 4-5 shows the dredging volume with and without training works under maintenance water depth 10m. Figure 4-27 shows the dredging volume with training works under maintenance water depth 8.5m, 10m, 12.5m and 15m respectively. The x-axis represents the simulated time, while the y-axis means the total dredging volume.

Table 4-4 gives the calculated annual dredging volume for different maintenance water depth, the dredging volume for the different construction phases, and also the available statistics or analyzed results from other researchers and institutes. The annual dredging volume is the averaged value from annual dredging volume in dry season (Feb.22-Mar.22) and in flood season (Sep.1-30). The dredging volume for construction means that at the very beginning of the different construction phases, the navigation channel needs to be dredged during the building of groins and training dikes, and then it depends on regular dredging to maintain the objected water depths.

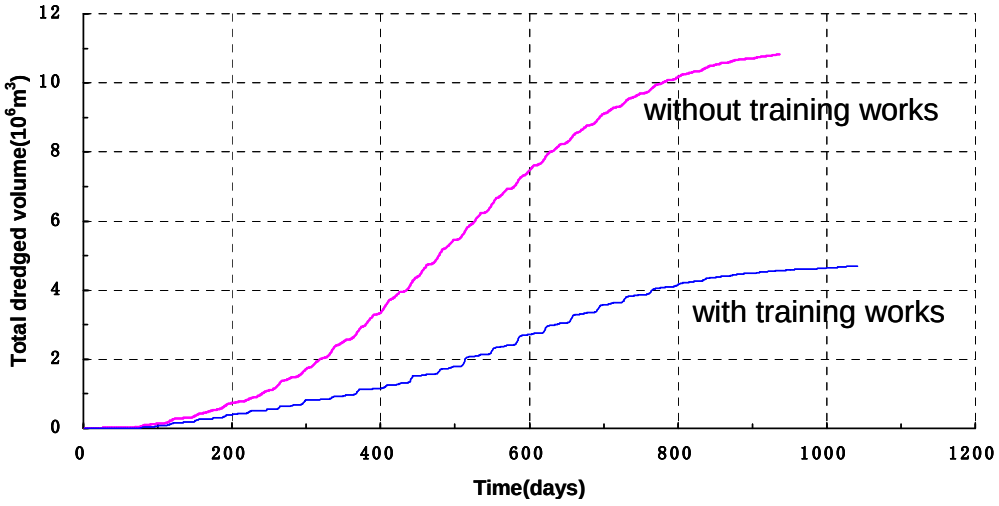

Figure 4-26 calculated dredging volume with and without training works (under maintenance water depth 10m)

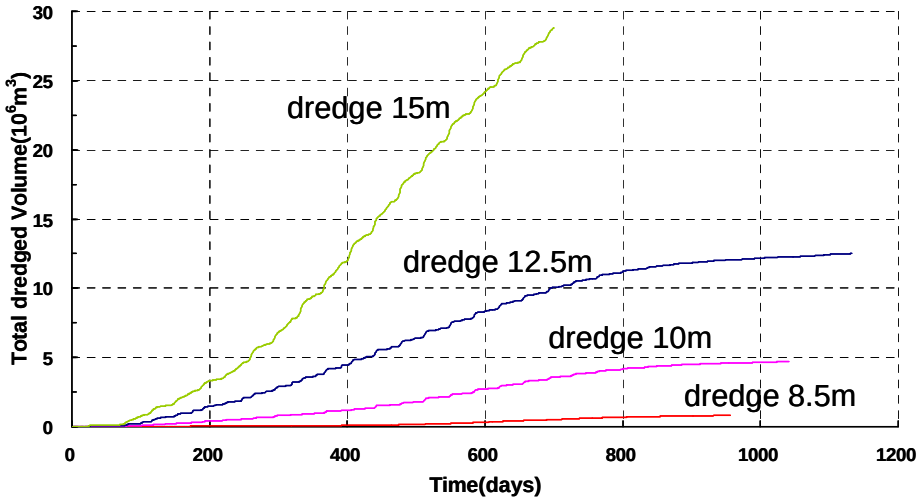

Figure 4-27 Calculated dredging volume with training works under different maintenance water depth

Table 4-4 Dredging volume with training works
(mea.= measured; cal.= calculated)

Maintenance water depth (m)	Annual dredging volume (m^3)	Statistics or referenced results (m^3)	Dredging volume for construction (m^3)
8.5	7,227,151	7,000,000 (Yan,2002,mea.) 10,054,000 (Wang,1999,cal.) 12,000,000 (Dou,2006,cal.)	1,558,476
10	21,376,282	14,972,000 (Wang,1999,cal.) 20,420,000 (Dou,2006,mea.) 40,400,000 (SWEDC,2008,mea.)	14,668,884
12.5	53,160,046	21,148,000 (Wang,1999,cal.) 72,600,000 (SWEDC,2008,mea.)	83,885,336
15	70,759,735		175,459,568

Discussion

From the simulated results in figure 4-26 we can see that, the dredging volume without training works is much higher than that with training works. With the simulation time 400 days, the dredging volume without training works is twice as that with the training works, but with 800 days, it is 2.5 times. So as time increases, the difference is bigger. The training works have reduced deposition in the navigation channel which fulfills one of its important functions.

The results in figure 4-27 show that, to maintain the water depth as 8.5m, 10m, 12.5m and 15m, the dredging volume is increasing. The dredging volume of each case increases rapidly at beginning. However after two years, the increasing speed slows down and reaches a stable increasing rate for water depth 8.5m, 10m and 12.5m, the dredging volume for maintaining 15m water depth is still increasing rapidly.

The annual dredging volume for maintaining 8.5m and 10m is acceptable, but for 12.5m the dredging volume is much higher. With different numerical models and computational methods, the calculated results are different. However the calculated results from TIMOR are between those of results. From this point of view, even there are no predictions from others available for maintaining 15m water depth, we can say the result for 15m is possible and reasonable.

4.4 Prediction of morphological changes under engineering measures

The morphology changes occur greatly in two or three years after the building of the training works. This huge human engineering works has definitely affected the hydrodynamic and sediment environment in its area. On the contrary, the changed hydrodynamics and morphodynamics will also exert influence on function of the training works.

From the above simulations and analysis, we can easily see that the middle section of the channel is under deposition. The dredging volume for maintaining 12.5m water depth reaches nearly 60 Million m^3, which is not only high financial pressure, but also for the sustainable development of the navigation channel. The reason for the deposition in the middle section has been analyzed in the above section. The sediment source, the hydrodynamic conditions and the bathymetry conditions are possible causes. Engineers, scholars and institutes have done intensive research on how to reduce the deposition with physical models, site surveys, and numerical models. Liu (2008) studied carefully on the morphological evolution in the North Passage after the DWRP based on rich measured data. He has put up six suggestions to deal with this problem. (1) Heightening the south training dike to prevent the sediment from Jiuduansha shore coming into the North Passage. (2) Repairing Ruifengsha to reduce the sediment source from the upstream. (3) Adjusting the axis of the channel to reduce the angle between the upper section of the channel and the talweg. (4) Extending the groins to narrow the river. (5) Enlarging the curvature radius of the regulation line. (6) Limiting the current in the South Passage by engineering measures to enhance the ebb tide motion. It is necessary to predict the changes of hydrodynamics and morphodynamics that could happen before implementing those engineering improvement measures.

In this section, the influence of the engineering approach-heightening the south training dike is studied by numerical simulation with TIMOR. The bathymetry is taken as the same with simulation of the original training works. The morphological factor is 45. Both dry season and flood season has been simulated. The influence of them will be compared. Comparison has also made between the original training works, and those with heightening the south training work by 1m and 2m.

4.4.1 Bathymetry changes

Effect of dry season and flood season

Figure 4-28, 4-29, 4-30, 4-31 are the results of bathymetry changes in half a year and one year by heightening the south training dike 1m under dry season and flood season respectively. The simulation set to bagger the navigation channel for maintaining 12.5m water depth. The bathymetry changes in half a year under dry season is minor, most of the area is under balance, and only the lower section is under light erosion. After one year, the pattern changed, in the upper section of the channel, light deposition appeared. Both bathymetry changes in half a year and one year under flood season are much bigger than that under dry season. Furthermore, the function of heightening south training work is much more obvious. The areas among those groins along the south training dike are less deposited compared to those along the north dike.

Comparing to the results under dry season, the bathymetry changes under flood season is much more significant. According to the statistics, the deposition happens intently in the flood season (May to October), which accounts for 72.6~95.8% of the whole year, after the implementation of Phase I and II of DWRP (Tab.4-5). The effect of flood season on the bathymetry is bigger, so the following comparisons and analysis will be concentrated on results in flood season.

Table 4-5 ratio of deposition during flood season
from 2001 to 2005 (data from Liu, 2008)

Year	Ratio	Month with maximum deposition
2000		August
2001	72.6%	March
2002	90.1%	July
2003	78.3%	August
2004	95.8%	September
2005	75.8%	August
Average	82.5%	July

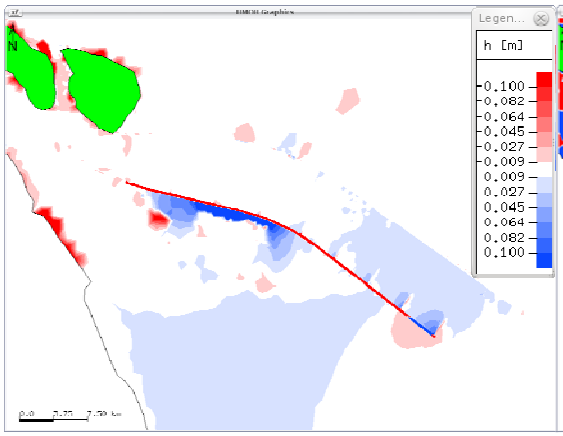

Figure 4-28 in half a year under dry season

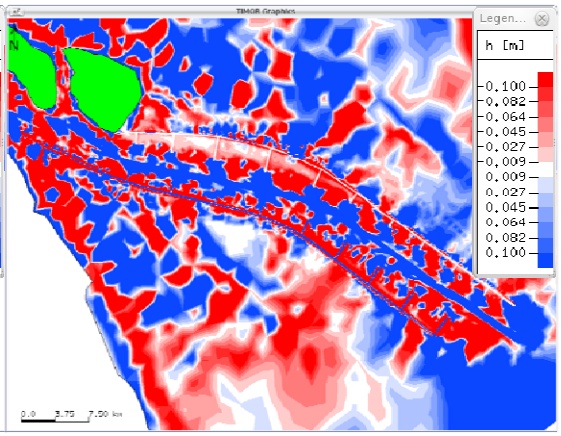

Figure 4-29 in half a year under flood season

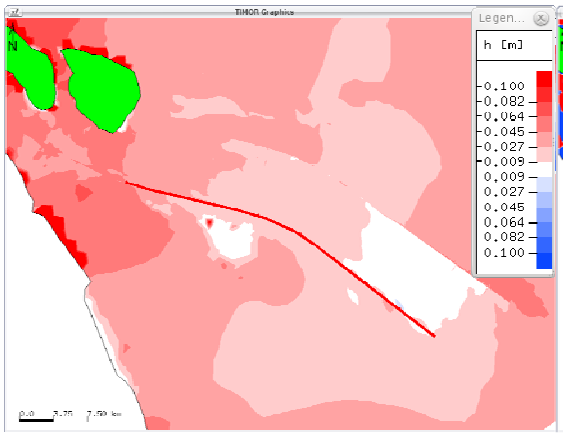

Figure 4-30 in one year under dry season

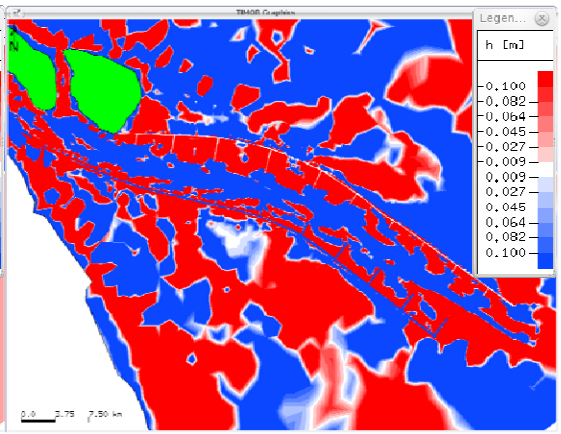

Figure 4-31 in one year under flood season

Note: the above figures are calculated bathymetry changes between the original training work system and the one with the south training dike heightening for 1m. For all the figures here, blue=erosion; red=accumulation

Difference of bathymetry changes

Comparison has been made on the difference of bathymetry changes between original

training work and those with heightening the south training work with 1m and 2m under flood season with the maintaining water depth 12.5m. Figure 4-32 (a-d) are bathymetry changes difference between original training work and the one with heightening 1m of the south training work in half a year, one year, two years and three years. Figure 4-33(a-d) are those between original training work and the one with heightening 2m of the south training work.

The deposition and erosion pattern of these two comparison group is very similar. The areas among groins along the north training dikes are under deposition with heightening the south training works either 1m or 2m, but those among the south training dikes are not deposited. Heightening the training work in this case has its effect to reduce the deposition along the south dike, especially in the upper section, but the difference with heightening 1m or 2m is not obvious.

Figure 4-32 & Figure 4-33
Bathymetry difference between original training work system 0m and the ones with south training wall heightening 1m and 2m, for maintaining 12.5m water depth in deep channel.
For all the figures, blue= erosion, red=deposition

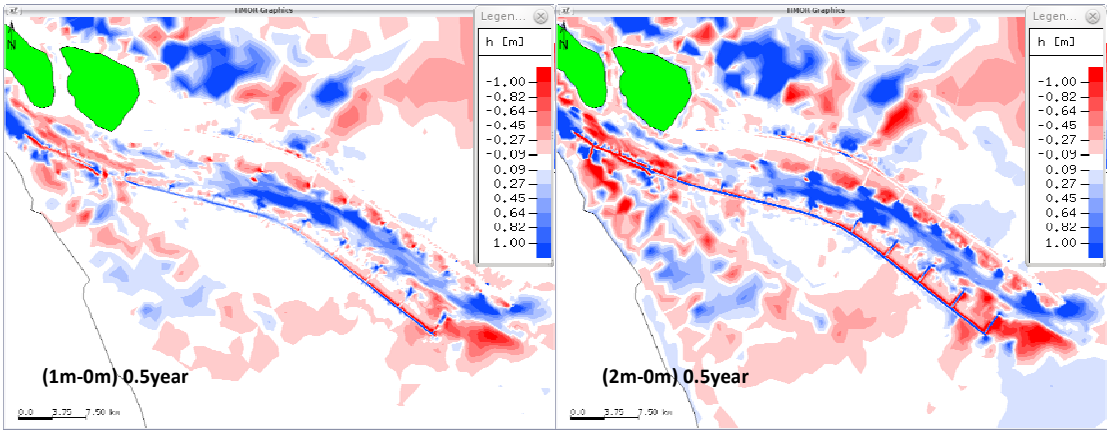

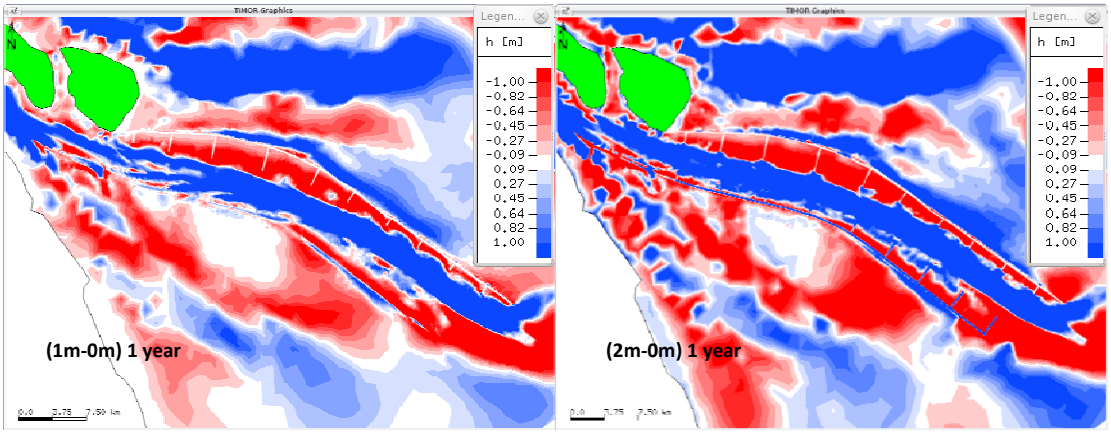

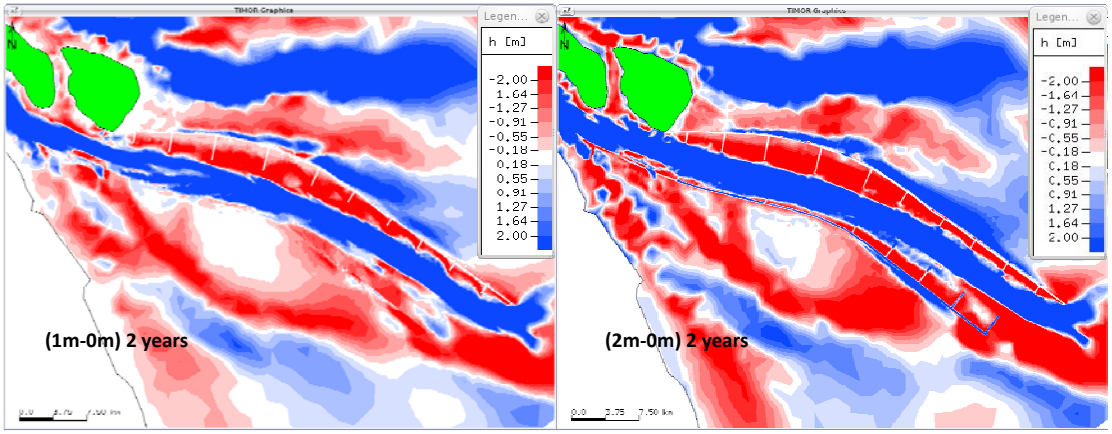

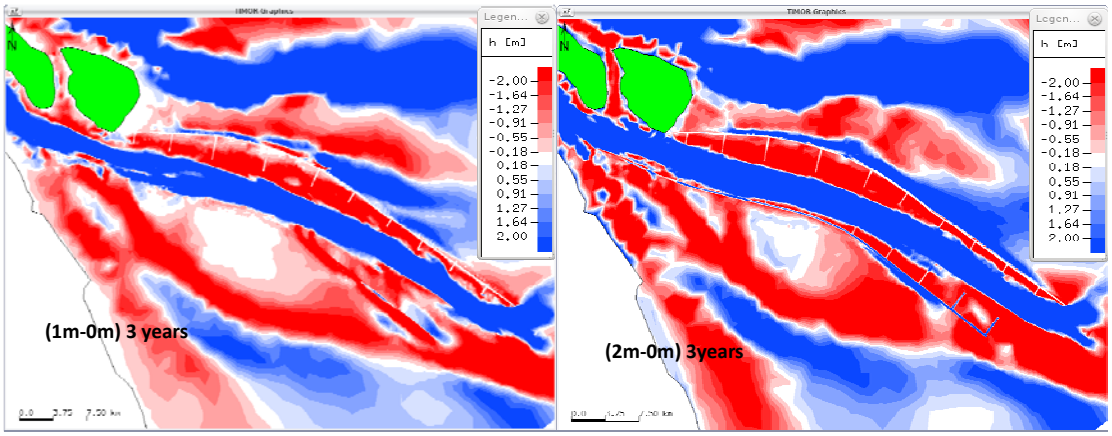

Figure 4-32: system (1m)-system (0m)

Figure 4-33: system (2m) - system (0m)

4.4.2 Hydrodynamic changes

The hydrodynamic conditions take a dominant role in transporting the sediment. How the tidal current reacts to the enhanced training dike needs to be analyzed. Figure 4-34 and Figure 4-35 give the velocity distribution along the middle line of the navigation channel, when Point A (position see.Fig.4-34) reaches maximum ebb velocity and maximum flood velocity respectively. When Point A reaches maximum ebb velocity, the velocity along the whole channel in all cases are above 1m/s, and they are in the tendency of increasing along the channel. However, the original training work system has higher velocities than the others. Comparing to the ebb velocity, the velocities along the channel in all cases are generally lower when Point A reaches maximum flood velocity (Fig.4-35). They are not always increasing, but have troughs in the middle of the channel. The original training work system has lower velocity comparing to the others. The comparison show that the ebb tidal current with original training work system has more power than others, which is good for transporting more sediment into the sea; the flood tidal current with original training work has less power, which can bring little sediment into the channel than others. So it is seen from Figure 4-34 and Figure 4-35 that heightening the south training work with 1m and 2m will not help reducing the deposition.

Figure 4-36 to Figure 4-39 give the one year velocity difference of the original training work system as well as the system with 1m heightening of the south training wall, when Point A in the channel reaches maximum ebb velocity and flood velocity respectively. The pattern looks the same, but the difference between the two systems exists.

Figure 4-40 show the one year velocity difference between the original training work system (0m) and the system with 1m heightening of the south training wall (1m), when Point A reaches maximum ebb velocity and flood velocity respectively. Comparing to the original training work, the one with heightening 1m of the south training wall has higher ebb velocity in the upper section of the channel and lower ebb velocity in the lower section of the channel. Heightening the south training wall with 1m will get higher flood velocity in the middle section, but lower velocity in the upper section and the end of the channel. The difference tells us that with heightening 1m of the south training dike, the deposition will decrease in the upper section, but increase in the middle section. At the end of the channel, it is hard to say whether deposition or erosion is easier to happen.

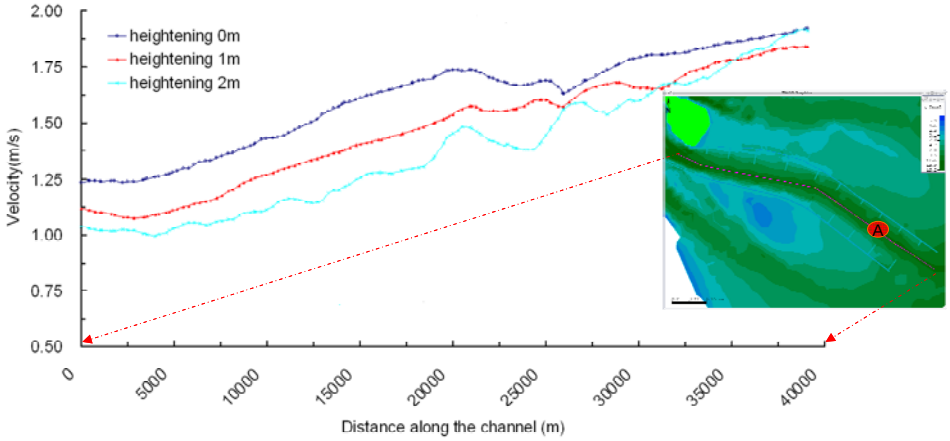

Figure 4-34 Ebb velocity distribution along the channel (red line), when Point A reaches maximum ebb velocity.
The south training wall is heightened for 0m, 1m, 2m in the model.

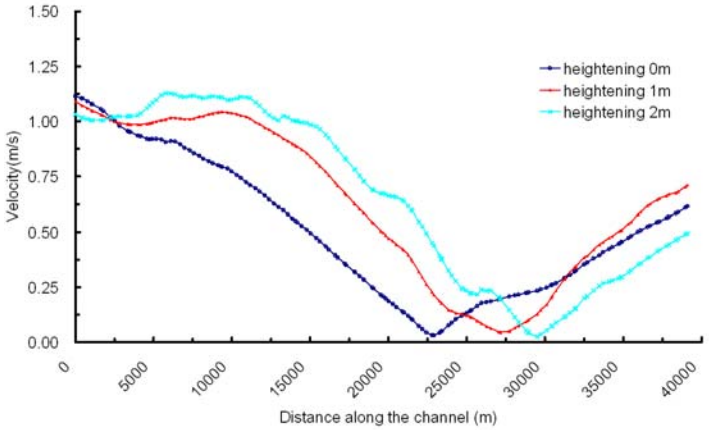

Figure 4-35 Flood velocity distribution along the channel (red line), when Point A reaches maximum flood velocity.
The south training wall is heightened for 0m,1m, 2m in the model.

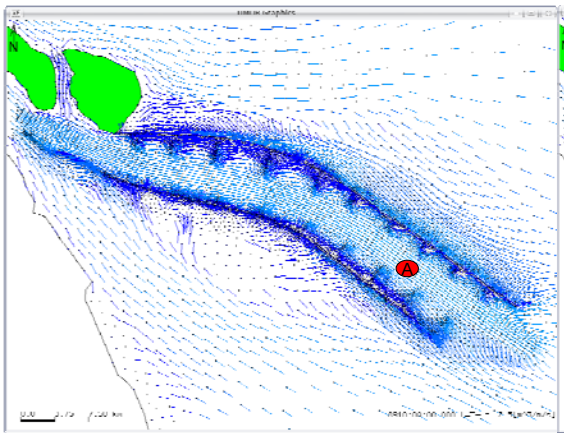

Figure 4-36 Ebb velocity distribution when Point A reaches maximum ebb velocity (heighten for 0m)

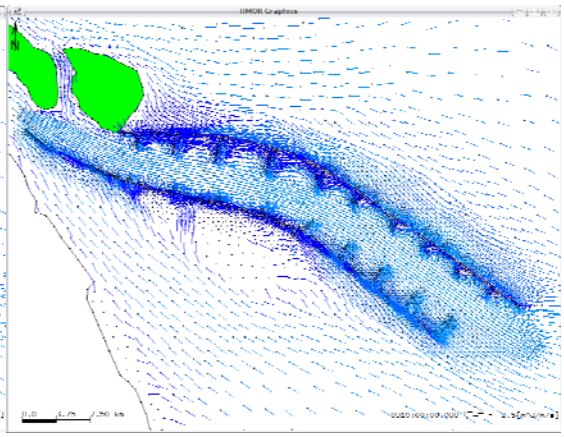

Figure 4-37 Ebb velocity distribution when Point A reaches maximum ebb velocity (heighten for 1m)

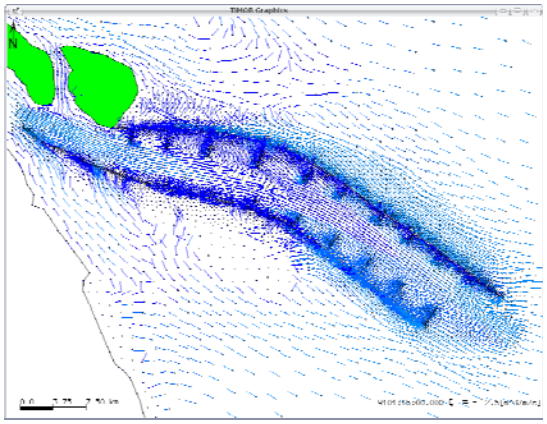

Figure 4-38 Flood velocity distribution when Point A reaches maximum flood velocity (heighten for 0m)

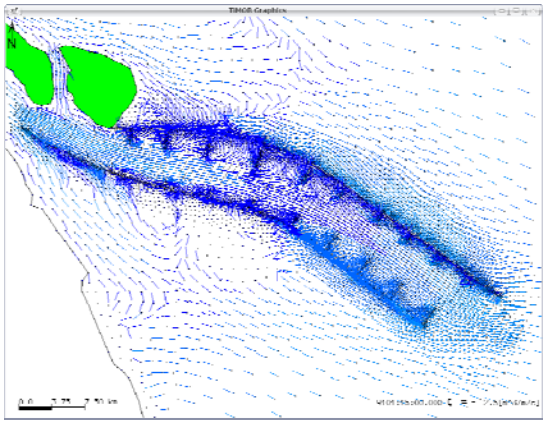

Figure 4-39 Flood velocity distribution when Point A reaches maximum flood velocity (heighten for 1m)

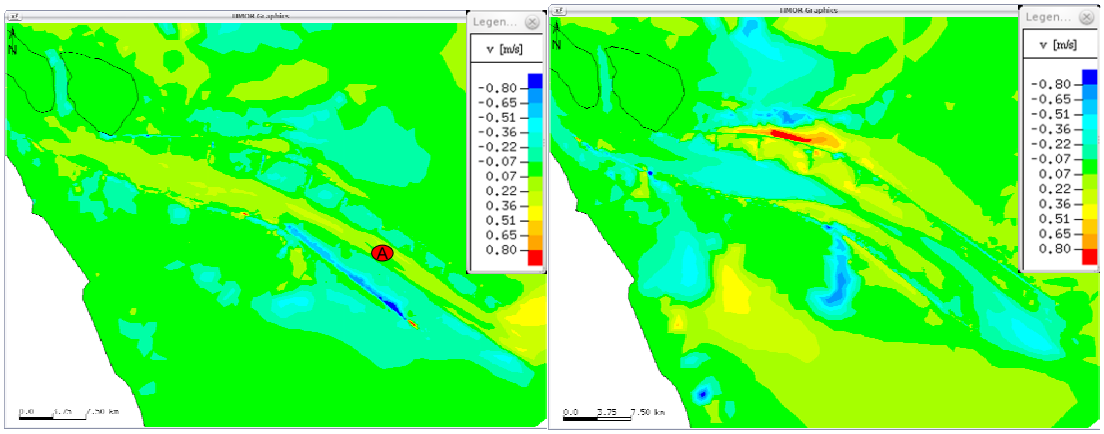

Figure 4-40 One year velocity difference, when Point A reaches maximum ebb velocity(left) and maximum flood velocity(right),between the original system(0m), and the system(1m) with the south training wall heighten for 1m

4.4.3 Dredging volume

According to the calculation results (Tab.4-4), the annual dredging volume for maintaining 12.5m water depth is 53,160,046 m^3. When heightening the south training dike, the calculated annual dredging volume reaches 57,616,737m^3 with 1m heightening. Figure 4-42 shows the tendency of dredging volume between them. From the perspective of dredging, it is not deserved to heighten the south training dike.

4.5 Prediction of morphological changes under extreme hydrological conditions

The hydrological data of above mentioned simulations is based on the water discharge in 2002. It is necessary to have the averaged water discharge as input data. Chapter 2 (Tab.2-2) has analyzed the hydrological changes in the past 50 years at Datong station. The averaged water discharge in flood season from 1950 to 2006 is 40128m^3/s. The maximum water discharge during flood season in history is 92600m^3/s. The averaged water discharge in dry season from 1950 to 2006 is 16710m^3/s. The recorded minimum water discharge during dry

season is 4620 m^3/s. Hereby the simulations with maximum and minimum water discharges and with averaged water discharge in dry and flood seasons are carried out, in order to predict and compare the morphological changes of the channel under extreme hydrological conditions. The roughness coefficient for dry season is taken as 0.0012, and for flood season is taken as 0.0015.

4.5.1 Morphological changes under extreme high water discharge

Figure 4-41 and 4-42 show the bathymetry changes under maximum water discharge in half a year and one year respectively, with the maintaining water depth 12.5m of the navigation channel. Figure 4-43 and 4-44 give the bathymetry changes under averaged water discharge during flood season in half a year and one year, still with the maintaining water depth 12.5m. Under maximum water discharge, the whole channel is under erosion. There is deposition in the middle area among the groins in half a year, but after one year, the deposition in the middle is gone, alternatively in the upper and lower section, deposition appear.

Comparing to those results under maximum water discharge, the difference of bathymetry changes under averaged water discharge in half a year (Figure 4-43) and one year (Figure 4-44) is obvious. The whole channel is under erosion in half a year, but as time increasing, the pattern changes. After one year, the middle part of the channel is under erosion. The upper and lower section is much more deposited.

To analyze the hydrodynamics is good for understanding the bathymetry changes. Figure 4-45 and 4-46 show the velocity distribution along the channel under averaged water discharge in flood season, when Point A in the channel reaches maximum ebb velocity and maximum flood velocity. The flood tide brings sediment from seaside, while the ebb tide transports the sediment outside of the channel. The ebb velocity in half a year keeps a minor increase. After one year, the ebb velocity keeps increasing above 1 m/s, but after two years, it decreases. At the end of the channel, the ebb velocity is always decreasing a little bit.

Meanwhile, the flood velocity in half a year tends to increase along the channel, this will together with the ebb velocity tendency, has a minor erosion in the upper and middle section of the channel, but at the end of the channel, deposition appears due to the decreased ebb velocity. The flood velocity in one year decreases along the channel, reaches a lowest point in the middle channel and than begins to rise. The deposition in the middle in Figure 4-46 is reasonable, with lower flood velocity and higher ebb velocity. The ebb velocity after two years decreases in the middle part, but the flood velocity in this part is increasing, so deposition is possible to happen in the middle of the channel.

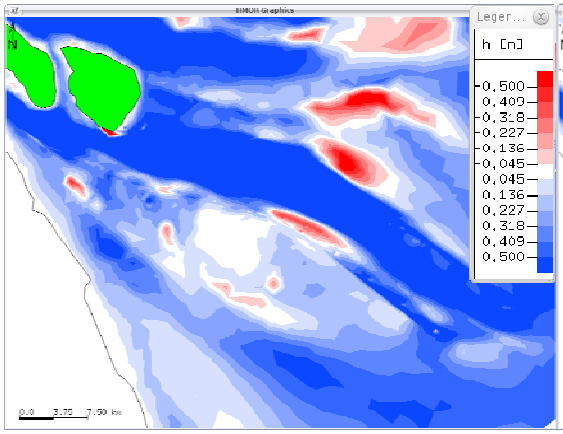

Figure 4-41 Calculated bathymetry changes under max. water discharge (92600m^3/s) in half a year

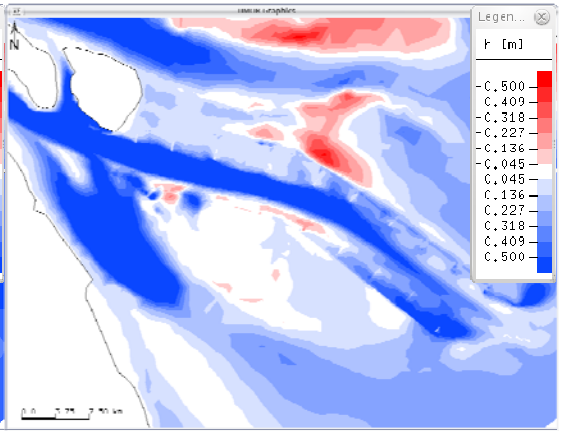

Figure 4-43 Calculated bathymetry changes under averaged water discharge (40128m^3/s) in half a year

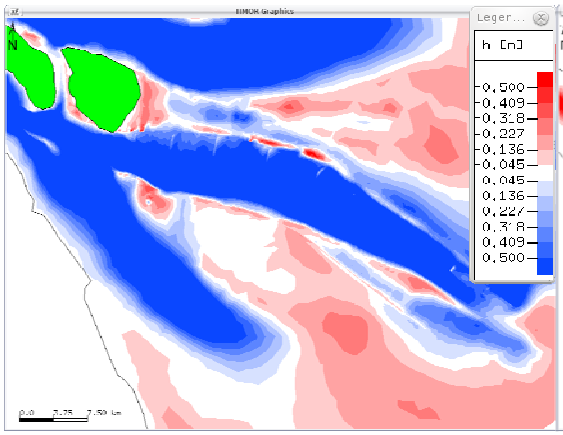

Figure 4-42 Calculated bathymetry changes under max. water discharge (92600m^3/s) in one year

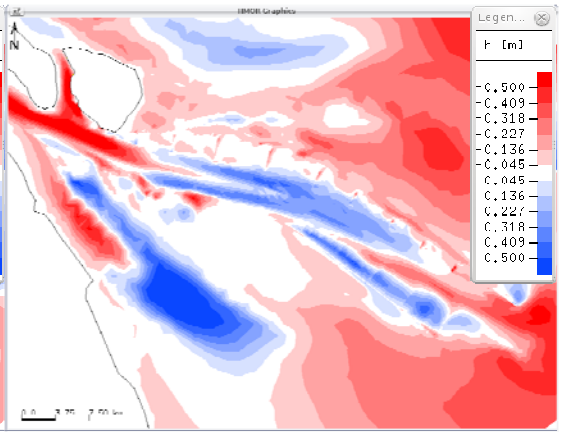

Figure 4-44 Calculated bathymetry changes under averaged water discharge (40128m^3/s) in one year

(for all the above figures blue=erosion; red=deposition)

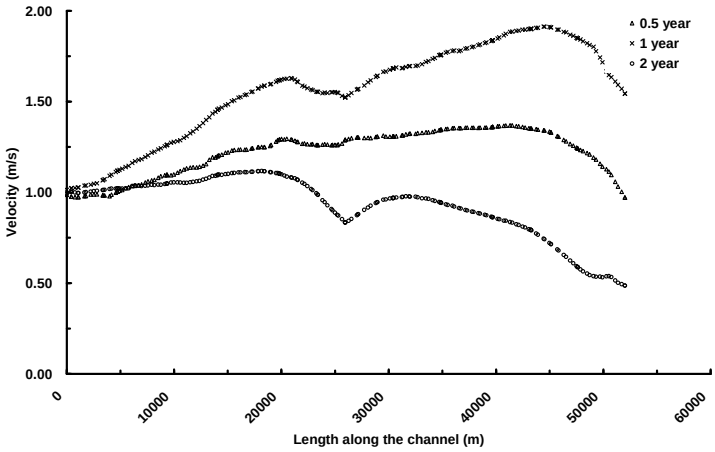

Figure 4-45 Predicted ebb velocity along the channel under averaged water discharge 40128m^3/s with Point A reaching the maximum ebb velocity

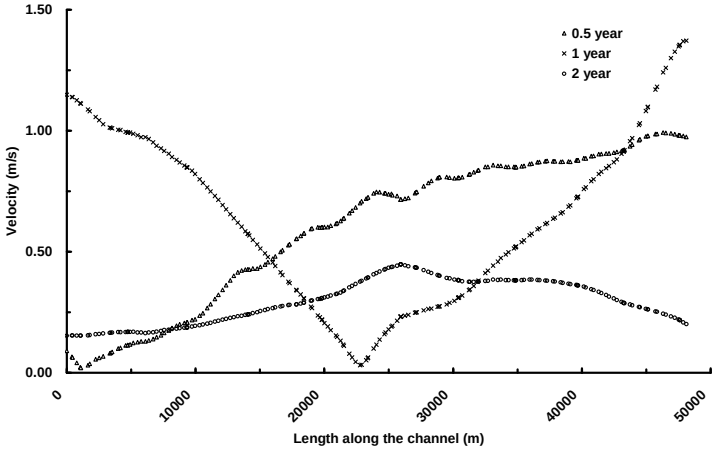

Figure 4-46 Predicted flood velocity along the channel
under averaged water discharge 40128m^3/s
with Point A reaching the maximum flood velocity

4.5.2 Morphological changes under extreme low water discharge

Corresponding to the above calculation, the bathymetry changes under minimum water discharge in half a year and one year, with the maintaining water depth 12.5m of the navigation channel, are shown in figure 4-47 and 4-48. The bathymetry changes under averaged water discharge during dry season are given in figure 4-49 and 4-50. Under minimum water discharge, the whole channel is under erosion in half a year, but after one year, deposition appears in the upper section of the channel. The same pattern appears with the averaged water discharge. In the middle section, there is erosion in half a year, but after one year, the erosion area is getting smaller and the upper section is under deposition.

Figure 4-51 and 4-52 reveals the hydrodynamic changes along the channel. The same like in figure 4-45, the ebb velocity is increasing in half a year and one year, but decrease after two years. However, under dry season, the ebb velocity is relatively lower than that during flood season. The flood velocity in half a year decreases at the upper section of the channel, and then keeps increasing along the channel, thus erosion appears in the upper section. The flood velocity in one year reaches highest in the upper section and lowest in the lower section, since the corresponded ebb velocity is increasing, deposition appears in the upper section and erosion happens in the lower section of the channel.

The prediction of morphological changes under extreme hydrological conditions is meaningful, however in the future research much work has to be done to analyze the joint effect of hydrological conditions from riverside and seaside, like the maximum water discharge happening together with typhoon or storm surges or spring tides.

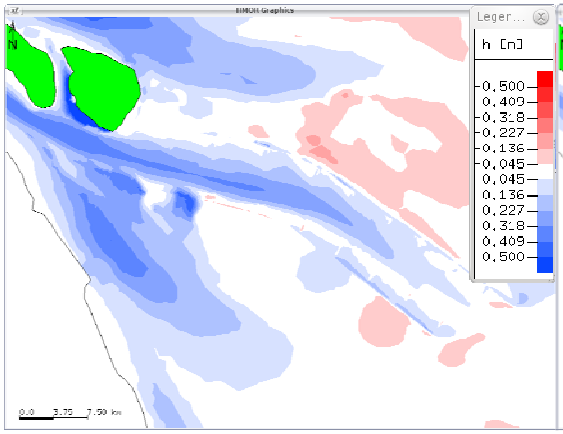

Figure 4-47 Calculated bathymetry changes under minimum water discharge (4620m^3/s) in half a year

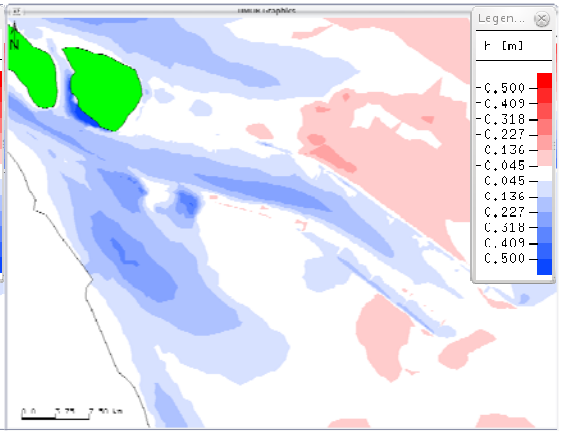

Figure 4-49 Calculated bathymetry changes under averaged water discharge (16710m^3/s) in half a year

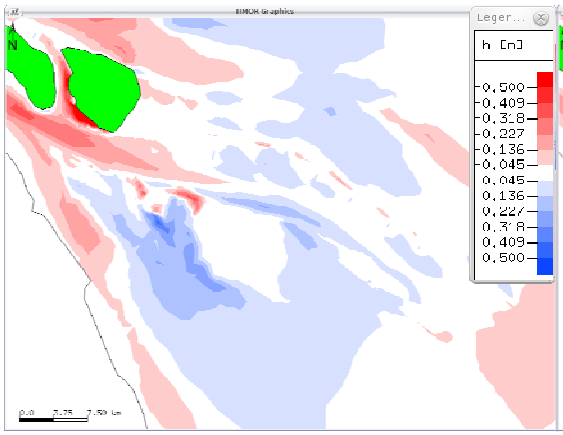

Figure 4-48 Calculated bathymetry changes under minimum water discharge (4620m^3/s) in one year

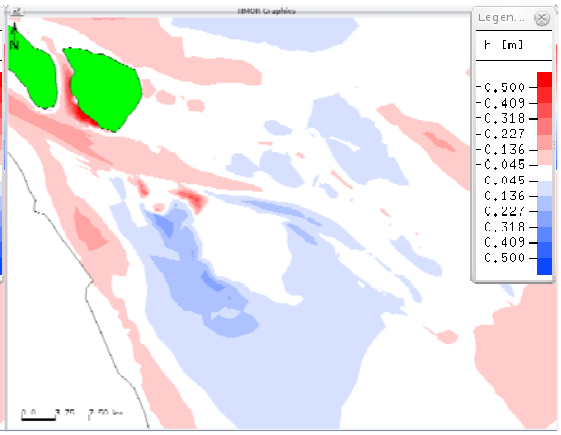

Figure 4-50 Calculated bathymetry changes under averaged water discharge (16710m^3/s) in one year

(For all the figures above, blue=erosion; red=accumulation)

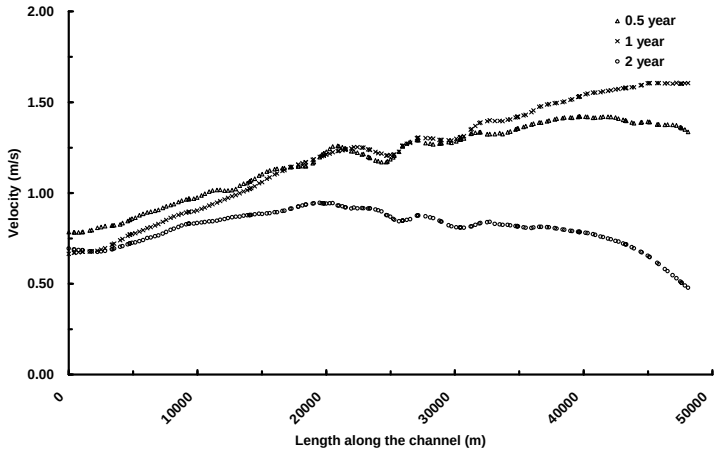

Figure 4-51 Predicted ebb velocity along the channel
with averaged water discharge 16710m^3/s
when Point A (position see Fig.4-34) reaches maximum ebb velocity

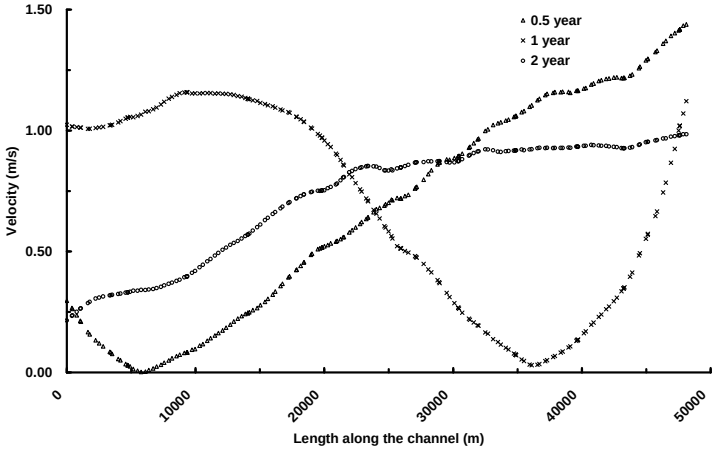

Figure 4-52 Predicted flood velocity along the channel
with averaged water discharge 16710m^3/s
when Point A(position see Fig.4-34) reaches maximum flood velocity

4.6 Summary

The effect of human interferences on morphodynamics in Yangtze Estuary has been analyzed, from the perspective of dams and reservoirs, the ongoing water diversion project, and the Chinese Water and soil Conservation project. Each human activity has different influences but it is hard to tell their joint effects on morphodynamics.

The regulation works carried out in different estuaries in the world has been reviewed briefly. Their effects on morphodynamics have been discussed and analyzed. Detailed description about the regulation work in Yangtze Estuary, the DWRP has been given after then.

Simulations have been made to check the morphodynamic evolution induced by regulation work at Yangtze Estuary.

Firstly, a simple case and the case of DWRP have been simulated with the purpose of getting intuitive impression of training works. The simple case showed that the simulation result is reasonable to the basic regular pattern of sediment transportation. The training dikes can narrow the flow and enhance the flow velocity. The groins which guide the current in the one hand and trap the sediment on the other hand. The case of DWRP has done a more detailed examination of the morphological changes with and without the regulation works. The bathymetry changes in one year with and without training works have been given. The difference of bathymetry changes in one and two years have been compared between two systems. The deposition and erosion area corresponds well to the changes of maximum ebb and flood velocities.

Secondly, the long-term morphological changes with regulation works have been simulated. The observed geomorphology before and after DWRP were presented with a quantitative analysis on the changed morphodynamics. The simulated morphological changes between 2002 and 2005 have been compared with available measured data, which enhanced the feasibility of this model. Then the bathymetry and hydrodynamic changes between 2005 and

2007 have been presented and analyzed. The maximum ebb velocity is decreasing and the maximum flood velocity is increasing, thus resulting in deposition in the channel, which corresponds to the simulated morphological result. The dredging volume with different objective water depth has been calculated systematically. Calculated results from TIMOR are between those results from other institutes or by other calculating means.

After implementing the Phase I and Phase II, the evolution pattern showed that: A Smooth and microbend tidal channel talweg which connects upper, middle and lower sections is formed, the original mouth bar disappeared. The obvious positive effect of DWRP has exhibited. But for maintaining 15m water depth, the yearly dredging volume will be larger than 70 million m^3.

Thirdly, to tackle the deposition problem in the middle channel after Phase II, the south training dike has been heightened to 1m and 2m by numerical method. Results showed that heightening the south training dike could not reduce the needed dredging volume. Besides, the hydrodynamics along the channel revealed no positive improvement. No obvious advantage of heightening the south training dike is exhibited.

Fourthly, simulations to predict the morphological changes under extreme hydrological conditions were carried out. The extreme high water discharges in the history and the averaged water discharge during flood season have been put into the model as boundary conditions. Simulated results showed that the channel is under heavier erosion with extreme high water discharge than with the averaged discharge in half a year. But hydrodynamics showed that after two years, the maximum ebb velocity along the channel is decreasing, while the maximum flood velocity along the channel is increasing, especially in the middle section of the channel. This could result in deposition in the middle section of the channel due to the weakened ebb current power and the increased flood current power.

CHAPTER 5

MORPHODYNAMIC RESPONSE TO THE SEA LEVEL RISE AT YANGTZE RIVER ESTUARY

5.1 The global climate change and sea level rise

Weather changes all the time. The average pattern of weather, called climate, usually stays pretty much the same for centuries. However, people are taking actions that can change the earth and its climate in significant ways. The human activity that is most likely to have a large impact on the climate is the burning of fossil fuels such as coal, oil and gas. These fuels contain carbon. Burning them makes carbon dioxide (CO_2) gas (the greenhouse gas). Since the early 1800s, when people began burning large amounts of coal and oil, the amount of carbon dioxide in the earth's atmosphere has increased by nearly 30%. The Fourth Assessment Report (AR4) of the Intergovernmental Panel on Climate Change (IPCC) shows that the Earth's average surface temperature has risen by 0.76°C since 1850. Without action to reduce these emissions, the global average temperature is likely to rise by a further 1.8-4.0°C this century, and by up to 6.4°C in the worst case scenario (IPCC, 2007). Most of the warming over the past 50 years is very likely to have been caused by emissions of carbon dioxide and other greenhouse gases from human activities. The potential for runaway greenhouse warming is real and has never been more present. As more carbon dioxide is added to the atmosphere, solar heat has more trouble getting out. The result is that the average temperature of the atmosphere would increase. If global warming occurs, not every day or every place will be warmer. But on average most places will be warmer. This will cause changes in the amount and pattern of rain and snow, in the length of growing seasons, in the frequency and severity of storms, and in sea level. Farms, forests, and plants and animals in the natural environment, will all be affected. IPCC (2007) presented a schematic framework representing anthropogenic drivers, impacts of, and responses to climate change and their linkages as shown in Figure 5-1.

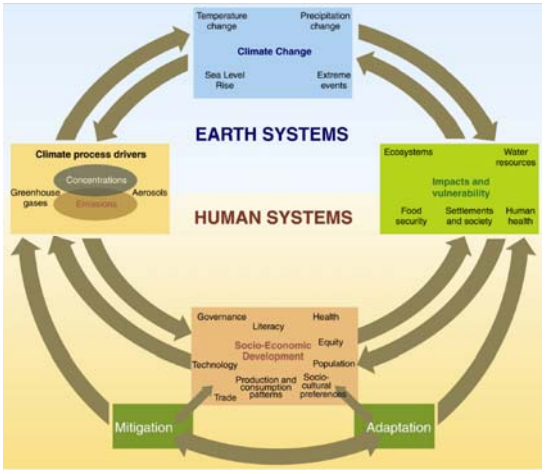

Figure 5-1 Schematic framework representing anthropogenic drivers, impacts of, and responses to climate change and their linkages. (IPCC, 2007)

In the 1980s, evidence of climate change was mounting and a number of international conferences raised worldwide concern about the issue. Governments realized how big a threat climate change was and that they had to do something about it. They also realized that they had to work together to have any chance of success. Climate change is a global issue because all countries will be affected by it and all contribute, in varying degrees. In 1988, the United Nations set up the Intergovernmental Panel on Climate Change (IPCC) which brings together thousands of scientists from around the world. Their task is to assess existing research and knowledge about climate change and its effects and to provide comprehensive reports at regular intervals. The most recent report, known as the Fourth Assessment Report (AR4), was published in 2007. It concluded beyond all reasonable doubt that greenhouse gas concentrations in the atmosphere have increased mainly as a result of human activities, and gave a grave warning of the consequences if nothing is done. In 1992, governments agreed the United Nations Framework Convention on Climate Change (UNFCCC). This international agreement has been formally accepted by 191 countries. The objective of the convention is to stabilize greenhouse gas concentrations in the atmosphere at a level that would prevent dangerous, man-made interference with the climate system. Under the convention, governments monitor and report the greenhouse gases they produce, develop climate change strategies, and help the poorer among them address climate change. They meet once a year to review progress and decide what to do next. The convention was designed as an umbrella under which more action would be agreed in the future. In 1997, Kyoto Protocol was agreed. This treaty commits industrialized countries to reduce or limit their greenhouse gas emissions and reach certain emission targets by 2012. Recently, the UNFCCC 15th Conference of the Parties (COP15) meeting was held in Copenhagen in December 2009. It resulted in the Copenhagen Accord under which several developing and developed countries outlined intentions and commitments on carbon emissions, pledged support for technology transfer and acknowledged the importance of forest systems in combating climate change.

Increasing temperatures result in sea level rise (SLR). Two primary processes contribute to sea level rise. First is the thermal expansion which is the increase in water volume resulting from heat uptake. Second is the mass input that is the transfer of freshwater from land to the ocean. The largest portion of mass inputs is from the loss of land-based ice as warming proceeds. Mountain glaciers at all latitudes, large ice sheets in the polar regions, and frozen soils all can contribute water to the ocean (Houghton et al., 2001). Over the past million years, the earth has undergone a repeating cycle of cold ice ages alternating with warm interglacial periods. Sea level at the Last Glacial Maximum, about 20000 years ago, was 120 m lower than the current level (Kopp et al., 2009). Recently in the Fourth Assessment Report (AR4) of the IPCC, it was estimated that the mean rate of sea level rise for the past century is 1.8 mm/yr, and more recently, the satellite measurement shows the rate increased to 3.1±0.7 mm/yr from 1993 to 2003. Because of the short time span of the satellite record, confirmation of this recent acceleration will require more time. Until recently, scientists assumed that thermal expansion dominated contemporary SLR (Houghton et al. 2001). Recent progress has changed that perception, and it now appears that mass contributions from glaciers and ice sheets dominate, with the latter comprising at least half of total SLR over the past decade (Nerem et al. 2006). Recent measurements of glaciers and ice sheets show increased mass loss (Cazenave 2006), which is consistent with the larger than expected

contribution from land-based ice to contemporary SLR. The discovery of a large mass input contribution is one of the most important recent advances in our understanding of SLR.

There are currently over $1.2x10^{12}$ people living within 100 km of the coast and less than 100 m above sea level, the broad area that will be affected by global rising sea levels (Small and Nicholls, 2003). The rise of sea level has a potential impact on coastal regions, such as increased coastal erosion, more extensive coastal inundation, higher storm surge flooding, landward intrusion of seawater in estuaries and aquifers, and changes in surface water quality and groundwater characteristics. This would flood low-lying islands such as the Maldives, coastal and estuary areas such as the Bangladesh, Nile Delta in Egypt, and Yangtze Delta in China. A number of studies (Han et al., 1995; French et al., 1995; Olsthoorn et al., 2002; Zeidler, 1997) have provided estimates of the potential impacts for specific developed countries (e.g. France, the Netherlands, Poland, Singapore and the United States); developing countries (e.g. Bangladesh, Benin, China, Nigeria, and Senegal); or specific areas of individual countries (e.g. deltas of the Nile and Bengal; Rhine Delta, Thames Estuary and Rhone Delta). The indicators of impacts used in the studies generally include land loss, population affected, capital loss value and wetlands loss, different studies have used different subsets of indicators or regions. Only a limited number of studies have assessed the impacts of SLR on a broader regional or world scale. Such studies include: Nicholls (2002), Nicholls and Tol (2006) and Nicholls et al. (2008). Some of these studies examine the impact of 'extreme climate scenarios' such as a 5m SLR (e.g. Nicholls et al., 2008). The significant impacts found in the global model shows that the response to abrupt sea-level rise is worthy of further research.

5.2 Projection of sea level rise at Yangtze Estuary

Many reports or studies presented various projections of sea level rise (IPCC, 2007; Rahmstorf, 2007; Grinsted et al., 2009; Vermeer and Rahmstorf, 2009; Siddall et al., 2009). IPCC (2007) estimates that the global average sea level will rise by 0.18-0.59m by 2100 (see Figure 5-2) relative to 1980-1999 under a range of scenarios. The central value of the quantity is 0.39m which is 2-4 times of the rate over 20th century. However these estimates assume that ice flow from Greenland and Antarctica will continue at the same rates as observed from 1993-2003. If the Greenland ice sheet melted completely, sea levels could rise by as much as 7m. The Antarctic ice sheets contain enough water to raise the sea level by almost 70m (Church et al., 2001), small changes in their volume would have a significant effect for the global sea level. Grinsted et al. (2009) presented that the sea level 2090–2099 is projected to be 0.9 to 1.3 m for the IPCC A1B scenario. Rahmstorf (2007) said the projected sea level rise in 2100 is from 0.5 to 1.4 m above the 1990 level. Vermeer and Rahmstorf (2009) proposed a simple relationship linking global sea-level variations to global mean temperature. Their relationship projects a sea-level rise ranging from 0.75 to 1.9 m for the period 1990–2100. Siddall et al. (2009)'s model predicts 0.07 to 0.82 m of sea-level rise by the end of this century. According to the IPCC, current model projections indicate substantial variability in future sea level rise between different locations. Some locations could experience sea level rise higher than the global average projection, while others could have a fall in sea level. Changes in winds, atmospheric pressure and ocean currents will also cause the quantity of sea level rise. Regionally sea-level rise will depart from the global-mean trend due to a range of meteorological, oceanographic and geological effects (Nicholls, 2002).

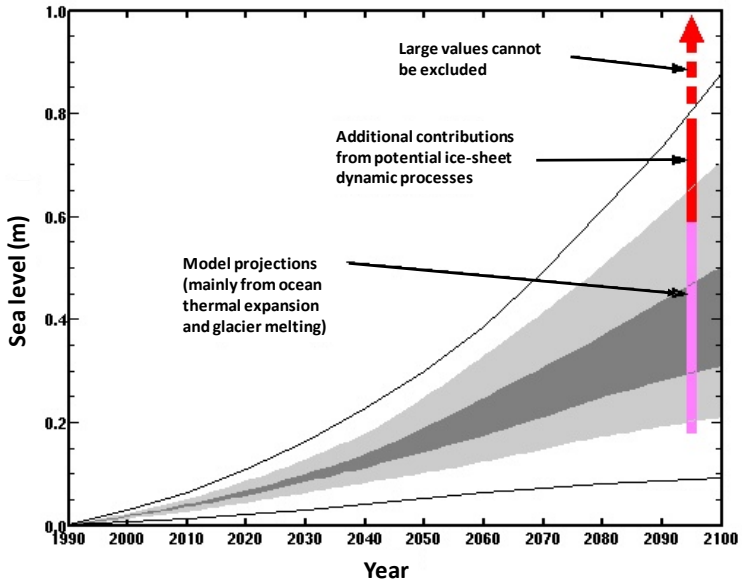

Figure 5-2 Projected sea-level rise for the 21st century

(The lines and shadings are from IPCC 2001 Assessment Report. The central dark shading is an average of models for the range of scenarios. The light shading is the range for all models and all scenarios and the outer bold lines include an allowance for land-ice uncertainty. The updated IPCC AR4 projections announced in 2007 are shown by the bars plotted at 2095. Introductions of the bars are in the figure)

China's coastline is approximately 18000 km long. The long coastline is the base for about 70 percent of the large cities, over a half of the domestic population and nearly 60 percent of the national economy. According to the latest observations from tide stations, the sea level along China's coastline has maintained a rapidly rising speed over the past five decades (Chen, 1997). The elevation even accelerated in recent years with an annual increase of 2.6 mm/yr. It is nearly twice of the global average rate (1.8 mm/yr for 20th century, announced by IPCC AR4). Figure 5-3 shows the trends of sea level rise at Chinese coasts (SOA, 2009). Compared to the mean sea level from 1975 to 1993, it has been raised 68 mm in average. Table 5-1 shows the values of Chinese seas. It is predicted that the sea level will rise 80 to 130mm at 30 years later (in 2040), compared to the mean sea level in 2009. Furthermost, at the end of this century, the sea level at Chinese coasts will rise 30 to 70 cm than today. Recently, the climate scientist of China said that the upper range of sea level rise in China by 2100 could be in the range of about 1 m, or possibly more (academic reference wasn't found yet). Large sections of Chinese coastal regions will gradually disappear under rising sea levels, severely impairing the country's social and economic progress.

Table 5-1 Trend of sea level rise at Chinese marginal seas (SOA, 2009)

	Rising rate (mm/yr)	Rising sea level related to MSL 1977-1993 (mm)	Rising sea level related to MSL 2009 (mm)	Prediction of rising sea level 30 years later (~2040) (mm)
Bohai Sea	2.3	53	-1	68～118
Yellow Sea	2.6	65	1	82～126
East China Sea	2.9	62	15	86～138
South China Sea	2.7	88	18	73～127
Average	2.6	68	8	80～130

Note: MSL (Mean Sea Level)

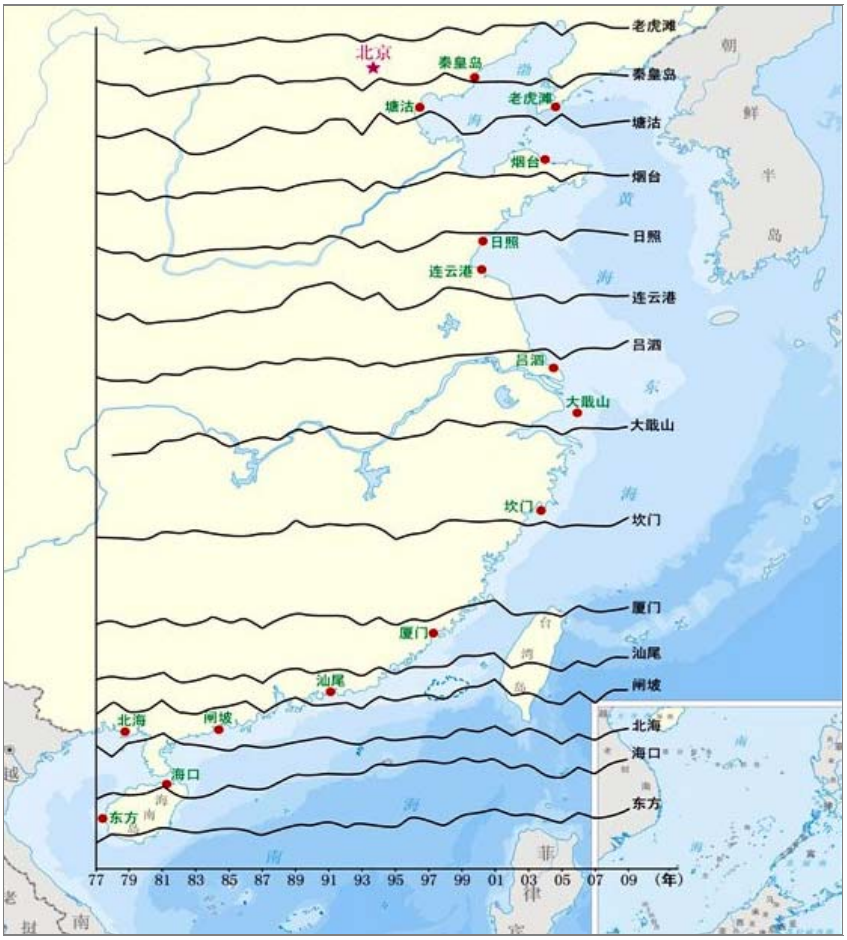

Figure 5-3 Trend sea level rise at Chinese coasts (SOA, 2009)

Sea level rise is creating great challenges for the coastal area especially for the river estuaries. In China, the Yangtze River Delta, Pearl River Delta (S. China) and Yellow River Delta (N. China) regions located along the coast with the country's most developed economies may all face to the large impacts if the sea level kept rising at the current speed, even faster. Among them, the Yangtze delta that is low-lying region (~2m above m.s.l.) and highly vulnerable to flooding, is interested by this study. Although regional factors could affect sea level, changes in sea level trends in the Yangtze Estuary were uniform with global sea level over the last 100 years (Chen, 1990; Shi et al, 2000). However based on latest tidal data, the forecasted rate of sea level at Shanghai is 2.5 mm/yr by the beginning of the 21st century and 3.5 mm/yr by the middle of the 21st century (Wei and Gong, 1998). Figure 5-4 is the trend of sea level fluctuation at station Lvsi (32.08N, 121.37E) done by this study. The station locates very close to the Yangtze Estuary (as shown in Figure 5-4) and has long-term tide data (1961-2009). The field data are from PSMSL (Permanent Service for Mean Sea Level) RLR (Revised Local Reference) database. Using linear analysis for fitting to the trend, it is found the annual rate of sea level is 5.412 mm/yr. Since the simulation of future SLR project is not the work in this study, we apply IPCC's result to estimate SLR quantity for Yangtze Estuary. The projection of SLR for global ocean is from 0.18m-0.59m in 2100 based on the 1.8 mm/yr mean rate in 20th century. It is estimated that the sea level at Yangtze Estuary will rise from 0.54m to 1.77m in 2010. More true values should be simulated by theoretical based model.

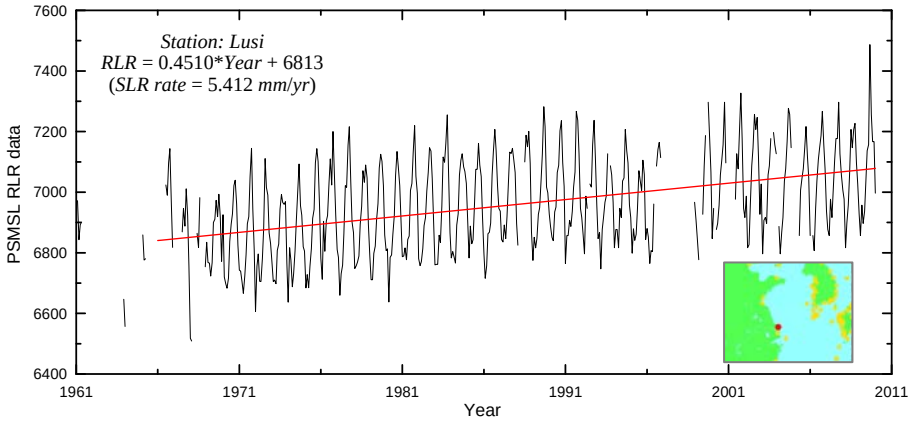

Figure 5-4 Trend of sea level fluctuation at station Lvsi

In additional to the effect of sea level rise, the land has subsided continuously in this region, resulting from the combined effects of tectonism, compaction, isotatic subsidence and groundwater over-pumping (Wu et al., 2003; Chen and Stanley, 1998). Join effects of sea level rise and land subsidence results to the relative sea level rise (RSLR). The subsidence rate at Shanghai is around 10.2 mm/yr (Wu et al., 2003) that is several times of the sea level rising rate. Given global or eustatic change superimposed by local factors such as land subsidence, the magnitude of future relative sea level rise at Yangtze Estuary can be estimated as tentative scenarios. Prediction of its possible quantity during the next century is uncertain due to the incompleteness of our knowledge. This study summarizes the projections of sea level rise for Yangtze Estuary area, as shown in Table 5-2.

Consequences of this relative rise include difficulty in expelling water from the low-lying delta plain to the coast and associated hydrodynamic conditions changes (Chen and Stanley, 1998). Since the implement of TGD can control flooding of the Yangtze river but decrease sediment accumulation on the delta plain that, in turn, is likely to accelerate saline inundation and estuary erosion. Join effects of the natural sea level rise and the human interferences largely bring possibility of morphological changes for the Yangtze Estuary.

Table 5-2 Summary of the assessment of sea level rise at Yangtze Estuary for 2100

	Projected sea level rise [1][2] (m)	Land subsidence effect (relative sea level rise)[3] (m)	Joint effect of sea level rise and land subsidence (m)	Remark
IPCC (2007)	0.18-0.59	0.92	1.1 – 1.5	・Global base ・relative to 1980-1999 MSL
SOA (2009)	0.26-0.41	0.92	1.2 – 1.3	・Marginal sea scale ・Relative to 1977-1993 MSL ・constant rate assumption
Referred studies	0.07-1.9	0.92	1.0 – 2.8	・Global scale ・See Section 5-2
This study	0.54-1.77	0.92	1.46-2.69	・Based on Yangtze Estuary tidal data analysis result

Note:
[1] Melting of Greenland ice sheets, sea level rise +7m
[2] Melting of Antarctic ice sheets, sea level rise +70m
[3] Land subsidence rate at Yangtze Estuary (Shanghai) 10.2 mm/yr, resulting 0.92 m total land subsidence (relative sea level rise) in 2010 by the constant rate assessment.

5.3 Morphology under various projection of sea level rise (SLR)

The world's estuaries are on the front line of climate change, from sea level rise, floods and droughts, to saltwater intrusion, habitat degradation and biodiversity loss. It is therefore essential to understand the response of the estuary under global climate changes impacts. This study focuses on the morphological changes based on various scales of sea level rise. The nature and phenomena by the changes can be simulated using morphodynamics models, though not so much such kind of studies available yet. Verhaar et al. (2008) modified a one-dimensional morphodynamic model SEDROUT to invest how the changing hydrology of the St-Lawrence River in Canada. In this paper, the TIMOR3 is used to simulate the morphodynamic response to the sea level rise at Yangtze Estuary.

Topographic changes

Morphological simulations are made under different SLR (0.18m, 0.59m, 1m, and 2m), based on the assessment of SLR at Yangtze Estuary for 2100 (Tab.5-2). Seasonal variations of water discharges have been considered in the simulations. Figure 5-5 (a-h) show the two year topographic difference between systems with different SLR and system without SLR influence (0m) under dry and wet season respectively. The deep waterway channel in the North Passage, as studied in detail in chapter 4, set in the following simulations to maintain 12.5m water depth by dredging.

From the figures it can be found that the SLR has generally much more significant impact on the morphological evolution under dry season than under wet season. The topographic changes in dry season with different SLR are obvious. This may be due to the fact that under dry season, the water discharge from riverside is less than that in wet season, so the tidal current is much easier to get into and out of the estuary under SLR circumstances, thus shaping the topography greatly.

During dry season, the pattern and degree of erosion and deposition under SLR (0.18m, 0.59m, 1m and 2m), comparing to the system without SLR (0m), is more or less the same. Deposition takes dominant position. The SB, SP as well as the groins area in NP are under deposition, but the waterway channel is obvious to be in erosion.

During wet season, the topographic difference with SLR 0.18m is very minor, which may be due to the influence of huge water discharge from riverside. With SLR 0.59m and 1m, the topographic differences are comparatively obvious. But comparing to those results during dry season, erosion is generally much more severe. Attention is needed at the North Passage, the erosion dominates in this area but at the end of North Passage the mouth sand bar appears. The topographic difference with SLR 2m showed more erosion in the South Branch, North Channel, South Channel, and North Passage. The South Passage has balanced deposition and erosion pattern. The deposition area in North Branch decreased. The deposition degree of the mouth sand bar at the end of North Passage increased.

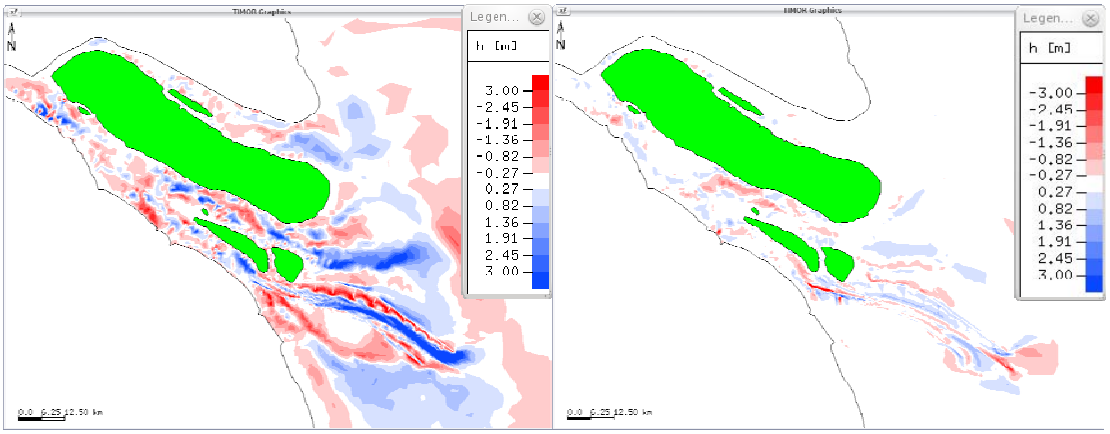

(a) (0.18m-0m) dry season (b) (0.18m-0m) wet season

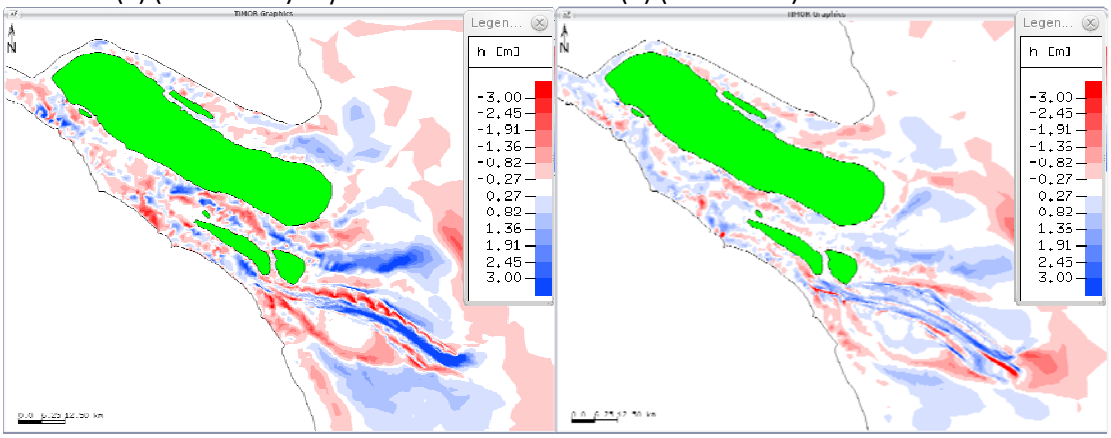

(c) (0.59m-0m) dry season (d) (0.59m-0m) wet season

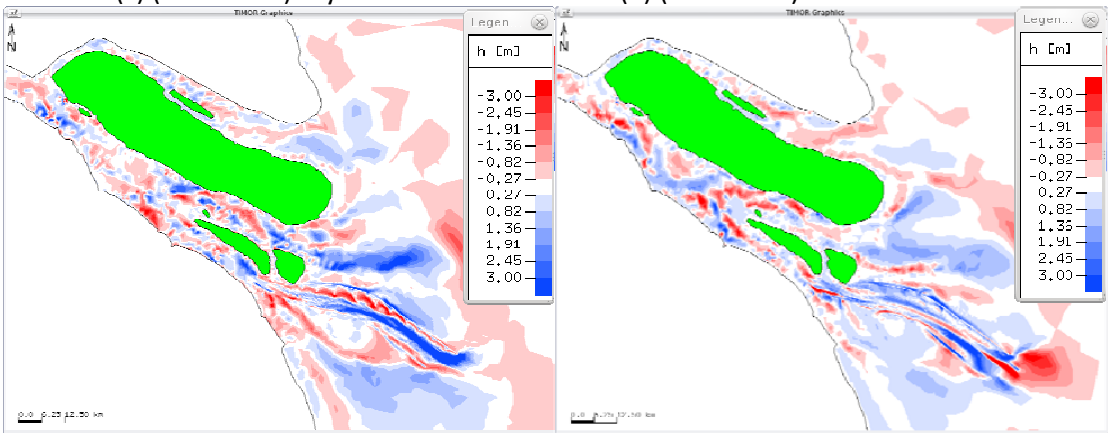

(e) (1m-0m) dry season (f) (1m-0m) wet season

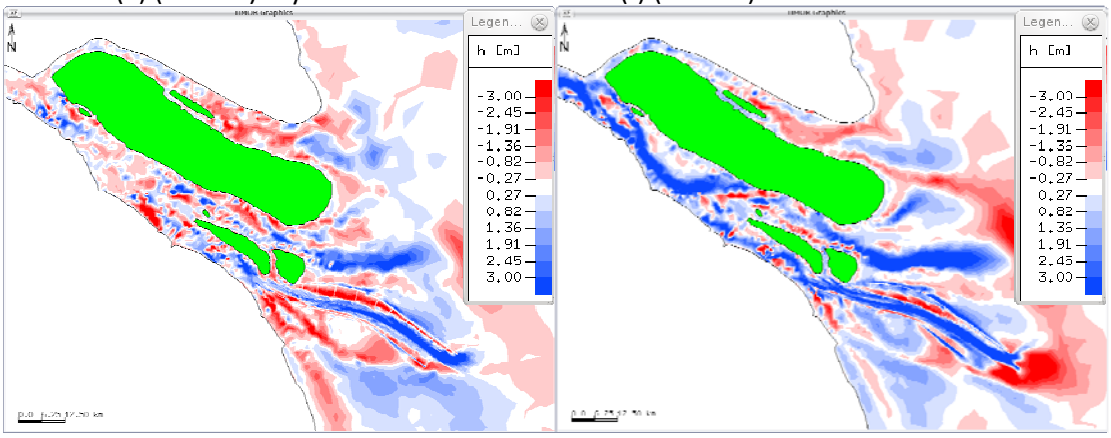

(g) (2m-0m) dry season (h) (2m-0m) wet season

Figure 5-5 two years topographic difference among different SLR (0.18m, 0.59m, 1m, 2m) and SLR (0m). Blue=erosion; red=accumulation

Hydrodynamic changes

The hydrodynamics, which can somehow explain the morphological evolution, contains the information of tidal current, river runoff, wind and waves. Therefore it is always important to study on it very carefully. The ebb velocity and flood velocity can reflect the power of ebb current and flood current. Both currents take important role in transporting sediment. The ebb velocity difference and flood velocity difference among the systems with different Sea Level Rise (SLR) 0.18m, 0.59m, 1m, 2m and the system with SLR 0m is shown in Figure 5-6 (a-p). Seasonal variations of water discharges have been considered respectively.

The ebb velocity difference and flood velocity difference with SLR 0.18m during dry season is given in (a) and (c). It is obvious that the increase of flood velocity in South Passage is bigger than that of ebb velocity. But in North Passage, the ebb velocity in the waterway channel increases, while the areas near it like the shallow shoal has suffered decrease of ebb velocity. During wet season, the ebb velocity difference with SLR 0.18 (b) is minor comparing to the flood velocity difference (d), which has difference around 0.3m/s. The increase and decrease pattern of flood velocity is complicate. North Passage has major increase of flood velocity, while the South Branch has both increase and decrease of flood velocities.

With SLR 0.59m the pattern of ebb and flood velocity difference (e, g) is almost the same like with SLR 0.18m during dry season. In North Passage, the ebb velocity increases while in its surrounding area, the flood velocity increases. During wet season there are zones with increased ebb and flood velocities (f,h). The ebb velocity increases in the area near North Passage, while the end of South Branch has increased flood velocity. One notable difference with SLR 0.59 comparing to SLR 0.18m is that, there are changes of flood and ebb velocities in North Branch, which actually has very shallow water depth with only 2 or 3m. The difference may be due to that the raised SLR has pushed more water into North Branch than before.

The difference pattern of ebb velocity and flood velocity with SLR 1m during dry season (i, k) is more or less the same. Both ebb and flood velocities are generally decreased. At the beginning of South Channel and North Channel, increase zone of ebb velocity is found. The increase zone of flood velocity with more than 0.3m/s is found at the end of South Branch. During wet season, decrease of velocity is the major pattern. However, ebb velocity increases in the waterway channel in North Passage but at the end of North Passage, the flood velocity increase, which explain the deposition and erosion pattern in this area in Figure 5-5 (d)(f).

With SLR 2m the pattern are similar during dry season (m, o) and wet season (n, p), which can be further explained that with increasing SLR, the seasonal variations of river runoff has few influence on the ebb and flood velocities. During dry season, the ebb velocity is getting smaller. However, the ebb velocity is still increasing at the deep waterway channel in North Passage. The two increase zone of ebb velocity at the beginning of South Channel and North Channel under SLR 1m disappeared. The flood velocity is similar to those under SLR 1m. At the beginning section of South Chanel and North Channel, there are two zones with increased flood velocity, but at the middle section of them, the flood velocity decrease.

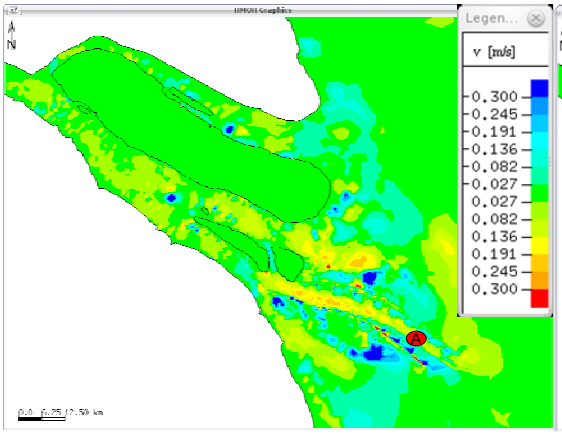

(a) (0.18m-0m) ebb velocity diff. in dry season

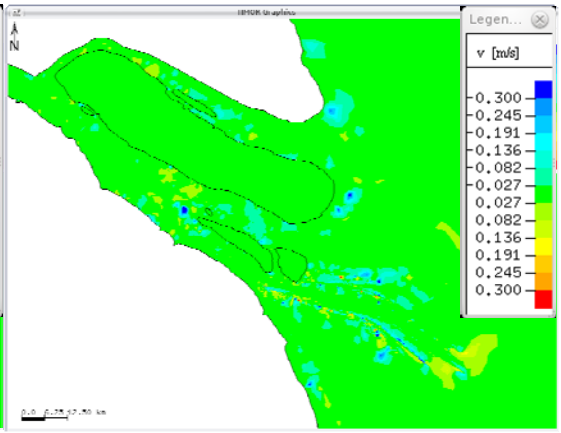

(b) (0.18m-0m) ebb velocity diff. in wet season

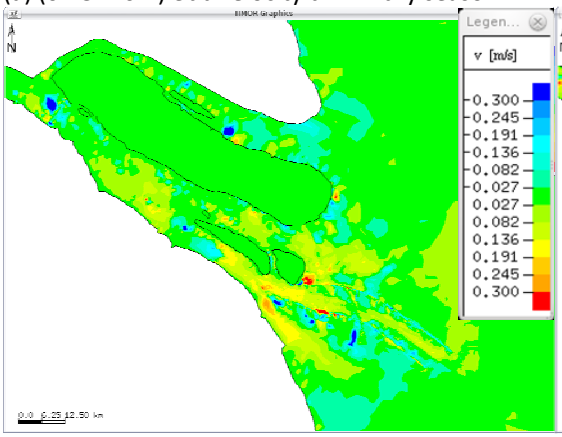

(c) (0.18m-0m) flood velocity diff. in dry season

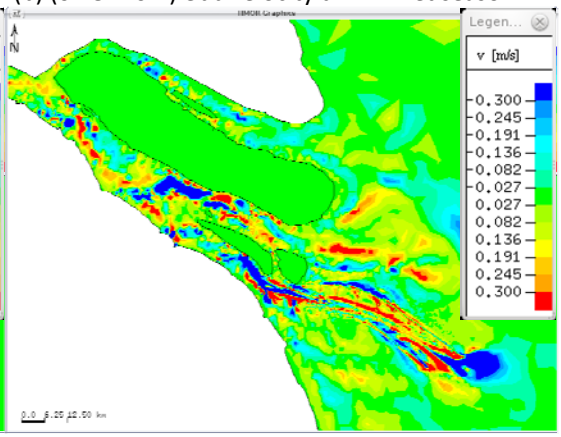

(d) (0.18m-0m) flood velocity diff. in wet season

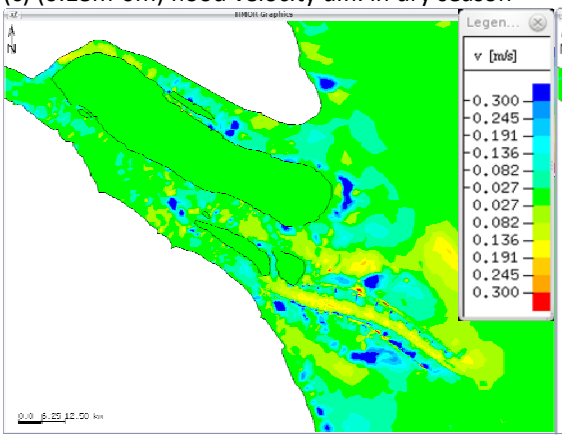

(e) (0.59m-0m) ebb velocity diff. in dry season

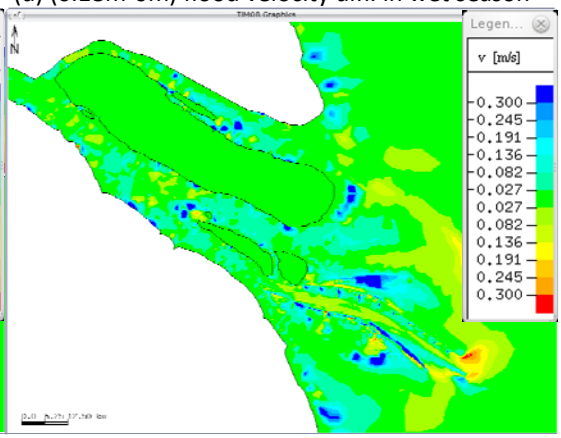

(f) (0.59m-0m) ebb velocity diff. in wet season

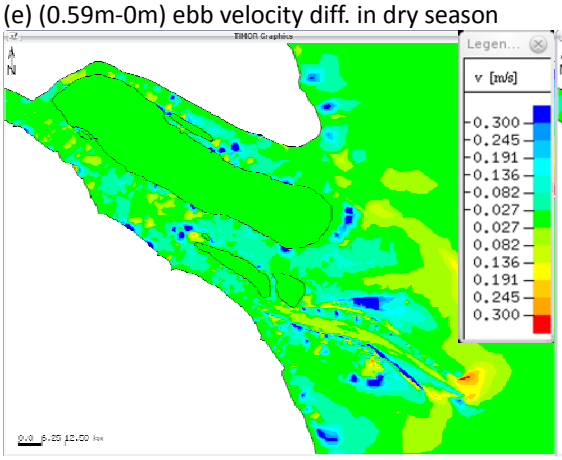

(g) (0.59m-0m) flood velocity diff. in dry season

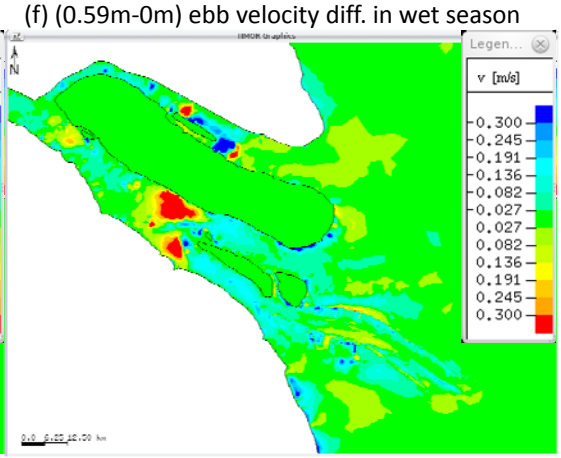

(h) (0.59m-0m) flood velocity diff. in wet season

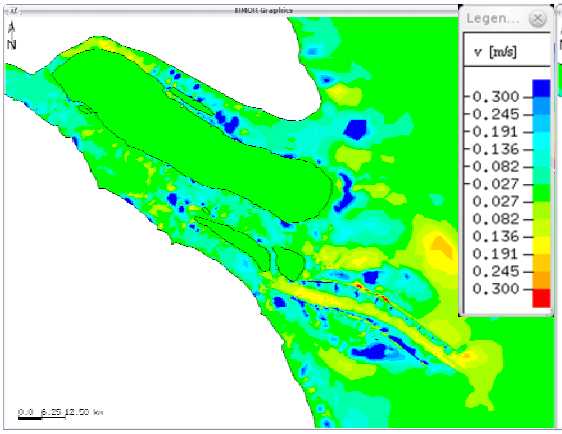

(i) (1m-0m) ebb velocity diff. in dry season

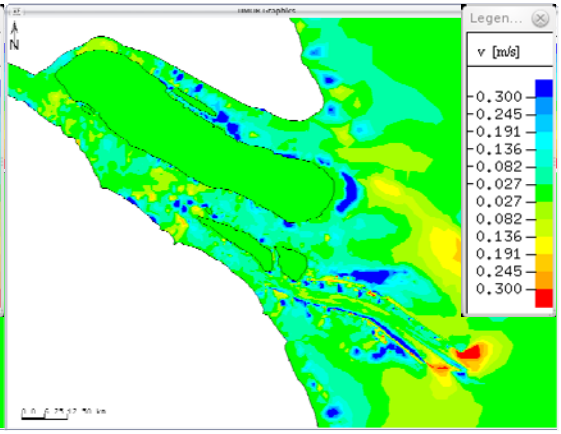

(j) (1m-0m) ebb velocity diff. in wet season

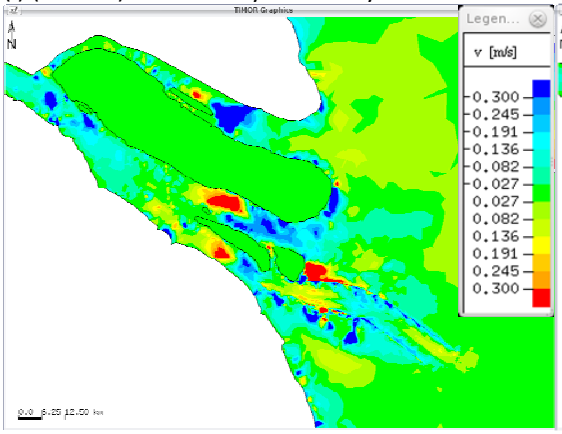

(k) (1m-0m) flood velocity diff. in dry season

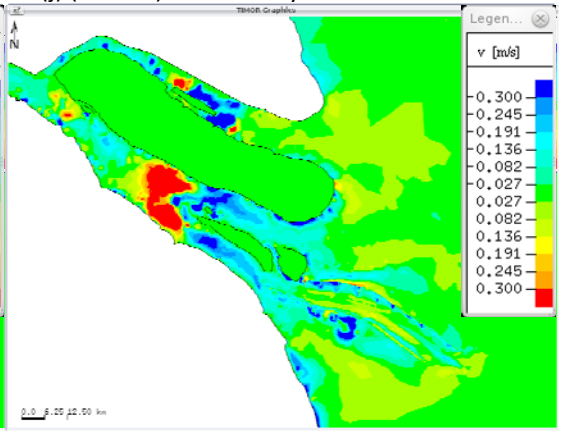

(l) (1m-0m) flood velocity diff. in wet season

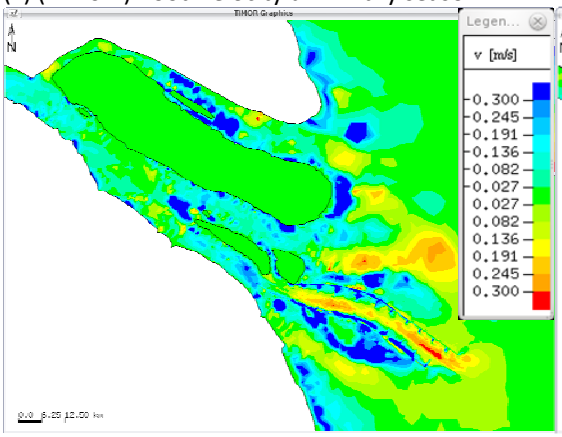

(m) (2m-0m) ebb velocity diff. in dry season

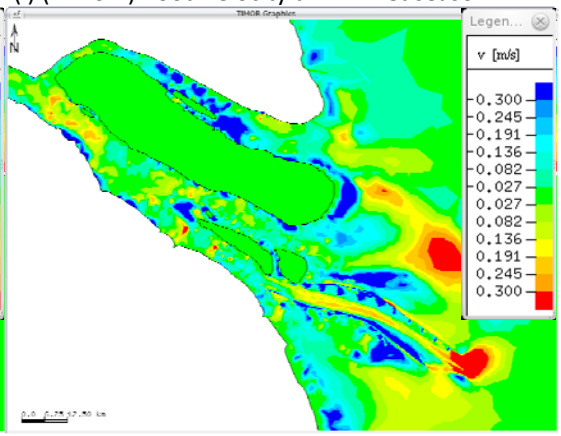

(n) (2m-0m) ebb velocity diff. in wet season

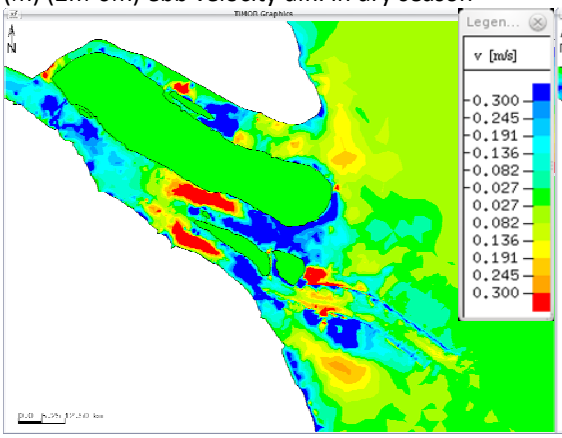

(o) (2m-0m) flood velocity diff. in dry season

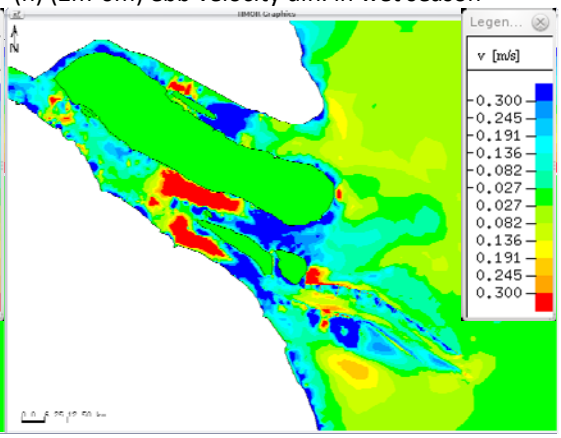

(p) (2m-0m) flood velocity diff. in wet season

Figure 5-6 Difference of ebb velocity and flood velocity among different Sea Level Rise (0.18m, 0.59m, 1m, 2m) and Sea Level Rise (0m) when Point A reaches max. flood velocity and max. ebb velocity

Quantitative analysis on Ebb Velocity and Flood Velocity

The spatial distribution of velocity difference is intuitive. However a more quantitative analysis on the changes of ebb velocity and flood velocity is shown in Figure 5-7 to Figure 5-10. The figures show the ebb and flood velocity along the deep waterway channel in North Passage with different Sea Level Rise during dry season and wet season respectively.

The ebb velocity along the channel during dry season with different Sea Level Rise (Fig. 5-7) keeps increasing. The ebb velocity with Sea Level Rise 0m is always bigger than others, with maximum 1.8m/s at the end of the channel. The ebb velocity with Sea Level Rise 0.18m is similar to the ebb velocity with Sea Level Rise 0.59m. The ebb velocity with Sea Level Rise 1m is a little bigger than that with Sea Level Rise 0.18m and Sea Level Rise 0.59m; however it decreases at the end of the channel. The ebb velocity with Sea Level Rise 2m is always the lowest one except at the very beginning of the channel. It seems that during dry season, the ebb velocity decreases with increased Sea Level Rise.

The trend of flood velocity along the channel during dry season (Fig. 5-8) is single, with increasing at the upper section of the channel, reaching the maximum at the middle and then going down. The ebb velocity with Sea Level Rise 0m is bigger than others in the most sections of channel. The flood velocity with Sea Level Rise 018m and 0.59m are more or less the same. At the very beginning, the former is a little bit smaller than the latter. But at the middle section of the channel, the flood velocity with Sea Level Rise 0.59m reaches the maximum than others with 1.55m/s. At the upper section, the flood velocity with Sea Level Rise 1m and 2m are smaller than those with Sea Level Rise 0.18m and 0.59m but they exceed the latter at the lower section of the channel. It seems that during dry season, the flood velocity decreases with increased Sea Level Rise at the upper section of the channel, but keeps no big change at the lower section of the channel.

The pattern of ebb velocity during wet season (Fig.5-9) has big difference with that during dry season. The ebb velocity is not always increasing, but has a jump towards down at the middle of the channel. The ebb velocity with Sea Level Rise 0m is not any more the biggest one than others but stays between them. The ebb velocity with Sea Level Rise 0.18m is very similar to that with Sea Level Rise 0m, only a little bit bigger at some local areas. The ebb velocity with Sea Level Rise 0.59m is relatively smaller than with Sea Level Rise 0m and 0.18m. The ebb velocity with Sea Level Rise 1m is the highest than others at the upper section, with maximum 1.9m/s but jumps down to 1.68m/s, and then stays between the others. The ebb velocity with Sea Level Rise 2m is always the smallest one, with 1.61 m/s at the middle of the channel. It can not be concluded that the ebb velocity during wet season increase or decrease with Sea Level Rise. As the Sea Level Rise 1m has the highest ebb velocity and the Sea Level Rise 2m has the lowest. The hydrodynamic changes during wet season are complicate under Sea Level Rise.

The trend of flood velocity during wet season (Fig.5-10) is similar to the trend during dry season, generally increasing at the upper section and then decreasing at the lower section of the channel. The flood velocities under all cases are similar, only except that the flood

velocity with Sea Level Rise 2m is relatively smaller than others at the upper section of the channel. The flood velocity with Sea Level Rise 0.59m reaches the biggest value about 1.6m/s at the middle section of the channel. The flood velocity with Sea Level Rise 1m is relatively small at the upper section, but is biggest at the lower section.

In general, during dry season, the ebb and flood velocities decrease with Sea Level Rise comparing to without Sea Level Rise. During wet season, the hydrodynamic changes are complicate. With different level of Sea Level Rise, the ebb and flood velocity can go rise or down along the channel.

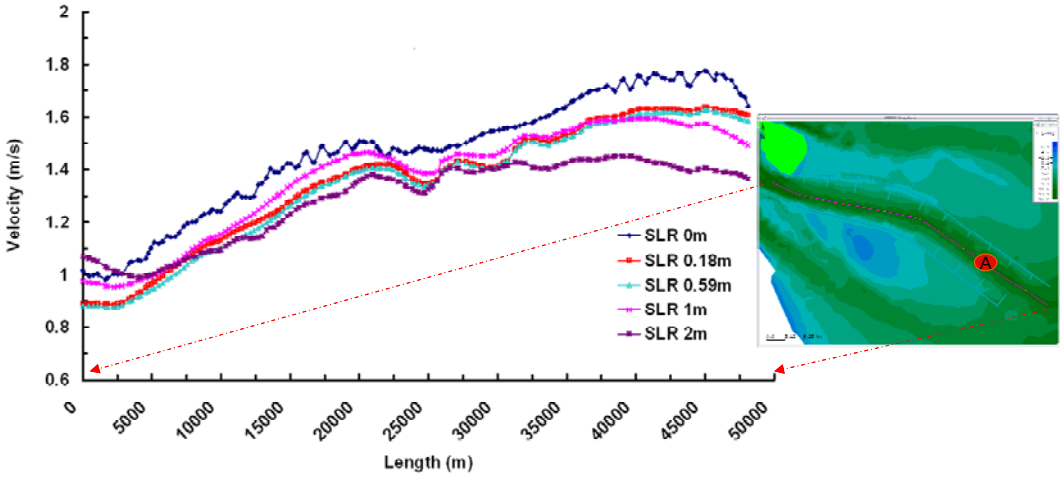

Figure 5-7 Ebb velocity along the channel during dry season with Sea Level Rise 0m, 0.18m, 0.59m, 1m and 2m when Point A reaches maximum ebb velocity

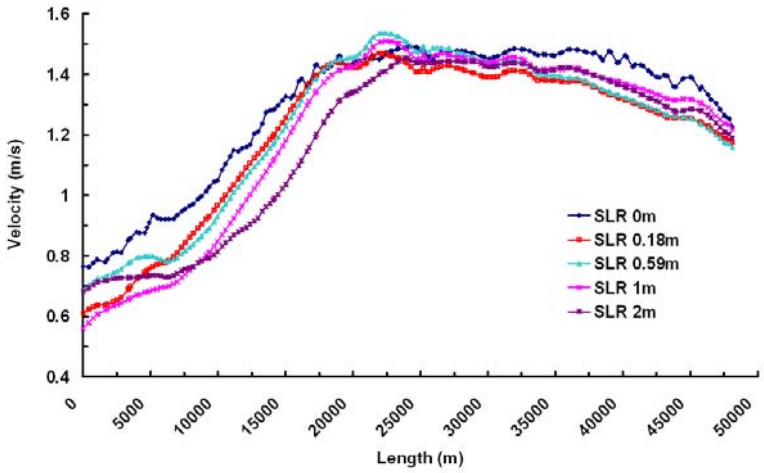

Figure 5-8 Flood velocity along the channel during dry season with Sea Level Rise 0m, 0.18m, 0.59m, 1m and 2m when Point A reaches maximum flood velocity

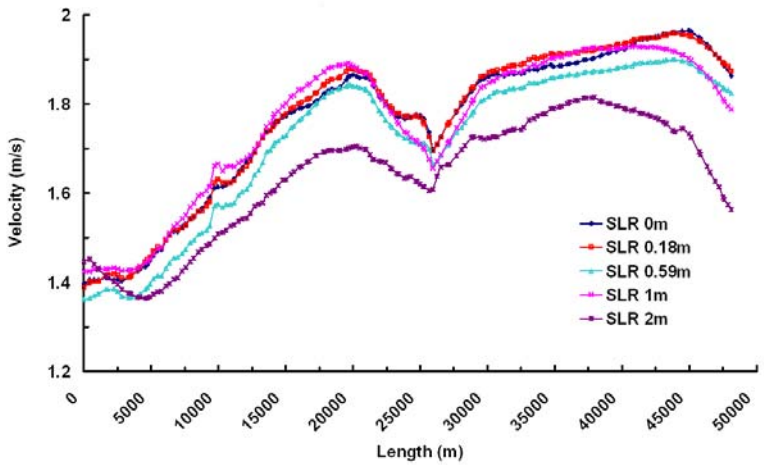

Figure 5-9 Ebb velocity along the channel during wet season with Sea Level Rise 0m, 0.18m, 0.59m, 1m and 2m when Point A reaches maximum ebb velocity

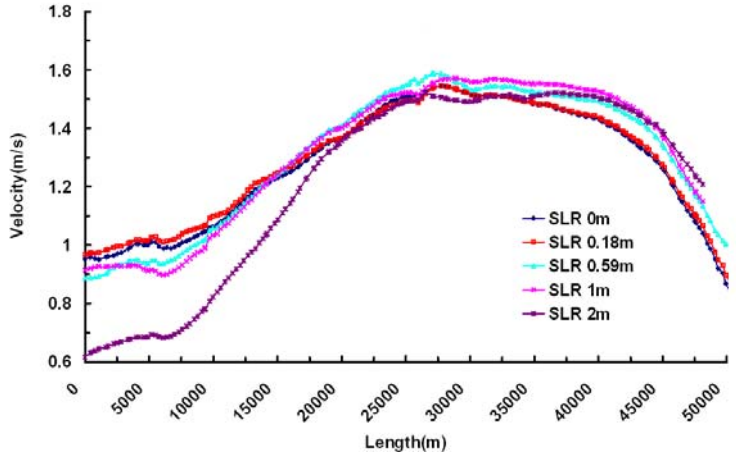

Figure 5-10 Flood velocity along the channel during wet season with Sea Level Rise 0m, 0.18m, 0.59m, 1m and 2m when Point A reaches maximum flood velocity

5.4 Joint effect of sea level rises and typical discharges

5.4.1 Projection of water discharge

Human activities already have a strong influence on the hydrological processes in the world's rivers as well as at Yangtze River. Such as the large-scale water diversions may greatly reduce the water discharge into the sea especially during dry season. Almost all of China's major rivers have been dammed. Before the TGD constructed, it was found that the annual mean discharge from the upper Yangtze basin has shown a significant decreasing trend since the end of the 19th century (Chen et al., 2001). Since the 1970s, the monthly mean discharge to the sea has also shown a dramatic decrease during dry seasons. Though the reservoirs and dams can regulate seasonal water discharge, their overall impact is a reduction of water discharge. Drawing experiences from the past, the Farakka Dam on the Ganges River in India has led to 75% reduction of water flowing to Bangladesh (Chen 2000). The Aswan Dam on the Nile River reduced freshwater and sediment flux entering the Mediterranean (Chen 2000). Constructions and dams on the Yellow River in China, combined with low rainfall due to El Nino effects, have led to about 50% drop of water discharge to the Bohai Sea in recent years (Milliman 1997). In the middle basin discussions are focused on the effect of decreasing lake area, of increasing reservoir capacity, and of irrigated agriculture on the temporal changes of water discharge since the 1950s. The human impacts on water discharge from the lower basin to the sea are mostly attributed to water transfer to both tributary and neighboring drainage basins by a large number of electric pumping stations and sluices (Chen et al., 2001). At the present time, it is difficult to predict the percentage reduction and seasonality of the Yangtze River discharge after damming. If damming is solely for the generation of hydroelectric power, the regulated discharge will likely have a reduced seasonal variation, but the net discharge per year will change little. If some of the water is retained for other usage, then the net annual discharge will be reduced as well. Actually large and episodic drop in flow and water stage at Yangtze River during dry season has been found by Chen et al. (2002). Table 5-3 shows the influence on Yangtze annual runoff by human activities or large engineering.

Table 5-3 Human activities on the influence on the runoff of Yangtze River

Known human activities or large engineering	Influence on annual runoff	Remark
South-to-North Water Diversion Project (SNWDP)	-450×10^8 m^3	full operation in 2030.
Water Diversion Projects in lower Yangtze (WDP)	-8×10^8 m^3	Started from 1990-
Damming, incl. Three Gorges Dam (TGD), Water and Soil Conservation Project (WSCP), Deepwater Waterway Regulation Project (DWRP)	-	
Reclamation, Sand mining…etc.	-	

Note: Annual runoff of Yangtze River is 8994×10^8 m^3

Meanwhile, the global warming is expected to cause an increase of the seasonal variability of discharge from the Yangtze into the sea. Some studies focus on the simulation of variations of hydrological variables such as water discharge under impacts of global climate changes. Lu (2004)'s paper provided an overview on the water discharge changes occurring in major Chinese rivers and their vulnerability to environmental change. He mentioned the stable value in the annual mean and the annual maximum discharges, but a significant decrease in the annual minimum discharges of Yangtze River has been observed. Jiang et al. (2008) analyzed the meteorological and hydrological data at Yangtze River Basin from 1961 to 2000. They found the summer runoff and flood discharge of the lower Yangtze region show an increasing trend in the last 40 years which was influenced by the increasing summer precipitation and rainstorm trends. Groundwater discharge (corresponding to the baseflow in the river) is the major contributor to stream flow in most rivers, especially during extreme drought period. The baseflow is influenced by the extreme climate and human activities. It is found that the contribution of groundwater discharge to streamflow due to human activities is about 8% during the wet season, 13% during the dry season and 10% in the whole year, results from the analysis in a extreme drought year 2006 in Yangtze River (Dai et al., 2010). Bueh et al. (2003) applied atmospheric general circulation model and a hydrological discharge model to study the present-day climate (1971 to 1980) and the mid 21st century (2041 to 2050) climate in East Asia. The changes of the monsoon and the related river discharge under global warming conditions are investigated. The simulation showed that the Yangtze River discharge will increase in the early and mid-summer, due to the large increase in precipitation. However it will decrease in the late summer and autumn. Wang et al. (2008) reconstructed the long-term sediment flux from the river to the sea since the 1860s using water discharge data. Sediment flux sensitivity to climate change (e.g., temperature and precipitation) in upper reaches was documented by Zhu et al. (2008). Dam impacts on sediment discharge, channel variations, and delta erosion have been further studied by Yang et al. (2006a, 2007) and Yang et al. (2006b). Jin et al. (2009) used statistical approach with a conceptual model to study the influences of Yangtze River discharge based on various scenarios in IPCC AR4 report. They found preliminary the Yangtze River discharge will slight decrease in the coming 30 years however the discharge will increase significantly after 2060 due to increasing of precipitation.

There are still not confident quantitative investigations on the projection of Yangtze River discharge under individual influence of climate change or human interferences, or their joint effects in the academic research publication. For the study of morphodynamics changes at Yangtze Estuary in this chapter, the historical maxima water discharge (92600 m^3/s, occurred in January 1979), historical minima water discharge (4620 m^3/s, occurred in August 1954), average water discharge in wet season (40128 m^3/s) and in dry season (16710 m^3/s) are used to be the input of the model. Responses on the hydrodynamic and morphodynamic conditions at Yangtze Estuary under these water discharge assumptions are presented in next section.

5.4.2 Morphology forecast

For forecasting the joint effect of Sea Level Rise and different typical water discharges, Sea Level Rise 2m is taken as input in this study since it takes consideration of the joint effect of Sea Level Rise and land subsidence (Tab.5-2). The deep waterway channel in the North

Passage is set in the following simulations to maintain 12.5m water depth by dredging. It is of interest to see how the topography response to the joint effect of Sea Level Rise under different water discharges. The topographic changes are the difference between two systems. One is with Sea Level Rise 2m and related typical water discharge, while the other one is original case without Sea Level Rise.

Topographic changes

The two year difference of topographic changes under joint effect of Sea Level Rise 2m and different water discharges is shown in Figure 5-11.

The pattern of topographic changes under small water discharges (the averaged water discharge during dry season 16710m^3/s; the historical minima water discharge 4620 m^3/s) is mainly deposition. It can be found in (a) that only the deep waterway channel in North Passage is under erosion. The North Branch and South Passage are totally under deposition. The South Branch has a little erosion at the beginning but then deposition with about 1-1.5m. With joint effect of Sea Level Rise 2m and historical minima water discharge (b), the deposition degree is getting smaller. The South Branch and South Passage are under balance between deposition and erosion.

The pattern of topographic changes under big water discharges (the averaged water discharge during wet season 40128m^3/s; the historical minima water discharge 92600m^3/s) is mainly erosion. With joint effect of Sea Level Rise 2m and averaged water discharge during wet season (c), the South Channel, North Channel, North Passage are obviously under erosion with about 1-3m. The North Branch, South Passage and upper section of South Branch are under balance between erosion and deposition. The pattern of topographic changes under joint effect of Sea Level Rise 2m and historical maxima water discharge is sole. Most areas are under erosion with about 2-3m, like South Branch, South Channel, North Channel, and South Passage. However, the North Branch and South Passage, though not so heavy, are still under deposition. Attention is needed that a deposition zone becomes obvious at each end of channel outside of the estuary comparing to those under small water discharges. This may be due to the huge water discharge from riverside carry the sediment down to the further part of the estuary.

The historical minima and maxima water discharges are extreme hydrological conditions, thus (b) and (d) are very seldom chances to happen. It is of great significance to pay more attention to the case in (a) and (c), which is of great possibility to come true. With Sea Level Rise 2m, the pattern of topographic changes under small water discharges is mainly deposition, while under big water discharges is mainly erosion. One common point of both cases is that the North Channel enjoys pretty good hydrodynamic conditions.

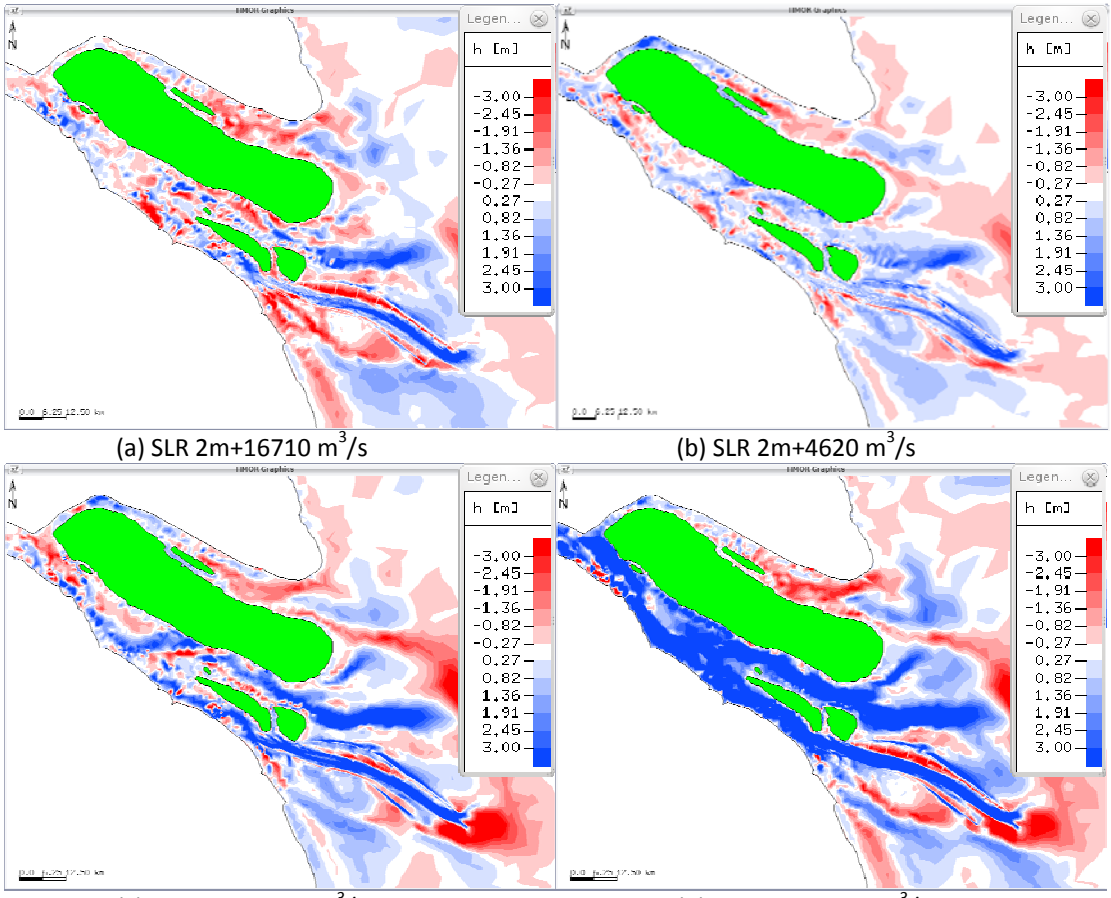

(a) SLR 2m+16710 m^3/s (b) SLR 2m+4620 m^3/s

(c) SLR 2m+40128 m^3/s (d) SLR 2m+92600 m^3/s

Figure 5-11 two year topographic changes under joint effect of Sea Level Rise (SLR) and different water discharges

(a) is under average water discharge in dry season (16710 m^3/s)

(b) is under historical minima water discharge (4620 m^3/s)

(c) is under average water discharge in wet season (40128 m^3/s)

(d) is under historical maxima water discharge (92600 m^3/s)

Hydrodynamic changes

The difference of ebb velocity and flood velocity under joint effect of Sea Level Rise 2m and different water discharges is shown in Figure 5-12. The difference pattern of ebb and flood velocity between Sea Level Rise 2m with averaged water discharge during dry season and Sea Level Rise 2m with historical minima water discharge, are similar. The pattern of ebb velocity between Sea Level Rise 2m with averaged water discharge during wet season and Sea Level Rise 2m with historical maxima water discharge is also very similar but their flood velocity pattern are totally different.

The ebb velocity has not so much difference under Sea Level Rise 2m and averaged water discharge during dry season (a), only at the North Passage, the ebb velocity is increasing. The flood velocity, shown in (c), has obvious difference. The flood velocity at the upper section of South Branch is decreasing. But it is increasing at the South Channel, North Channel, and South Passage.

The ebb velocity decreased generally under Sea Level Rise 2m and historical minima water discharge (b). The North Channel and South Channel have obvious decreased ebb velocity. Correspondently, the flood velocity in North Channel and South Channel (d) increases, but the deposition and erosion pattern in this case (Fig.5-11-b) is under balance. So the ebb and flood velocities are factors which could effect the topographic changes but not the only and decisive factors.

Under Sea Level Rise 2m and averaged water discharge during wet season, the ebb velocity (e) is generally increasing, but the change of flood velocity (g) is not sole. The North Passage and the end of the North Channel have increased ebb velocities. The upper section of South Channel and North Channel has increased flood velocities, but the lower section of them has decreased flood velocities.

The ebb velocity under Sea Level Rise 2m and historical maxima water discharge is generally decreased, only increases at the deep waterway channel and the end section of North Channel. The flood velocity under Sea Level Rise 2m and historical maxima water discharge (h) has obvious distinctions. The upper section of the whole estuary has decreased flood velocities, but the whole lower section of the estuary has increased flood velocities, especially the upper section of North Passage, the South Passage as well as the North Channel.

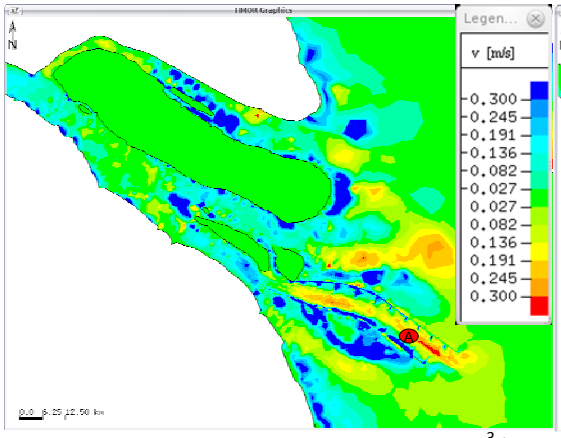

(a) Ebb velocity difference (SLR 2m+16710 m^3/s)

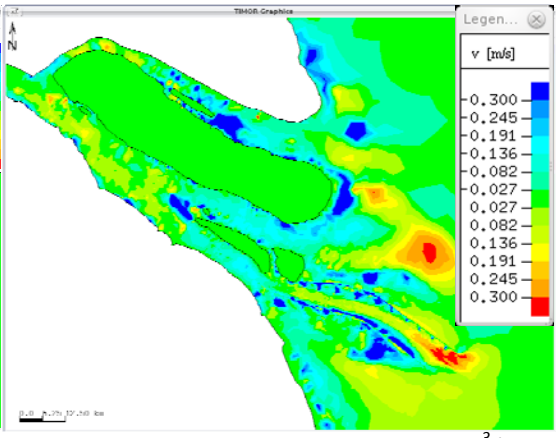

(b) Ebb velocity difference (SLR 2m+4620 m^3/s)

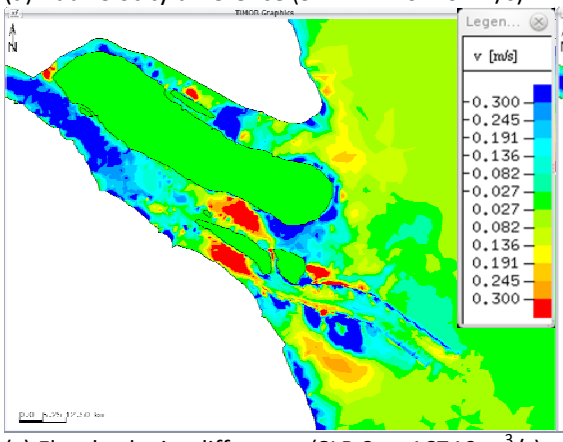

(c) Flood velocity difference (SLR 2m+16710 m^3/s)

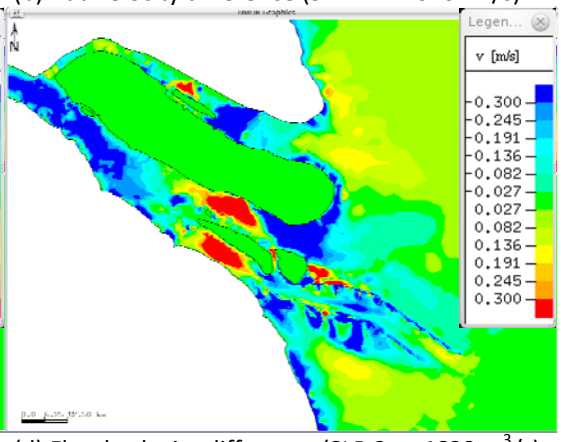

(d) Flood velocity difference (SLR 2m+4620 m^3/s)

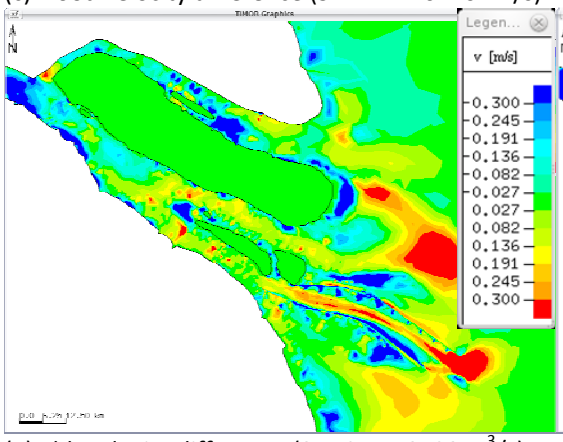

(e) Ebb velocity difference (SLR 2m+40128 m^3/s)

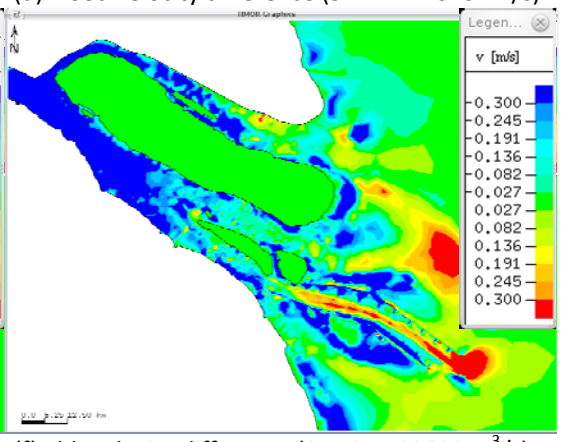

(f) Ebb velocity difference (SLR 2m+92600 m^3/s)

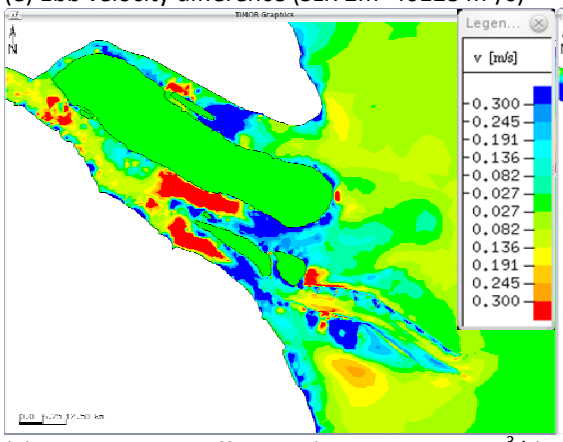

(g) Flood velocity difference (SLR 2m+40128 m^3/s)

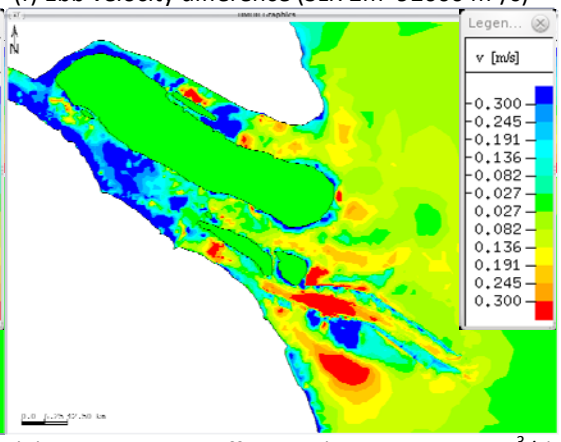

(h) Flood velocity difference (SLR 2m+92600 m^3/s)

Figure 5-12 Difference of ebb velocity and flood velocity
under joint effect of Sea Level Rise (SLR) and different water discharges,
when Point A reaches max. ebb velocity and max. flood velocity
(a)&(c) are under average water discharge in dry season (16710m^3/s)
(c)&(d) are under historical minima water discharge (4620m^3/s)
(e)&(f) are under average water discharge in wet season (40128m^3/s)
(g)&(h) are under historical maxima water discharge (92600m^3/s)

Quantitative analysis on Ebb Velocity and Flood Velocity

Figure 5-13 and Figure 5-14 show the ebb velocity and flood velocity along the channel under joint effect of Sea Level Rise (SLR) 2m and different water discharges.

The trend of ebb velocity (Fig.5-13) under the four different combinations of input (a, b, c, d) is almost the same. The ebb velocity keeps increasing at the upper section of the channel, then drop down to a lower point at the middle section, and then keeps slowing increasing. The ebb velocity under (d) is a little bit smaller than that under (c) at the upper section, but then gets bigger at the lower section of the channel with maximum value of 1.72 m/s. The ebb velocity under (b) is always the smallest one with 1.32 m/s at the middle section of the channel. With historical minima or maxima water discharge, the ebb velocity is little bigger than that with averaged water discharge respectively. The joint effect is that, the ebb velocity under big water discharges (the historical maxima water discharge and the averaged water discharge during wet season), is generally bigger than that under small water discharges (the historical minima water discharge and averaged water discharge during dry season).

The pattern of flood velocity (Fig.5-14) is much simple. The flood velocity under the four input combinations keeps increasing rapidly at the upper section of the channel, then holds on for a moment and then gets a little bit smaller at the lower section of the channel. Unlike the ebb velocity, the flood velocities under big water discharges are not always bigger than those under small water discharges. The flood velocity under (a) is larger than the others with maximum value of 1.48m/s at the middle. The flood velocity under (c) is the smallest one comparing to the others. However, between averaged water discharges, the flood velocity under big water discharge (d) is still larger than that under small water discharge (b). It can be concluded that under extreme minima water discharge with Sea Level Rise 2m, the flood velocity is much bigger than that under extreme maxima water discharge with Sea Level Rise 2m. The raised water level from seaside, together with the small water discharge from riverside, leads increasing flood velocity along the channel.

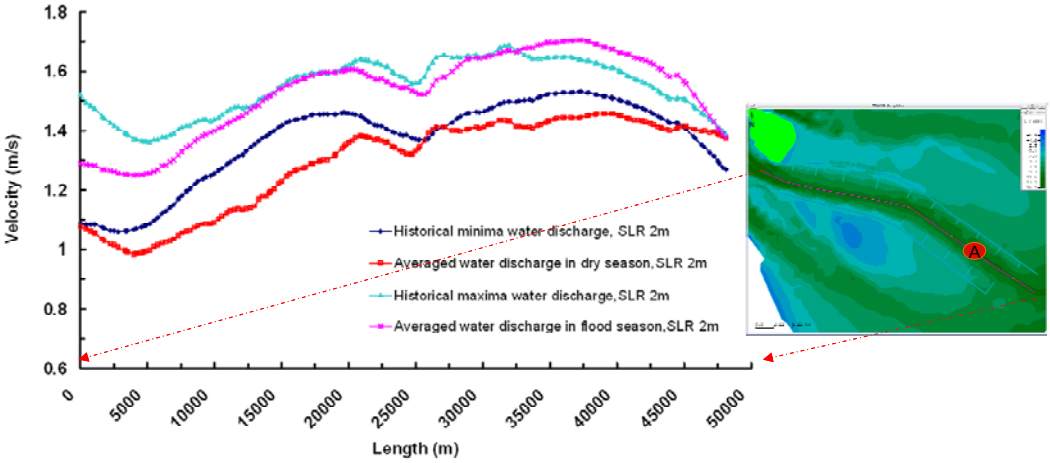

Figure 5-13 Ebb velocity along the channel under joint effect of Sea Level Rise 2m and different water discharges when Point A reaches maximum ebb velocity

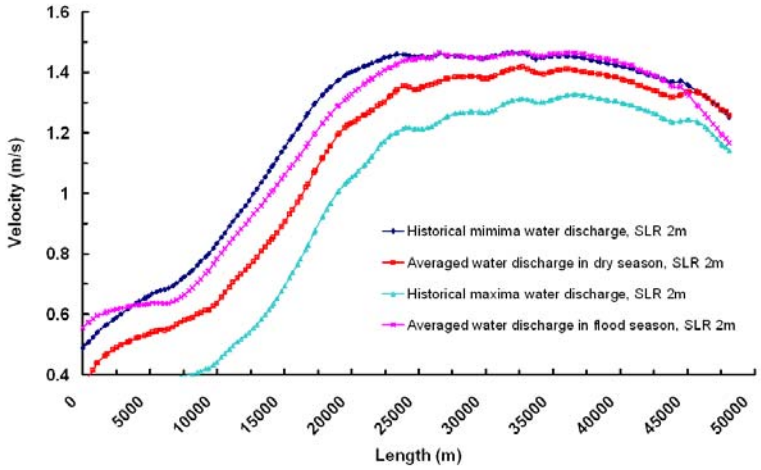

Figure 5-14 Flood velocity along the channel under joint effect of Sea Level Rise and different water discharges when Point A reaches maximum flood velocity

(a) SLR 2m + average water discharge in dry season (16710m^3/s)

(b) SLR 2m + historical minima water discharge (4620 m^3/s)

(c) SLR 2m + average water discharge in wet season (40128m^3/s)

(d) SLR 2m + historical maxima water discharge (92600m^3/s)

5.5 Summary

This global warming is going on since the end of the last ice age. 10.000 years ago, the sea level was about 50cm below that of today. The average rise of sea level in the past 200 years was approx.25-30cm. Based on computer models, different scientists expect an acceleration of sea level rise, especially due to green house effect. With or without this effect, the sea level rises and thus causes an impact on the coasts.

However the current model projections indicate substantial variability in future sea level rise between different locations. Although regional factors could affect sea level, changes in sea level tends in the Yangtze Estuary were uniform with global sea level over the past 100 years. In this study, the linear analysis is done for fitting to the trend of sea level fluctuation at Station Lvsi, based on long-term tide data. It is found the annual rate of sea level at station Lvsi is 5.412 mm/yr, considering the effect of both sea level rise and land subsidence. Based on this study, a summary of the joint effects of sea level rise and land subsidence at Yangtze Estuary in the long-term has been made in the second section of this chapter.

The main content of this chapter is, based on the projections of sea level rise at Yangtze Estuary, to use numerical model TIMOR3 to simulate the morphodynamic response. Two major groups of simulations have been carried out. One group is the systematic morphological simulations under a series of sea level rises (0.18m, 0.59m, 1m and 2m) during dry season and wet season respectively. The other group is morphological simulations under joint effect of sea level rise and typical discharges. The sea level rise in this joint effect combination is taken as 2m. The typical discharges are the averaged water discharges during dry season and wet season from 1950 to 2008, the historical minima and maxima water discharges.

The simulated results of topographic changes and the hydrodynamic changes have been analyzed. The quantitative analysis on ebb and flood velocity along the deep waterway channel in the North Passage has been done. By analyzing the hydrodynamics, it is helpful to get more idea of morphodynamic changes.

In the first group of simulations, the sea level rise during dry season has generally much more significant impact on the morphological evolution than during wet season. The pattern and degree of erosion and deposition under Sea Level Rise (SLR 0.18m, 0.59m, 1m and 2m), comparing to the system without SLR (0m), is more or less the same. Deposition takes dominant position. During wet season, erosion is generally much more severe especially with SLR 2m. The pattern of hydrodynamic changes remains similar for SLR 0.18m and 0.59m during dry season, but both ebb and flood velocity increase during wet season.

The pattern of hydrodynamic changes with SLR 1m and 2m are similar during dry season and wet season, which can be further explained that with increasing SLR, the seasonal variations of river runoff has few influence on the ebb velocity and flood velocity. In general, during dry season, the ebb and flood velocities decrease with SLR comparing to without SLR. During wet season, the hydrodynamic changes are complicate. With different level of SLR, the ebb and flood velocity can go rise or down along the channel.

In the second group of simulations, the pattern of topographic changes under small water discharges (the averaged water discharge during dry season 16710m^3/s; the historical minima water discharge 4620 m^3/s) is mainly deposition. The pattern of topographic changes under big water discharges (the averaged water discharge during wet season 40128m^3/s; the historical minima water discharge 92600m^3/s) is mainly erosion. A deposition zone becomes obvious at each end of channel outside of the estuary under big water discharges. The historical minima and maxima water discharges are extreme hydrological conditions, thus are very seldom to happen. It is of great significance to pay more attention to the averaged water discharges with SLR.

The pattern of ebb and flood velocities under joint effect of SLR 2m and small water discharges are similar. Under joint effect of SLR 2m and big water discharges, the pattern of ebb velocity is also similar, but the pattern of flood velocity is totally different. The ebb and flood velocities could effect the topographic changes but they are not the only and most decisive factors. Quantitative analysis on ebb velocity and flood velocity has been made along the channel under the four different combinations of input. Joint effect results show that, the ebb velocity under big water discharges is generally bigger than that under small water discharges. The flood velocity, under extreme minima water discharge with SLR 2m, is much bigger than that under extreme maxima water discharge with SLR 2m. The raised water level from seaside, together with the small water discharge from riverside, leads increasing flood velocity along the channel.

CHAPTER 6

CONCLUSIONS AND RECOMMENDATIONS

6.1 Conclusions

The main objectives of this study are to increase the understanding of the complex hydrodynamic and morphodynamic conditions as well as the historical morphological evolution of Yangtze Estuary; to simulate the morphological process with and without human interference under variations of hydrodynamic conditions, based on various unknown scenarios and known project plans; to predict the morphological response to joint effect of sea level rise and typical water discharges.

1. **For better understanding the hydrodynamic and morphodynamic conditions as well as the historical morphological evolution of Yangtze Estuary, the following processes are taken:**

The natural and human interferences factors affecting estuary morphodynamics worldwide are described. The morphology changes with available historical data in the past two thousand years of the Yangtze Estuary have been briefly discussed. The major human activities either finished or ongoing large water-related projects along the Yangtze River in the past century as well as their influences are summarized.

Regular field measurements conducted by governmental institutes, short-term measurements by local institutes or universities, as well as the data from referred papers or reports of Yangtze River Basin, are collected. Monthly data of water discharge, sediment discharge, surface suspended sediment concentration (SSC) and the median particle diameter (d_{50}) measured at Datong station from 1950 to 2008 are used for analyzing long-term trend of water and sediment variations.

The measured water level, flow velocity, sediment properties, as well as recorded wind and wave data at water level stations or profile stations are analyzed for understanding the hydrodynamic and sediment conditions, as the tidal motion, flow velocity and direction, the flow bifurcation ration and sediment bifurcation ration in Yangtze Estuary.

Topographical maps of different periods are analyzed with Topographic Change Method to learn the historical evolution of morphological changes at lower reach of Yangtze River and the estuary area.

The following conclusions are drawn:

- The natural factors affect the estuary morphodynamic seasonally and periodically. Human interferences break the sediment balance of the system. The morphology of

Yangtze Estuary changed a lot in the past two thousand years. The present three-stage bifurcation of the river mouth has been stabilized. The sediment has been blocked in the upper Yangtze River as well as been extracted of huge amount along the river. The water discharge has been diverged from large diversion projects or regional pumping plans. In additional, big artificial construction is developing directly at the river mouth. All these activities change the water and sediment discharges of Yangtze Estuary into the sea.

- The annual water discharge in the past 50 years in Yangtze Estuary has no significant change, but the monthly water discharge in wet season decreases while in dry season increases. Decreasing trends were found on the sediment discharge and concentration in the past few decades, especially after 1986. Increasing trend of the bed-load size is found. However, there is no significant change for suspended load in the past 30 years.

- The duration of ebb-tide is longer than it is during flood tide period either in dry season or wet season. In addition, the duration of flood tide gradually shortens and that of ebb tide gradually increases when the tidal water propagates from river mouth into the river channel. The tidal range decreases during the propagation. A time lag exists between the intrusions of tidal water and tidal current. The flow velocity in ebb tide period is higher than that in the flooding tide period; higher in wet season than in dry season.

- A linear correlation between the deposition volumes with the ratio of water to sediment discharges is found. The variation of sediment discharge, not the water discharges, dominated the scouring at the Near-River Estuary Reach (N-RER). The erosion rate increased 10 times in the past two decades for this reach. For the reach of North Branch (NB), it has been also scoured since 1992. The deposition volume increased after the implementation of TGD in 2003.

2. Before simulating the morphological process with and without human interference, a hydrodynamic and morphodynamic model is set up. The sensitive parameters are calibrated. The model is fully calibrated and validated.

The sensitive parameters such as the friction coefficient, the entrainment factor, the grain size distribution, and the eddy viscosity coefficient are calibrated with field data. The TIMOR is validated with field data both from wet and dry season as a reasonable model for the hydrodynamic and morphodynamic simulations for Yangtze Estuary area.

Simulations are done to check the seasonally bathymetry results in 3 years, 6 years and 9 years, due to the uneven seasonally water runoff distribution in the Yangtze Estuary. The long-term morphological simulations within 6 years, 12 years, 24 years and 36 years are made; and the spatial and temporal pattern of bathymetry changes in the Yangtze Estuary is analyzed.

Major conclusions are as follows:

- The model results have good agreements with the field measurements.

- The simulated hydrodynamics show that, the tide comes into the estuary from a direction between south and east, and leaves the estuary from a direction between north and west. The suspended sediment concentration is greatly influenced by tide propagation and it is in proportion to the current velocity.

- In long-term scale, the general pattern of morphological evolution is under balance. The whole North Branch is under obvious deposition. The South Branch and North Channel has deposition along the river banks. The right bank of South Passage is under deposition.

3. One of the major exploratory works in this study is by using the efficient numerical method to check the influences of one of the huge human activities, the regulation works at Yangtze Estuary.

The effect of different human activities on morphodynamics in Yangtze Estuary has been reviewed. Regulation works, as one of major human interference on the river and estuary systems, have been reviewed in worldwide scale. Detailed information about the regulation work in Yangtze Estuary, the Deep Waterway Regulation Project, has been described.

Simulations are done to check the morphodynamic evolution induced by regulation work at Yangtze Estuary. The morphological changes with and without the regulation works are examined. To tackle the deposition in the middle channel after Phase II, the south training dike has been heightened to 1m and 2m by numerical method. Simulations on predicting the morphological changes under extreme hydrological conditions are carried out. Quantitative analysis on the maintenance dredging volume is done under different model conditions.

Major conclusions are as follows:

- The flow velocity in the channel is enhanced with the training dikes. The groins also guide the current in and trap the sediment. The maximum ebb velocity is decreasing and the maximum flood velocity is increasing. The dredging volume for maintaining different objective water depths has been calculated systematically. The annual dredging volume for maintaining 8.5m and 10m are around 7.2 million m^3 and 21.4 million m^3 respectively, but for 12.5m the dredging volume amounts to 53.16 million m^3. The simulated annual dredging volume for 15m could be more than 70.75 million m^3. With different numerical models and computational methods, the calculated results are different. However the calculated results from TIMOR are between those results from other institutes or by other calculating means. All have the same trend.

- After implementing the Phase I and Phase II, the evolution pattern showed that: A Smooth and microbend tidal channel talweg which connects upper, middle and lower sections is formed, the original mouth bar disappeared. A navigation channel with 10m can be maintained through dredging. The obvious positive effect of DWRP has exhibited.

- The heightening of south training wall has reduced the deposition along this side, but the dredging volume needed has not been reduced. Besides, the hydrodynamics along

the channel revealed no positive improvement. The idea to heighten the South Training Wall may not be effective to tackle the deposition problem according to the dredging volume needed as well as the ebb and flood velocities in the channel.

- The deep waterway channel is under heavier erosion with extreme high water discharge than with the averaged discharge at half a year from the beginning. This is the extreme case as the Yangtze River could not meet the extreme high water discharge everyday. However after two years, the ebb velocity along the channel is decreasing, while the flood velocity along the channel is increasing, especially in the middle section of the channel. This could still result in deposition in the middle section of the channel due to the weakened ebb current power and the increased flood current power.

4. Attempt simulations are made to predict the morphological response under joint effect of sea level rise and typical water discharges.

The current projections indicate substantial variability in future sea level rise between different locations. Based on long-term tide data, the linear analysis is done for fitting to the trend of sea level fluctuation at Station Lvsi, which is near the Yangtze Estuary.

The systematic morphological simulations under a series sea level rise 0.18m, 0.59m, 1m and 2m during dry season and wet season respectively are done.

The influence on Yangtze annual runoff by human activities or large engineering works is analyzed. However, to project the discharge of Yangtze River under individual influence of climate change or human interferences, or their joint effects is still beyond confident quantitative investigations. Morphological simulations under joint effect of sea level rise 2m and the historical maxima and minima as well as averaged discharges in Yangtze Estuary are carried out.

Major conclusions are made as follows:

- The annual rate of sea level at station Lvsi is found to be 5.412 mm/yr. The projection of SLR for global ocean is from 0.18m-0.59m in 2100 based on the 1.8 mm/yr mean rate in 20th century. It is estimated that the sea level will rise from 0.54m to 1.77m in 2010 at Yangtze Estuary. More true values should be simulated by theoretical based model.

- The sea level rise during dry season has generally much more significant impact on the morphological evolution than during wet season. Deposition takes dominant position. During wet season, erosion is generally much more severe especially with sea level rise 2m. In general, during dry season, the ebb and flood velocities decrease with sea level rise comparing to without sea level rise. During wet season, the hydrodynamic changes are complicate. With different level of sea level rise, the ebb and flood velocity can go rise or down along the channel.

- The ebb and flood velocities are factors which could effect the topographic changes but not the only and most decisive factors. The ebb velocity under big water discharges is

generally bigger than that under small water discharges. The flood velocity, under extreme minima of water discharge, is much bigger than that under extreme maxima water discharge with joint effect of sea level rise 2m. The raised water level from seaside, together with the small water discharge from riverside, leads increasing flood velocity along the channel.

- The pattern of topographic changes under small water discharges (the averaged water discharge during dry season 16710m^3/s; the historical minima water discharge 4620 m^3/s) is mainly deposition. The pattern under big water discharges (the averaged water discharge during wet season 40128m^3/s; the historical minima water discharge 92600m^3/s) is mainly erosion. A deposition zone is found at each end of channel outside of the estuary under big water discharges.

6.2 Recommendations

Field data analysis is based on the data from Datong station, which is the only one long-term station, 640 km far from the river mouth. The water pumping along the Yangtze River from Datong to the Estuary area should be considered. Since the hydrodynamic environment changes greatly either from natural factors or by human interferences, much more long-term stations are urgently needed for the Near-River Estuary Reach (N-RER), the River Estuary Reach (RER), and the Offshore Estuary (OE).

Large-scaled long-term morphological simulations are still challenged by simultaneously coupled modeling of physical properties as waves, salinity and finer sediments, especially in the seasonally uneven hydrodynamic-conditioned estuaries.

Heightening the training dike has no obvious improvement on the hydrodynamic conditions in the navigation channel. More other engineering approaches can be tried. In the future, the joint effect of hydrological conditions from riverside and seaside is suggested to be considered, like the maximum water discharge happening together with typhoon or storm surges, as well as under sea level rises.

REFERENCES

[1] Acker, P., White, W.R., 1973. Sediment transport: new approach and analysis. *Journal of Hydraulic Division*, 99 (Hy11), 2041-2060.

[2] Antonelli, C., Provansal, M., Vella, C., 2004. Recent morphological channel changes in a deltaic environment the case of the Rhone River, France. *Geomorphology* 57, 385–402.

[3] Bai, X.F., Li, S.R., Gong, D.J., Xu, Y.P., Jiang, J.B., 2009. Estimation of suspended sediment concentrations using Pulse-coherent Acoustic Doppler Profiler (PCADP). *Chinese Journal of Oceanology and Limnology* 27 (2), 260-265.

[4] Baumann, R.H., 1984. Mississippi deltaic wetland survival: sedimentation versus coastal submergence. *Science* 224, 1093–1095.

[5] Benkhaldoun, F., Sahmim, S., Seaid, M., 2009. A two-dimensional finite volume morphodynamic model on unstructured triangular grids. *International Journal for Numerical Methods in Fluids.* Published online in Wiley InterScience (www.interscience.wiley.com). DOI: 10.1002/fld.2129

[6] Bueh, C., Cubasch, U., Hagemann, S., 2003. Impacts of global warming on changes in the East Asian monsoon and the related river discharge in a global time-slice experiment. *Climate Research* 24, 47–57.

[7] Biswas, A.K., 1983. *Long-distance water transfer: a Chinese case study and international experiences.* Tycooly International Publishing Ltd, Dublin, Ireland.

[8] Boyd, R., Dalrymple, R., 1992. Classification of clastic coastal depositional environments. *Sedimentary Geology* 80, 139– 150.

[9] *Bulletin of Yangtze River Sediment (2000–2004)*, Ministry of Water Resources of the People's Republic of China, Beijing.

[10] Cañizares, R., Irish, J.L., 2008. Simulation of storm-induced barrier island morphodynamics and flooding. *Coastal Engineering* 55, 1089–1101.

[11] Casulli, V., Zanolli, P., 1998. A three-dimensional Semi-Implicit Algorithm for Environmental Flows on Unstructured Grids. *Proceedings of the conference on Numerical Methods for Fluid Dynamics*, University of Oxford.

[12] Cazenave, A. 2006. How fast are the ice sheets melting? *Science* 314, 1250-1252.

[13] Chadwick, A., Morfett, J., Borthwick, M., 1996. *Hydraulics in Civil and Environmental Engineering.* Taylor & Francis, London.

[14] Chen, B., Wang, K., 2008. Suspended sediment transport in the offshore near Yangtze Estuary. *Journal of Hydrodynamics* 20(3).

[15] Chen, C.T.A., 2000. The Three Gorges Dam: Reducing the upwelling and thus productivity in the East China Sea. *Geophysical Research Letters* 27 (3), 381-383.

[16] Cheng, H.Q., Kostaschuk, R., Shi, Z., 2004. Tidal currents, bed sediments, and bedforms at the South Branch and the South Channel of the Changjiang (Yangtze) Estuary, China: implications for the ripple-dune transition. *Estuaries* 27 (5), 861-866.

[17] Chen, J.Y., 1997. The impact of sea level rise on China's coastal areas and its disaster hazard evaluation. *Journal of coastal research* 13 (3), 925-930.

[18] Chen, J.Y., Chen, S.L., 2003. The Changes of Ecologic Environment in Yangtze River Estuary and Some Suggestions for Estuary Regulation. *Water Resources and Hydropower Engineering* 34 (1), 19-25. (in Chinese)

[19] Chen, M.R., Hang, X.F., Liu, S.Q., 2000. The effects of reclamation and sustainable development on the coastal zone in Shanghai. *China Soft Science* 120(12), 115-120. (in Chinese).

[20] Chen, S.L., Zhang, G.A., Yang, S.L., 2003. Temporal and spatial changes of suspended sediment concentration and resuspension in the Yangtze River estuary. *Journal of Geographical Sciences* 13(4), 498-506.

[21] Chen, X.Q., 1990. Sea level changes from 1922 to 1987 in the Changjiang River Mouth and its significance, Acta Geographica Sinica, 45 (4), 387. (in Chinese)

[22] Chen, X.Q., 2000. Cross-border rivers, inter-basin water transfer and the basic problems of China's South-North Water Diversion. *Resources and Environment in the Yangtze Basin* 9(1), 92-97. (in Chinese)

[23] Chen, X.Q., Yan, Y.X., Tong, C.F., Song, Z.Y., Dou, X.P., Li, J.Y., 2007. Changes and mechanism studies on the bed load size of Yangtze Estuary reach. *Progress in Natural Sciences* 17 (2), 233-239. (in Chinese)

[24] Chen, X.Q., Zhang, E. F., Mu, H.Q., Zong, Y., 2005. A preliminary analysis of human impacts on sediment discharges from the Yangtze, China, into the sea. *Journal of Coastal Research* 21 (3), 515–521.

[25] Chen, X.Q., Zhang, D.Z., Zhang, E.F., 2002. The south no north water diversions in China: review and comments. *Journal of Environmental Planning and Management*, 45(6), 927-932. DOI: 10.1080/0964056022000024415

[26] Chen, X.Q., Zhang, E.F., Mu, H.Q., Zong, Y., 2005. A Preliminary Analysis of Human Impacts on Sediment Discharges from the Yangtze, China, into the Sea. *Journal of Coastal Research* 21 (3), 515-521.

[27] Chen, X.Q., Zhang, E.F., Xu, J.G., 2002. Large and episodic decrease of water discharge from the Yangtze River to the sea during the dry season. *Hydrological Sciences* 47 (1), 41-48.

[28] Chen, X.Q., Zong, Y., Zhang, E., Xu, J. Li, S., 2001. Human impacts on the Changjiang (Yangtze) River basin, China, with special reference to the impacts on the dry season water discharges into the sea. *Geomorphology* 41 (2), 111-123.

[29] Chen, Z., Gupta, A., 2001. The Yangtze River: an introduction. *Geomorphology* 41, 73-75.

[30] Chen, Z.Y., Chen, D.C., Xu, K.Q., Zhao, Y.W., Wei, T.Y., Chen, J., Li, L.Q., Watanabe, M., 2007. Acoustic Doppler current profiler surveys along the Yangtze River. *Geomorphology* 85, 155–165.

[31] Chen, Z.Y., Stanley, D.J., 1998. Sea-Level Rise on Eastern China's Yangtze Delta. *Journal of Coastal Research* 14 (1), 360-366.

[32] Chen, Z.Y., Stanley, D.J., 1995. Quaternary Subsidence and River Channel Migration in the Yangtze Delta Plain, Eastern China. *Journal of Coastal Research* 11 (3), 927-945.

[33] Chen, Z.Y., Li, J.F., Shen, H.T., Wang, Z.H., 2001. Yangtze River of China: historical analysis of discharge variability and sediment flux. *Geomorphology* 41 (3-3), 77-91.

[34] Chinese Three Gorges Project Corporation (CTGPC), 2002. *Flooding on the Yangtze in 1998*. April 20. (in Chinese).

[35] Chu, Z.X., Zhai, S.K., 2008. Yangtze River sediment: in response to Three Gorges Reservoir (TGR) water impoundment in June 2003. *Journal of Coastal Research* 24(sp1), 30-39.

[36] Church, J.A., Gregory, J.M., Huybrechts, P., Kuhn, M., Lambeck, K., Nhuan, M.T., Qin, D., Woodworth, P.L., 2001. Changes in sea level. In: Houghton, J.T., Ding, Y., Griggs, D.J., Noguer, M., van der Linden, P.J., Xiaosu, D. (eds) *Climate Change 2001*. *The Scientific*

Basis. Cambridge University Press, Cambridge, 639–693.

[37] Cronin, K.M., Devoy, R.J.N., Gault, J., 2007. Modelling estuarine morphodynamics on the south coast of Ireland. *Journal of Coastal Research* 50, 474 – 479.

[38] Cui, Y., Parker, G., Paola, C., 1996. Numerical simulation of aggradation and downstream fining. *Journal of Hydraulic Research* 34, 185-203.

[39] Dai, S.B., Lu, X.X., Yang, S.L., Cai, A.M., 2008. A preliminary estimate of human and natural contributions to the decline in sediment flux from the Yangtze River to the East China Sea. *Quatern. Int.* 186(1), 43–54.

[40] Dai, Z.J., Chu, A., Du, J.Z., Stive, M., Hong, Y., 2010. Assessment of extreme drought and human interference on baseflow of the Yangtze River. *Hydroogical. Processes* 24, 749–757. DOI: 10.1002/hyp.7505

[41] Dalrymple, R.W., Zaitlin, B.A., Boyd, R., 1992. Estuarine facies models: conceptual basis and stratigraphic implications. *Journal of Sedimentary Petrology* 62(6), 1130-1146.

[42] Davies, J.L., 1964. A morphogenic approach to world shorelines. *Zeitschrift fur Geomorphologie* 8, 27–42.

[43] Dennis, K., Niang-Diop, I., Nicholls, R.J., 1995. Sea-level rise and Senegal: Potential impacts and consequences. *Journal of Coastal Research* 14, 242-261.

[44] Ding, P.X., 2004. Prediction model of storm-induced erosion and deposition in the Yangtze Estuary. *Coastal Engineering.*

[45] Dong, Y.H., 2009. Contrast study on estimation of river deposition-erosion amount by sediment budget method and morphological change method. *Journal of Yangtze River Scientific Research Institute* 26(8). (in Chinese)

[46] Dou, X.P., 2003. Sedimentation problems related to regulation of deep channel in the Yangtze Estuary. *Proceedings of the International Conference on Estuaries and Coasts*, Hangzhou, China, 36-45.

[47] Dyer, K.R., 1986. *Coastal and estuarine sediment dynamics*. John Wiley and Sons, 358pp.

[48] Dyer, K.R., 1998. *Estuaries: A Physical Introduction.* John Wiley & Sons. 210pp.

[49] Edmonds, D.A., 2007. Mechanics of river mouth bar formation: Implications for the morphodynamics of delta distributary networks. *Journal of Geophysical Research.*

[50] Eidsvlk, K.J., 2004. Some contributions to the uncertainty of sediment transport predictions. *Continental Shelf Research* 24, 739-754.

[51] Eisma, D., 1998. *Intertidal Deposits: river mouths, tidal flats and coastal lagoons*. CRC Press. 459pp.

[52] Engelund, F., Hansen, E., 1967. A monograph on sediment transport in alluvial streams. Danish Tech. Press, Copenhagen, Denmark.

[53] Engelund, F., Fredsoe, J., 1976. A sediment transport model for straight alluvial channels. *Nordic Hydrology* 7, 296-306.

[54] Fanos, A.M., 1995. The impact of human activities on the erosion and accretion of the Nile delta coast. *Journal of Coastal Research* 11(3), 821–833.

[55] FitzGerald, D.M., Knight, J., 2005. *High Resolution Morphodynamics and Sedimentary Evolution of Estuaries (Coastal Systems and Continental Margins)*. Springer, 364pp.

[56] French, G.T., Awosika, L.F., Ibe, C.E., 1995. Sea-level rise in Nigeria: Potential impacts and consequences. *Journal of Coastal Research* 14, 224-242.

[57] Fryirs, K., Brierley, G.J., 2001. Variability in sediment delivery and storage along river courses in Bega catchment, NSW, Australia: implications for geomorphic river recovery. *Geomorphology* 38, 237–265.

[58] Frihy, O.E., 1992. Sea-Level Rise and Shoreline Retreat of the Nile Delta Promontories, Egypt. *Natural Hazards* 5, 65-81.

[59] Fuggle, R., Smith, W.T., 2000. *Large dams in water and energy resource development in the People's Republic of China.* Country Review Paper, Cape Town.

[60] Gao, M., 2008. *A Pre-feasibility study of navigation channel regulation works in north channel, Yangtze Estuary.* MSc thesis, UNESCO-IHE Institute for Water Education, The Netherlands.

[61] Gao, A., Yang, S.L., Li, G., Li, P., Chen, S.L., 2010. Long-term morphological evolution of a tidal island as affected by natural factors and human activities, the Yangtze Estuary. *Journal of Coastal Research* 26(1), 123–131.

[62] Gartner, J.W., 2004. Estimating suspended solids concentrations from backscatter intensity measured by acoustic Doppler current profiler in San Francisco Bay, California. *Marine Geology* 211, 169–187.

[63] Gleizon, P., Punt, A.G., Lyons, M.G., 2003. Modelling hydrodynamics and sediment flux with a macrotidal estuary: Problems and solutions. The Science of the Total Environment.

[64] Gleik, P.H., 2009. Three Gorges Dam Project, Yangtze River, China. *The World's Water 2008-2009.*

[65] Grinsted, A., Moore, J.C., Jevrejeva, S., 2009. Reconstructing sea level from paleo and projected temperatures 200 to 2100 AD. *Climate Dynamics*, DOI 10.1007/s00382-008-0507-2

[66] Giardino, A., Ibrahim, E., Adam, S., Toorman, E.A., Monbaliu, J., 2009. Hydrodynamics and Cohesive Sediment Transport in the IJzer Estuary, Belgium: Case Study. *Journal of Waterway,Port, Coastal, and Ocean Engineering* 135(4), 176-184.

[67] Giosan, L., Constantinescu, S., Clift, P.D., Tabrez, A.R., Danish, M., Inam, A., 2006. Recent morphodynamics of the Indus delta shore and shelf. *Continental Shelf Research* 26 (14), 1668–1684.

[68] Gornitz, V., 2000. In: Douglas, B.C. et al. (Eds), *Sea Level Rise: History and Consequences*. Academic Press, San Diego, CA, 97–119.

[69] Guillén, J., Palanques, A., 1997. A historical perspective of the morphological evolution in the lower Ebro River. *Environmental Geology* 30, 174-180.

[70] Han, M., Hou, J., Wu, I., 1995. Potential impacts of sea-level rise on China's coastal environment and cities: A national assessment. *Journal of Coastal Research* 14, 79-95.

[71] Han, Z., Jin, Y.Q., Yun, C.X., 2006. Suspended sediment concentrations in the Yangtze River estuary retrieved from the CMODIS data, *International Journal of Remote Sensing* 27(19), 4329-4336.

[72] He, Q., et al., 2003. Field measurements of surface suspended sediment concentration in the Yangtze Estuary. CHINA. *Proceedings of International Conference on estuarine and coasts*, Hangzhou, China. 27-232.

[73] Hervouet, J.M., 2007. *Hydrodynamics of free surface flow, finite elements system.* Wiley.

[74] Hervouet, J.M., Bates, P., 2000. The TELEMAC modeling special issue. *Hydrological*

Process.

[75] Heyer, H., Plüß, A., 2007. Morphodynamic Multi-Model Approach for the Elbe Estuary. *Proceedings of the International Symposium of River*, *Coastal and Estuarine Morphodynamics (RCEM)*. Enschede, The Netherlands.

[76] Hirano, M., 1971. On riverbed variation with armoring. *Proceedings of the Japan Society of Civil Engineering* 195, 55-65.

[77] Hoitink, A.J.F., Hoekstra, P., 2005. Observations of suspended sediment from ADCP and OBS measurements in a mud-dominated environment. *Coastal Engineering* 52(2), 103-118.

[78] Holdaway, G.P., Thorne, P.D., Flatt, D., Jones, S.E., Prandle, D., 1999. Comparison between ADCP and transmissometer measurements of suspended sediment concentration. *Continental Shelf Research* 19, 421-441.

[79] Holz, K.P., Milbradt, P., 1995. Large area simulation of beach processes In Pahl/Werner, *Computing in Civil and Building Engineering*, A.A. Balkema, Rotterdam, Netherlands.

[80] Houghton, J.T., Ding, Y., Griggs, D.J., Noguer, M., van der Linden, P.J., Dai, X., Maskell, K., Johnson, C.A., 2001. *Climate Change 2001: The Scientific Basis. Contribution of Working Group I to the Third Assessment Report of the Intergovernmental Panel on Climate Change*. Cambridge University Press, New York.

[81] Hsu, T.W., Ou, S.H., Liau, J.M., 2005. Hindcasting nearshore wind waves using a FEM code for SWAN, *Coastal Engineering*, Vol. 52, pp. 177-195.

[82] Hu, B.Q., Yang, Z.S., Wang, H.J., Sun, X.X., Bi, N.H., Li, G.G., 2009. Sedimentation in the Three Gorges Dam and the future trend of Changjiang (Yangtze River) sediment flux to the sea. *Hydrology and Earth System Sciences* 13, 2253–2264.

[83] Hu, K., Ding, P.X., Zhu, S.X., Cao, Z.Y., 2000. 2-D Current field numerical simulation iIntegrating Yangtze Estuary with Hangzhou Bay. *China Ocean Engineering* 14(1), 89-102.

[84] Hu, K., Ding, P.X., Wang, Z.B., and Yang, S.L., 2009. A 2D/3D hydrodynamic and sediment transport model for the Yangtze Estuary, China. *Journal of Marine Systems* 77(1-2), 114-136.

[85] Huntley, D. A., Coco, G., O'hare, T.J., 2004. Abstracted modelling as a tool for understanding and predicting coastal morphodynamics. *Journal of Coastal Research*, 39.

[86] Institute of Hydraulics and Water Resources at the Technical University of Darmstadt, 2004. Manual of TIMOR Modeling System.

[87] Intergovernmental Panel on Climate Change (IPCC), Working Group I Contribution to the Fourth Assessment Report, Climate change 2007—the physical science basis, Chapter 5 observations—oceanic climate change and sea level, 409.

[88] Ippen A. T., 1968. Salinity Intrusion in Estuaries. In: Ippen AT (Eds), *Estuary and Coastline Hydrodynamics*, McGraw-Hill Inc., 598-629.

[89] Jin, L., Yu, Z., He, Q., 2006. On the relationship between maintenance condition of Yangtze Estuary Deepwater Channel and water & sediment transport from the Valley. *Port & Waterway Engineering* 3, 46-51 (in Chinese)

[90] Jia, L.W., Luo, Z.G., Yang, Q.S., Ou, S.Y., Lei, Y.P., 2007. Impacts of the large amount of sand mining on riverbed morphology and tidal dynamics in lower reaches and delta of

the Dongjiang River. *Journal of Geographical Sciences* 17(2), 197-211.

[91] Jiang, T., Kundzewicz, Z.W., Su, B., 2008. Changes in monthly precipitation and flood hazard in the Yangtze River Basin, China. *International Journal of Climatology* 28 (11), 1471-1481. Doi: 10.1002/joc.1635

[92] Kappenberg, J., Grabemann, I., 2001. Variability of the mixing zones and estuarine turbidity maxima in the Elbe and Weser Estuaries. *Estuaries* 24, 699-706.

[93] Kausch, H., 1993. Ecological characteristics, anthropogenic alterations, and the need for restoration of German tidal estuaries, exemplified by the Elbe Estuary, northern Germany. In: Kurihara, Y. (Eds), *Restoration and Preservation of Urban Estuarine Ecosystems*. Report of International Science Research Project, Sendai, Japan.

[94] Kempe, S. (1982b). Valdivia Cruise, October 1981: carbonate equilibria in the estuaries of the Elbe, Weser, Ems, and in the Southern German Bight. In Degens, E. T. (Ed.) Transport of Carbon and Minerals in Major World Rivers, Vol. I, pp. 719-742.

[95] Kesel, R.H., 1989. The role of the Mississippi River in wetland loss in Southeastern Louisiana, USA. *Environmental Geology and Water Sciences* 13, 183–193.

[96] Kesel, R.H., 2003. Human modifications to the sediment regime of the Lower Mississippi River flood plain. *Geomorphology* 56, 325–334.

[97] Kondolf, G.M., 1997. HungryWater: Effects of Dams and Gravel Mining on River Channels. *Environmental Management* 21, 533–551.

[98] Kopp, R.E., Simons, F.J., Mitrovica, J.X., Maloof, A.C., Oppenheimer, M., 2009. Probabilistic assessment of sea level during the last interglacial stage. *Nature* 462, 863-867. doi:10.1038/nature08686

[99] Lafite, R., Roman˜ a, L.-A., 2001. A man-altered macrotidal estuary: the Seine estuary (France): introduction to the special issue. *Estuaries* 35 (6B), 939.

[100] Latteux, B., 1995. Techniques for long-term morphological simulation under tidal action. *Marine Geology* 126.

[101] Leopold, L.B., Wolman, M.G., Miller, J.P., 1964. *Fluvial Processes in Geomorphology.* W.H. Freeman & Company, San Francisco, 535 pp.

[102] Lesourd, S., Lesueur, P., Brun-Cottan, J.-C., Auffret, J.-P., Poupinet, N., Laignel, B., 2001. Morphosedimentary evolution of the macrotidal Seine estuary subjected to human impact. *Estuaries* 24 (6B), 940e949

[103] Lesser, G.R., Roelvink, J.A., van Kester, J.A.T.M., Stelling, G.S., 2004. Development and validation of a three-dimensional morphological model. *Coastal Engineering* 51, 883–915.

[104] Li, J. Y., 2007. *Research on Hydrodynamic and Sediment Characteristics at Datong and Xuliujing Reach of Yangtze River*. Ph.D thesis, Hohai University, China, (in Chinese).

[105] Li, J., Wan, X., Ying, M., Chen, X., 2005. Field observations on bed sediments and sand waves in Changjiang estuary. *International Journal of Sediment Research* 20 (2), 129-135.

[106] Li M.T., Chen Z.Y., 2004. Analysis of Jiujiang reach of Changjiang river evolution in recent forty years using DEM. *Advance in Water Science* 15(3), 330–335 (in Chinese).

[107] Li, W.H., Cheng, H.Q., Li, J.F., Dong, P., 2008. Temporal and spatial changes of dunes in the Changjiang (Yangtze) estuary, China. *Estuarine, Coastal and Shelf Science* 77, 169-174.

[108] Lin, H., Lu, G.N., Song, Z.Y., 2000. Study on modeling the tide wave system of East China

Sea and coastal evolution. *Science Press*, Beijing. (in Chinese)

[109] Lisle, T.E., Iseya, F., Ikeda, H., 1993. Response of a channel with alternate bars to a decrease in supply of mixed-size bed load: a flume experiment. *Water Resource Research* 29 (11), 3623-3629.

[110] Liu, H., 2006. Hydrodynamic problems associated with construction of sea-crossing bridges. *Journal of Hydrodynamics.*

[111] Liu, J.W., 2008. *Application of ELCIRC model in saltwater intrusion of Yangtze Estuary.* MSc thesis, Hohai University, China, (in Chinese).

[112] Liu, J.P., Xu, K.H., Li, A.C., Milliman, J.D., Velozzi, D.M, Xiao, S.B., Yang, Z.S., 2007. Flux and fate of Yangtze River sediment delivered to the East China Sea. *Geomorphology* 85, 208–224.

[113] Liu, Z., 2004. Soil and water conservation in China, *Proceedings of the Ninth International Symposium on River Sedimentation*, Yichang, China. 137-142.

[114] Livingston, R.J., 1991. Historical relationships between research and resource management in the Apalachicola River estuary. *Ecological Applications* 1, 361–382.

[115] Lu, J.Y., Zheng, W.Y., 2004. Progress of Sedimentation Research for the Yangtze River. *Proceedings of the Ninth International Symposium on River Sedimentation, Yichang, China*. 95-104.

[116] Lu, X.X., 2004. Vulnerability of water discharge of large Chinese rivers to environmental changes: an overview. *Regional Environmental Change 4*, 182–191. DOI: 10.1007/s10113-004-0080-0

[117] Malcherek, A., 2005. Mathematical Module SediMorph – Standard Validation Document Version 1.1, Technical. Rep. Bundesanstalt für Wasserbau.

[118] Meehl, G.A., Washington, W.M., Collins, W.D., Arblaster, J.M., Hu, A., Buja, L.E., Strand, W.G., Teng, H., 2005. How much more global warming and sea level rise? *Science* 307, 1769-1772.

[119] Mei, J.S., 2006. The South to North Water Transfer Project of China. *Proceedings of the World Environmental and Water Resources Congress*.

[120] Mewis, P., 2002. Morphodynamisch-numerische Modellierung von Flußkurven, Doktorarbeit an der Teschnische Universität Darmstadt.

[121] Mewis, P., 2007. Numerische Simulation von Strömungsvorgängen im Wasserbau, TU Darmstadt.

[122] Meyer, P., Müller, 1948. Formulas for bed load transport, Report on second meeting of international association for Hydraulics Research, Stockholm, Sweden

[123] Mikkelsen, N., 1980. Experimental dissolution of Pliocene diatoms. Nova Hedwigia **33**, pp. 893–907.

[124] Milliman, J.D., Meade, R.H., 1983. World-Wide Delivery of River Sediment to the Oceans. *Journal of Geology* 91, 1–21.

[125] Milliam, J.D., 1997. Blessed dams or dammed dams. *Nature* 386, 325-326.

[126] Milliman, J.D., Syvitski, J.P.M., 1992. Geomorphic/tectonic control of sediment discharge to the ocean: the importance of small mountainous rivers. *Journal of Geology* 100 (5), 525–544.

[127] Milliman, J.D., 1997. Blessed dams or damned dams? *Nature* 386, 325–327.

[128] Milliman, J.D., 2001. Delivery and fate of fluvial water and sediment to the sea: a

marine geologist's view of European rivers. *Scientia Marine* 65, 121-132.

[129] Milne J.A., Sear D.A., 1997. Modelling river channel topography using GIS. *International Journal Geographical Information Science* 11(5), 499–519.

[130] Mu, H.Z., Xu, J.L., Ke, X.X., Tang, L., Chen, D.L., 2006. Application of high resolution numerical model to wind energy potential assessment. *Journal of Applied Meteorological Science* 17(2), 152-159.

[131] Nerem, R.S., Leuliette, E., Cazenave, A., 2006. Present-day sea-level change: A review. *Comptes Rendus Geoscience* 338, 1077-1083.

[132] Nghiem, L.T., Stive, M.J.F., Verhagen, H.J., Wang, Z.B., 2006. Morphodynamic modelling for thuan an inlet, Vietnam. *International Conference on Estuaries and Coasts(ICEC-2006)*, Guangzhou, China.

[133] Nichols, M.M., 1991. *Response of Coastal Plain Estuaries to Episodic Events in the Chesapeake Bay Region.* Springer, New York.

[134] Nichols, M.M., Biggs, R.B., 1985. Estuaries. In: Davis, R.A. (Eds), *Coastal Sedimentary Environments.* Springer, Berlin, 77-186.

[135] Nicholls, R.J., 2002. Analysis of global impacts of sea-level rise: a case study of flooding, Physics and Chemistry of the Earth 27, 1455–1466.

[136] Nicholls, R.J., Tol, R.S.J., 2006. Impacts and responses to sea-level rise: a global analysis of the SRES scenarios over the twenty-first century. *Philosophical Transactions of the Royal Society A* 364(1841), 1073-1095.

[137] Nicholls, R.J., Tol, R.S.J., Vafeidis, A.T., 2008. Global estimates of the impact of a collapse of the West Antarctic ice sheet: an application of FUND. *Climatic Change*, 91(1-2), 171-191. doi:10.1007/s10584-008-9424-y

[138] Nilsson, C., et al., 2005, Fragmentation and flow regulation of the world's large river systems. *Science* 308, 405-408.

[139] O'Brien, M.P., Field and laboratory studies navigation channels of the Columbia River Estuary, Hydraulic Engineering Laboratory, University of California at Berkeley, *Report* HEL-24-4 (1971), p. 35.

[140] Olsthoorn, X., van der Werff, P., Bouwer, L., Huitema, D., 2002. Neo-Atlantis: Ducth Responses to Five Meter Sea Level Rise, *Working Papers FNU-78, Research unit Sustainability and Global Change*, Hamburg University.

[141] Osterwald, J., Oellerich, J., Wittmüß, D., 2008. Deeping of the lower and outer Elbe Estuary. *Proceedings of the International Conference on Coastal Engineering (ICCE)*.

[142] Overpeck, J.T., Otto-Bliesner, B.L., Miller, G.H., Muhs, D.R., Alley, R.B., Kiehl, J.T., 2006. Paleoclimatic Evidence for Future Ice-Sheet Instability and Rapid Sea-Level Rise. *Science* 311, 1747-1750.

[143] Parthiot, F. (1981). Development of the river Seine estuary: case study. J.of the Hydraulics div., ASCE, vol.107, HY11, 1283-1303.

[144] Parker, G., 1990. Surface-based bedload transport relation for gravel rivers. Journal of Hydraulic Research 28(4), 417-436.

[145] Pennant-Rea, R., 1994. Chainsaw Massacres. *The Economist* 331(7869), 39.

[146] Perez, B.C., Day, J.W., 2000. Influence of atchafalaya river discharge and winter frontal passage on suspended sediment concentration and flux in fourleague bay, louisiana. *Estuarine, Coastal and Shelf Science* 50, 271–290

[147] Portela, L.I., 2008. Sediment transport and morphodynamics of the Douro River estuary. Geo-Marine Letters, Vol.28.No.2., pp.77-86

[148] Pritchard, D.W., 1952. Estuarine hydrography. In: Advances in Geophysics, Vol. 1, Academic Press Inc., New York, 243-280.

[149] Pritchard, D.W., 1955. Estuarine circulation patterns. *Proceeding of the America Society of Civil Engineering*. 1-11

[150] Pritchard, D.W., 1967. What is an estuary: physical viewpoint. pp.3-5 in: G. H. Lauf (ed.) Estuaries, A.A.A.S. Publ. No. 83, Washington, D.C.

[151] Qi, D.M., Zhang, Y., 2003. Numerical Investigations on effects of the reclamation project on Hengsha east beach in the Yangtze estuary deepwater channel. *Proceedings of International Conference on Estuaries and Coasts*, Hangzhou, China. 937-943.

[152] Qing, H.E., Yu, Z.Y., Wang, Y.Y., Yun, C.X., 2003. Field measurements of surface suspended sediment concentration in the Yangtze Estuary. *Proceedings of the International Conference on Estuaries and Coasts*, Hangzhou, China. 228-232.

[153] Rahmstorf, S., 2007. A Semi-Empirical Approach to Projecting Future Sea-Level Rise. *Science* 315, 368-370.

[154] Ramos, S.C., Cowen, R.K., Paris, C., Re, P., Bordalo, A.A., 2006a. Environmental forcing and larval fish assemblage dynamics in the Lima River estuary (northwest Portugal). *Journal of Plankton Research 28*, 275-286

[155] Roelvink, J.A., 2006. Coastal morphodynamic evolution techniques. *Coastal Engineering* 53 (2-3), 277-287.

[156] Roland, A., 2008. Development of WWM II: Spectral wave modelling on unstructured meshes. Ph.D. thesis of Technische Universität Darmstadt, Institute of Hydraulic and Water Resources Engineering.

[157] Rouse, H., 1937. Modern conceptions of the mechanics of turbulence. *Transactions of the American Society of Civil Engineers* 102(1965), 463-543.

[158] Sa' nchez-Arcilla, A., Jime'nez, J.A., Valdemoro, H.I., 1998. The Ebro Delta: morphodynamics and vulnerability. *Journal of Coastal Research* 14(3), 754–772.

[159] Savenije, H.H.G., 2005. *Salinity and Tides in Alluvial Estuaries*. Elsevier, 208pp.

[160] Scott, T.R., Mason, D.C., 2007. Data assimilation for a coastal area morphodynamic model: Morecambe Bay. C*oastal Engineering* 54, 91–109.

[161] Sheng, Y.P., 1987. On Modeling Three-Dimensional Estuarine and Marine Hydrodynamics. In: Nihoul, J.C.J., Jamart, B.M. (Eds), *Three-Dimensional Models of Marine and Estuarine Dynamics.* Elsevier Oceanography Series, Elsevier, 35-54.

[162] Sheng, Y.P., Eliason, D.E., Chen, X.J., and Choi, J.K., 1991. *A Three-dimensional numerical model of hydrodynamics and sediment transport in lakes and estuaries: Theory, Model Development and Documentation*. U.S. Environmental Protection Agency, Athens GA.

[163] Shen, G.Z., Xie, Z.Q., 2004. Three Gorges project: chance and challenge. *Science* 304.

[164] Shi, Y.F., Zhu, J., Xie, Z., Ji, Z.X., 2000. Prediction and prevention of the impacts of sea level rise on the Yangtze River Delta and its adjacent areas. *Science in China, Series D.*

[165] *Shore Protection Manual (SPM)*. 1984. U.S. Army Engineer Waterways Experiment Station, U.S. Government Printing Office, Washington, DC.

[166] Siddall, M., Stocker, T.F., Clark, P.U., 2009. Constraints on future sea-level rise from past sea-level change. *Nature Geoscience* 2, 571 – 575. doi:10.1038/ngeo587

[167] Small, C., Nicholls, R.J., 2003. A global analysis of human settlement in coastal zones. *Journal of Coastal Research* 19 (3), 584–599.

[168] Smith, L.M. and Winkley, B.R., 1996. The response of the Lower Mississippi River to river engineering. *Engineering Geology* 45, 433–455.

[169] State *Ocean* Administration (SOA). 2009. *State Sea-level bulletin*. Beijing.

[170] Stanley, D.J., Warne, A.G., 1993. Nile Delta: recent geological evolution and human impact. *Science* 260 (5108), 628–634.

[171] Stanley, D.J., Warne, A.G., 1994. Worldwide initiation of Holocene marine deltas by deceleration of sea-level rise. *Science* 265, 228– 231.

[172] Stive, M.J.F., Capobianco, M., Wang, Z.B., Ruol, P., Buijsman, M.C., 1998, Morphodynamics of a tidal lagoon and adjacent coast. *Proceedings of 8th International Biennial Conference on Physics of Estuaries and Coastal Seas*. Hague, Netherlands, 397-407.

[173] Su, C.W., Tan, G.M., 2009. Advances in calculation methods for river sedimentation. *Journal of Sediment Research* 4. (in Chinese).

[174] Sutherland, J., Peet, A.H., Soulsby, R.L., 2004a. Evaluating the performance of morphological models. *Coastal Engineering* 51, 917–939.

[175] Sutherland, J., Walstra, D.J.R., Chesher, T.J., van Rijn, L.C., Southgate, H.N., 2004b. Evaluation of coastal area modelling systems at an estuary mouth. *Coastal Engineering* 51, 119–142.

[176] Syvitski, J.P.M., Vorosmarty, C.J., Kettner, A.J., Green, P., 2005. Impact of humans on the flux of terrestrial sediment to the global coastal ocean. *Science* 308, 376–380.

[177] Talmon, M.C.L.M., van Mierlo, N., Struiksma, N. 1995. Laboratory measurements of the direction of sediment transport on transvere alluvial bed slopes. *Journal of Hydraulic Research*, 33 (4).

[178] Thomas et al., 2002. C.G. Thomas, J.R. Spearman and M.J. Turnbull, Historical morphological change in the Mersey Estuary. *Continental Shelf Research* 22 11–13 (2002), pp. 1775–1794

[179] Tong, C.F., Lei, Z.Y., Yan, Y.X., Li, J.Y., 2008. Multiple time-scale analysis on flow and sediment of Yangtze River into the sea. *Proceedings of the forth Chinese-German joint symposium on coastal and ocean engineering*. 197-205.

[180] Toorman, E.A., 2001. Cohesive sediment transport modelling: European perspective. In: McAnally, W.H., Mehta, A. J. (Eds). P*roceedings of Marine Sciences, Coastal and Estuarine Fine Sediment Processes*, Elsevier Science, Amsterdam, The Netherlands. 1–18.

[181] Toro-Escobar, C.M., Parker, G., Paola, C., 1996. Transfer function for the deposition of poorly sorted gravel in response to streambed aggradation. *Journal of Hydraulic Research*, 34(1), 35-53.

[182] Trenhaile, A.S., 1997. *Coastal dynamics and landforms*. Oxford University Press, New York. 366pp.

[183] U.S. Army Corps of Engineers (USACE), 2008. Coastal Engineering Manual (CEM), Washington.

[184] Van Rijn, L. 1984. Sediment Pick-up Functions. *Journal of Hydralic Engineering*, ASCE, 110(10).

[185] Van Rijn, L.C., 1989. *Handbook, sediment transport by currents and waves*. Rep. H461,

Delft Hydraulics, Delft, the Netherlands.

[186] Van Rijn, L.C., 1991. Bed-load transport measurements in the River Waal near Woudrichem and near Druten. Delft Hydraulics, Delft, the Netherlands.

[187] Van Rijn, L.C., 1993. Principles of sediment transport in rivers, estuaries, coastal seas and oceans. Aqua Publications, Amsterdam, the Netherlands.

[188] Van Rijn, L.C., Davies, A.G., Van de Graaff, J., Ribberink, J.S., 2001. *Sediment transport modelling in marine coastal environments.* Aqua Publications, Amsterdam, 415pp.

[189] Vermeer, M., Rahmstorf, S., 2009. Global sea level linked to global temperature. *Proceedings of the National Academy of Sciences* 106 (51), 21527–21532.

[190] Verhaar, P.M., Biron, P.M., Ferguson, R.I., Hoey, T.B., 2008. A modified morphodynamic model for investigating the response of rivers to short-term climate change, *Geomorphology* 101, 674–682.

[191] Vriend, H.J., 1991. Mathematical modeling and large-scale coastal behavior. Journal of Hydraulic *Research.*

[192] Vriend, H.J., 1993. Approaches to long-term modeling of coastal morphology: a Review. *Coastal Engineering.*

[193] Vriend, H.J., 2003. Advances in Morphodynamics of tidal rivers and estuaries, *Proceedings of the International Conference on Estuaries and Coasts*, Hangzhou, China. 3-10.

[194] Villaret, C. 2005. *Sisyphe release 5.5—User manual*, EDFLNHE report HP76/05/009.

[195] Villaret, C., Hervouet, J.M., Huybrechts, N., Van, L.A., Davies, A.G., 2010. Effect of bed friction on morphodynamic modelling: Application to the central part of the Gironde estuary. In Vionnet et al. (eds). *River, Coastal and Estuarine Morphodynamics (RCEM) 2009*. 899-905.

[196] Vörösmarty, C.J., Meybeck, M., Fekete, B., Sharma, K., Green, P., Syvitski, J.P.M., 2003. Anthropogenic sediment retention: major global impact from registered river impoundments. *Global andPlanetary Change* 39, 169–190.

[197] Walling, D.E., 1999. Linking land use, erosion and sediment yields in river basins. *Hydrobiologia* 410, 223–240.

[198] Walling, D.E., 2006. Human impact on land-ocean sediment transfer by the world's rivers. *Geomorphology* 79, 192–216.

[199] Walter, H., and E. Stadelmann, 1974. A new approach to the water relations of desert plants. In G.W. Brown Jr., ed., Desert Biology: Special Topics on the Physical and Biological Aspects of Arid Regions, 2:213-310. *New York: Academic Press*.

[200] Wang, H., Yang, Z., Saito, Y., Liu, J.P., Sun, X., Wang, Y., 2007. Stepwise decreases of the Huanghe (Yellow River) sediment load (1950–2005): impacts of climate change and human activities. *Global and Planetary Change* 57 (3–4), 331–354.

[201] Wang, H.J., Yang, Z.S., Wang, Y., Saito, Y., Liu, J.P., 2008. Reconstruction of sediment flux from the Changjiang (Yangtze River) to the sea since the 1860s. Journal of Hydrology.

[202] Wang, J., Bai, S.B., Liu, P., Li, Y.Y., Gao, Z.G., Qu, G.X., Cao, G.G., 2009. Channel sedimentation and erosion of the Jiangsu reach of the Yangtze River during the last 44 years. *Earth Surface Processes and Landforms* 34, 1587–1593.

[203] Wang, Y., Ren, M.E., Syvitski, J.P.M., 1997. Sediment transport and terrigenous flux. In: The Sea. In: Robinson, A.R., Brink, K.H. (Eds), *The Global Coastal Ocean: Processes and*

Methods, vol. 10. Wiley, New York, 346–401.

[204] Ward, J.V., Stanford, J.A., 1979. *The ecology of regulated streams*. Plenum Press, New York.

[205] World Commission on Dams (WCD), 2000. *Dams and Development: A New Framework for Decisionmaking*, Earthscan, London and Sterling, VA.

[206] Wei, Z.X., Gong, S.L., 1998. Sea level rising and its possible impacts on Shanghai in future, Shanghai Geology 1, 14-20. (in Chinese)

[207] Witting, M., Zanke, U., Mewis, P., 2004. Multiple grain size morphodynamic modeling at Teigmouth (UK). *Proceedings of the 5th International Conference on Hydroscience and Engineering (ICHE)*, Brisbane, Australian.

[208] Witting, M., Zanke, U., 2004. Development of an equilibrium bay: A long-term morphodynamic modeling study. *Proceedings of the 29th International Conference on Coastal Engineering (ICCE)*, Lisbon, Portugal.

[209] Witting, M., 2004. S*imulation von Küstenlängs-und Küstenquertransport im 2DH-morphodynamischen Modell TIMOR3*, Doktorarbeit an der Teschnische Universität Darmstadt.

[210] Wright, L.D., 1971. Hydrography of South Pass, Mississippi River. *J. Waterway Port Coastal and Ocean Div., ASCE 97 (WW3).*

[211] WL|Delft Hydraulics, 2005. *Delft3D-FLOW, User manual*, Version 3.12

[212] Wu, Q., Zheng, X.X., Xu, H., Ying, Y.F., Hou, Y.S., Xie, X.C., Wang, S.X., 2003. Relative sea-level rising and its control strategy in coastal regions of China in the 21st century. *Science in China* 46 (1), 74-83.

[213] Wurpts, A., 2006. *Numerische Simulation von Dichteeffekten am Beispiel der Umlagerung von Baggergut im Ästuarbereich,* Doktorarbeit an der Teschnische Universität Darmstadt.

[214] Xu, A.X., Zhou, G.Y., 2009. Application of new technology in measuring Hydrology of Yangtze River

[215] Xu, F.M., Perrie, W., Zhang, J.L., 2005. Simulation of typhoon-driven waves in the Yangtze Estuary with multiple-nested wave models. *China Ocean Engineering* 19(4), 613-624.

[216] Xu, K., Milliman, J.D., Yang, Z., Wang, H., 2006. Yangtze Sediment Decline Partly From Three Gorges Dam. *Eos* 87 (19), 185-196.

[217] Xu, K., Milliman, J.D., 2009. Seasonal variations of sediment discharge from the Yangtze River before and after impoundment of the Three Gorges Dam. *Geomorphology* 104 (3-4), 276-283.

[218] Yan, K., 1981. Yangtze Regulation Research. Vol.1, Yangtze Regulation Group

[219] Yan, Y.X., Gao, J., Zhu, Y.L., Zheng, J.H., 2001. Preliminary study on relationship between deepwater channel regulation and riverbed evolution. *Journal of Hohai University*. (in Chinese)

[220] Yan, Y.X., Gao, J.Y., Tong, C.F., 2006. Wind Waves in East China. *Proceeding of the 25th International Conference on Offshore Mechanics and Artic Engineering, Germany.*

[221] Yang, J.C., 1985. *Geographic*, High Education Press, Beijing, 53-60. (in Chinese)

[222] Yang, S., Ding, P.X., Zhu, J., Zhao, Q., Mao, Z., 2000. Tidal flat morphodynamic processes of the Yangtze estuary and their engineering implications. *China Ocean Engineering* 14 (3), 307–320.

[223] Yang, S.L., 1999. A study of coastal morphodynamics on the Muddy Islands in the Changjiang River estuary. *Journal of Coastal Research* 15 (1), 32–44.

[224] Yang, S.L., Ding, P.X., Chen, S.L., 2001. Changes in progradation rate of the tidal flats at the mouth of the Changjiang (Yangtze) River, China. *Geomorphology* 38 (1), 167-180.

[225] Yang, S.L., Zhao, Q.Y., Belkin, I.M., 2002. Temporal variation in the sediment load of the Yangtze River and the influences of human activities. *Journal of Hydrology* 263 (1–4), 56–71.

[226] Yang, S.L., Belkin, I.M., Belkina, A.I., Zhao, Q.Y., Zhu, J., Ding, P.X., 2003. Delta response to decline in sediment supply from the Yangtze River over the last 50 years and predictions for the future, *Estuarine, Coastal and Shelf Science* 57 (4), 689-699.

[227] Yang, S.L., Shi, Z., Zhao, H.Y., Li, P., Dai, S.B., Gao, A., 2004. Research Note: Effects of human activities on the Yangtze River suspended sediment flux into the estuary in the last century. *Hydrology and Earth Systems Sciences* 8 (6), 1210-1216.

[228] Yang, S.L., Gao, A., Hotz, H.M., Zhu, J., Dai, S.B., Li, M., 2005. Trends in annual discharge from the Yangtze River to the sea (1865–2004). *Hydrological Sciences* 50 (5), 825–836.

[229] Yang, S.L., Zhang, J., Zhu, J., Smith, J.P., Dai, S.B., Gao, A., and Li, P., 2005. Impact of dams on Yangtze River sediment supply to the sea and delta intertidal wetland response. *Journal of Geophysical Research* 110.

[230] Yang, S.L., Li, M., Dai, S.B., Liu, Z., Zhang, J., Ding, P.X., 2006a. Drastic decrease in sediment supply from the Yangtze River and its challenge to coastal wetland management. *Geophysical Research Letters* 33, L06408.

[231] Yang, Z.S., Wang, H.j., Saito, Y., Milliman, J.D., Xu, K.H., Shi, G.Y., 2006b. Dam impacts on the Changjiang (Yangtze River) sediment discharge to the sea: the past 55 years and after the Three Gorges Dam. *Water Resource Research* 42.

[232] Yang, S.L., Zhang, J., Dai, S.B., Li, M., Xu, X.J., 2007a. Effect of deposition and erosion within the main river channel and large lakes on sediment delivery to the estuary of the Yangtze River. *Journal of Geophysical Research*, 112.

[233] Yang, S.L., Zhang, J., Xu, X.J., 2007b. Influence of the Three Gorges Dam on downstream delivery of sediment and its environmental implications, Yangtze River. *Geophysical Research Letters* 34.

[234] Yin, H.F., Li, C.G., 2001. Human impact on floods and flood disasters on the Yangtze River. *Geomorphology* 41 (2–3), 105–109.

[235] Yu, D.S., Tian, C., 2003. Vertical distribution of suspended sediment at the Yangtze River Estuary. *Proceedings of the International Conference on Estuaries and Coasts*, Hangzhou, China. 214-220.

[236] Yu, D.S., 2006. Analysis on impact of the Coriolis forces on flow in the Yangtze River Estuary. *Proceedings of the third Chinese-German Joint Symposium on Coastal and Ocean Engineering*, Tainan, Taiwan.

[237] Yangtze Estuary Waterway Administration Bureau (YEWAB), 2007: Project Description.

[238] Zaitlin, B.A., Dalrymple, R.W., Boyd, R.W., 1994. The stratigraphic organization of incised-valley systems associated with relative sea-level change. In: Dalrymple R., Boyd R. and Zaitlin B. A. (Eds), *Incised – valley systems: origin and sedimentary sequences.* SEPM Society of Sedimentary Geology Special Publication, 51, 45-60.

[239] Zanke, U., 1993. *Report on development of a numerical model with movable bed*. (Hydro-Consult-Hannover)

[240] Zanke, U., 1994. *Zur Entwicklung eines numerischen Modells mit beweglicher Sohle*. Wasser und Boden, Heft 12.

[241] Zanke, U., 1995. *Report on development of a numerical with movable bed Part Ⅱ-Fractional sediment bed* (Hydro- Consult-Hannover)

[242] Zanke,U., Mewis P., 2002. *Morphodynamisches Simulationssystem TIMOR.* Wasser und Boden, Bodenschutz und Abfallwirtschaft, Parey Buchverlag, Berlin.

[243] Zanke, U., 2002. *Hydromechanik der Gerinne und Küstengewässer*, Parey Verlag.

[244] Zeidler, R.B., 1997. Climate change variability and response strategies for the coastal zones of Poland. *Climate Change* 36, 151-173.

[245] Zhang, A.F., Chen, X.Q., 2003. Changes of water discharge between Datong and the Changjiang Estuary during the dry season. *Journal of Geographical Science*. (in Chinese)

[246] Zhang, A.F., 2004. *A Study about impacts of human activities in the Mid-lower Yangtze on fluvial sediment supply from river basin and sediment discharge from the Yangtze into the Sea*. Doctoral Dissertation, East China Normal University, Shanghai, China (in Chinese)

[247] Zhang, Q., Xu, C.Y., Becker, S., Jiang, T., 2006. Sediment and runoff changes in the Yangtze. River basin during past 50 years. *Journal of Hydrology* 331, 511-523.

[248] Zhang, Q., Xu, C.Y., Singh, V.P., Yang, T., 2009. Multiscale variability of sediment load and streamflow of the lower Yangtze River basin: Possible causes and implications. *Journal of Hydrology* 368 (1-4), 96–104.

[249] Zhang, Q.F., 2009. The South-to-North Water Transfer Project of China. *Environmental Implications and Monitoring Strategy, Journal of the American Water Resources Association* 45 (5), 1238-1247.

[250] Zhao, J., 2006. *Research of the response of the morphological process at Yangtze River Estuary to the changes of water and sediment discharges.* Master Dissertation, Hohai University, Nanjing, China (in Chinese)

[251] Zheng, G., 2002. *3-D Current numerical model for the Yangtze River estuary with baroclinic-diagnosis mode.* Ph.D thesis, Hohai University, China. (in Chinese).

[252] Zheng, J.H., Mase, H., Demirbilek, Z., Lin, L., 2008. Implementation and evaluation of alternative wave breaking formulas in a coastal spectral wave model. *Ocean Engineering.*

[253] Zhou, G, Wang, H., Shao, X.J., Jia, D.D., 2009. Numerical model for sediment transport and bed degradation in the Yangtze River channel downstream of Three Gorges Reservoir. *Journal of Hydraulic Engineering* 135 (9), 729-740.

[254] Zhou, H., 2008. *The erosional evolution and the morphological response to the water and sediment discharges at the Yangtze River Estuary based on GIS*. Doctoral Dissertation, Hohai University, Nanjing, China. (in Chinese)

[255] Zhou, X.Y., Dahlem, G., Zanke, U., 2009. Beispiele Morphodynamischer Modelluntersuchungen in China und Brasilien. *Verfahren des 1 Darmstädter Ingenieurkongress Bau und Umwelt*, Darmstadt.

[256] Zhou, X.Y., Zanke, U., Yan, Y.X., Zheng, J.H., 2009. Morphodynamic Simulation at South Branch of Yangtze Estuary. *Proceedings of the ASME 28th International Conference on Ocean, Offshore and Arctic Engineering (OMAE)*, Hawaii.

[257] Zhou, X.Y., Zanke, U., Yan, Y.X., 2008. Flow and Morphodynamics Simulation in Yangtze Estuary Using TIMOR3. *Proceedings of Fourth Chinese-German Joint Symposium on Hydraulic and Ocean Engineering*, Darmstadt, Germany.

[258] Zhu, K., Zhang, Y.X., 2008. South-to-North Water Diversion Project in China. In: Lambert, M., Daniell, T.M., Leonard, M., (Eds). *Proceedings of Water Down Under 2008*. Causal Productions, Modbury, Australia, 785-794.

[259] Zhu, S., Shi, F., Zhu, J., Ding, P.X., 2001a. Numerical study on residual current and its impact on mass transport in the Hongzhou Bay and Yangtze Estuary, I. A 3-D joint model of the Hangzhou Bay and Changjiang Estuary. *Acta Oceanologica Sinica* 20, 1–13.

[260] Zhu, S., Shi, F., Ding, P.X., Zhu, J., 2001b. Numerical study on residual current and its impact on mass transport in the Hangzhou Bay and Yangtze Estuary, II. Residual current and its impact on mass transport in winter. *Acta Oceanologica Sinica* 20, 14–30.

[261] Zhu, Y.M., Lu, X.X., Zhou, Y., 2008. Sediment flux sensitivity to climate change: a case study in the Longchuanjiang catchment of the upper Yangtze River, China. *Global and Planetary Change* 60 (3–4), 429–442.

[262] Zhu, Y.L., Yan, Y.X., Jia, L.W., Mao, L.H., 2001. Numerical model of unsteady flow and suspended-sediment transport in river networks with junction control method. *Journal of Hydrodynamics.* (in Chinese)

GESAMTVERZEICHNIS

der bisherigen „Technischen Berichte über Ingenieurhydrologie und Hydraulik“ *)

Nr. 1/1965 (vergriffen)
H. Lacher — Über das Kriechverhalten destillierter Bitumina unter Zugrundelegung der Theorie der linearen Viskosität

Nr. 2/1966
J. Bock — Einfluß der Querschnittsform auf die Widerstandsbeiwerte offener Gerinne

Nr. 3/1967 (vergriffen)
P. Unger — Berechnung instationärer Abflußvorgänge in natürlichen Gerinnen unter Verwendung eines von der Gerinneform unabhängigen Rauhigkeitsmaßes

Nr. 4/1968 (vergriffen)
W. Tiedt — Berechnung des laminaren und turbulenten Reibungswiderstandes konzentrischer und exzentrischer Ringspalte

Nr. 5/1969
R. Schröder — Häufigkeitsanalyse hydrologischer Daten
B. Scherer — Unverzerrtes Hele-Shaw-Modell für instationäre Grundwasserströmungen mit freier Oberfläche

Nr. 6/1970
D. Krause — Einfluß der Trassierungselemente auf den Spiegelverlauf in gekrümmten Schussrinnen

Nr. 7/1971
W. Tiedt — Hydrodynamische Untersuchung des Teilfüllungsproblems, Gesetzmäßigkeiten des Abflusses in technisch rauhen Kreisgerinnen bei laminarer und turbulenter Strömung

Nr. 8/1972
M. T. Monzavi — Widerstandsgesetz auf statistischer Basis für extreme natürliche Rauhigkeiten in Druckrohren

Nr. 9/1973
B. Scherer — Die Entwicklung und Anwendung eindimensionaler Modelle der zweidimensionalen Grundwasserbewegungen in Fluß-, Graben- und Drainnähe

Nr. 10/1973 (vergriffen)
diverse Autoren — Sammlung von Kurzberichten 1965 – 1972

*) Bestellungen beim

Institut für Wasserbau und Wasserwirtschaft
Fachgebiet Ingenieurhydrologie und Wasserbewirtschaftung
Petersenstraße 13, D-64287 Darmstadt

Nr. 11/1974 (vergriffen)

E. Zäschke — Widerstandsmindernde Wirkung hochmolekularer Zusätze beim Transport Newtonscher Flüssigkeiten in geschlossenen Leitungen

R. Schröder u. D. Knauf — Über das hydraulische Widerstandsverhalten von Beton- und Stahlbetonrohren im Übergangsbereich

H. Lacher — Konstruktionshilfe für Strömungsnetze ebener Potentialströmungen mittels Elementarströmungen

H. Lacher u. M. T. Monzavi — Einfluß von Teilfüllungsgrad und von Wanddicke des porösen Rohrmantels auf die Ergiebigkeit von Betonfilterrohren

H. Lacher u. K. J. Ueker — Untersuchung zur Ermittlung der Abflußleistung poröser Betonfilterrohre unter natürlichen Bedingungen

G. Euler u. A. Koussis — Berechnung von Hochwasserabläufen mit Näherungsverfahren und Anwendung

H. Lacher — Neuere Methoden der Wissensvermittlung im Fach „Hydraulik“, erläutert am Lehrbeispiel „Hydrostatik räumlich gekrümmter Oberflächen“

Nr. 12/1974

H. J. Dallwig — Fließformeln und Formbeiwert - eine kritische Untersuchung üblicher Berechnungsmethoden für Gerinneströmungen

R. Schröder — Wirkung periodischer Wandwelligkeiten auf den Strömungswiderstand

Nr. 13/1974 (vergriffen)

D. Belke — Die statistische Analyse von Grundwasserständen mit dem Ziel der Extremwertprognose

Nr. 14/1975 (vergriffen)

G. Euler — Die Simulation der Niederschlagsaufteilung für Hochwasserabfluß-Modelle

Nr. 15/1975

A. Koussis — Ein verbessertes Näherungsverfahren zur Berechnung von Hochwasserabläufen

Nr. 16/1975

G. Lass — Berechnung von Horizontalfilterbrunnen mit beliebig angeordneten Filterrohren

Nr. 17/1976 (vergriffen)

D. Knauf — Die Abflußbildung in schneebedeckten Einzugsgebieten des Mittelgebirges

Nr. 18/1977

H. Bischoff — Die Berechnung von Potentialfeldern mit der Randintegralmethode, dargestellt am Beispiel der ebenen Grundwasserbewegung

Nr. 19/1977

I. David — Grundwasserfassungsanlagen mit Filterrohren

Nr. 20/1977 (vergriffen)

diverse Autoren — Sammlung von Kurzberichten 1972 - 1977

Nr. 21/1978

O. Gieseler — Einfluß der äquivalenten Sandrauhigkeit auf die Lage des Wechselsprungs bei Umlenkung eines frei fallenden runden Flüssigkeitsstrahls an einer ebenen Platte

Nr. 22/1978

R. Schröder	Forschungsarbeiten des Instituts für Hydraulik und Hydrologie
D. Belke u.	Simulation zur Nutzraumoptimierung einer Talsperre
G. Euler u.	Ein detailliertes mathematisches Modell zur Simulation von
R. Wackermann	Hochwasserwellen am Beispiel der Nidda
T. Brandt	Der Austausch von Oberflächen- und Grundwasser
R. Schröder	Gestaltung von Offshore-Bauwerken für die Kühlwasserversorgung thermischer Kraftwerke
H. Lacher u. F. Thiele	Zum Problem des Regenwasserabflusses auf Fahrbahnen
W. Tiedt	Druckspüler/Spülkasten - ein Beitrag zur Hydraulik zweier Spülsysteme der Sanitärtechnik
O. Gieseler	Hydraulische und mechanische Verfahren zur Ermittlung von Rauhigkeiten

Nr. 23/1978

A. Holderbaum	Hydraulische Untersuchung zur Ermittlung der Wasserfilmdicken auf beregneten Fahrbahnoberflächen

Nr. 24/1979

T. Brandt	Modell zur Abflußgangliniensimulation unter besonderer Berücksichtigung des grundwasserbürtigen Abflusses

Nr. 25/1980

N. Könemann	Der wechselseitige Einfluß von Vorland und Flußbett auf das Widerstandsverhalten offener Gerinne mit gegliederten Querschnitten

Nr. 26/1981

R. Wackermann	Ein Rasterverfahren mit flächenvariabler Systemfunktion zur Simulation von Hochwasserganglinien aus großen Einzugsgebieten

Nr. 27/1981

A. Holderbaum	Modellversuche zum Abfluß von Niederschlagswasser auf Verwindungs-Strecken

Nr. 28/1982

H. J. Dallwig	Zur Leistungsfähigkeit von Kelchüberfällen

Nr. 29/1982

R. Schröder	In memoriam Hannes Lacher - Geleitwort
H. Lacher	Über die viskoelastischen Eigenschaften von destilliertem Bitumen
H. Lacher u. R. Schröder	Experimentelle Erfahrungen mit Filterrohren als Grundlage ihrer hydraulischen Bemessung
H. Lacher	Grundwasserabfluß mit freier Oberfläche, Auszug aus dem Textbuch zur Technischen Hydraulik
H. Lacher B. Söhngen H. Bischoff	Anwendung der Randintegralmethode zur Berechnung der Leistungsfähigkeit von teilgefüllten Rohren
H. Lacher	Verallgemeinertes Berechnungsverfahren nach Dupuit-Forchheimer für Grundwasserleiter beliebig hoher Durchlässigkeit
H. Lacher H. Bischoff B. Söhngen	Anwendung der Feldintegralmethode zur Berechnung der Durchströmung von Steinschüttdämmen
F. Zior u. H. Lacher	Ein neues Meßverfahren für die Bestimmung der Oberflächenrauhigkeit von Kanalwandungen
H. Gerdes u. H. Lacher	Die Berechnung dreidimensionaler Grundwasserströmung mit Mitteln der ebenen Potentialtheorie
F. Zior u. H. Lacher	Entwicklung einer konduktometrischen Sonde zur Messung von Wasserfilmdicken auf Fahrbahnoberflächen

Fortsetzung Heft 29

H. Lacher u. E. Zäschke — Schiffahrtsbedingte Wasserdruckausbreitung in Kanalböschungen

F. Thiele u. H. Lacher — Probleme der Straßenentwässerung und neue Bemessungsmethoden

B. Söhngen, H. Bischoff u. H. Lacher — Die Berechnung der Ergiebigkeit von Drainagesystemen in horizontal ausgedehnten Grundwassersystemen

H. Lacher — Zur Begründung der Konzentrationszeit aus der Sicht der Hydraulik

H. Lacher — Humor im Wasserbaulichen Versuchswesen: Versuchsanordnung zur Bestimmung der äquivalenten Sandrauhigkeit von Steinzeugrohren

Nr. 30/1983

diverse Autoren — Sammlung von Kurzberichten 1978 - 1983

Nr. 31/1983

F. Thiele — Fahrbahnlängsentwässerung im Straßengerinne und ein Entwurf für zukünftige Richtlinien zur Bemessung

Nr. 32/1984

U. Höfer — Beginn der Sedimentbewegung bei Gewässersohlen mit Riffeln oder Dünen

Nr. 33/1985

G. Euler, C. Heinzelmann, D. Jacobi — Die Berechnung des Schmutzwasserabflusses aus Niederschlägen: Eine vergleichende Darstellung und Wertung der Modellansätze

Nr. 34/1985

H. Gerdes — Berechnung dreidimensionaler Grundwasserströmung mit Mitteln der ebenen Potentialtheorie am Beispiel des Sickerstollens

Nr. 35/1986

diverse Autoren — Stofftransport im Wasser - Darmstädter Wasserbauliches Kolloquium 1985: Zusammenstellung der Referate

Nr. 36/1986

R. Schröder — Diskontinuierliche Abflußvorgänge in Freispiegelrinnen: Randwalzen

R. Schröder — Die turbulente Strömung im freien Wechselsprung: Deckwalze

C. Kraus — Walzenbildung im Kolk

Nr. 37/1987

C. Heinzelmann, U. Höfer — Transportbeginn auf geriffelter Sohle unter dem Einfluß einer stationär gleichförmigen Strömung mit überlagerter Schwallwelle

Nr. 38/1987

F. Zior — Regenwasserabfluß auf Fahrbahnoberflächen: experimentelle und theoretische Untersuchungen

Nr. 39/1987

B. Söhngen — Das Formbeiwertkonzept zur Berechnung des Fließwiderstandes in Rohren und Gerinnen

Nr. 40/1988

diverse Autoren — Lösungsansätze zu aktuellen Problemen im Wasserbau - Darmstädter Wasserbauliches Kolloquium 1987: Zusammenstellung der Referate

Nr. 41/1987

G. J. Weiß — Abfluß- und Wasserstandssteuerung in offenen Gerinnen mit Hilfe selbstregulierender Schwimmkörper

Nr. 42/1989
H. Zaiß — Simulation ereignisspezifischer Einflüsse des Niederschlag-Abfluß-Prozesses von Hochwasserereignissen kleiner Einzugsgebiete mit Niederschlag-Abfluß-Modellen

Nr. 43/1990
diverse Autoren — Hydraulik und Hydrologie im Stadtbauwesen - Darmstädter WasserbaulichesKolloquium 1989: Zusammenstellung der Referate

Nr. 44/1990
H. Wegner — Steuerung für kleine Hochwasserschutzräume

Nr. 45/1991
U. Drechsel — Repräsentanz und Übertragbarkeit von Niederschlagsersatz-belastungen zur Durchführung von Schmutzfrachtberechnungen

Nr. 46/1991
J. Lang — Analyse und Simulation des Feuchtekontinuums auf Straßenoberflächen

Nr. 47/1992
G. J. Weiß — Sohlenbeanspruchung und Sedimenttransport unter Einzelwellen

Nr. 48/1992
C. Heinzelmann — Hydraulische Untersuchung über den Einfluß benthischer Diatomeenfilme auf Strömungswiderstand und Transportbeginn ebener Sandsohlen

Nr. 49/1993
J. Kühlborn — Wachstum und Wanderung von Sedimentriffeln

Nr. 50/1995
M. Schuster — Transportkritische Schubspannungen bei verschiedenen Sohlenzuständen, insbesondere unter Einzelwellenbelastung bei stationärer Grundströmung

Nr. 51/1993 (vergriffen)
diverse Autoren — Dezentraler Hochwasserrückhalt - Darmstädter Wasserbauliches Kolloquium 1992: Zusammenstellung der Referate

Nr. 52/1994
N. Engel — Hydrologische Simulation der Abflußtransformation in Kanalisationsnetzen

Nr. 53/1995
diverse Autoren — Die modellgestützte Bewirtschaftung intensiv genutzter Einzugsgebiete - Darmstädter Wasserbauliches Kolloquium 1994: Zusammenstellung der Referate

Nr. 54/1996
S. Wallisch — Ein mathematischen Modell zur Berechnung der hydromechanischen Beanspruchung von Riffelsohlen

GESAMTVERZEICHNIS (ISSN 0340-4005)
der bisherigen `Wasserbau-Mitteilungen der TH Darmstadt *)
(teilweise Kurztitel)

Heft 1/März 66		(vergriffen)
	Bassler, F.	Vorwort des Herausgebers
	Linder, R.	Hochwasserentlastung von Staustufen durch Schiffsschleusen
	Bassler, F.	Beginnt die Epoche der Gezeitenkraftwerke?
	Elshazli, S.	Die Bedeutung der Wasserkraft für die ägyptische Wirtschaft
Heft 2/Juli 67		(vergriffen)
	Uhlig, D.	Probleme des landwirtschaftlichen Wasserbaus in Lybien
	Bassler, F.	Eindrücke vom ICID-Kongreß in Indien
	Sauer, H.-D.	Zentral messendes Wasserstands-Registriergerät für Modelle mit instationärer Strömung
	Bassler, F.	Die Nutzung von Meerwasser in der Kattara-Senke/Ägypten
Heft 3/Dez. 68		(vergriffen)
	Müller, J.	Weltregister der Pumpspeicherkraftwerke
	Bassler, F.	Wasserwirtschaftliche Sonderaufgaben in Entwicklungsländern
	Bayer, E.	Die Versuchseinrichtungen des Instituts für Wasserbau und Wasserwirtschaft
	Mäder, Ch.	Die Exkursionen des Lehrstuhls für Wasserbau und Wasserwirtschaft
	Bassler, F.	Scheme for Qattara Depression/Egypt
Heft 4/Aug. 69		
	Bayer, E.	Gestaltung der Rampenbauwerke für Flussfähren
Heft 5/Nov. 69		
	Sauer, H.-D.	Industriewasserentnahme aus schwebstoffreichen Flüssen
Heft 6/Okt. 70		
	Schröder, W.	Ausbaugefällebemessung alluvialer Bachstrecken nach dem Sandtransportvermögen
Heft 7/Feb. 71		
	Müller, J.	Auswirkungen eines Unterbeckens für Pumpspeicherung auf die Wasserwirtschaft
	Bassler, F.	Nuklearausbruch und Pumpspeicherung als Kostenfaktoren der Wasserkraftanlage in der Kattara-Senke/Ägypten

---

*) Selbstkostenpreis EURO 20,-- je Heft. Bestellungen beim
Institut für Wasserbau und Wasserwirtschaft, Fachgebiet Wasserbau
Petersenstraße 13, D-64287 Darmstadt,
per Fax: 06151/16-3223, per e-mail: zeitler@wb.tu-darmstadt.de

Heft 8/Juli 71

Bassler, F.	10 Jahre Lehre und Forschung in Wasserbau und Wasserwirtschaft an der Technischen Hochschule Darmstadt
Mäder, Ch.	Modellversuche zur Umgestaltung des Mains bei Aschaffenburg
Schmidtke, R.	Projektstudie zur Regelung des Rio Mantaro in der Hochebene von Huancayo/Peru
Schröder, W.	Projektstudie zur Ufersicherung am Amazonas bei Iquitos/Peru
Sulser, P.	Gedanken zu den Exkursionen eines Wasserbaulehrstuhls
Täubert, U.	Modellversuche für Hochwasserentlastungsanlage Staudamm Poza Honda/Ecuador
Uhlig, D.	Das Bewässerungsprojekt Al Hassa/Saudi Arabien
Bassler, F.	Studieneinführung Bauingenieurwesen, Fachgebiet Wasserbau und Wasserwirtschaft

Heft 9/Nov. 71

Mäder, Ch.	Strömungen durch Luftblasenschleier in stehenden und fließenden Gewässern

Heft 10/Aug. 72

Schmidtke, R.	Ein Kostenzurechnungsmodell für wasserwirtschaftliche Mehrzweckprojekte

Heft 11/Dez. 73 (vergriffen)

Sulser, P.	Berührungslose Wasserstandsmessung mittels kontinuierlicher Kondensator-umladung
Börner, R.	Internationale Pumpspeicherbibliographie 1900 bis 1960
Bassler, F.	Solar Depression Power Plant of Qattara/Eqypt
Täubert, U.	Der Abfluß in Schußrinnenversuchen
Bassler, F.	Pumpspeicherkraftwerke an schiffbaren Wasserstraßen u. a.

Heft 12/Apr. 74

Täubert, U.	Wasserwirtschaftliche Systemanalyse des Wärmehaushalts von Flüssen

Heft 13/Dez. 75 (vergriffen)

Bassler, F.	Neue Vorschläge für die Entwicklung der Kattara-Senke/Ägypten
Bassler, F.	New Proposals to Develop Qattara Depression/Egypt
Börner, R.	Moorentwässerung in Finnland
Börner, R.	Internationale Pumpspeicherbibliographie 1961 bis 1965
Gräb, E.	Konstruktion und Umbau einer Kipprinne
Sulser, P.	Die Wasserbau-Exkursionen des Instituts in den Jahren 1970 bis 1975, Forschungsvorhaben und Veröffentlichungen 1970 bis 1975

Heft 14/März 77

Kriesel, E.	Wasserwirtschaftliche Aspekte thermischer Energiequellen

Heft 15/Mai 77

Börner, R.	Einsatzmöglichkeiten der Mehrzweckpumpspeicherung in Entwicklungsländern

Heft 16/Juli 77 (vergriffen)

Franzius, V.	Der Sickerwasserabfluß aus Mülldeponien - Ein mathematisches Modell

Heft 17/ Aug. 77 (vergriffen)

Tönsmann, F.	Verringerung des Feststoffbetriebs in Entnahmebauwerken an Bächen

Heft 18/Dez. 77 (vergriffen)

Bassler, F.	Die Energiequellen Fluss- und Meerwasser
Bassler, F.	Speisung der Schiffahrtskanäle mit Scheitelhaltung
u.a.	
Bassler, F.	100 Jahre Bauingenieurwesen Arab Republic of Egypt : Qattara Depression
Bassler, F.	Tätigkeiten als Ordinarius für Wasserbau und Wasserwirtschaft

Heft 19/Dez. 78

Sulser, P.	Drucklufteinleitung in Flüsse zur Steuerung des Geschiebetransports

Heft 20/Juni 79 (vergriffen)
Friedrich Bassler 70 Jahre/Ansprache und Aufsätze zu seiner Emeritierung

Heft 21/März 81

Döring, M.	Einflüsse der Wassernutzung thermischer Kraftwerke auf Gewässer

Heft 22/Aug. 83

Albert, W.	Solarteich - Kollektor und Wärmespeicher
Gonsowski, P.	Bodenluftkompression bei Wasserinfiltration
Gonsowski, P.	Selbstdichtung von Fließgewässern
Kaiser, W.	Modellversuch HW-Entlastung Sösetalsperre
Wieland, H.	
Krier, H.	Erfahrungen bei Beregnungsanlagen im Hessischen Ried
Krier, H.	Erosionsbeginn bei kohäsiver Wasserlaufsohle
Wieland, H.	Modellversuch zur Hochwasser-Entlastung der Kulmke-Sperre/Harz

Heft 23/Sep. 84 (vergriffen)
Kaiser, W. Fließwiderstandsverhalten in Gerinnen mit durchströmten Ufergehölzzonen

Heft 24/Feb. 85 (vergriffen)
Darmstädter Wasserbauliches Kolloquium 1984 „Hochwasser am Oberrhein“

Heft 25/Aug. 87

Wieland, H.	Hydraulische Bemessung von Tosbecken für Überfallstrahlen und der Druckbelastung der Sohle

Heft 26/Feb. 87 Darmstädter Wasserbauliches Kolloquium 1986 „Planungsansätze Ökologie - Wasserwirtschaft, so nicht! - wie dann?“

Heft 27/Juli 87

Krier, H.	Zum Langzeiterosionsverhalten kohäsiver Fließgewässersohlen

Heft 28/Sep. 87

Gonsowski, P.	Der Einfluß der Bodenluftkompression auf die vertikale Infiltration von Wasser in Sanden

Heft 29/Dez. 89 Darmstädter Wasserbauliches Kolloquium 1988 `Fließgewässer – Stillgewässer

Heft 30/Dez.89 (vergriffen)
Albert, W. Die Gebietsverdunstung von Waldstandorten aus der Simulation von Grundwasserganglinien mit klimatischem Bodenwasserhaushaltsmodell

Heft 31/Feb. 90

Weiß. J.	Berücksichtigung der Hysterse der Wasserspannung bei der Berechnung der vertikalen Wasserbewegung in natürlichen Sandböden

Heft 32/März 90 Festschrift zum 60. Geburtstag von Prof. Dr.-Ing. Josef Mock

Heft 33/Aug. 90
Theune, Ch. Hydrological and Economical Aspects of Agronomically Productive Perculation Systems

Heft 34/Dez. 90 (vergriffen)
Darmstädter Wasserbauliches Kolloquium 1990 `Umweltverträglichkeitsprüfung in der Wasserwirtschaft

Heft 35/Nov. 91 (vergriffen)
Nuding, A. Fließwiderstandsverhalten in Gerinnen mit Ufergebüsch - Entwicklung eines Fließgesetzes für Fließgewässer mit und ohne Gehölzufer, unter besonderer Berücksichtigung von Ufergebüsch

Heft 36/Dez. 91 Darmstädter Wasserbauliches Kolloquium 1991 „Boden- und Grundwasserschutz - anwendungsorientierte Forschung und Verfahren“

Heft 37/März 92
Zimmermann, E. Phänomenologische Untersuchungen bei der Erosion einer kohäsiven Sohle

Heft 38/Dez. 93 Darmstädter Wasserbauliches Kolloquium 1993 `Ökologisch orientierte Gewässersanierung und –pflege

Heft 39/Dez. 93
Ruiz Rodriguez, E. Bodenluftströmung in teilgesättigten Böden

Heft 40/Dez. 95 Darmstädter Wasserbauliches Kolloquium 1995 „Hochwassergefahren am Oberrhein“ und Fachseminar „Abflußabhängigkeit der morphologischen und biologischen Verhältnisse von Fließgewässern bei Niedrigwasser“

Heft 41/Juli 99
von der Hude, Die Kapillarsperre als Oberflächenabdichtungssystem von Deponien und Altlasten - Rinnenversuche und Bemessungsregeln

Die Reihe der „Wasserbau-Mitteilungen der TH Darmstadt“ wird zusammen mit den „Technischen Berichten über Ingenieurhydrologie und HydraulikA“ als „Mitteilungen des Instituts für Wasserbau und Wasserwirtschaft der TU Darmstadt“ (ISSN 1430-3434) fortgesetzt. Die neue Nummerierung ergibt sich aus der Summe der Hefte beider Vorgängerreihen.

GESAMTVERZEICHNIS (ISSN 1430-3434) **)

Heft 96/1996 (vergriffen)
Träbing, K. Ökomorphologische Kenngrößen für die Strukturvielfalt von Fließgewässern

Heft 97/1997
Jelinek, D. Die Kapillarsperre als Oberflächenbarriere für Deponien und Altlasten - Langzeitstudien und praktische Erfahrungen in Feldversuchen

Heft 98/1997 Darmstädter Wasserbauliches Kolloquium 1996 `Numerische Simulationen im Wasserbau

Heft 99/1997 Berichte zur Ingenieurhydrologie und Wasserbewirtschaftung

Heft 100/1998
Kilian, T. Abflußcharakteristika und potentiell natürliche Gerinnegrundrißformen hessischer Fließgewässer

Heft 101/1997 (vergriffen)
Döring, M.

Heft 102/1998
Schmidt, T.R. Einfluß der Wandrauhigkeitsstruktur auf die Geschwindigkeitsverteilung ausgebildeter, turbulenter Strömungen in Kreisrohren

Heft 103/1998 Darmstädter Wasserbauliches Kolloquium 1997 „Betrieb und Steuerung von Speichern und Stauhaltungen unter sich ändernden Randbedingungen“

Heft 104/1998
Bettmann, T. Dezentrale Regenwasserbewirtschaftung und deren Auswirkungen auf die Regenwasserbehandlung in urbanen Gewässereinzugsgebieten

Heft 105/1998
Seid, A.H. Modelling the Influence of Shrinkage Cracks on Overland Flow

Heft 106/1999 (Nachdruck)
Zanke, U. Zur Physik von strömungsgetriebenem Sediment (Geschiebetrieb)

Heft 107/1999
Obermann, I. Modellierung des Wasserhaushaltes von Deponien vorbehandelter Siedlungsabfälle

Heft 108/1999 Darmstädter Wasserbauliches Kolloquium 1998
Mischwasserbehandlung - Planung, Prüfung, Vollzug -

Heft 109/2000
Kämpf, M. Fließprozesse in Kapillarsperren zur Oberflächenabdichtung von Deponien und Altlasten - Grundlagen zur hydraulischen Bemessung

Heft 110/2000
Lempert, M. Ein GIS gekoppeltes rasterbasiertes Modell zur Berechnung des Wasserhaushaltes kleiner Einzugsgebiete

Heft 111/2000 (vergriffen)
Darmstädter Wasserbauliche Kolloquium 1999 „Fließ- und Ausbreitungsvorgänge in aquatischen Grenzräumen“

Heft 112/2000 100-Jahr-Feier des Instituts für Wasserbau und Wasserwirtschaft mit Festvortrag von Prof. Dr.-Ing., Dr.-Ing. E.h. J. Plate

Heft 113/2000 (vergriffen)
Mehler, R. Mischwasserbehandlung - Verfahren und Modellierung

Heft 114/2000 (Nachdruck)
Lenk, M. Hydraulische Austauschvorgänge zwischen fließender Welle und Interstitial - Felduntersuchungen in einer Pool-Riffle-Sequenz an der oberen Lahn

Heft 115/2000 (Nachdruck)
Saenger, N. Identifikation von Austauschprozessen zwischen Fließgewässer und hyporheischer Zone

Heft 116/2000
Sieker, H. Generelle Planung der Regenwasserbewirtschaftung in Siedlungsgebieten

Heft 117/2001
Hailu, D. Optimal planning and water management of irrigation systems

Heft 118/2001
Lohr, H. Simulation, Bewertung und Optimierung von Betriebsregeln für wasserwirtschaftliche Speichersysteme

Heft 119/2001
Bente, St. Eine Software-gestützte Methodik zur Voreinschätzung der wasserwirtschaftlichen Auswirkungen von Maßnahmen der naturnahen Regenwasserbewirtschaftung

Heft 120/2001
Zanke, U. Zum Einfluß der Turbulenz auf den Beginn der Sedimentbewegung

Heft 121/2002
Hirschhäuser, T., Zanke, U. Morphologische Langfristprognose für das System Tidebecken-Außensände am Beispiel Sylts und der Dithmarscher Bucht

Heft 122/2002 Darmstädter Wasserbauliches Kolloquium 2000
Integrierte Gewässerbewirtschaftung in Verwaltung, Wissenschaft und Praxis

Heft 123/2002
Kraus, T. Rauheitsänderung durch Biofilmbewuchs in Druckrohrleitungen

Heft 124/2002
Luckner, T. Zum Bewegungsbeginn von Sedimenten

Heft 125/2002
Holfelder, T. Temperaturbeeinflußte Transportprozesse in Kapillarsperren zur Oberflächenabdichtung von Deponien und Altlasten

Heft 126/2003
Mewis, P. Morphodynamisch-numerische Modellierung von Flußkurven

Heft 127/2003
Wetzstein, A. Berechnung von Entlastungsabflüssen an gedrosselten Streichwehren auf der Basis von gemessenen Wasserständen

Heft 128/2003
Hirschhäuser,T. Sedimentologische und biologische Aspekte der morphodynamischen Modellierung von Tidebecken

Heft 129/2003 Darmstädter Wasserbauliches Kolloquium 2003 „Hochwasserschutz“

Heft 130/2003 Darmstädter Wasserbauliches Kolloquium 2001
Aktuelle Themen aus Hydromechanik, Wasserbau und Hydrologie

Heft 131/2003
Witting, M. Simulation von Küstenlängs- und Küstenquertransport im 2DH-morphodynamischen Modell TIMOR3

Heft 132/2003
Krebs, M. Untersuchung instationärer oszillierender Strömungen in buhnenverbauten Flußabschnitten und ihre Bedeutung für morphodynamische Berechnungen

Heft 133/2004
Kudo, Eiji Sustainable Water Management in an Urbanizing River Basin in Japan, Based on Integrated Modeling Technique

Heft 134/2005
Gebrewubet, Y. Numerical Modeling of Koka Reservoir Sedimentation

Heft 135/2006
Schadrac, I. Nouvelle approche méthodologique pour l‘analyse de la sécurité hydrologique des barrages en contexte sahélien soumis à une variabilité climatique

Heft 136/2006
Link, O. Untersuchung der Kolkung an einem schlanken zylindrischen Pfeiler in sandigem Boden

Heft 137/2006
Muschalla, D. Evolutionäre multikriterielle Optimierung komplexer wasserwirtschaftlicher Systeme

Heft 138/2006
Klawitter, A Ein Modellkonzept zur integrativen Betrachtung von Urban- und Ruralhydrologie auf Einzugsgebietsebene

Heft 139/2006 Darmstädter Wasserbauliches Kolloquium / DWA-Seminar 2005
„Feststofftransportmodelle“

Heft 140/2006
Wurpts, A. Numerische Simulation von Dichteeffekten am Beispiel der Umlagerung von Baggergut im Ästuarbereich

Heft 141/2007
Seydell, I. Einlagerung von Feinstoffen in eine Flusssohle und Wasseraustausch zwischen Fluss und Interstitial – Naturuntersuchungen an einer Kiesquerbank der Lahn bei Marburg

Heft 142/2007
Döring, M. Römische Häfen, Aquädukte und Zisternen in Campanien: Bestandsaufnahme der antiken Wasserbauten

Heft 143/2007
Winterscheid, A. Szenariotechnik im Hochwasserrisikomanagement

Heft 144/2008
Zanke, U.C.E. On Applicability of Morphodynamic Acceleration in Morphodynamic Simulations

Heft 145/2009
Schröter, K.A. Contribution to the Uncertainty Analysis of Distributed Hydrological Models

Heft 146/2009
Roland, A. Entwicklung von WWM II -Zur Seegangsmodellierung auf unregelmäßigen Gitternetzen-

Heft 147/2009
Wiesemann, J.-U. Zum Sedimenttransport auf quergeneigter Sohle

Heft 148/2011
Zhou, X. Morphodynamic Response of Yangtze River Estuary to Sea Level Rise and Human Interferences

---

**) Selbstkostenpreis EURO 20,-- je Heft. Bestellungen beim

Institut für Wasserbau und Wasserwirtschaft
Fachgebiet Ingenieurhydrologie und Wasserbewirtschaftung
Petersenstraße 13, D-64287 Darmstadt

oder

Institut für Wasserbau und Wasserwirtschaft, Fachgebiet Wasserbau
Petersenstraße 13, D-64287 Darmstadt,
per Fax: 06151/16-3223, per E-Mail: zeitler@wb.tu-darmstadt.de

ISSN-Nr.: 1430-3434

ISBN: 3-936146-28-4